

DECODING HEAVY HEARTS

Molecular Insights into Hypertrophic
Cardiomyopathy



Anne Elisabeth de Leeuw

Decoding Heavy Hearts

Molecular Insights into Hypertrophic Cardiomyopathy

Anne Elisabeth de Leeuw

Printed by: TOSAM Studio
Lay-out: Anne de Leeuw
Cover: Rob Buitink
ISBN/EAN: 978-90-393-7657-7

Decoding Heavy Hearts

Molecular Insights into Hypertrophic Cardiomyopathy

Decodering van het Zware Hart

Moleculaire inzichten in Hypertrofische Cardiomyopathie
(met een samenvatting in het Nederlands)

Proefschrift

ter verkrijging van de graad van doctor aan de
Universiteit Utrecht
op gezag van de
rector magnificus, prof. dr. H.R.B.M. Kummeling,
ingevolge het besluit van het college voor promoties
in het openbaar te verdedigen op

donderdag 28 maart 2024 des middags te 12.15 uur

door

Anne Elisabeth de Leeuw

geboren op 3 februari 1991
te Leiden

Promotor:

Prof. dr. E. van Rooij

Copromotor:

Dr. M. Wehrens

Beoordelingscommissie:

Prof. dr. ir. J.P.W.M. Bakkers

Prof. dr. R.A. de Boer

Prof. dr. D.P.V. de Kleijn (voorzitter)

Prof. dr. ir. H.M. den Ruijter

Prof. dr. J.P.G. Sluiter

The research described in this thesis was supported by a grant from the Leducq Foundation (14CVD04) and by a grant from the Dutch Heart Foundation (DHF number 2017-B018: ARENA-PRIME)

Financial support by the Dutch Heart Foundation for the publication of this thesis is gratefully acknowledged.

Contents

| | | |
|-----------|--|-----|
| Chapter 1 | General Introduction | 6 |
| Chapter 2 | Single-cell transcriptomics provides insights into hypertrophic cardiomyopathy | 28 |
| Chapter 3 | Spatial transcriptomic to define the septal transcriptional program in hypertrophic cardiomyopathy | 80 |
| Chapter 4 | Molecular mechanisms driving Hypertrophic Cardiomyopathy in Mybpc3 mouse models | 120 |
| Chapter 5 | General Discussion | 170 |
| Appendix | Nederlandse samenvatting Acknowledgements Curriculum Vitae List of Publications | 188 |



1

Heavy hearts, or hypertrophic hearts, were first mentioned in the 17th century by European physicians and anatomists, who described the anatomical hearts of young people who suffered from a sudden death as “hearts larger than that of any bull-ock”. Initially, the condition was named idiopathic hypertrophy in absence of a clear explanation for the enlargement of the heart muscle (Coats & Hollman, 2008). Later, cardiac idiopathic hypertrophy was separated from cardiac hypertrophy caused by (among others) renal disease, or hypertension (Bright, 1836; Coats & Hollman, 2008). Donald Teare first described asymmetrical hypertrophy as ‘a tumour of the heart’ in 8 different cases coming from a series of 16.000 autopsies (**Figure 1A**). Soon after, the term ‘Hypertrophic cardiomyopathy’, or HCM, was adopted in the medical society; which literally means “increased nutrition disease of the cardiac muscle” [Greek: *hyper* = over, *trophe* = nourishment, *cardiomyo* = heart muscle, *pathy* = disease] (B. J. Maron et al., 2009; Teare, 1957).

Nowadays, HCM is characterized as a thickening of the left ventricular heart muscle, in the absence of loading conditions such as hypertension, aortic valve disease, systemic infiltrative- or storage diseases (Marian & Braunwald, 2017). HCM is an autosomal dominant disease in which a single mutation can cause the disease phenotype (Marian & Braunwald, 2017). In the general western population, 1:500 to 1:200 people are estimated to suffer from this disease, making it the most prevalent of genetic heart diseases (Semsarian et al., 2015). Nevertheless, it is estimated that only 10% of the cases are clinically diagnosed and 6% are symptomatic (Antunes & Scudeler, 2020; B. J. Maron, 2018). Additionally, women and minorities are more affected by underrecognition which might partially be attributed to complex social and socioeconomic factors, and a possible provider bias, indicating that we might be only looking at “the tip of the iceberg” when speaking of the HCM prevalence (B. J. Maron, 2018; Wells et al., 2018).

Histologically, HCM can be characterized by hypertrophy and disorganization of the cardiomyocytes (disarray) (**Figure 1B**), and (perivascular) fibrosis (Lamke et al., 2003). Hypertrophic remodelling can occur throughout the left ventricle, and has a high inter- and intrafamilial variation. Despite this variation, the intraventricular septum (IVS, **Figure 1A**), is involved in most cases (Canepa et al., 2016). Although research has made great advances over time, many HCM features remain largely unknown, such as disease triggers, penetrance, and how clinical outcome can be predicted.

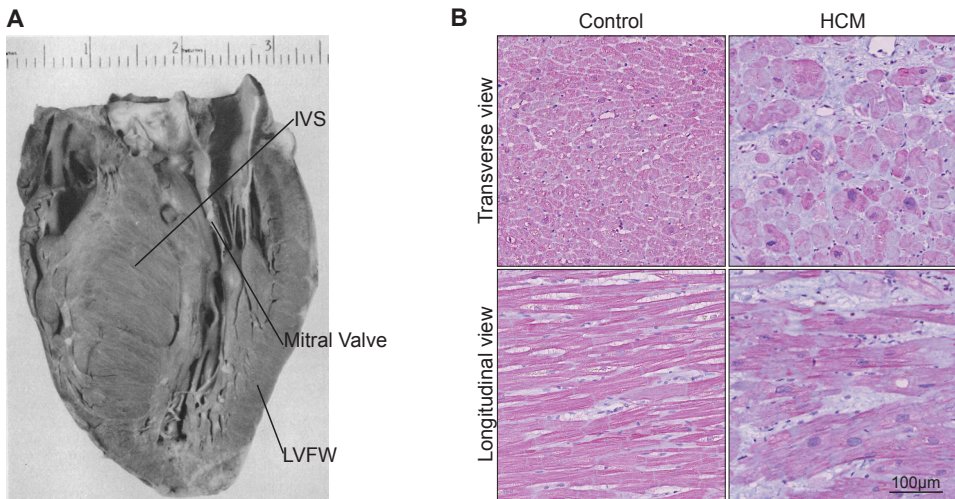


Figure 1: Pathological and histological characteristics of HCM. (A) One of the eight reported cases with a 'cardiac tumor' by Donald Teare. A 14-year-old boy had collapsed on the playground of his school in 1951, diseased with cardiac defects. The autopsy showed that the boy had an enlarged IVS when compared to the LVFW, and clearly had a very close proximity between the mitral wall and the septum (copied from Teare, 1957). (B) Histology of a healthy control heart and an HCM heart, stained for the cardiac contractile protein; Titin (pink) and nuclei are counterstained (blue). From histology, we can detect cardiomyocyte disarray, indicated in misalignment of the cardiomyocytes in the longitudinal view. Furthermore, cardiomyocyte hypertrophy can be detected in the transverse view compared to control cardiomyocytes and enlarged nuclei. Lastly, HCM tissue displays interstitial and perivascular fibrosis, which is shown in white. Intraventricular septum (IVS), Left ventricular free wall (LVFW).

Clinical perspectives

Although the majority of mutation carriers remain asymptomatic, patients who do develop HCM present varying symptoms. The disease can start with mild hypertrophy and disarray in the cardiomyocytes or patients can suffer from angina, syncope, and arterial/ventricular arrhythmias. Arrhythmias can lead to the formation of blood clots or inefficient blood pumping, increasing the risk at SCD. In fact, HCM is the primary cause of SCD in young adults (<30 years old) and athletes (B. J. Maron & Maron, 2013). Among the symptomatic patients, 10% progresses to a dilated phase and end stage heart failure (Semsarian et al., 2015).

Diagnosis of HCM

A patient may come to the clinic with symptoms such as: chest pain, shortness of

breath, fatigue, fainting, dizziness or palpitations (Association, 2014). Patients are typically diagnosed by 2D echocardiography (ECG), or magnetic resonance (MRI) which can provide information regarding heart muscle thickness and blood flow.

1 ECG is used to determine the thickness of the IVS (>15mm for patients with HCM). About two thirds of the patients will suffer from obstructive cardiomyopathy, indicating left ventricular outflow tract (LVOT) obstruction. In the absence of LV hypertrophy, other abnormalities can be investigated, such as fibrosis (imaged with Cardiac Magnetic Resonance; CMR) and collagen biomarkers, mitral valve abnormalities (elongation) and filling of the crypts with blood, which can be both be studied with MRI (B. J. Maron et al., 2014). Furthermore, atrial enlargement can be observed because of increased ventricular stiffness, which can lead to increased workload.

Another important diagnostic tool in HCM is genetic testing. Remarkably, already in 1705 HCM was described as an inheritable disease, when Giovanni Maria discovered reoccurrence of the disease in four generations, investigating an epidemic of sudden deaths in Rome (Coats & Hollman, 2008). HCM was the first heart disease linked to a mutation on chromosome 14 in 1989 (Canepa et al., 2016). The first mutation was described by the Seidman lab in myosin heavy chain- β (MYH7) (Geisterfer-Lowrance et al., 1996). Nowadays, it is known that roughly 40-60% of HCM patients carry a disease driving mutation in the contractile apparatus (the sarcomere) of cardiomyocytes (Marian & Braunwald, 2017; S. B. Marston, 2011; Zamorano et al., 2014). (Figure 2A). The most commonly mutated genes are MYH7 (30-35%), Cardiac myosin binding protein-C3 (MYBPC3 20-30%), and Troponin-T (TNNT, 10-15%) (Figure 2B) (Canepa et al., 2016; Chung et al., 2003). When a patient is tested positive for a disease driving mutation, direct relatives of HCM patients harboring an HCM-causing mutation may be submitted for genetic testing as well. Although genetic testing is a valuable tool to identify patients at risk (relatives carrying a mutation will be classified as HCM patients at an earlier stage; when the IVS exceeds 13mm), it does not influence the treatment strategy (B. J. Maron et al., 2014).

Mutation carriers that do not display clear signs of HCM (genotype+, phenotype- patients) will be kept under continued surveillance with imaging (B. J. Maron et al., 2014). Patients with confirmed clinical HCM will undergo more screenings to monitor LVOT obstruction, or other clinical manifestations such as diastolic dysfunction, arrhythmias, mitral regurgitation, ischemia, decreased cardiac output, increased arterial pressure, atrial fibrillation and ventricular arrhythmia (Enriquez & Goldman, n.d.; B. J.

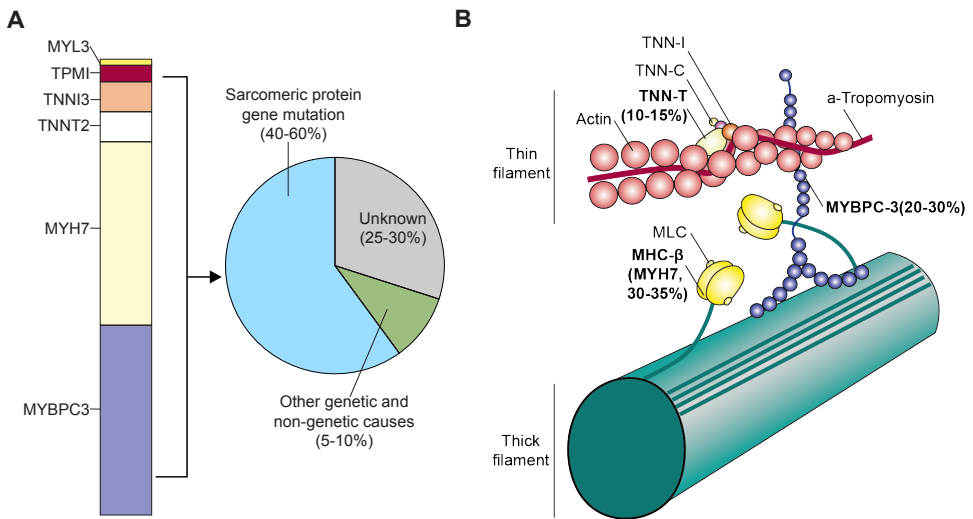


Figure 2: The genetic background of HCM. (A) Underlying causes for HCM with the majority of the cases (40-60%) is found to have a disease-causing mutation in a sarcomeric protein. 25-30% of the cases have an unknown cause (idiopathic) and 5-10% of the cases is found to have a different cause, for example patients with inborn errors of metabolism, mitochondrial diseases, neuromuscular diseases, amyloidosis, or drug-induced HCM by p.e. steroids. (Adapted from ESC guidelines 2014) (B) Schematic structure of the sarcomere with the genes which are most frequently found to be mutated in patient with HCM labeled. (Adapted from Nabel et al.). MLC = myosin light chain; MYL3= myosin light chain 3; MYBPC3 = myosin binding protein C, cardiac-type; MYH7 = myosin heavy chain 7, TNNC = troponin C; TNNI3 = troponin I, cardiac; TNNT2 = troponin T, cardiac, TPMI = tropomyosin I alpha chain.

Maron et al., 2014). Based on the symptoms and clinical manifestations, a risk stratification will be made according to the New York Heart Association Classes (NYHA) II-IV ranging from mildly symptomatic (Class II) to severely symptomatic (Class III/IV).

Treatment options

Based on their classes, patients will receive medical (pharmacological) therapy or surgical interventions to reduce HCM symptoms (B. J. Maron & Maron, 2014). Additionally, a patient will be evaluated for the risk of SCD, by looking at family history, blood pressure response and unexplained syncope (B. J. Maron & Maron, 2014). To decrease the risk of SCD, a patient might be recommended lifestyle interventions such as the avoidance of heavy exercise (Atteya et al., 2017; Weissler Snir et al., 2021).

Pharmacological treatment normally includes β -Adrenergic antagonists (β -blockers), calcium channel blockers, and anti-arrhythmic agents. These drugs are aimed

1 to alleviate symptoms by slowing the heart rate and thereby improving LV filling, decreasing myocardial oxygen demand through negative inotropic effects (weakening of heart contraction and slowing down the heart rate). β -blockers such as propranolol are considered the first line of therapy in symptomatic patients, they are known to have an effect on outflow gradients, alleviation of dyspnoea, chest pain, palpitations, dizziness and syncope. Calcium channel blockers such as verapamil also improve outflow gradients and diastolic function. These are however considered second in line therapy because adverse reactions such as hypotension due to its vasodilatory effects (Enriquez & Goldman, n.d.). Recently, a myosin inhibitor (Mavacamten) was added to the treatment options. These inhibit active myosin heads (**Figure 2B**), thereby reducing the contraction of the heart muscle. Mavacamten has been proven to reduce symptom burden and LVOT, giving a very interesting perspective on the future of pharmacological treatment of HCM (Ho et al., 2020; Tuohy et al., 2020).

Class III/IV patients, suffering from LVOT obstruction will undergo an intervention to remove a part of the IVS by surgical intervention or by alcohol ablation. (Canepa et al., 2016). Septal reduction therapy is considered a very safe and effective option to treat HCM patients; it frequently improves the mortality of patients up to a normal life expectancy. However, in some cases (roughly 10% of HCM patients), pathological remodeling proceeds after surgery. In progressive remodeling, there is an accumulation of fibrosis in the ventricular wall, which leads to a weakening, and eventually thinning of the heart muscle. In this case, the disease may evolve to end stage heart failure (ESHF) with reduced ejection fraction (EF). Patients with ESHF will have to receive a heart transplant in order to survive (B. J. Maron & Maron, 2013; Zamorano et al., 2014). In the Netherlands, roughly 130 people are on the waiting list for a heart transplant, with an annual addition of 50-70 patients, and transplantations are performed roughly 40 times a year (*Cijferoverzicht*, 2020).

Disease penetrance

Efforts are being made to better define patients who will remain asymptomatic or will develop severe progressive heart disease. The wide variation in phenotype may depend on the mutation itself, and a wide range of other non-genetic influences (Marian & Braunwald, 2017; Michels et al., 2009).

The role of environmental factors (or non-genetic influences) remains speculative. Potential modifiers of HCM are ageing (increased risk at a higher age), pregnancy,

ethnicity, sex (male predominance), and lifestyle habits such as exercise, diet and fluid intake (Finocchiaro et al., 2017; B. J. Maron et al., 2001). Heavy exercise is thought to trigger life threatening arrhythmias in patients carrying an HCM mutation (Atteya et al., 2017). However, moderate exercising is favored over a more sedentary lifestyle, mostly due to the fact that the prevalence of obesity in HCM patients is much higher compared to the general population. Additionally, increased body mass index (BMI) is associated with the level of LVOT obstruction and adverse events. (Balaji et al., 2019; Finocchiaro et al., 2017; Fumagalli et al., 2020; Olivotto et al., 1999). Other potential co-morbidities influencing the outcome and development of the disease are hypertension, obstructive sleep apnea and coronary artery disease (Finocchiaro et al., 2017; Semsarian & Semsarian, 2020).

The molecular mechanisms driving cardiac hypertrophy

All in all, HCM is a complex disease leading to impaired heart function and an increased risk of arrhythmias and heart failure. Delving into the molecular mechanism driving HCM can unravel key insights into the disease origin, progression and potential therapeutic targets. By doing so, researchers can work towards more personalized treatment strategies, or develop better diagnostic tools, potentially helping with early detection and timely interventions. HCM is an important disease to study for scientific reasons, but also withholds the promise of transforming clinical approaches and ultimately enhancing the quality of life of patient with a mutation, or with the disease.

Pathological hypertrophic remodeling ensues via diverse mechanistic pathways: (1) impaired calcium cycling and sensitivity in CMs; (2) increased myocardial fibrosis, (3) disturbed biomechanical stress sensing, (4) altered energy homeostasis and (5) microvascular dysfunction (Frey et al., 2012). Moreover, hypertrophic growth of cardiomyocytes, the principal HCM characteristic, is considered a physiological or pathological process in which there is an enhanced protein synthesis and heightened organization of the sarcomere. In case of pathological hypertrophic remodeling, there is a serial addition of sarcomere protein in response to stress. Ribosome production is enhanced during this process to be able to cope with the increased demand of translation of mRNA into proteins (Dorn & Force, 2005).

On a genetic level, the pathological hypertrophic response in cardiomyocytes cor-

1 responds to a gene pattern observed in the heart during embryonic development. (Carreño et al., 2006; Frey et al., 2004; Samak et al., 2016) Transcription factors (TFs) are important proteins that modulate this response, through upregulation in their expression or translocation into the nucleus, thereby exerting a profound genetic response. Examples of relevant TFs are; NFAT, GATA's, NKX2-5, MEFs and SRF. (Carreño et al., 2006; Dirx et al., 2013) Because of the importance of TFs in augmenting genetic response, and due to their small size, they have been of interest as therapeutic targets to treat hypertrophy. (Akazawa & Komuro, 2003; Lacraz et al., 2017)

Activation of TFs leads to the expression of, among others, atrial natriuretic peptide (ANP, *nppa*) and brain natriuretic peptide (BNP, *nppb*). These two genes are specific to cardiac stress by stretch-induction. Because of the specificity during cardiac stress, the protein product, pro-BNP has become an interesting biomarker (D'Amato et al., 2013; Jansen et al., 2022). Additionally, a switch towards a more fetal state in energy substrate metabolism can be detected in cardiac stress; instead of using free fatty acids, cardiomyocytes will start using glucose as the main source of ATP generation to be able to cope with the increase in energy demand (Bertero & Maack, 2018). Lastly, the expression of contractile proteins in the sarcomere will change, such as an increased expression of myosin light chains (MYL1/MYL2), skeletal α -actin (ACTA1), Cardiac troponins (TNN) and Desmin (DES) (Dirx et al., 2013). A myosin-switching is also observed where there is an increase in the slow twitch beta-myosin heavy chain (β -MHC), accompanied by the downregulation of the fast twitch alpha-myosin heavy chain (α -MHC) (Krenz & Robbins, 2004).

Myosins and hypertrophy

As mentioned, the genes which are most prevalently found to cause HCM are MYH7 and MYBPC3. Together, these account for roughly 70% of the patients (Chou & Chin, 2021). In the Netherlands specifically, most cases of HCM are caused by a mutation in MYBPC3 (Christiaans et al., 2010). MYBPC3 interacts with the thick filaments at the N-terminus side, and contains titin binding sites on the C-terminus side (Figure 2B) (Moolman et al., 2000). It contains 8 immunoglobulin-like (Ig-) domains, and 3 fibronectin-like (Fn-) domains, and the N-terminal also includes a cardiac-specific domain. This explains why mutations in Mybpc3 can lead to a cardiac phenotype specifically (Van Dijk et al., 2009).

MYBPC3 reduces part of the availability of myosin heads which generate contractile force. Consequently, it impedes both contractile force and energy expenditure. If

less MYBPC3 is present or functional, more myosin heads are utilized for contraction, leading to a more forceful contraction (McNamara et al., 2019). Mutations in MYBPC3 often lead to aberrant splicing, or a premature stop codon. However, generally there is no truncated form of the protein found in human tissues from patients carrying Mybpc3 mutations (Carrier et al., 2015; S. Marston et al., 2012; Moolman et al., 2000; Van Dijk et al., 2009). This would indicate that haploinsufficiency, where only the healthy allele is expressed and there is a 50% reduction of the protein. This might be the trigger to induce hypertrophy in patients with HCM. However, haploinsufficiency is not detected in all models, indicating an extra trigger might be required in the onset of HCM.

Models to study HCM-causing mutations in MYBPC3

HCM has been studied in different mouse models using knockouts (KO) of (among others) Mybpc3 (Barefield et al., 2015; Carrier et al., 2004; Farrell et al., 2018; Harris et al., 2002). Here, it was shown that a homozygous KO of Mybpc3 inevitably leads to hypertrophy in the heart; an upregulation of stress genes, increased fibrosis, and deterioration of the heart function, measured with echocardiography (Barefield et al., 2015; Carrier et al., 2004; Farrell et al., 2018; Harris et al., 2002). For heterozygous knockout mice, there was often a reduction detected in the transcript levels of Mybpc3, but the protein levels were either indistinguishable from the wildtype (WT) (Harris et al., 2002), or seemed to decrease after a longer period of time or a stressor, which was associated with hypertrophy or worsened cardiac function (Barefield et al., 2015; Carrier et al., 2004). These data suggest that haploinsufficiency of the protein precedes a phenotype. On the other hand, it was suggested that heterozygous genotype positive-phenotype negative models already show alterations in force development (Barefield et al., 2014). Although these models provide valuable insight into the pathology of HCM in case of a half or full reduction of MYBPC3 protein levels, it does not exactly recapitulate the patient situation, with a single point mutation.

A big leap was made in biomedical research with the discovery of clustered regularly interspaced short palindromic repeats (CRISPR)-Cas9; this enabled us to induce a mutation of interest very specifically (Cong et al., 2013; Doudna & Charpentier, 2014; Jinek et al., 2013; Mali et al., 2013). Furthermore, the development of stem cell research has enabled us to generate human induced pluripotent stem cells (hiP-SCs), which can be differentiated into any kind of cell type, including cardiomyocytes (hiPSC-CMs) (Andrysiak et al., 2021; Brodehl et al., 2019; Omole & Fakoya, 2018; Takahashi & Yamanaka, 2006). By using these two techniques, researchers have been

1

able to study the effect of Mybpc3 reduction; by a mutation or by using siRNA (Birket et al., 2015), by studying hiPSC-CMs from patients carrying a mutation in MYBPC3, and their reverted control (in which the mutation is reverted into the WT sequence) or by inducing a mutation in a healthy control line (Bhagwan et al., 2020; Birket et al., 2015; Eschenhagen et al., 2015; Eschenhagen & Carrier, 2019; Ojala et al., 2016; Prondzynski et al., 2017). Using these models, they successfully mimicked and studied several HCM hallmarks, including changes in calcium handling, force generation, marker genes and multinucleation. Nevertheless, the challenge with these models lies in attaining hypertrophy comparable to that observed in the adult heart.

Multomics to study the heart and HCM

Deep sequencing techniques have advanced greatly in the last decade, contributing substantially to the unbiased elucidation of molecular changes. Several studies performed either transcriptomic or proteomic analysis in order to identify new genes as drivers for the HCM phenotype (Bos et al., 2020; Lim et al., 2001; B. A. Maron et al., 2021; Pei et al., 2021; Pisano et al., 2022; C. W. Ren et al., 2016; Schuldt et al., 2021; Zhao et al., 2022). However, bulk sequencing only takes into account a small area of the myocardium, and is done on a mixed cell population. In HCM, there is a very large cellular, and regional heterogeneity in the myocardial wall (Becker et al., 2020; Canepa et al., 2016; Cheng et al., 2021; Kirschner et al., 2005; Kraft & Montag, 2019; J. Liu et al., 2022; Sepehrkhoy et al., 2017). Further development of RNA-sequencing techniques allowed for the investigation of genetic patterns in much greater detail. Hence, Tomo-sequencing (Tomo-Seq) is a technique in which the tissue is dissected into thin slices, which are sequenced separately, allowing the detection of spatial gene expression patterns within one sample (Junker et al., 2014; Kruse et al., 2016). This technique has been successfully used by our group to identify relevant TFs in cardiac pathologies (Boogerd et al., 2019; Lacraz et al., 2017). To get a more in-depth understanding of disease heterogeneity on a cellular level, single cell RNA sequencing (scRNA-seq) can be performed. Several studies have used scRNA-seq to study cardiac biology by looking at (among others) differences between cell clusters of the same cell type in diseased states versus healthy, identifying new cell types, or by looking at intercellular communication (Codden et al., 2022; Farbehi et al., 2019; Gladka et al., 2018; Hu et al., 2018; Koenig et al., 2022; Kretzschmar et al., 2018; Larson & Chin, 2021; Molenaar et al., 2021; Nomura et al., 2018; Z. Ren et al., 2020; Sereti et al., 2018; Skelly et al., 2018). Recently, studies have also focused on the HCM heart, revealing new insights on changes in cell composition and intercellular communication, in the diseased septum and ventricle (Chaffin et al., 2022; Larson et

16

al., 2022; X. Liu et al., 2023). Further investigation can enhance our understanding of the segregation between a severely diseased CM, and a comparatively healthier CM. Furthermore, delineating the spatial localization in the more diseased CM, and elucidating the genomic pathways activated in the transition towards a hypertrophic state will help us getting a better understanding of the molecular mechanisms driving HCM.

Thesis outline

In this thesis, we will dive deeper into the driving molecular mechanisms behind the development of HCM hallmarks. By focusing on the intercellular and spatial heterogeneity, we hope to broaden the general knowledge and prediction of progression of this complex disease. In the studies described here, we made use of different models and sequencing techniques to investigate regional and cell to cell differences on a transcriptional level. Thereby we delve deeper into potential regulators of pathological remodeling in HCM.

In **Chapter 2** we study transcriptional differences in adult human cardiomyocytes from HCM patients by subjecting myectomy tissue to digestion and scRNA-seq. By doing so, we found that cardiomyocytes coming from patients with HCM could be clustered into different states of disease. With bioinformatical models we were able to predict transcription factors which might push genetic programs in these cardiomyocytes. Furthermore, we were able to detect a gene program which was linked to more hypertrophic cells.

In **Chapter 3**, we performed Tomo-seq to find out whether the expression of disease related genes is specific to certain regions in the (explanted) HCM heart. We selected part of the IVS and part of the left ventricular free wall and sequenced thin slices of the cross section. Thereby, we were able to detect translational patterns, specifically detecting regional expression of genes related to hallmarks of HCM, indicating areas of hypertrophy and fibrosis. With further analysis, we focused on the hypertrophy-related gene program in the septum specifically, and identified NR2F2 as a potential transcription factor to be driving this genetic pattern and we studied its downstream function in hiPS-CMs.

In **Chapter 4** we generated mouse models to study HCM by knocking in two of

the most common Dutch mutations in MYBPC3 in the Netherlands; p.Trp792fs and p.Arg943X, which corresponded to p.Trp796fs and p. p.Arg947X in mice. Both of these mutations give rise to PTCs Here, we compared heterozygous male and female mice, we studied the influence of pressure-induced stress on cardiac function, and we studied the effect of a homozygous mutation on HCM pathogenesis.

Chapter 5 combines the data and will put all our findings in context, where the current papers and literature will be discussed.

References

- Akazawa, H., & Komuro, I. (2003). Roles of cardiac transcription factors in cardiac hypertrophy. *Circulation Research*, 92(10), 1079–1088. <https://doi.org/10.1161/01.RES.0000072977.86706.23>
- Andrysiak, K., Stępniewski, J., & Dulak, J. (2021). Human-induced pluripotent stem cell-derived cardiomyocytes, 3D cardiac structures, and heart-on-a-chip as tools for drug research. *Pflugers Archiv European Journal of Physiology*, 473(7), 1061–1085. <https://doi.org/10.1007/s00424-021-02536-z>
- Antunes, M. de O., & Scudeler, T. L. (2020). Hypertrophic cardiomyopathy. *IJC Heart and Vasculature*, 27, 100503. <https://doi.org/10.1016/j.ijcha.2020.100503>
- Association, A. H. (2014). What is hypertrophic cardiomyopathy (HCM). *A Guide to Hypertrophic Cardiomyopathy*, 1–122. <https://doi.org/10.1002/9781118725498.ch1>
- Atteya, G., Day, S., & Lampert, R. (2017). Sports and Exercise in Patients with Hypertrophic Cardiomyopathy: More Questions than Answers. *American College of Cardiology*, 5–7. <https://www.acc.org/latest-in-cardiology/articles/2017/02/20/08/06/sports-and-exercise-in-patients-with-hypertrophic-cardiomyopathy>
- Balaji, S., Dilorenzo, M. P., Fish, F. A., Etheridge, S. P., Aziz, P. F., Russell, M. W., Tisma, S., Pflaumer, A., Sreeram, N., Kubus, P., Law, I. H., & Kantoch, M. J. (2019). Impact of Obesity on Left Ventricular Thickness in Children with Hypertrophic Cardiomyopathy. *Pediatric Cardiology*, 40(6), 1253–1257. <https://doi.org/10.1007/s00246-019-02145-9>
- Barefield, D., Kumar, M., de Tombe, P. P., & Sadayappan, S. (2014). Contractile dysfunction in a mouse model expressing a heterozygous MYBPC3 mutation associated with hypertrophic cardiomyopathy. *American Journal of Physiology - Heart and Circulatory Physiology*, 306(6), 807–815. <https://doi.org/10.1152/ajpheart.00913.2013>
- Barefield, D., Kumar, M., Gorham, J., Seidman, J. G., Seidman, C. E., de Tombe, P. P., & Sadayappan, S. (2015). Haploinsufficiency of MYBPC3 exacerbates the development of hypertrophic cardiomyopathy in heterozygous mice. *Journal of Molecular and Cellular Cardiology*, 79, 234–243. <https://doi.org/10.1016/j.yjmcc.2014.11.018>
- Becker, R. C., Owens, A. P., & Sadayappan, S. (2020). Tissue-level inflammation and ventricular remodeling in hypertrophic cardiomyopathy. *Journal of Thrombosis and Thrombolysis*, 49(2), 177–183. <https://doi.org/10.1007/s11239-019-02026-1>
- Bertero, E., & Maack, C. (2018). *Metabolic remodelling in heart failure*. <https://doi.org/10.1038/s41569>
- Bhagwan, J. R., Mosqueira, D., Chairez-Cantu, K., Mannhardt, I., Bodbin, S. E., Bakar, M., Smith, J. G. W. W., & Denning, C. (2020). Isogenic models of hypertrophic cardiomyopathy unveil differential phenotypes and mechanism-driven therapeutics. *Journal of Molecular and Cellular Cardiology*, 145(March), 43–53. <https://doi.org/10.1016/j.yjmcc.2020.06.003>
- Birket, M. J., Ribeiro, M. C., Kosmidis, G., Ward, D., Leitoguinho, A. R., van de Pol, V., Dambrot, C., Devalla, H. D., Davis, R. P., Mastroberardino, P. G., Atsma, D. E., Passier, R., & Mummery, C. L. (2015). Contractile Defect Caused by Mutation in MYBPC3 Revealed under Conditions Optimized for Human PSC-Cardiomyocyte Function. *Cell Reports*, 13(4), 733–745. <https://doi.org/10.1016/j.celrep.2015.09.025>
- Boogerd, C. J., Lacraz, G. P., Vértessy, Á., Perini, I., de Ruiter, H., Brodehl, A., van der Kraak, P., Huibers, M., de Jonge, N., Junker, J. P., Vink, A., & van Rooij, E. (2019). Spatial Transcriptomics Unveil ZBTB11 as a Regulator of Cardiomyocyte Degeneration in Arrhythmogenic Cardiomyopathy. *Circulation Research*, 125(Suppl_1), 1–15. <https://doi.org/10.1161/>

res.125.suppl_1.510

- Bos, J. M., Hebl, V. B., Oberg, A. L., Sun, Z., Herman, D. S., Teekakirikul, P., Seidman, J. G., Seidman, C. E., dos Remedios, C. G., Maleszewski, J. J., Schaff, H. V., Dearani, J. A., Noseworthy, P. A., Friedman, P. A., Ommen, S. R., Brozovich, F. V., & Ackerman, M. J. (2020). Marked Up-Regulation of ACE2 in Hearts of Patients With Obstructive Hypertrophic Cardiomyopathy: Implications for SARS-CoV-2-Mediated COVID-19. *Mayo Clinic Proceedings*, 95(7), 1354–1368. <https://doi.org/10.1016/j.mayocp.2020.04.028>
- BRIGHT, & R. (1836). Cases and observations illustrative of renal disease accompanied with the secretion of albuminous urine. *Guy's Hospital Report*, 10, 338–340. <http://ci.nii.ac.jp/naid/10030343458/en/>
- Brodehl, A., Ebbinghaus, H., Deutsch, M. A., Gummert, J., Gärtner, A., Ratnavadivel, S., & Milting, H. (2019). Human induced pluripotent stem-cell-derived cardiomyocytes as models for genetic cardiomyopathies. *International Journal of Molecular Sciences*, 20(18). <https://doi.org/10.3390/ijms20184381>
- Canepa, M., Pozios, I., Vianello, P. F., Ameri, P., Brunelli, C., Ferrucci, L., & Abraham, T. P. (2016). Distinguishing ventricular septal bulge versus hypertrophic cardiomyopathy in the elderly. *Heart (British Cardiac Society)*, 102(14), 1087–1094. <https://doi.org/10.1136/heartjnl-2015-308764>
- Carreño, J. E., Apablaza, F., Ocaranza, M. P., & Jalil, J. E. (2006). Cardiac Hypertrophy: Molecular and Cellular Events. *Revista Española de Cardiología (English Edition)*, 59(5), 473–486. [https://doi.org/10.1016/s1885-5857\(06\)60796-2](https://doi.org/10.1016/s1885-5857(06)60796-2)
- Carrier, L., Knöll, R., Vignier, N., Keller, D. I., Bausero, P., Prudhon, B., Isnard, R., Ambroisine, M.-L., Fiszman, M., Ross, J., Schwartz, K., & Chien, K. R. (2004). Asymmetric septal hypertrophy in heterozygous cMyBP-C null mice. *Cardiovascular Research*, 63(2), 293–304. <https://doi.org/10.1016/j.cardiores.2004.04.009>
- Carrier, L., Mearini, G., Stathopoulou, K., & Cuello, F. (2015). Cardiac myosin-binding protein C (MYBPC3) in cardiac pathophysiology. *Gene*, 573(2), 188–197. <https://doi.org/10.1016/j.gene.2015.09.008>
- Chaffin, M., Papangelis, I., Simonson, B., Akkad, A. D., Hill, M. C., Arduini, A., Fleming, S. J., Melanson, M., Hayat, S., Kost-Alimova, M., Atwa, O., Ye, J., Bedi, K. C., Nahrendorf, M., Kaushik, V. K., Stegmann, C. M., Margulies, K. B., Tucker, N. R., & Ellinor, P. T. (2022). Single-nucleus profiling of human dilated and hypertrophic cardiomyopathy. *Nature*, 608(7921), 174–180. <https://doi.org/10.1038/s41586-022-04817-8>
- Cheng, Z., Qi, M., Zhang, C., & Mao, Y. (2021). Myocardial Fibrosis in the Pathogenesis, Diagnosis, and Treatment of Hypertrophic Cardiomyopathy. *Cardiovascular Innovations and Applications*, 5(4), 267–274. <https://doi.org/10.15212/cvia.2021.0008>
- Chou, C., & Chin, M. T. (2021). Pathogenic mechanisms of hypertrophic cardiomyopathy beyond sarcomere dysfunction. *International Journal of Molecular Sciences*, 22(16). <https://doi.org/10.3390/ijms22168933>
- Christiaans, I., Nannenbergh, E. A., Dooijes, D., Jongbloed, R. J. E., Michels, M., Postema, P. G., Majoor-Krakauer, D., van den Wijngaard, A., Mannens, M. M. A. M., van Tintelen, J. P., van Langen, I. M., & Wilde, A. A. M. (2010). Founder mutations in hypertrophic cardiomyopathy patients in the Netherlands. *Neth Heart J*, 18(5), 248–254. <https://doi.org/10.1007/BF03091771>
- Chung, M. W., Tsoutsman, T., & Semsarian, C. (2003). Hypertrophic cardiomyopathy: from gene defect to clinical disease. *Cell Res*, 13(1), 9–20. <https://doi.org/10.1038/sj.cr.7290146>
- Cijferoverzicht. (2020).
- Coats, C. J., & Hollman, A. (2008). Hypertrophic cardiomyopathy: Lessons from history. *Heart*, 94(10), 1258–1263. <https://doi.org/10.1136/hrt.2008.153452>
- Codden, C. J., Larson, A., Perera, G., & Chin, M. T. (2022). Single nucleus RNA-sequencing reveals altered intercellular communication and dendritic cell activation in nonobstruc-

- tive hypertrophic cardiomyopathy. *MedRxiv*, 1–48.
- Cong, L., Ran, A. F., Cox, D., Lin, S., Baretto, R., Habib, N., Hsu, P. D., Wu, X., Jiang, W., Marraffini, L. A., & Zhang, F. (2013). Multiplex Genome Engineering Using CRISPR/Cas Systems. *Science*, 339(February), 819–824. <https://doi.org/10.1126/science.1231143>
- D’Amato, R., Tomberli, B., Castelli, G., Spoladore, R., Girolami, F., Fornaro, A., Caldini, A., Torricelli, F., Camici, P., Gensini, G. F., Cecchi, F., & Olivotto, I. (2013). Prognostic value of N-terminal pro-brain natriuretic peptide in outpatients with hypertrophic cardiomyopathy. *American Journal of Cardiology*, 112(8), 1190–1196. <https://doi.org/10.1016/j.amjcard.2013.06.018>
- Dirkx, E., da Costa Martins, P. A., & De Windt, L. J. (2013). Regulation of fetal gene expression in heart failure. *Biochim Biophys Acta*, 1832(12), 2414–2424. <https://doi.org/10.1016/j.bbadis.2013.07.023>
- Dorn, G. W., & Force, T. (2005). Protein kinase cascades in the regulation of cardiac hypertrophy. *Journal of Clinical Investigation*, 115(3), 527–537. <https://doi.org/10.1172/JCI24178>
- Doudna, J. A., & Charpentier, E. (2014). The new frontier of genome engineering with CRISPR-Cas9. *Science*, 346(6213). <https://doi.org/10.1126/science.1258096>
- Enriquez, A. D., & Goldman, M. E. (n.d.). Management of Hypertrophic Cardiomyopathy. *Annals of Global Health*, 80(1), 35–45. <https://doi.org/10.1016/j.aogh.2013.12.004>
- Eschenhagen, T., & Carrier, L. (2019). Cardiomyopathy phenotypes in human-induced pluripotent stem cell-derived cardiomyocytes—a systematic review. In *Pflugers Archiv European Journal of Physiology* (Vol. 471, Issue 5). <https://doi.org/10.1007/s00424-018-2214-0>
- Eschenhagen, T., Mummery, C., & Knollmann, B. C. (2015). Modelling sarcomeric cardiomyopathies in the dish: From human heart samples to iPSC cardiomyocytes. *Cardiovascular Research*, 105(4), 424–438. <https://doi.org/10.1093/cvr/cvv017>
- Farbehi, N., Patrick, R., Dorison, A., Xaymardan, M., Janbandhu, V., Wystub-Lis, K., Ho, J. W. K., Nordon, R. E., & Harvey, R. P. (2019). Single-cell expression profiling reveals dynamic flux of cardiac stromal, vascular and immune cells in health and injury. *Elife*, 8, 1–39. <https://doi.org/10.7554/eLife.43882>
- Farrell, E., Armstrong, A. E., Grimes, A. C., Naya, F. J., De Lange, W. J., & Ralphe, J. C. (2018). Transcriptome analysis of cardiac hypertrophic growth in MYBPC3-null mice suggests early responders in hypertrophic remodeling. *Frontiers in Physiology*, 9(OCT), 1–14. <https://doi.org/10.3389/fphys.2018.01442>
- Finocchiaro, G., Magavern, E., Sinagra, G., Ashley, E., Papadakis, M., Tome-Esteban, M., Sharma, S., & Olivotto, I. (2017). Impact of demographic features, lifestyle, and comorbidities on the clinical expression of hypertrophic cardiomyopathy. *Journal of the American Heart Association*, 6(12), 1–11. <https://doi.org/10.1161/JAHA.117.007161>
- Frey, N., Katus, H. A., Olson, E. N., & Hill, J. A. (2004). Hypertrophy of the Heart: A New Therapeutic Target? *Circulation*, 109(13), 1580–1589. <https://doi.org/10.1161/01.CIR.0000120390.68287.BB>
- Frey, N., Luedde, M., & Katus, H. A. (2012). Mechanisms of disease: Hypertrophic cardiomyopathy. *Nature Reviews Cardiology*, 9(2), 91–100. <https://doi.org/10.1038/nrcardio.2011.159>
- Fumagalli, C., Maurizi, N., Day, S. M., Ashley, E. A., Michels, M., Colan, S. D., Jacoby, D., Marchionni, N., Vincent-tompkins, J., Ho, C. Y., Olivotto, I., & Investigators, S. (2020). Association of Obesity With Adverse Long-term Outcomes in Hypertrophic Cardiomyopathy. *JAMA Cardiol*, 5(1), 65–72. <https://doi.org/10.1001/jamacardio.2019.4268>
- Geisterfer-Lowrance, A. A., Christe, M., Conner, D. A., Ingwall, J. S., Schoen, F. J., Seidman, C. E., & Seidman, J. G. (1996). A mouse model of familial hypertrophic cardiomyopathy. *Science*, 272(5262), 731–734. <https://doi.org/10.1126/science.272.5262.731>
- Gladka, M. M., Molenaar, B., de Ruiter, H., Van Der Elst, S., Tsui, H., Versteeg, D., Lacraz, G. P. A. A., Huibers, M. M. H. H., Van Oudenaarden, A., & Van Rooij, E. (2018). Single-Cell

- Sequencing of the Healthy and Diseased Heart Reveals Cytoskeleton-Associated Protein 4 as a New Modulator of Fibroblasts Activation. *Circulation*, 138(2), 166–180. <https://doi.org/10.1161/CIRCULATIONAHA.117.030742>
- Harris, S. P., Bartley, C. R., Hacker, T. A., McDonald, K. S., Douglas, P. S., Greaser, M. L., Powers, P. A., & Moss, R. L. (2002). Hypertrophic cardiomyopathy in cardiac myosin binding protein-C knockout mice. *Circulation Research*, 90(5), 594–601. <https://doi.org/10.1161/01.RES.0000012222.70819.64>
- Ho, C. Y., Olivotto, I., Jacoby, D., Lester, S. J., Roe, M., Wang, A., Waldman, C. B., Zhang, D., Sehnert, A. J., & Heitner, S. B. (2020). Study Design and Rationale of EXPLORER-HCM: Evaluation of Mavacamten in Adults with Symptomatic Obstructive Hypertrophic Cardiomyopathy. *Circulation: Heart Failure*, June, 59–67. <https://doi.org/10.1161/CIRCHEARTFAILURE.120.006853>
- Hu, P., Liu, J., Zhao, J., Wilkins, B. J., Lupino, K., Wu, H., & Pei, L. (2018). Single-nucleus transcriptomic survey of cell diversity and functional maturation in postnatal mammalian hearts. *Genes Dev*, 32(19–20), 1344–1357. <https://doi.org/10.1101/gad.316802.118>
- Jansen, M., Algül, S., Bosman, L. P., Michels, M., van der Velden, J., de Boer, R. A., van Tintel, J. P., Asselbergs, F. W., & Baas, A. F. (2022). Blood-based biomarkers for the prediction of hypertrophic cardiomyopathy prognosis: a systematic review and meta-analysis. *ESC Heart Failure*, 9(5), 3418–3434. <https://doi.org/10.1002/ehf2.14073>
- Jinek, M., East, A., Cheng, A., Lin, S., Ma, E., States, U., Division, P. B., & Berkeley, L. (2013). RNA-programmed genome editing in human cells. *ELife*, 1–9. <https://doi.org/10.7554/eLife.00471>
- Junker, J. P., Noël, E. S., Guryev, V., Peterson, K. A., Shah, G., Huisken, J., McMahon, A. P., Berezikov, E., Bakkers, J., & Van Oudenaarden, A. (2014). Genome-wide RNA Tomography in the Zebrafish Embryo. *Cell*, 159(3), 662–675. <https://doi.org/10.1016/j.cell.2014.09.038>
- Kirschner, S. E., Becker, E., Antognozzi, M., Kubis, H. P., Francino, A., Navarro-López, F., Bit-Avragim, N., Perrot, A., Mirrakhimov, M. M., Osterziel, K. J., McKenna, W. J., Brenner, B., & Kraft, T. (2005). Hypertrophic cardiomyopathy-related β -myosin mutations cause highly variable calcium sensitivity with functional imbalances among individual muscle cells. *American Journal of Physiology - Heart and Circulatory Physiology*, 288(3 57-3), 1242–1251. <https://doi.org/10.1152/ajpheart.00686.2004>
- Koenig, A. L., Shchukina, I., Amrute, J., Andhey, P. S., Zaitsev, K., Lai, L., Bajpai, G., Brede-meyer, A., Smith, G., Jones, C., Terrebonne, E., Rentschler, S. L., Artyomov, M. N., & Lavine, K. J. (2022). Single-cell transcriptomics reveals cell-type-specific diversification in human heart failure. *Nature Cardiovascular Research*, 1(3), 263–280. <https://doi.org/10.1038/s44161-022-00028-6>
- Kraft, T., & Montag, J. (2019). Altered force generation and cell-to-cell contractile imbalance in hypertrophic cardiomyopathy. *Pflügers Archiv - European Journal of Physiology*, 471(5), 719–733. <https://doi.org/10.1007/s00424-019-02260-9>
- Krenz, M., & Robbins, J. (2004). Impact of beta-myosin heavy chain expression on cardiac function during stress. *Journal of the American College of Cardiology*, 44(12), 2390–2397. <https://doi.org/10.1016/j.jacc.2004.09.044>
- Kretschmar, K., Post, Y., Bannier-Helaouet, M., Mattiotti, A., Drost, J., Basak, O., Li, V. S. W., van den Born, M., Gunst, Q. D., Versteeg, D., Kooijman, L., van der Elst, S., van Es, J. H., van Rooij, E., van den Hoff, M. J. B., & Clevers, H. (2018). Profiling proliferative cells and their progeny in damaged murine hearts. *Proc Natl Acad Sci U S A*, 115(52), E12245–E12254. <https://doi.org/10.1073/pnas.1805829115>
- Kruse, F., Junker, J. P., van Oudenaarden, A., & Bakkers, J. (2016). Tomo-seq: A method to obtain genome-wide expression data with spatial resolution. In *Methods in Cell Biology* (Vol. 135). Elsevier Ltd. <https://doi.org/10.1016/bs.mcb.2016.01.006>

- Lacruz, G. P. A., Junker, J. P., Gladka, M. M., Molenaar, B., Scholman, K. T., Vigil-Garcia, M., Versteeg, D., De Ruiter, H., Vermunt, M. W., Creighton, M. P., Huibers, M. M. H., De Jonge, N., Van Oudenaarden, A., & Van Rooij, E. (2017). Tomo-Seq Identifies SOX9 as a Key Regulator of Cardiac Fibrosis during Ischemic Injury. *Circulation*, *136*(15), 1396–1409. <https://doi.org/10.1161/CIRCULATIONAHA.117.027832>
- Lamke, G. T., Allen, R. D., Edwards, W. D., Tazelaar, H. D., & Danielson, G. K. (2003). Surgical pathology of subaortic septal myectomy associated with hypertrophic cardiomyopathy: A study of 204 cases (1996-2000). *Cardiovascular Pathology*, *12*(3), 149–158. [https://doi.org/10.1016/S1054-8807\(03\)00036-X](https://doi.org/10.1016/S1054-8807(03)00036-X)
- Larson, A., & Chin, M. T. (2021). A method for cryopreservation and single nucleus RNA-sequencing of normal adult human interventricular septum heart tissue reveals cellular diversity and function. *BMC Medical Genomics*, *14*(1), 1–8. <https://doi.org/10.1186/s12920-021-01011-z>
- Larson, A., Codden, C. J., Huggins, G. S., Rastegar, H., Chen, F. Y., Maron, B. J., Rowin, E. J., Maron, M. S., & Chin, M. T. (2022). Altered intercellular communication and extracellular matrix signaling as a potential disease mechanism in human hypertrophic cardiomyopathy. *Scientific Reports*, *12*(1). <https://doi.org/10.1038/s41598-022-08561-x>
- Lim, D. S., Roberts, R., & Marian, A. J. (2001). Expression profiling of cardiac genes in human hypertrophic cardiomyopathy: insight into the pathogenesis of phenotypes. *Journal of the American College of Cardiology*, *38*(4), 1175–1180. [https://doi.org/10.1016/s0735-1097\(01\)01509-1](https://doi.org/10.1016/s0735-1097(01)01509-1)
- Liu, J., Zhao, S., Yu, S., Wu, G., Wang, D., & Liu, M. B. L. (2022). *Patterns of Replacement Fibrosis in Hypertrophic*.
- Liu, X., Yin, K., Chen, L., Chen, W., Li, W., Zhang, T., Sun, Y., Yuan, M., Wang, H., Song, Y., Wang, S., Hu, S., & Zhou, Z. (2023). Lineage-specific regulatory changes in hypertrophic cardiomyopathy unraveled by single-nucleus RNA-seq and spatial transcriptomics. *Cell Discovery*, *9*(1). <https://doi.org/10.1038/s41421-022-00490-3>
- Mali, P., Yang, L., Esvelt, K. M., Aach, J., Guell, M., DiCarlo, J. E., Norville, J. E., & Church, G. M. (2013). RNA-Guided Human Genome Engineering via Cas9. *Science*, *339*(823), 823–826. [http://www.sciencemag.org.cyber.usask.ca/content/339/6121/823.full.pdf%5Cn-file:///Articles/2013/Mali/Science 2013 Mali.pdf](http://www.sciencemag.org.cyber.usask.ca/content/339/6121/823.full.pdf%5Cn-file:///Articles/2013/Mali/Science%2013%20Mali.pdf)
- Marian, A. J., & Braunwald, E. (2017). Hypertrophic Cardiomyopathy: Genetics, Pathogenesis, Clinical Manifestations, Diagnosis, and Therapy. *Circ Res*, *121*(7), 749–770. <https://doi.org/10.1161/CIRCRESAHA.117.311059>
- Maron, B. A., Wang, R. S., Shevtsov, S., Drakos, S. G., Arons, E., Wever-Pinzon, O., Huggins, G. S., Samokhin, A. O., Oldham, W. M., Aguib, Y., Yacoub, M. H., Rowin, E. J., Maron, B. J., Maron, M. S., & Loscalzo, J. (2021). Individualized interactomes for network-based precision medicine in hypertrophic cardiomyopathy with implications for other clinical pathophenotypes. *Nature Communications*, *12*(1), 1–11. <https://doi.org/10.1038/s41467-021-21146-y>
- Maron, B. J. (2018). Clinical Course and Management of Hypertrophic Cardiomyopathy. *New England Journal of Medicine*, *379*(7), 655–668. <https://doi.org/10.1056/nejmra1710575>
- Maron, B. J., & Maron, M. S. (2013). Hypertrophic cardiomyopathy. *Lancet*, *381*(9862), 242–255. [https://doi.org/10.1016/S0140-6736\(12\)60397-3](https://doi.org/10.1016/S0140-6736(12)60397-3)
- Maron, B. J., & Maron, M. S. (2014). The 25-year genetic era in hypertrophic cardiomyopathy: Revisited. *Circulation: Cardiovascular Genetics*, *7*(4), 401–404. <https://doi.org/10.1161/CIRCGENETICS.114.000741>
- Maron, B. J., Niiimura, H., Casey, S. A., Soper, M. K., Wright, G. B., Seidman, J. G., & Seidman, C. E. (2001). Development of left ventricular hypertrophy in adults with hypertrophic cardiomyopathy caused by cardiac myosin-binding protein C gene mutations. *Journal of the American College of Cardiology*, *38*(2), 315–321. <https://doi.org/10.1016/S0735->

1097(01)01386-9

- Maron, B. J., Ommen, S. R., Semsarian, C., Spirito, P., Olivetto, I., & Maron, M. S. (2014). Hypertrophic cardiomyopathy: Present and future, with translation into contemporary cardiovascular medicine. *Journal of the American College of Cardiology*, *64*(1), 83–99. <https://doi.org/10.1016/j.jacc.2014.05.003>
- Maron, B. J., Seidman, C. E., Ackerman, M. J., Towbin, J. A., Maron, M. S., Ommen, S. R., Nishimura, R. A., & Gersh, B. J. (2009). Response to Elliott and McKenna. *Circulation: Cardiovascular Genetics*, *2*(1), 89. <https://doi.org/10.1161/CIRCGENETICS.108.835645>
- Marston, S. B. (2011). How do mutations in contractile proteins cause the primary familial cardiomyopathies? *Journal of Cardiovascular Translational Research*, *4*(3), 245–255. <https://doi.org/10.1007/s12265-011-9266-2>
- Marston, S., Copeland, O., Gehmlich, K., Schlossarek, S., & Carrier, L. (2012). How do MYB-PC3 mutations cause hypertrophic cardiomyopathy? *Journal of Muscle Research and Cell Motility*, *33*(1), 75–80. <https://doi.org/10.1007/s10974-011-9268-3>
- McNamara, J. W., Singh, R. R., & Sadayappan, S. (2019). Cardiac myosin binding protein-C phosphorylation regulates the super-relaxed state of myosin. *Proceedings of the National Academy of Sciences of the United States of America*, *116*(24), 11731–11736. <https://doi.org/10.1073/pnas.1821660116>
- Michels, M., Soliman, O. I. I., Phefferkorn, J., Hoedemaekers, Y. M., Kofflard, M. J., Dooijes, D., Majoor-Krakauer, D., & Ten Cate, F. J. (2009). Disease penetrance and risk stratification for sudden cardiac death in asymptomatic hypertrophic cardiomyopathy mutation carriers. *European Heart Journal*, *30*(21), 2593–2598. <https://doi.org/10.1093/eurheartj/ehp306>
- Molenaar, B., Timmer, L. T., Droog, M., Perini, I., Versteeg, D., Kooijman, L., Monshouwer-Kloots, J., de Ruiter, H., Gladka, M. M., & van Rooij, E. (2021). Single-cell transcriptomics following ischemic injury identifies a role for B2M in cardiac repair. *Communications Biology*, *4*(1), 1–15. <https://doi.org/10.1038/s42003-020-01636-3>
- Moolman, J. A., Reith, S., Kerstin, U. I., Bailey, S., Gautel, M., Jeschke, B., Fischer, C., Ochs, J., McKenna, W. J., Klues, H., & Vosberg, H. P. (2000). A newly created splice donor site in exon 25 of the MyBP-C gene is responsible for inherited hypertrophic cardiomyopathy with incomplete disease penetrance. *Circulation*, *101*(12), 1396–1402. <https://doi.org/10.1161/01.CIR.101.12.1396>
- Nomura, S., Satoh, M., Fujita, T., Higo, T., Sumida, T., Ko, T., Yamaguchi, T., Tobita, T., Naito, A. T., Ito, M., Fujita, K., Harada, M., Toko, H., Kobayashi, Y., Ito, K., Takimoto, E., Akazawa, H., Morita, H., Aburatani, H., & Komuro, I. (2018). Cardiomyocyte gene programs encoding morphological and functional signatures in cardiac hypertrophy and failure. *Nat Commun*, *9*(1), 4435. <https://doi.org/10.1038/s41467-018-06639-7>
- Ojala, M., Prajapati, C., Pölönen, R. P., Rajala, K., Pekkanen-Mattila, M., Rasku, J., Larsson, K., & Aalto-Setälä, K. (2016). Mutation-specific phenotypes in hiPSC-derived cardiomyocytes carrying either myosin-binding protein C or α -tropomyosin mutation for hypertrophic cardiomyopathy. *Stem Cells International*, *2016*. <https://doi.org/10.1155/2016/1684792>
- Olivetto, I., Maron, B. J., Monteregegi, A., Mazzuoli, F., Dolara, A., & Cecchi, F. (1999). Prognostic value of systemic blood pressure response during exercise in a community-based patient population with hypertrophic cardiomyopathy. *Journal of the American College of Cardiology*, *33*(7), 2044–2051. [https://doi.org/10.1016/S0735-1097\(99\)00094-7](https://doi.org/10.1016/S0735-1097(99)00094-7)
- Omole, A. E., & Fakoya, A. O. J. (2018). Ten years of progress and promise of induced pluripotent stem cells: Historical origins, characteristics, mechanisms, limitations, and potential applications. *PeerJ*, *2018*(MAY), 1–47. <https://doi.org/10.7717/peerj.4370>
- Pei, J., Schuldt, M., Nagyova, E., Gu, Z., el Bouhaddani, S., Yiangou, L., Jansen, M., Calis, J. J. A., Dorsch, L. M., Blok, C. S., van den Dungen, N. A. M., Lansu, N., Boukens, B. J., Efimov, I. R., Michels, M., Verhaar, M. C., de Weger, R., Vink, A., van Steenbeek, F. G., ...

- Harakalova, M. (2021). Multi-omics integration identifies key upstream regulators of pathomechanisms in hypertrophic cardiomyopathy due to truncating MYBPC3 mutations. *Clinical Epigenetics*, 13(1), 1–20. <https://doi.org/10.1186/s13148-021-01043-3>
- Pisano, A., Le, L., Carletti, R., Cerbelli, B., Pignataro, M. G., Pernazza, A., Ferre, F., Lombardi, M., Lazzeroni, D., Olivetto, I., Rimoldi, O. E., Foglieni, C., Camici, P. G., & Amati, G. (2022). *seq profiling reveals different pathways between remodeled vessels and myocardium in hypertrophic cardiomyopathy*. April, 1–11. <https://doi.org/10.1111/micc.12790>
- Prondzynski, M., Krämer, E., Laufer, S. D., Shibamiya, A., Pless, O., Flenner, F., Müller, O. J., Münch, J., Redwood, C., Hansen, A., Patten, M., Eschenhagen, T., Mearini, G., & Carrier, L. (2017). Evaluation of MYBPC3 trans-Splicing and Gene Replacement as Therapeutic Options in Human iPSC-Derived Cardiomyocytes. *Molecular Therapy - Nucleic Acids*, 7(June), 475–486. <https://doi.org/10.1016/j.omtn.2017.05.008>
- Ren, C. W., Liu, J. J., Li, J. W. H., Li, J. W. H., Dai, J., & Lai, Y. Q. (2016). RNA-seq profiling of mRNA associated with hypertrophic cardiomyopathy. *Molecular Medicine Reports*, 14(6), 5573–5586. <https://doi.org/10.3892/mmr.2016.5931>
- Ren, Z., Yu, P., Li, D., Li, Z., Liao, Y., Wang, Y., Zhou, B., & Wang, L. (2020). Single-Cell Reconstruction of Progression Trajectory Reveals Intervention Principles in Pathological Cardiac Hypertrophy. *Circulation*, 141(21), 1704–1719. <https://doi.org/10.1161/CIRCULATIONAHA.119.043053>
- Samak, M., Fatullayev, J., Sabashnikov, A., Zeroui, M., Schmack, B., Farag, M., Popov, A. F., Dohmen, P. M., Choi, Y. H., Wahlers, T., & Weymann, A. (2016). Cardiac Hypertrophy: An Introduction to Molecular and Cellular Basis. *Medical Science Monitor Basic Research*, 22, 75–79. <https://doi.org/10.12659/MSMBR.900437>
- Schuld, M., Pei, J., Harakalova, M., Dorsch, L. M., Schlossarek, S., Mokry, M., Knol, J. C., Pham, T. V., Schelfhorst, T., Piersma, S. R., Dos Remedios, C., Dalinghaus, M., Michels, M., Asselbergs, F. W., Moutin, M. J., Carrier, L., Jimenez, C. R., van der Velden, J., & Kuster, D. W. D. (2021). Proteomic and Functional Studies Reveal Detyrosinated Tubulin as Treatment Target in Sarcomere Mutation-Induced Hypertrophic Cardiomyopathy. *Circ Heart Fail*, 14(1), e007022. <https://doi.org/10.1161/CIRCHEARTFAILURE.120.007022>
- Semsarian, C., Ingles, J., Maron, M. S., & Maron, B. J. (2015). New Perspectives on the Prevalence of Hypertrophic Cardiomyopathy. *Journal of the American College of Cardiology*, 65(12), 1249–1254. <https://doi.org/10.1016/j.jacc.2015.01.019>
- Semsarian, C., & Semsarian, C. R. (2020). Variable Penetrance in Hypertrophic Cardiomyopathy: In Search of the Holy Grail. *Journal of the American College of Cardiology*, 76(5), 560–562. <https://doi.org/10.1016/j.jacc.2020.06.023>
- Sepehrkhoy, S., Gho, J. M. I. H., van Es, R., Harakalova, M., de Jonge, N., Dooijes, D., van der Smagt, J. J., Buijsrogge, M. P., Hauer, R. N. W., Goldschmeding, R., de Weger, R. A., Asselbergs, F. W., & Vink, A. (2017). Distinct fibrosis pattern in desmosomal and phospholamban mutation carriers in hereditary cardiomyopathies. *Heart Rhythm*, 14(7), 1024–1032. <https://doi.org/10.1016/j.hrthm.2017.03.034>
- Sereti, K. I., Nguyen, N. B., Kamran, P., Zhao, P., Ranjbarvaziri, S., Park, S., Sabri, S., Engel, J. L., Sung, K., Kulkarni, R. P., Ding, Y., Hsiai, T. K., Plath, K., Ernst, J., Sahoo, D., Mikkola, H. K. A., Iruela-Arispe, M. L., & Ardehali, R. (2018). Analysis of cardiomyocyte clonal expansion during mouse heart development and injury. *Nat Commun*, 9(1), 754. <https://doi.org/10.1038/s41467-018-02891-z>
- Skelly, D. A., Squiers, G. T., McLellan, M. A., Bolisetty, M. T., Robson, P., Rosenthal, N. A., & Pinto, A. R. (2018). Single-Cell Transcriptional Profiling Reveals Cellular Diversity and Intercommunication in the Mouse Heart. *Cell Reports*, 22(3), 600–610. <https://doi.org/10.1016/j.celrep.2017.12.072>
- Takahashi, K., & Yamanaka, S. (2006). *Induction of Pluripotent Stem Cells from Mouse Embryonic and Adult Fibroblast Cultures by Defined Factors*. 2, 663–676. <https://doi.org/10.1016/j.celrep.2017.12.072>

org/10.1016/j.cell.2006.07.024

Teare, D. (1957). Asymmetrical hypertrophy of the heart. *Medicine, Science, and the Law*, 20(1), 1–8.

Tuohy, C. V., Kaul, S., Song, H. K., Nazer, B., & Heitner, S. B. (2020). Hypertrophic cardiomyopathy: the future of treatment. *Eur J Heart Fail*, 22(2), 228–240. <https://doi.org/10.1002/ejhf.1715>

Van Dijk, S. J., Dooijes, D., Remedios, C. Dos, Michels, M., Lamers, J. M. J., Winegrad, S., Schlossarek, S., Carrier, L., Cate, F. J. T., Stienen, G. J. M., & Van Velden, J. Der. (2009). Cardiac myosin-binding protein C mutations and hypertrophic ardiomyopathy haploinsufficiency, deranged phosphorylation, and cardiomyocyte dysfunction. *Circulation*, 119(11), 1473–1483. <https://doi.org/10.1161/CIRCULATIONAHA.108.838672>

Weissler Snir, A., Connelly, K. A., Goodman, J. M., Dorian, D., & Dorian, P. (2021). Exercise in hypertrophic cardiomyopathy: restrict or rethink. *Am J Physiol Heart Circ Physiol*, 320(5), H2101–H2111. <https://doi.org/10.1152/ajpheart.00850.2020>

Wells, S., Rowin, E. J., Bhatt, V., Maron, M. S., & Maron, B. J. (2018). Association Between Race and Clinical Profile of Patients Referred for Hypertrophic Cardiomyopathy. *Circulation*, 137, 1973–1975.

Zamorano, J. L., Anastasakis, A., Borger, M. A., Borggrefe, M., Cecchi, F., Charron, P., Hagege, A. A., Lafont, A., Limongelli, G., Mahrholdt, H., McKenna, W. J., Mogensen, J., Nihoyannopoulos, P., Nistri, S., Piepe, P. G., Pieske, B., Rapezzi, C., Rutten, F. H., Tillmanns, C., ... Watkins, H. (2014). 2014 ESC Guidelines on diagnosis and management of hypertrophic cardiomyopathy: the Task Force for the Diagnosis and Management of Hypertrophic Cardiomyopathy of the European Society of Cardiology (ESC). *Eur Heart J*, 35(39), 2733–2779. <https://doi.org/10.1093/eurheartj/ehu284>

Zhao, W., Wu, T., Zhan, J., & Dong, Z. (2022). Identification of the Immune Status of Hypertrophic Cardiomyopathy by Integrated Analysis of Bulk- and Single-Cell RNA Sequencing Data. *Computational and Mathematical Methods in Medicine*, 2022. <https://doi.org/10.1155/2022/7153491>



Summary

Hypertrophic cardiomyopathy (HCM) is a genetic heart disease that is characterized by unexplained segmental hypertrophy, that is usually most pronounced in the septum. While sarcomeric gene mutations are often the genetic basis for HCM, the mechanistic origin for the heterogeneous remodeling remains largely unknown. A better understanding of gene networks driving the cardiomyocyte (CM) hypertrophy is required to improve therapeutic strategies. Patients suffering from HCM often receive a septal myectomy surgery to relieve outflow tract obstruction due to hypertrophy. Using single-cell RNA sequencing (scRNA-seq) on septal myectomy samples from patients with HCM we identify functional links between genes, transcription factors, and cell size relevant for HCM. The data show the utility of using scRNA-seq on the human hypertrophic heart, highlights CM heterogeneity and provide a wealth of insights into molecular events involved in HCM, that can eventually contribute to the development of enhanced therapies.

Introduction

Hypertrophic cardiomyopathy (HCM) is a genetic cardiac disorder with an incidence of 1 in 200-500 individuals (Maron et al., 2014; Semsarian et al., 2015). The phenotype can vary from essentially asymptomatic to end-stage heart failure or cause life-threatening arrhythmias (Maron & Maron, 2013). Typically, patients carry a pathologic DNA variant in genes encoding sarcomere proteins. β -myosin heavy chain (MYH7), and myosin binding protein C (MYBPC3) are the genes most commonly involved, however the causal genes in approximately 40% of patients with HCM remain to be identified (Marian, 2010). Clinically, HCM is characterized by unexplained segmental hypertrophy that is usually most pronounced in the basal interventricular septum (Marian & Braunwald, 2017). Myocyte disarray, a pathological hallmark of HCM, involves 5–40% of the myocardium, and is usually mainly present in areas of more severe hypertrophy. Other key histological features include interstitial fibrosis and vascular abnormalities (Marian & Braunwald, 2017).

To date, the molecular mechanisms that underlie the remodeling processes in HCM remain largely unclear. While it has been suggested that myocyte disarray and hypertrophy are a direct result from changes in sarcomere function induced by the HCM-related mutations (Di Domenico et al., 2012), recent work suggests that the HCM phenotype might also be triggered by a functional imbalance among individual cardiomyocytes (CMs). Unequal force generation between adjacent CMs can initiate CM and myofibrillar disarray and trigger stretch-induced signaling leading to development of interstitial fibrosis and hypertrophy (Montag et al., 2018; Parbhudayal et al., 2018).

Single-cell RNA sequencing (scRNA-seq) provides a detailed view on gene expression differences between cell types or transcriptome heterogeneity across cells of the same type (Grun et al., 2014; A. A. Kolodziejczyk et al., 2015). Recently, we developed an approach that allows us to obtain single cell transcriptomic data from all main cardiac cell types of the adult murine heart under both healthy and diseased conditions (Gladka et al., 2018). While several studies by now have used scRNA-seq to study adult cardiac biology in an in-depth manner (Farbehi et al., 2019; Gladka et al., 2018; Hu et al., 2018; Kretzschmar et al., 2018; Larson & Chin, 2021; Nomura et al., 2018; Ren et al., 2020; Sereti et al., 2018; Skelly et al., 2018), even on adult human CMs (Y. Cui et al., 2019; Nomura et al., 2018; L. Wang et al., 2020), so far this has not

been done on cells from human HCM myectomy samples.

Here we used scRNA-seq to study cellular transcriptional differences between healthy and hypertrophic CMs and employed this expressional heterogeneity to link gene expression profiles to cellular characteristics related to HCM. In depth analysis of the scRNA-seq data from HCM CMs indicated the presence of subpopulations of CMs to which each patient contributed. Additionally, we were able to identify HCM-related gene correlations. Using these data, we could identify groups of genes that are co-expressed (regulons (Aibar et al., 2017)) and we were able to link these to transcription factors (TFs) that are potentially responsible for their activation. Additionally, index-sorting data enabled us to correlate gene expression profiles to CM hypertrophy and confirmed myosin light chain (*MYL2/MLC-2*) expression in larger CMs. Together these data indicate CM heterogeneity in the human heart and show that scRNA-seq provides insights into cellular and molecular mechanisms that are potentially relevant for HCM.

Results

Single-cell gene expression analysis of septal myectomy samples from patients with HCM

Patients with HCM show a heterogeneous remodeling response which is characterized by localized CM hypertrophy, disarray and fibrosis (Marian & Braunwald, 2017). To explore the molecular mechanisms underlying the cellular heterogeneity observed in HCM, we aimed to examine differential gene expression between individual CMs. To this end, we collected cardiac tissue from patients with HCM who underwent a septal myectomy for outflow tract obstruction and processed the tissue for scRNA-seq (**Figure 1A**). Histological analysis of the myectomy samples confirmed key hallmarks of HCM (**Figure 1B**). To achieve this, we used our previously optimized digestion and sorting strategy (Gladka et al., 2018). We enzymatically dispersed cardiac tissue into a single cell suspension and sorted cells into 384-well plates, where we gated for larger, single cells to enrich for CMs (**Supplemental Figures 1A and 1B**). This gating strategy resulted in intact and nucleated cells, as resorting of this population indicated 82% of the cells to be DRAQ5 positive and DAPI negative (**Supplemental Figures 1C and 1D**). DRAQ5 is able to enter live cells and stain nuclear DNA (P. J. Smith et al., 2004), whereas DAPI selectively stains nuclei of compromised cells. Events that are DRAQ5+ and DAPI- must therefore contain uncompromised cells

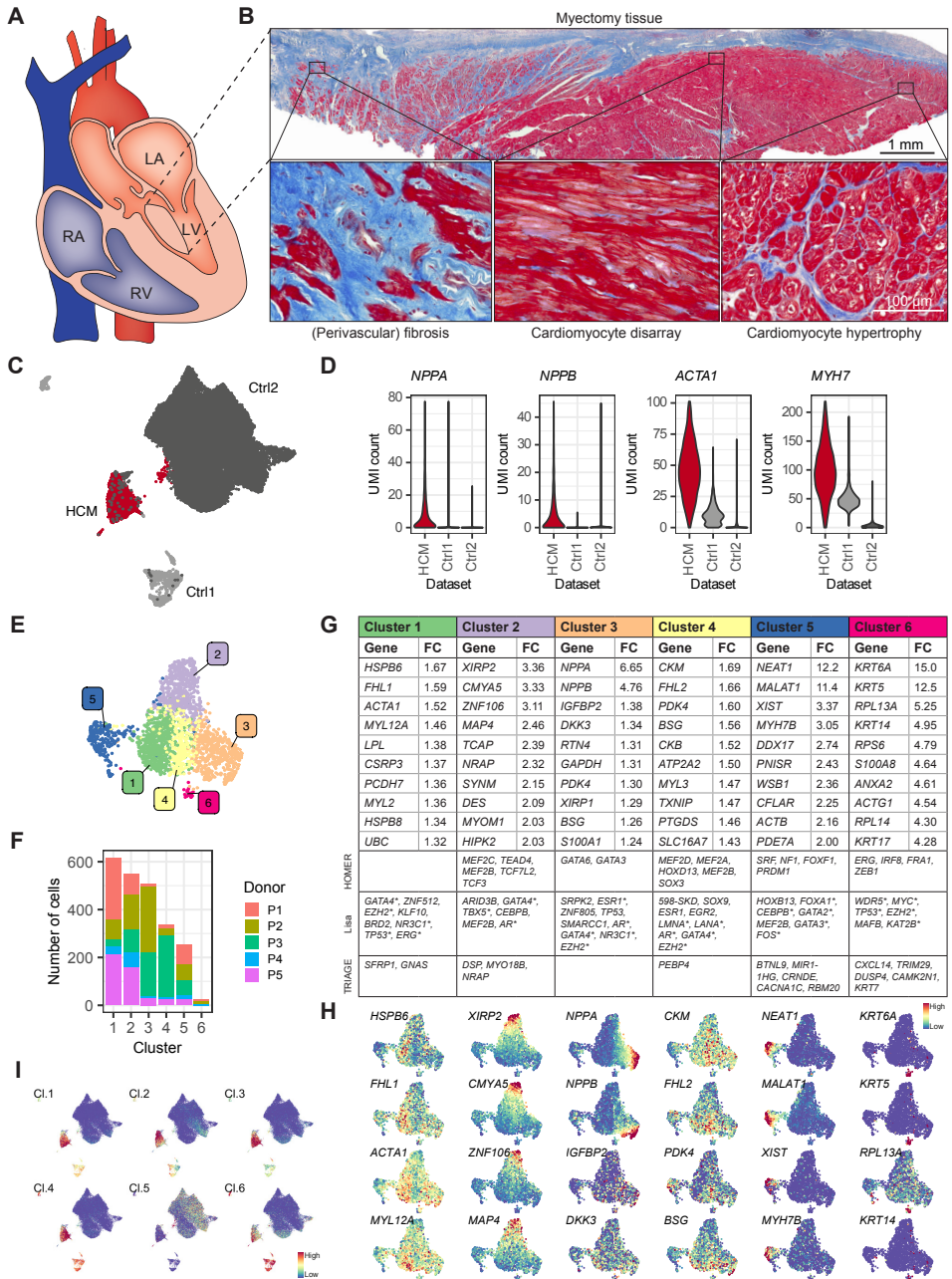


Figure. 1. Single cell analysis of septal myectomy samples from patients with HCM reveal different subpopulations of CMs. (A) Schematic representation of the human heart highlighting the septal myectomy sample used for this study. (B) Masson's trichrome staining of myectomy tissue from an HCM patient showing fibrosis, myocardial disarray and CM hypertrophy. (C) UMAP showing transcriptome similarities between HCM cells acquired in

2

this study (red dots), and cells from healthy donors from previously published studies (Ctrl1 and Ctrl2, respectively light gray and dark grey dots). **(D)** Violin plots of the normalized UMI counts for NPPA, NPPB, ACTA1 and MYH7 indicating an induction of stress markers in HCM CMs. **(E)** UMAP showing transcriptome similarities between HCM cells only. The colors represent the clusters identified by Seurat. **(F)** Bar graph showing the contribution of each of the five patients (P1-P5) to each of the Seurat clusters. **(G)** Top 10 most enriched genes in each cluster and their fold-change (FC) enrichment in the respective cluster. The bottom three rows show TFs potentially driving gene expression for each cluster (HOMER and Lisa) and cluster-enriched genes ($p < 0.01$) with the largest regulatory potential (TRIAGE). Enrichment was calculated for cells in the cluster over all cells outside the cluster. **(H)** UMAPs depicting the expression of the top 4 enriched genes for each cluster. Expression in UMAPs is shown as normalized transcript counts on a color-coded linear scale. **(I)** Composite expression of HCM-cluster enriched genes (see 1E-G), projected on UMAPs with pooled cells from HCM, Ctrl1 and Ctrl2 (see 1C). Composite expression is determined by cell-averaged Z-scores of enriched gene sets ($FC > 1.1$, $p < 0.05$) per cluster (Cl.1-5). RA, right atrium; RV, right ventricle; LA, left atrium; LV, left ventricle; UMAP, Uniform Manifold Approximation and Projection. See also Figures S1 and S2, and Tables S1 and S2.

with a nucleus. With each sort, we additionally collected cells for microscopy and RNA-quality control. Imaging the cells after sorting visually indicated that we were sorting intact cells (**Supplemental Figure 1D**). RNA quality from the dispersed and sorted cells was retained, as indicated by RNA Integrity Number (RIN) (Schroeder et al., 2006) (**Supplemental Figure 1E**). Together these data showed that our protocol allowed for the isolation of good quality RNA from individual, intact cells collected from human septal myectomy samples. To obtain single-cell transcriptomes of individual cardiac cells from myectomy samples we used the SORT-Seq protocol as described previously (Gladka et al., 2018; Grun et al., 2015).

Transcript abundance per gene was quantified by using a custom mapping pipeline using STAR and featureCounts (see methods for additional details). $33 \pm 12\%$ of transcripts mapped to the mitochondrial genome (**Supplemental Figure 1F**) which is consistent with results from previous studies (S. Kannan et al., 2019). Reads mapping to the mitochondrial genome were excluded from data, since they interfere with the downstream analysis. After filtering cells for a minimum of 1000 transcripts mapping to the nuclear genome, a total of 2292 cells from five different septal myectomy samples with an average number of 2201 unique non-mitochondrial reads per cell were included for downstream in-silico analysis (**Supplemental Figure 1G**). A UMAP map for MYH7, a well-known CM marker, confirmed the far majority of the remaining cells to be CMs (**Supplemental Figure 1H**). Together these data show we were able to collect reliable scRNA-seq data from HCM CMs to start exploring potential disease underlying mechanisms.

scRNA-seq identified HCM-related gene expression changes

To identify HCM-related gene expression changes we next combined our scRNA-seq data with gene expression data from healthy adult human CMs. To do so we included scRNA-seq data from healthy left ventricular (LV) CMs from Wang et al. (Ctrl1, n = 1400) (L. Wang et al., 2020) and from septal CMs from Litviňuková et al. (Ctrl2, n = 27604) (Litviňuková et al., 2020) (Table S1, S2). To prevent batch-effects stemming from bio-informatic analyses as much as possible, we downloaded raw FASTQ files and re-mapped Ctrl1 using our own pipeline. For Ctrl2, we downloaded available mapped data, as the Ctrl2 mapping pipeline closely matched our pipeline (see Methods for additional details).

Next, the Seurat algorithm was applied for identification and clustering of cells (Supplemental Figures 2A-C) (Stuart et al., 2018). Cells appeared to separate from each other based on origin, with the majority of HCM cells clustering away from cells coming from control hearts (Figure 1C). Clustering analysis identified 5 different CM clusters (Supplemental Figure 2A), with cluster 4 mainly representing CMs from HCM hearts (Supplemental Figure 2B). This HCM cluster was enriched for well-known cardiac stress marker genes, such as *MYH7*, *NPPA* and *XIRP2* (Supplemental Figure 2C and Supplemental Data 1), which is in line with these cells being diseased compared to the control cells. Also, when plotting the individual expression levels of these cardiac disease related genes, we could show a clear induction in the HCM CMs compared to both sets of control cells (Figure 1D). Functionally, the HCM cluster and cluster 5 – which mainly contains Ctrl1 cells – show similar enrichment of GO terms related to energy metabolism, which might be explained by the fact that HCM and Ctrl1 processed whole cells for sequencing, as opposed to Ctrl2, which mainly consists of sequenced CM nuclei (Supplemental Figure 2D). Nevertheless, these data indicate the HCM CMs to express disease related gene expression profiles that might provide insights into mechanisms relevant for cardiac remodeling during HCM.

scRNA-seq reveals different subpopulations of HCM CMs

To start exploring the gene expression profiles underlying the cellular heterogeneity in HCM, we next focused in on the CMs coming from HCM hearts. Clustering analysis on the 2292 included cells revealed 6 clusters to which every patient contributed (Figures 1E-G, S2E and Supplemental Data 2). Even though we were unable to detect a clear separation between clusters 1 to 4, we could confirm gene enrichment

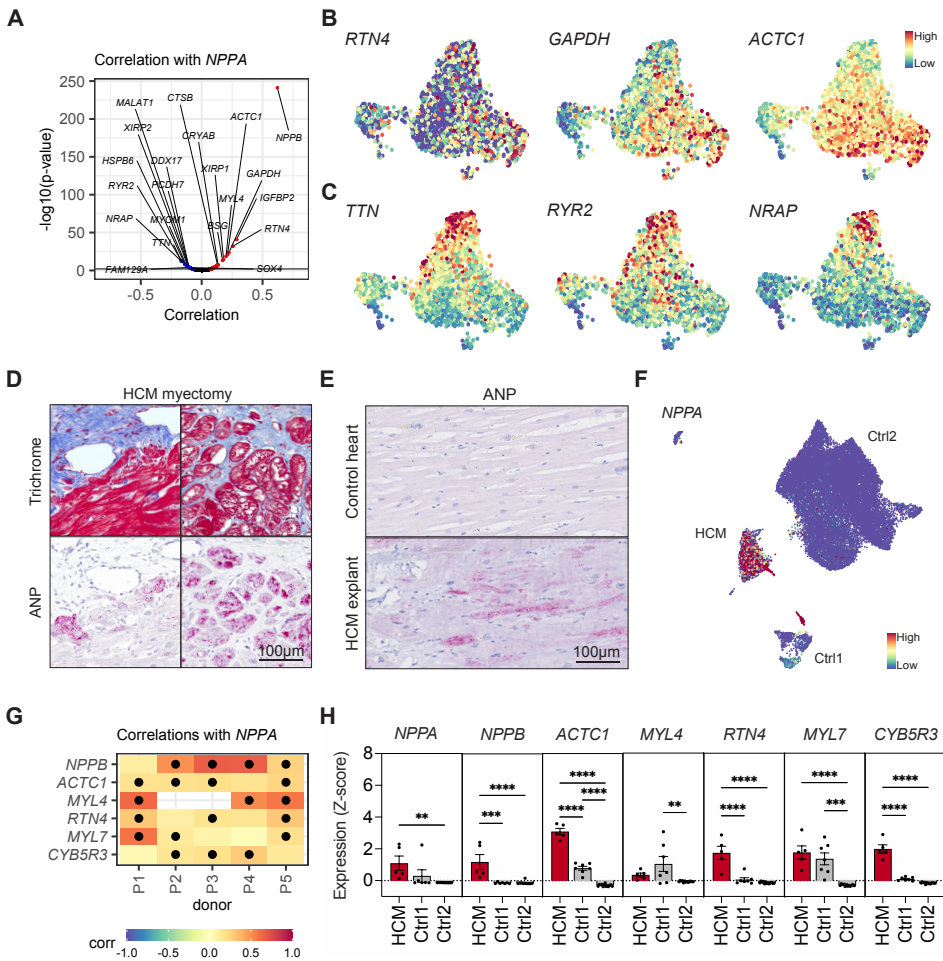


Figure 2. A subpopulation of HCM cardiomyocytes shows increased *NPPA* expression. (A) Volcano plot depicting genes positively (red dots) and negatively (blue dots) correlated to *NPPA* with an adjusted p-value < 0.01. (B-C) UMAPs showing the expression level of genes positively (B) and negatively (C) correlated to *NPPA*. Expression in UMAPs is shown as normalized transcript counts on a color-coded linear scale. (D) Representative Masson's trichrome staining (above) and ANP staining (below) on human HCM myectomy tissue showing ANP to be most expressed in CMs bordering areas of fibrosis. (E) Immunohistochemical staining showing ANP-expression in an explanted control and HCM heart. (F) UMAP of *NPPA* expression in all datasets showing HCM CMs to have more *NPPA* positive cells compared to healthy adult CMs. (G) Heatmap depicting *NPPA* correlation coefficients with listed genes determined from the respective Patients with HCM separately. A t-test was performed with Benjamin & Hochberg correction, black dots indicate that the correlation is considered significant ($p < 0.05$). (H) Comparison of expression of *NPPA* and *NPPA*-correlated genes between the HCM and Ctrl cells. Expression of each gene was first normalized (Z-score), after which average expression was determined per donor (black dots). Bars indicate averages per condition. Error bars show SEM. Outliers were removed by using the ROUT test with $Q=1\%$

and a one-way ANOVA test was performed. *, $P \leq 0.05$; **, $P \leq 0.01$, ***, $P \leq 0.001$; ****, $P \leq 0.0001$; UMAP, Uniform Manifold Approximation and Projection.

by UMAP (Figure 1H). This suggests gene expression differences in the clusters to be gradual instead of bimodal with heterogeneous cell-to-cell differences in gene expression. These clusters might represent differential gene regulation between different groups of single CMs, which could be related to functionally different pathology and/or disease progression at the single cell level. To identify potential drivers of this regulation, we then applied HOMER, Lisa and TRIAGE – which are software packages that can be used to identify regulatory factors based on gene subsets – to the lists of cluster-enriched genes (Figure 1G).

To explore the functional relevance of the different clusters we performed gene ontology (GO) analysis on the genes that showed significant enrichment per cluster (adjusted $p < 0.05$ and $FC > 1.1$) (Supplemental Figure 2F). Clusters 1-2 showed GO term enrichment for terms related to the sarcomere, suggesting this sub-population has more pronounced sarcomere remodeling (or retainment) compared to other cells. Clusters 3 and 4 on the other hand showed GO terms related to signaling and metabolic processes respectively. UMAPs containing both control and HCM CMs showed that genes enriched in HCM cluster 1 to 4 are HCM specific (Figure 1I).

In summary, scRNA-seq on human myectomy samples revealed the presence of functionally different subpopulations of CMs in the human HCM heart, which could be relevant for the disease.

NPPA expression is specific for a subset of CMs in patients with HCM

Classically, cardiac expression levels of Natriuretic Peptide A and B (NPPA/ANP and NPPB/BNP) have served as a hallmark for CM hypertrophy, stress or failure (Man et al., 2018). Though almost all HCM cells are expressing higher levels of NPPA compared to Ctrl samples (Figure 1D), our clustering analysis indicated the presence of a subpopulation of HCM CMs that is even more enriched for *NPPA* (cluster 3) (Figure 1G). The heterogeneity in *NPPA* expression was visualized by a UMAP indicating the *NPPA* expression per cell (Figure 1H). We next used our scRNA-seq data to determine which genes show a correlation with *NPPA*. By taking a cut-off of 0.01 for the adjusted p -value, we identified 83 positively correlated genes and 48 negatively correlated genes (Figure 2A and Supplemental Data 3). By far the strongest positive correlation was found for *NPPB*, which is in line with expectations (Kretzschmar et al.,

2018). UMAP confirmed the overlap for positively correlated genes (Figure 2B) and the negatively correlated genes (Figure 2C). Interesting to note is that genes related to muscle contraction (*TTN* and *RYR2*) and heart disease (*XIRP2* and *CRYAB*) showed a lower abundance in the cells with higher levels of *NPPA*.

Immunohistochemistry for ANP on myectomy samples indicated the ANP-positive cells to predominantly border fibrotic areas in the HCM samples (Figure 2D), while no positive cells could be detected in a control heart (Figure 2E). The HCM-specificity was further confirmed by comparing *NPPA* expression in HCM versus Ctrl cells, which showed very few Ctrl cells express *NPPA* (Figure 1D and 2F). The positive correlations for the top correlated genes were consistently found in multiple patients with HCM, indicating the correlation represents biology rather than it being by chance or dominated by data from a single patient (Figure 2G). The near absence of *NPPA* expression in the majority of CMs from control hearts made a comparable correlation analysis not applicable in those. In general, the *NPPA* positively correlated genes appeared more abundant in HCM CMs than cells coming from control hearts (Figure 2H).

These data indicate that while overall *NPPA* expression is higher in HCM CMs, there is a subpopulation of CMs that is enriched for *NPPA* and *NPPB* that are located in stressed, fibrotic regions in HCM hearts which is absent in control human heart samples. The gene expression profile of these cells could help us identify genes involved in the CM stress response.

XIRP2 correlations are more pronounced in HCM CMs

Xin Actin Binding Repeat Containing 2 (*XIRP2*) is expressed in cardiac and skeletal muscle where it interacts with actin and α -actinin. It localizes to the costamere and intercalated disks, two critical structures for cardiac function (Farrell et al., 2018). While relatively little is known about *XIRP2* function, mutations in *XIRP2* have been linked to dilated cardiomyopathy (DCM) (Long et al., 2015) and an increase in expression was observed in cardiac tissue from mice with a loss of cMyBP-C (Farrell et al., 2018). Based on our clustering, we found *XIRP2* to be the most enriched gene for cluster 2 (Figure 1G) and negatively correlated to *NPPA* expression (Figure 2A and Supplemental Data 3).

Correlation analysis for *XIRP2* showed the strongest positive correlation with *CMYA5*, *ZNF106* and *MAP4* expression, while genes like *ACTC1* and *MYBPC3* showed a neg-

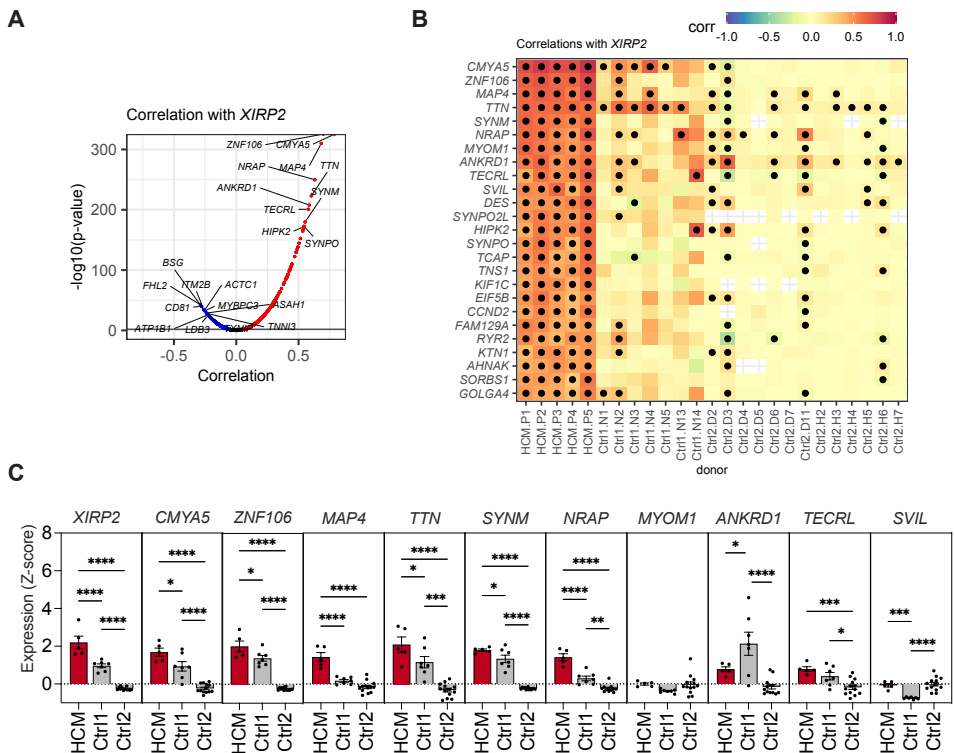


Figure 3. A subpopulation of HCM CMs shows increased *XIRP2* expression. (A) Volcano plot depicting genes positively (red dots) and negatively (blue dots) correlated to *XIRP2* in patients with HCM with an adjusted p-value < 0.01. **(B)** Heatmap depicting correlation coefficients between *XIRP2* and listed genes, determined in the listed donors. The top 25 genes most correlated to *XIRP2* in HCM are shown (based on average correlation coefficient in patients with HCM). A t-test was performed with Benjamin & Hochberg correction, black dots indicate that the correlation is considered significant ($p < 0.05$). **(C)** Comparison of expression of *XIRP2* and *XIRP2*-correlated genes between the HCM and Ctrl cells. Expression of each gene was first normalized (Z-score), after which average expression was determined per donor (black dots). Bars indicate averages per condition. Error bars show SEM. Outliers were removed by using the ROUT test with $Q=1\%$ and a one-way ANOVA test was performed. *, $P \leq 0.05$; **, $P \leq 0.01$, ***, $P \leq 0.001$; ****, $P \leq 0.0001$. See also Figure S3.

ative correlation (Figures 3A, S3A and Supplemental Data 4). To assert whether the *XIRP2*-gradient gene expression (Figure 1H) was based on biology and not by chance or dominated by the data from a single patient, we looked into *XIRP2* expression for each individual patient. Patient-specific UMAPs confirmed the presence of a *XIRP2*-gradient in each patient (Supplemental Figure 3B), and a comparable expression profile for the correlated genes *CMYA5* and *TTN* (Supplemental Figures 3C

and S3D). Histology confirmed the heterogeneity in *TTN* expression at the protein level (Supplemental Figure 3E). However, this heterogeneity was also observed in control tissue, indicating that healthy cells also show some degree of heterogeneity. These findings are in line with previous research showing that *TTN* is one of a set of proteins that have a mosaic expression pattern in the heart (T. Y. Wang et al., 2018).

To determine whether these co-expression patterns are specific for HCM, we next assessed these correlations in control CMs. This indicated the co-expression of these genes to be more pronounced in cells from HCM hearts compared to control CMs (Figures 3B and S3A), making them potentially disease relevant. Based on expression levels the majority of the *XIRP2* correlated genes also appeared to be more abundantly present in HCM CMs than in CMs from control hearts (Figure 3C).

Taken together, these data underline the validity of our observed gene expression profiles, and indicate the *XIRP2* gene correlations to be more pronounced in CMs from HCM hearts which could be relevant for the disease.

Regulon analysis reveals potential gene modules and TFs driving HCM

Clustering of cells offers a way to determine cellular subpopulations, which can be used to identify relevant gene expression patterns. However, many gene expression programs are likely to be active in the diseased heart, and they do not necessarily all need to coincide with subpopulations identified by clustering. Thus, to further identify gene expression patterns that might be relevant to HCM, we used SCENIC (Aibar et al., 2017) to look for patterns in our heterogenous HCM single cell expression data. The aim of this software is to identify potential regulons: groups of co-expressed genes driven by a specific TF. To achieve this, it uses machine learning methods to fit expression patterns of genes to expression patterns of TFs. These fits are used to determine potential regulons, which are further refined through TF motif analysis. We ran SCENIC separately on data of each of the five patients. To narrow down regulons of general importance to HCM, we first selected regulons identified in three or more (of five) patients (Figure 4A), and then selected regulons most consistently linked to the same group of genes (Figure 4B). This identified 22 regulons (Figure 4C and Supplemental Data 5) that showed heterogeneous expression over our single cells, as determined by the average expression Z-score of member genes (Figure 4D). GO analysis of these regulons showed functional differences between the regulons that might be related to processes relevant for hypertrophy and cell-signaling in HCM; for example, some regulons could be linked to energetic or metabolic processes, whilst some others were linked to sarcomere or cytoskeleton

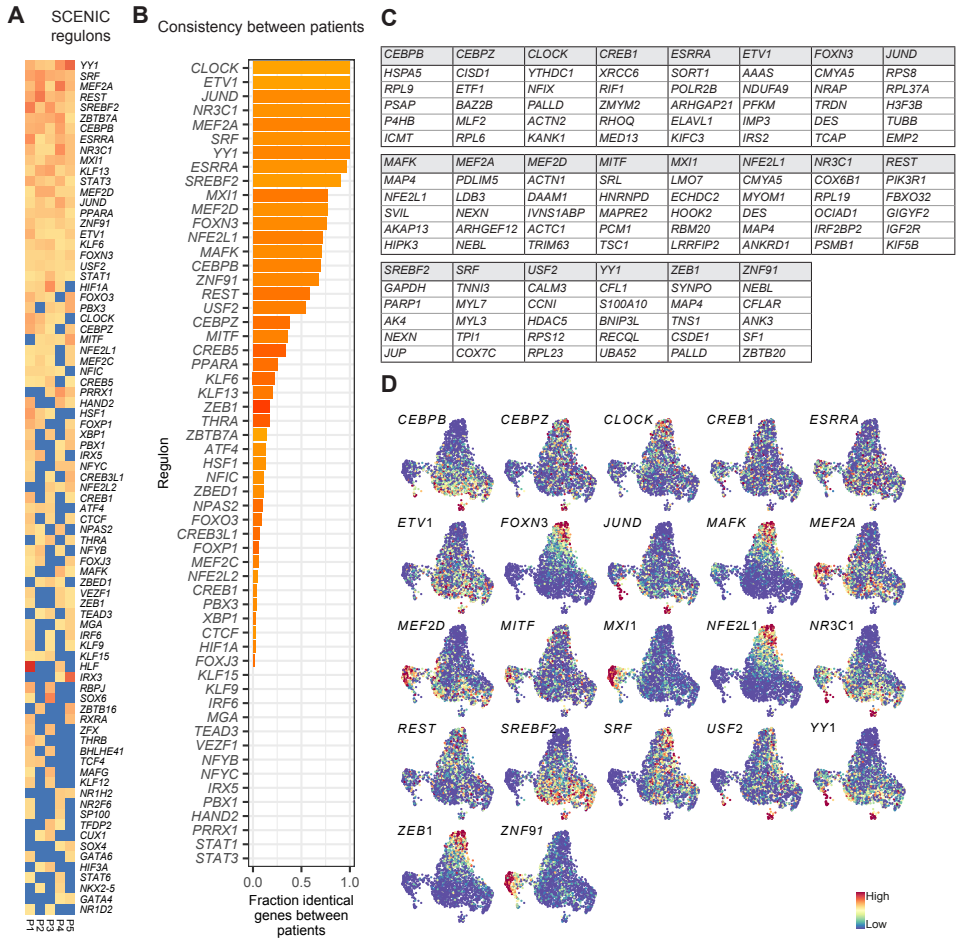


Figure 4. SCENIC analysis of gene expression heterogeneity reveals potential regulatory interactions. (A) Regulons determined in each HCM patient using SCENIC. Regulons are named according to the TF suggested to regulate them. Color coding indicates the normalized area under the curve score (NES), which relates to the confidence in the link between the TF and its associated genes (yellow to red). Blue indicates a regulon was not detected in respective patient. Only regulons identified in >1 patient are listed. (B) Graph showing the fraction of identical genes between patients. (C) Table depicting the 5 top genes within each regulon based on median gene importance scores. (D) Projection of the composite expression of indicated regulons on the HCM dataset UMAP. Composite expression is calculated by first normalizing gene expression (Z-score), and then calculating the mean of regulon member genes expression per cell. Expression is shown by a color-coded linear scale. UMAP, Uniform Manifold Approximation and Projection. See also Figures S4 and S5.

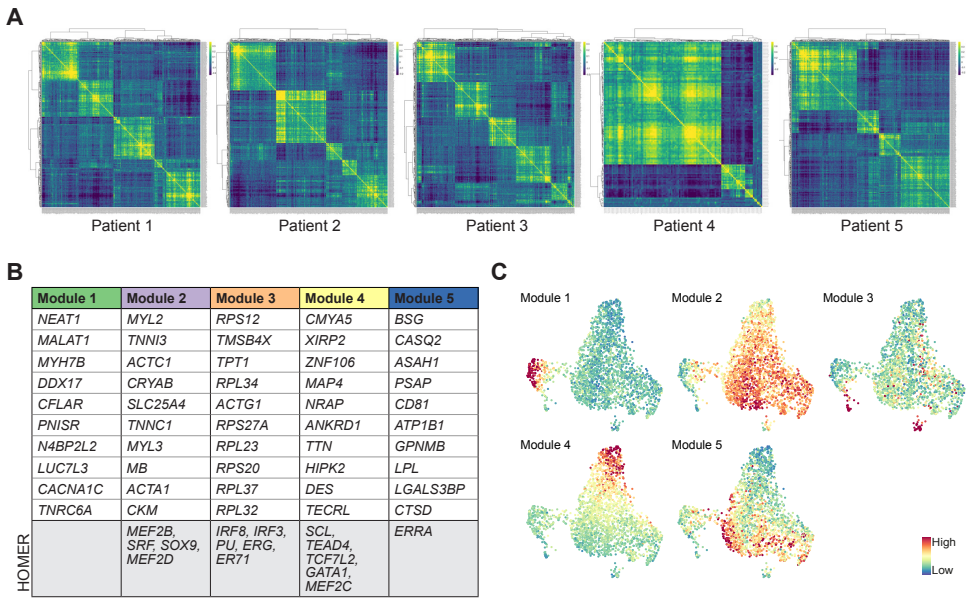


Figure 5. Gene expression heterogeneity reveals patterns of gene co-regulation. (A) Patient-specific heatmaps of the Pearson correlation matrix of a subset of detected genes that are expressed in >20% of cells and have a significant ($p < 0.001$) correlation with at least 10 other genes. Hierarchical clustering was used to identify regulons in each of the patients. **(B)** Top 10 genes found in each module (based on average correlation to other module member genes). The bottom row indicates TFs potentially regulating respective modules, as determined by HOMER analysis. **(C)** UMAPs showing the composite module expression in the HCM dataset. Composite expression is mean Z-score of the member gene expression levels, represented by a linear color-coded scale. See also Figures S4 and S5.

organization, and again others to membrane targeting of proteins (Supplemental Figure 4A).

Gene expression is often determined by posttranscriptional activation of TFs, rather than by differential expression of TFs. As SCENIC is based on TF differential expression data (Aibar et al., 2017), we next searched for groups of co-expressed genes (modules) independently of TF expression patterns. To do so, we selected genes that were detected in all patients and expressed in at least 5% of all cells (1871 genes) and generated gene-gene correlation matrices for each patient. We then selected all genes that had a significant correlation with at least 10 other genes (respectively 356, 334, 382, 120, 389 genes per patient). Hierarchical clustering analysis on the correlation matrix for these genes resulted in patient-specific modules

(Figure 5A). Strikingly, patient-to-patient comparison of the identified modules gave rise to 5 shared modules that were consistently identified in each of the patients (Figure 5B, Supplemental Figures 4B, 4C and Supplemental Data 6), indicating the modules to be of biological significance. The expression of these shared modules mark different cell populations as can be seen when visualized on a UMAP (Figure 5C). Based on gene content, we again see functional differences between the modules, where terms related to mitochondrial and ATP (module 2), sarcomere organization (module 4) and calcium signaling and conduction (module 5) are consistent with HCM-related processes (Supplemental Figure 4D). To identify TFs that could potentially be involved in the coregulation of the genes per module, we screened the promotor regions of these genes for binding site enrichment using HOMER. This yielded several potential transcriptional regulators (Figure 5B). Shared module 2 for example showed an enrichment for myogenic enhancer factor 2 (MEF2) binding sites, a well-known regulator of muscle genes (Black & Olson, 1998), SRF and SOX9, which have all been shown to regulate CM hypertrophy (Schauer et al., 2019; Zhang et al., 2001). This suggest that module 2 genes might be involved in CM hypertrophy.

Having identified regulons and modules from differential gene expression within the HCM population of cells, we next aimed to determine which of these regulons and modules show upregulation in HCM hearts compared to healthy hearts. We first applied the SCENIC algorithm to all donors from the Ctrl samples, and found all of the selected 22 regulons are also identified in healthy donor CM populations (Supplemental Figures 4E and 4F). This suggests that regulatory interactions underlying this co-expression are also active in healthy CM populations. We additionally tested whether the co-expression groups are unique in terms of member genes, and found that there is limited overlap between the individual regulons and/or modules (Supplemental Figure 4G). To more directly determine HCM-specificity of the regulons and modules, we assessed their expression in each of the patients and donors. Strikingly, this shows that the majority of the SCENIC regulons show enrichment in HCM, with the regulons *ZEB1*, *FOXN3*, *NFE2L1* and *MAFK* showing the largest contrast between HCM and Ctrl (Supplemental Figure 5A). In addition, we observe that co-expression modules 4 and 5 show a clear HCM-enrichment (Supplemental Figure 5B).

Integration of cell size with scRNA-seq reveals hypertrophy-associated genes

As one of the hallmarks of HCM is CM hypertrophy, it is of great interest to integrate cell size with the transcriptomic data obtained from scRNA-seq. Previously, index

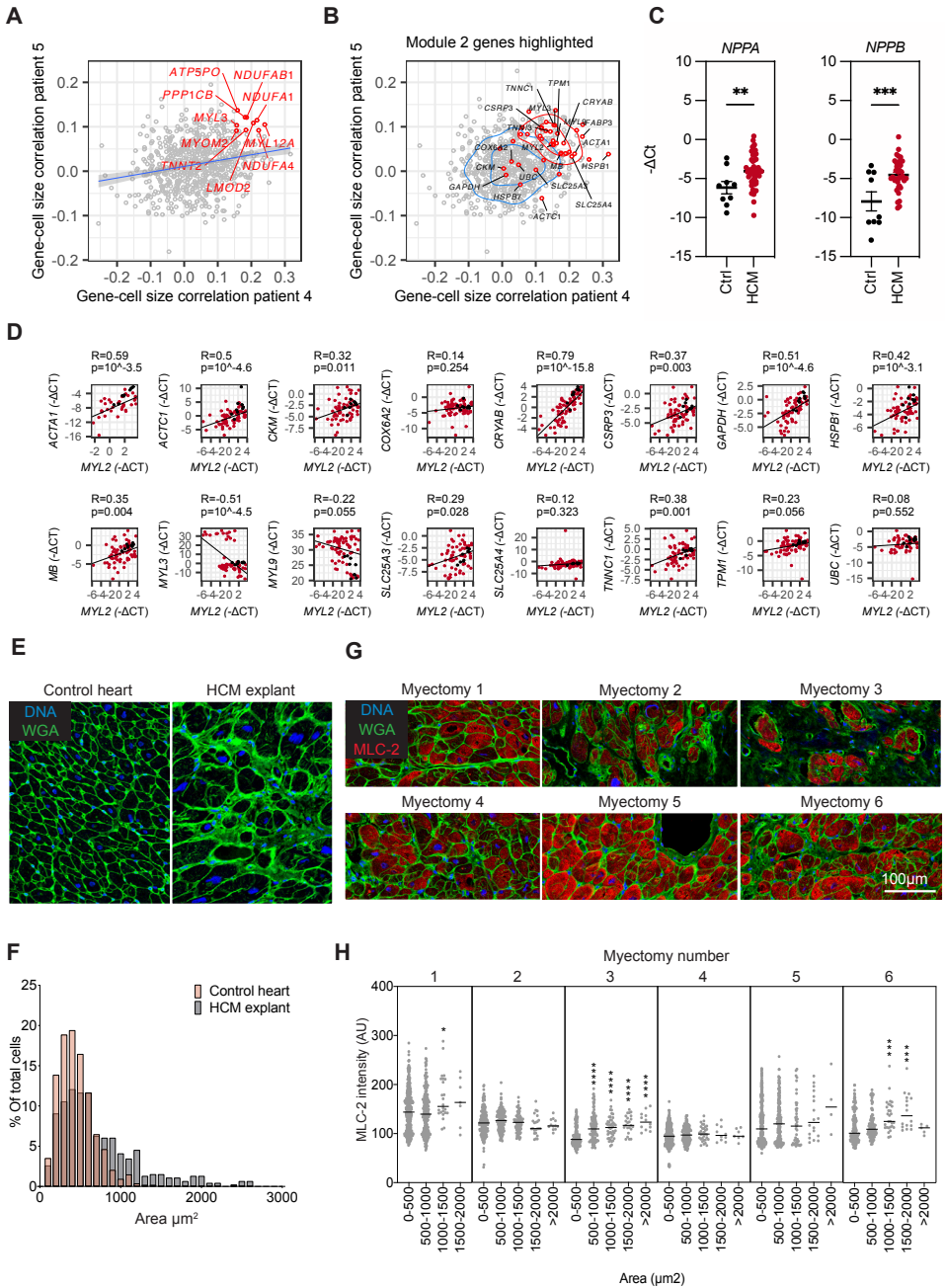


Figure 6. Index sorting provides a gene expression profile for enlarged CMs. (A-B) Correlations between FSC-A and gene expression determined from patient 4 (X-axis) versus those correlations determined from patient 5 (Y-axis). Each grey dot corresponds to a gene. In **(A)** genes that occur in the top 10% FSC-A correlated genes of both patient 4 and 5 are highlighted in red, and in **(B)** genes that occur in Module 2 are highlighted in red. **(C)** RT-

PCR showing an increase in *NPPA* and *NPPB* expression levels in patients with HCM. Outliers were removed by using the ROUT test with $Q=1\%$, t-tests were performed. For *NPPA*, there are $n = 9$ Ctrl and $n = 49$ HCM samples, for *NPPB*, there are $n = 9$ Ctrl and $n = 36$ HCM samples, mean and SEM are indicated. **(D)** RT-PCR validation of correlation between genes identified in Module 2. Pearson's correlation coefficients (indicated with an R) were calculated and t-tests were performed based on HCM samples. Samples were normalized to *RPL32*. Per gene, n-values are: *ACTA1*, 33; *ACTC1*, 65; *CKM*, 62; *COX6A2*, 68; *CRYAB*, 71; *CSRP3*, 64; *GAPDH*, 62; *HSPB1*, 61; *MB*, 66; *MYL3*, 59; *MYL9*, 74; *SLC25A3*, 59; *SLC25A4*, 66; *TNNC1*, 66; *TPM1*, 69; *UBC*, 52. In addition $n = 9$ Ctrl values are shown in each plot. **(E)** Representative immunofluorescent images from a control heart and an explanted HCM heart stained for WGA. **(F)**, Histogram showing the different distributions in CM cross-sectional area between a control heart and an explanted HCM heart. **(G)**, Representative images of WGA (green) and MLC-2 (red) co-staining on 6 HCM myectomy samples. **(H)** Quantification of CM cross-sectional area and MLC-2 fluorescence intensity (AU) in the samples from G. Outliers were removed by using the ROUT test with $Q=1\%$. Differences were tested by using a one-way ANOVA followed by a Tukey's multiple comparisons test. FSC-A indicates Forward scatter area; WGA, Wheat germ agglutinin; A.U., Arbitrary units; *, $P \leq 0.05$; **, $P \leq 0.01$, ***, $P \leq 0.001$; ****, $P \leq 0.0001$. See also Figure S6 and Table S1.

sorting data has been used to integrate morphological parameters obtained from flow cytometry with gene expression data obtained from scRNA-seq from bone marrow stem cells (Tan et al., 2017). To determine the enriched genes in hypertrophic CMs, we gathered FSC-A data in patients 4 and 5 as a proxy for cell size, which we subsequently linked to the gene expression profile of single CMs.

To first test the validity of this approach, we correlated FSC-A with total single cell mRNA read count, since bigger cells are expected to contain more mRNA. This showed a positive correlation between mRNA read count and FSC-A values for both patients (**Supplemental Figures 6A and B**). Further correlation analysis revealed genes that were both positively and negatively correlated with cell size (**Figure 6A and Supplemental Data 7**). While some of these genes have previously been linked to hypertrophy (Lim et al., 2001), we are among the first to show the correlation of these genes to CM size on a single-cell level rather than on the organ-wide level. Interestingly, the genes constituting shared module 2 show much higher correlations to cell size than other genes ($p = 2 \times 10^{-12}$ and $p = 5 \times 10^{-8}$ for patients 4 and 5 resp.) (**Figures 6B, Supplemental Figure 6C and D**).

In conjunction with our earlier observation that hypertrophy-related TFs are linked to this module, this suggests module 2 might be of extra importance to hypertrophy. We therefore aimed to validate the correlations between genes in this module in 97

additional septal myectomy samples from patients with HCM (HCM) and nine left ventricle RNA samples from non-failing donor hearts as controls (Control). Out of the 97 patients with HCM, 42 (43%) had a known pathogenic HCM mutation (MYBPC3, n=26; MYH7, n=7; multiple, n=3; other, n=6) while the causal mutation was unknown for the rest of the patients with HCM (**Supplemental Table 1**).

RT-PCR analysis for NPPA and NPPB validated the disease phenotype in the HCM samples compared to control (**Figure 6C**). RT-PCR confirmed that the majority of pair-wise correlations between the top-ranked gene in module 2, MYL2, and other module 2 genes are positive (**Figure 6D**). In addition, pair-wise comparison of all genes in module 2 showed 81% of correlations to be positive (**Supplemental Figure 6E, Supplemental Data 8**). These data independently confirmed the validity of the correlations in gene expression that were identified by scRNA-seq.

To visualize the distribution in cell size we performed WGA staining on control and HCM tissue and were able to show that CMs in HCM samples were on average larger than in control samples and showed a wider range in CM size (**Figures 6E and 6F**). In the sarcomere, myosin is formed by two heavy chains (encoded by *MYH6* and *MYH7*) and two myosin light chains (encoded by *MYL2* and *MYL3*). *MYL2* encodes the regulatory light chain (MLC-2) whereas *MYL3* encodes the essential myosin light chain (Sheikh et al., 2015). In both patients 4 and 5, *MYL3* and *MYL2* were present among the genes positively correlated to cell size (**Figure 6A**). To further examine the correlation between *MYL2* expression and cell size, we performed MLC-2 immunostainings on 6 septal myectomy samples (**Figure 6G**) and quantified both MLC-2 intensity and cell size. In 3 out of 6 samples we could confirm an increase in MLC-2 protein in the larger cells (**Figure 6H**). Together these data indicate that index sorting allows us to link cell morphological parameters to gene expression profiles and enables us to identify genes linked to CM hypertrophy.

Discussion

In this study we used scRNA-seq to define gene expression patterns that are relevant for HCM. By comparing gene expression profiles from healthy and diseased subjects we were able to show an enrichment for known and markers of CM stress induced in HCM hearts. In depth analysis of genetic profiles and gene correlations in diseased CMs revealed intercellular gene expression differences. Based on this heterogeneity we bioinformatically clustered transcriptionally related cells or genes, each of which are likely related to different cellular functions. Additionally, based on

scatter properties of HCM CMs we were able to correlate gene expression to cell size, which contributes to a better understanding of disease driving mechanisms in HCM.

In comparing healthy versus HCM CMs, we could detect clear transcriptional differences between the two. This included an HCM-related enrichment of well-known markers genes for cardiac stress, but additionally revealed genes that previously had not been functionally linked to HCM, such as myoglobin (encoded by *MB*). Myoglobin serves as an oxygen storage unit in muscle cells and is known as a circulating biomarker for muscle injury (Berenbrink, 2021). Our data show a strong transcriptional induction of *MB* in HCM CMs compared to healthy cells. This might be because *MB* is induced under hypoxic conditions (Kanatous et al., 2009), which is a key feature of cardiac hypertrophy (Mirtschink & Krek, 2016). Whether this actively contributes to HCM pathogenesis or whether circulating levels of *MB* can serve to track HCM disease progression is currently unknown and warrants further investigation.

CM heterogeneity has been shown to occur at many levels (Montag et al., 2018; Parbhudayal et al., 2018; Remme et al., 2009; van der Velden et al., 2011). This heterogeneity in adult CMs has more recently been confirmed by single cells studies (Gladka et al., 2018; Nomura et al., 2018; L. Wang et al., 2020), including the one described here. As the primary genetic origin of HCM lies within the sarcomere, and CM heterogeneity is a key hallmark in HCM, we focused on the analysis of CMs only. Based on the inter-myocyte transcriptomic heterogeneity, our algorithm clustered the CMs into 6 distinct subpopulations, with one cluster being highly enriched for *NPPA*. Correlation analysis revealed a positive correlation between *NPPA* and known stress marker genes, such as *NPPB*, *ACTC1* and *XIRP1*, but also showed a positive correlation with genes with relatively unknown cardiac functions, like reticulon 4 (*RTN4*). This suggests these lesser-known genes could also play an active part in the CM stress response. For example, *RTN4* is related to a variety of functions, it is known as a neurite outgrowth inhibitor, might play a role in the ER stress response in human DCM and cardiac ischemia (Ortega et al., 2014). In addition, it affects lipid homeostasis, AKT signaling, and cytoskeleton modulation in cancer (Pathak et al., 2018). Moreover, it is induced in mouse HCM models (Sasagawa et al., 2016) and it was recently shown that a knockdown of *RTN4* might be cardioprotective (Fan et al., 2021). However, a clear functional role in the CM stress response still remains to be defined. Nevertheless, given these previous observations, and our observation that *RTN4* expression correlates with *NPPA*, suggests that *RTN4* might play a role in HCM

pathogenesis.

Additionally, we noticed a positive correlation between *NPPA* expression and *GAPDH*, implying that *GAPDH* might not be suitable as housekeeping gene when studying stressed CMs. Interesting to note is the negative correlation with key genes related to CM contractility, such as *TTN* and *RYR2*, suggesting different contractile properties in cells expressing high levels of *NPPA*.

2 To investigate the gene regulatory network and TFs that drive HCM, we used SCENIC. Twenty-two regulons were consistently identified in patients with HCM, of which most were also expressed at higher levels in HCM CMs. Some, like MEF2 and SRF, are well-known regulators of HCM (Chai & Tarnawski, 2002; S. M. Kolodziejczyk et al., 1999; Passier et al., 2000; Zhang et al., 2001), validating our approach. However, not all of the most HCM-enriched factors, i.e. *ZEB1*, *FOXN3*, *NFE2L1* and *MAFK*, are currently known to play a role in heart disease. To our knowledge, *ZEB1* and *FOXN3* have not yet been shown to have a clear function in HCM. *NFE2L1* has been shown to be cardioprotective (M. Cui et al., 2021), and we have previously identified *MAFK* to be induced in failing CMs (Vigil-Garcia et al., 2021). The role of *MAFK* might thus not be restricted to genetic forms of heart failure. UMAPs indicated a clear overlap between the cells enriched for the regulons related to *NFE2L1* and *MAFK*. This is interesting as these TFs heterodimerize for DNA binding (M. B. Kannan et al., 2012) and have both been shown to provide cellular protection against oxidative stress through the induction of antioxidant genes (Itoh et al., 1999; Numazawa et al., 2003). Our data imply that *NFE2L1* and *MAFK* are cooperatively induced in a set of HCM CMs to drive a gene program involved in sarcomere organization and muscle contraction. While the regulons for *FOXN3* and *ZEB1* also appear enriched in the same set of cells, there is currently no known functional relationship between these 4 factors. However, based on the SCENIC analysis and the fact that the majority of the *XIRP2* correlated genes defined in Figure 3 are predicted to be regulated by 1 or more of these factors, these TFs together might drive at least part of the *XIRP2* correlated gene program.

Based on index sorting data we were able to show that several genes in shared module 2 were positively correlated to CM size at the single-cell level. Motif analysis of module 2 member genes indicated an enrichment for MEF2 binding sites, which would be in line with the well-known function of MEF2 in hypertrophic remodeling (Dirkx et al., 2013). Recently, Nomura et al. (Nomura et al., 2018) used scRNA-seq to

identify modules of co-expressed genes that correlated with CM size in mice one week after transverse aortic constriction (TAC). The genes in our hypertrophy-associated regulon 2 match surprisingly well (57%) with the hypertrophy-associated modules (M1, M2, M5, M11 & M16) in the paper by Nomura et al. This reinforces our observations to originate from biological regulation, and confirms the validity of using index-sorting to link gene expression to cell size.

It is evident that a lot of experimental choices regarding cell collection and obtaining sequencing data can influence the outcome when using scRNA-seq. This might be an explanation for the observed separation between the two sets of control CMs that we included in our analyses. scRNA-seq of CMs is challenging simply due to the size of the cells. Several strategies are currently used to separate single cells into individual wells or droplets, some of which allow for the high-throughput processing of thousands of transcriptomes in a cost-effective manner. However, all these high-throughput strategies have physical constraints regarding the size of the cells. Commercially available single-cell sorting platforms like Fluidigm C1 and Chromium can currently only sort cells that are up to 25-50 μM in diameter. This is considerably smaller than adult mammalian CMs, which can be approximately 125 μM along the longitudinal axis (Sorenson D.; Sonnenblick, E.H., Robinson, T.F.; Capasso J.M., 1985). This challenge has been circumvented by performing single nucleus RNA-sequencing on cardiac tissue, but with the drawback that there will be enrichment for RNAs residing predominantly in the nucleus (Selewa et al., 2020).

The percentage of mitochondrial reads is regarded as an additional indicator of CM scRNA-seq library quality, as cytoplasmic transcripts leak out of damaged cells, whereas mitochondrial transcripts do not. Mitochondrial reads are expected to fall within 30-50% of total reads (S. Kannan et al., 2019). If techniques are used that damage CMs this can increase to even 70% (Fluidigm C1 (DeLaughter et al., 2016) or handpicking myocytes (Nomura et al., 2018)) or 90% (conventional FACS (Gladka et al., 2018)). Thus, the 33% mitochondrial reads in the CMs that we sequence, corroborates that we sequenced intact myocytes.

The pathogenic processes and gene programs that occur in HCM are a complex interplay between many genes and gene programs, with cross-talk between different physiological pathways. Our study identifies many correlations, co-expression patterns, regulatory factors and relations to cell-size that offer an insight in this complex world. Our study provides a valuable data source to identify and further study

molecular mechanism that might be relevant for many HCM processes. This detail in insight will lead to new discoveries related to HCM and other areas of heart disease.

Limitations of the study

In our study, we collected single cardiomyocytes from patients with HCM to analyze gene expression patterns and heterogeneity. Both enzymatic digestion of patient material and FACS might introduce bias in cell recovery. For example, fibrotic tissue might be harder to digest, and certain cells might be more susceptible to FACS-induced damage. In addition, we focused on CMs in this study, disregarding other cell types in the heart. To compare diseased cardiomyocytes to healthy cells, we have included reference data from healthy cells from two other studies. While we tried to minimize batch effects by closely matching bio-informatic pipelines, variation from different experimental protocols might still introduce batch effects, as also discussed above. In addition, since the five patients analyzed in our study have either an MYBPC3 mutation or unknown genotype, we are unable to investigate the effects of specific HCM genotypes. To analyze our single cell data, we have used established bio-informatic analyses, and focused on effects that are observed in multiple patients and depend as a little as possible on analysis settings. Nevertheless, analysis choices can potentially affect identified features and analysis outcomes, such as cluster assignments of cells. While many observations we make based on single cell data are consistent with literature and additional experiments, further follow-up studies will be required to validate and investigate functional implications of many of our findings.

Methods

Lead contact

Further information and requests for resources and reagents should be directed to and will be fulfilled by the Lead Contact, Eva van Rooij (e.vanrooij@hubrecht.eu).

Materials availability

This study did not generate new unique reagents.

Data and code availability

RNA-Seq data is deposited on Gene Expression Omnibus, accession number GSE138262, and analysis scripts are available through GitHub (<https://github.com/>

vanrooij-lab/scRNAseq-HCM-human) and Zenodo (DOI: 10.5281/zenodo.6282659). Microscopy data reported in this paper will be shared by the lead contact upon request. Any additional information required to reanalyze the data reported in this paper is available from the lead contact upon request.

Human heart samples

Cardiac tissue from the interventricular septum was obtained from myectomy surgery in patients with HCM to relieve left ventricular outflow tract obstruction (n=5 for scRNA-seq, of which n=2 were used for additional index sorting analysis and n=97 for real-time PCR (RT-PCR) analysis). Written informed consent was obtained from each patient before surgery, and approval for the use of human tissue samples was obtained from the local ethics committee (fresh myectomy samples, and bulk myectomy RNA samples) or the local scientific advisory board of the biobank of the University Medical Center Utrecht (explanted heart tissue for histology). Cardiac tissue samples from non-failing donor hearts were used as control (n=9). Four of these were obtained from BioChain (Lots B607033, B711068, B711065 and A504241), the other five were obtained from the Sydney Heart Bank (dos Remedios et al., 2017).

Histology and Immunohistochemistry

Myectomy samples were fixed in PFA (4%) and incubated for 48 h rotating at room temperature. Next, the tissues were washed 3x for 10 min in PBS and stored in 70% ethanol (EtOH) at 4 °C. For tissue embedding, 3 consecutive incubations were performed. Firstly, 96% EtOH for 2 hours at 4 °C, followed by 100% EtOH for 2h at 4 °C and lastly Xylene for 2 hours at 4 °C. Finally, the tissue was incubated overnight in liquid paraffin at 60 °C and embedded in paraffin blocks. Then, 5 µm sections were cut on the HM 355S Automatic Microtome (#905200, Thermo Scientific) and placed on glass coverslips for further staining procedures. Explanted heart tissue was cut into 3 µm sections. For staining, sections were deparaffinized and rehydrated using xylene and ethanol graded series. Antigen retrieval was done by boiling the slides in EDTA buffer (pH 9.0) for 20 min and subsequently cooling them down to 37 °C. Masson trichrome staining was performed by using the Artisan Link Pro (Agilent) stainer according to manufacturer's protocol. For the immunostaining, sections were incubated overnight at 4°C with primary antibodies against titin (TTN, 9D10, Developmental Studies Hybridoma Bank, 1:400), ANP (CBL66, Millipore, 1:800) and MLC-2 (MLC-2V, 310-003, Synaptic Systems, 1:500). For immunohistochemistry, after 1x PBS wash, slides were incubated with BrightVision poly-AP anti-rabbit IgG antibody (VWRKDPVR110AP, Immunologic) for 30 min at room temperature and with liquid

2

permanent red (K0640, Agilent Dako) for 10 min at room temperature. Slides were counterstained with hematoxylin and mounted using Clearvue Mountant Xyl (ThermoFisher Scientific). Slides were digitalized using Nanozoomer XR (Hamamatsu). For immunofluorescence, slides were incubated overnight with primary antibody against MLC-2. After 3x PBS wash, slides were incubated with Alexa 647-labeled secondary antibody (A-21443, ThermoFisher Scientific, 1:500). Additionally, DAPI (#D3571, Invitrogen, 1:1000) and Wheat Germ Agglutinin (WGA, W11261, ThermoFisher Scientific, 100 µg/ml) were added. Slides were incubated for 1 h in the dark at room temperature. Slides were subsequently washed 3x in PBS and mounted with prolong gold antifade (P36934, Life Technologies). Immunofluorescent imaging was done with the SPE Confocal Microscope (Leica).

Tissue digestion

The tissue was digested into a single-cell suspension as described before (Gladka et al., 2018). In short, tissue was minced into fine pieces using a scalpel and transferred into a glass vial with 1.5 mL of cold digestion buffer. Tissues were digested by wheeling the vial for 15 minutes in a 37 °C water bath. Subsequently, the solution was pipetted up and down 10 times and transferred onto a 100 µm cell strainer (EASYS-trainer, #542000, Greiner Bio-One) placed on top of a 50 mL Falcon tube. The tissue was gently rubbed through the strainer using the plunger of a 1 mL syringe (#303172, BD Plastipak), after which the strainer was rinsed with 8.5 mL of DMEM (Dulbecco's Modified Eagle Medium, high glucose, GlutaMAX Supplement, pyruvate (Gibco, #31966021)) to obtain a total volume of 10 mL. This suspension was centrifuged for 6 min at 4 °C at 300 g. The supernatant was discarded and cells were resuspended in 1 mL fresh DMEM and kept on ice for immediate single-cell sorting.

Flow cytometry to sort single cells

Flow cytometry gating was performed according to our previously optimized protocol (Gladka et al., 2018). Briefly, cytometry was performed on a FACS Aria III (BD Biosciences) using a 130 µm nozzle. Debris was excluded based on forward (FSC-A) and side scatter (SSC-A). area. Cells were selected for autofluorescence between 530 nm and 600 nm. Using FSC-W, the larger cells were selected in order to sort CMs rather than other cell types. Cells were single-cell sorted into 384-well plates, immediately centrifuged and frozen at -80 °C until further processing. Additionally, 1000 cells were sorted into TRIzol reagent (Invitrogen, #15596026) for RNA quality control and 5000 cells were sorted into DMEM for imaging. Index sorting data was collected to correlate FSC-A (as a proxy for cell size) to gene expression on an indi-

vidual cell basis.

To show our sorted cells were viable, we gated for DAPI negative cells (DAPI #D3571, Invitrogen, 1:1000). To ensure our DAPI-negative events were nucleated, we next counterstained our sorted DAPI negative cells with DRAQ5 (65-0880-92, eBioscience, 1:1000) and re-analyzed the cells by FACS (P. J. Smith et al., 2004).

Imaging of single cells

After digesting the tissue into a single-cell suspension, cells were imaged before and after sorting using Axiovert 40C (Zeiss) to visualize the morphology of the cells.

RNA isolation and quality control

Total RNA was isolated from 1000 cells bulk-sorted into 100 μ l TRIzol reagent. RNA quality, measured as RNA integrity number, was determined using a Bioanalyzer 2100 (Agilent) and RNA 6000 Pico chips (Agilent, #5067-1513). Single-cell RNA sequencing was only performed when the RIN was above 7.5.

Library preparation and sequencing of single cells

The SORT-seq procedure was performed by Single Cell Discoveries, Utrecht as described previously (Gladka et al., 2018; Grun & van Oudenaarden, 2015; Muraro et al., 2016) with minor adaptations. In short: cells were sorted into 384 well plates containing 10 μ l of mineral oil and an aqueous solution of 50 nL containing primers derived from the CEL-seq2 protocol. CEL-seq2 primers consisted of a 24 bp polyT sequence followed by a 6bp unique molecular identifier (UMI), a cell-specific barcode, the 5' Illumina TruSeq2 adapter and a T7 promotor sequence. Cells were lysed by 5 min incubation at 65 °C, after which cDNA libraries were generated by dispersion of the RT enzyme and second strand mixes with the Nanodrop II liquid handling platform (GC biotech). cDNA libraries from all wells were pooled, followed by separation of the aqueous phase from the oil phase and subsequent in vitro transcription for linear amplification as performed by overnight incubation at 37 °C. Next, Illumina sequencing libraries were prepared using the TruSeq small RNA primers (Illumina), followed by PCR amplification for 12-15 rounds depending on the amount of RNA after in vitro transcription. Afterwards, libraries were sequenced paired-end at 75 bp read length with Illumina NextSeq500. 5% of the sequencing run (15×10^6 reads) were allotted to each 384-well plate. Four 384-well plates were sequenced per patient, two for the patient where index-sorting was applied.

Mapping of HCM sequencing data

2

After sequencing, each of the HCM samples were mapped. Read 1 (R1) contains respectively the UMI (positions 1-6) and barcode (positions 7-14) followed by the poly-T sequence (theoretically 24 nt) and sample mRNA sequence, read 2 (R2) contains the mRNA transcript sequence only. UMI and cell barcode (BC) information was attached to R2 metadata, and only R2 was used for mapping. In addition, we discarded reads that did not show ≥ 10 thymine nucleotides after the BC in R1. Reads were then trimmed for sequencing primers and repeating single nucleotides using the Cutadapt (Martin, 2011) wrapper Trim Galore (default settings). We then filtered out ribosomal RNA reads by discarding reads that mapped to the human rRNA genes using Burrows-Wheeler Alignment Tool (bwa merge of bwa aln and bwa mem -h 15) (Li & Durbin, 2009). These pre-processed reads were then mapped using Spliced Transcripts Alignment to a Reference (STAR --outFilterMultimapNmax 20) (Dobin et al., 2013), assigned to genes using featureCounts (-R BAM) (Liao et al., 2014), where multi-mappers were ignored (featureCounts default behavior), and processed into UMI count tables using UMI-tools (umi_tools count; default settings) (T. Smith et al., 2017). As reference genome, we used the human genome (GRCh38.93) and gene annotation (gtf file) acquired from ensembl.org. The gtf file was filtered to only contain genes with a gene_biotype annotation of protein_coding, lincRNA or antisense. After mapping, HCGN symbols were linked to Ensembl IDs using the R biomaRt package.

Obtaining Ctrl1 and Ctrl2 count tables

We included cells from healthy donor hearts from two different studies, Wang et al. (L. Wang et al., 2020) (referred to as Ctrl1) and Litviňuková et al. (Litviňuková et al., 2020) (Ctrl2). From Wang et al., we used samples N1, N2, N3, N4, N5, N13 and N14, as they came from healthy donors and included LV cells. We obtained raw FASTQ files from Gene Expression Omnibus (GEO, accession numbers GSE121893 and GSE109816) using the NCBI SRA Toolkit (fasterq-dump command) and SRR identifiers obtained from the provided metadata files. We collected FASTQ data for cells annotated as LV cells (clusters LV1-9) into files per donor and plate (we note that these selected cells were filtered for quality already by Wang et al.). This data was collected with the iCell8 platform from Takara Bio, R2 again contained the biological information that was mapped, and R1 contained only the BC (11 nt) followed by the UMI (ranging from 10-14 nt), of which we used only the first 10 nucleotides to deal with the variable length. (A reference BC file was obtained from the Cogent NGS Analysis Pipeline, v. 1.0, Takara Bio.) We mapped the obtained FASTQ files using the same pipeline as the HCM samples. For Litviňuková et al. (who used 10x Genomics)

we downloaded count tables for CMs for all available samples (D1-7, D11, H2-7) from <https://www.heartcellatlas.org/> (h5ad files) and selected only cells taken from the septum. These tables were generated by the Cell Ranger pipeline (v. 3.0.2, 10x Genomics), which, identical to our pipeline, uses the STAR aligner in combination with human genome GRCh38.93 and gene annotation (ensembl.org), and only considers uniquely mapped reads (10x Genomics documentation). The downloaded Litviňuková et al. raw count tables were converted to h5seurat format and used directly for analysis in Seurat.

Analysis of single cell transcriptomics data using Seurat

We used Seurat to analyze our data (Seurat v. 4.0.3, SeuratDisk v. 0.0.0.9019, SeuratObject v. 4.0.2, loomR v. 0.2.1.9000, hdf5r v. 1.3.3) (Stuart et al., 2018). Raw count tables were loaded into Seurat for all three datasets (HCM, Ctrl1, Ctrl2), and the Seurat “merge” function was applied to perform pooled analysis. Separate Seurat objects based on this data were also created for separate donors. Similar Seurat analyses were then performed for the pooled data, the HCM, Ctrl1, Ctrl2 sets, and donors separately. Mitochondrial read counts were determined, after which mitochondrial genes were removed from the count table. Cells were then filtered based on total read count, cells with total UMI count >1000 were taken along (we note that for Ctrl1 and Ctrl2 data, cell quality filtering was already performed by respective authors). Genes detected in <5 cells were discarded. Total UMI counts were 1780041, 1614560, 2028833, 396894 and 1418990 for patients 1-5 respectively (excluding mitochondrial counts), corresponding to mean UMI counts per well of 3779, 2660, 3241, 2795 and 3182. Then, to perform the analysis, the following Seurat functions were applied with default parameters unless explicitly stated: NormalizeData (with normalization.method = ‘RC’, and median total cell transcript count as scale.factor), FindVariableFeatures, ScaleData (with do.scale = F, do.center = F, scale.max = Inf), RunPCA (npcs = 30, using the top 2000 variable features), RunUMAP, FindNeighbors, FindClusters (resolution = 0.1 or 0.4 for pooled and HCM datasets, respectively). We use the FindMarkers function (min.pct = 0.05) to identify differentially expressed genes for the clusters. For gene expression plots, the scale was set from 0 to the 97th or 98th percentile for UMAPs and violin plots respectively, to exclude outliers from the scale. To determine patient-level gene expression values for genes, gene expression values were first normalized to Z-scores and then averaged per patient. To determine composite gene expression values for groups of genes (such as regulons or modules, see below), we also first normalized expression to Z-scores, and then averaged over the genes belonging to the group of interest. To determine

patient-averaged composite expression for groups of genes, these two strategies were combined.

Gene ontology analysis

For gene ontology (GO) analysis, gene names were mapped to Entrez Gene IDs. Mappings between Entrez Gene IDs and GO terms were then obtained from R-package `org.Hs.eg.db`⁵⁷. A background set of genes was constructed by selecting all genes expressed in >5% of cells. A set of genes of interest was then determined based on genes that were significantly enriched ($FC > 0$, adjusted $p < 0.05$) between cluster and non-cluster, or by their presence in a gene module (see below). Enrichment of GO terms were then analyzed using the tools from the GSEABase R-package (v. 1.54.0) (Morgan et al., 2021). The `pvalueCutoff` parameter of the `hyperGTest` function was set to 0.05.

Correlation analyses

For correlation analyses, the Pearson correlation between the parameter of interest (either expression of a gene of interest or FSC-A) and every (other) gene was calculated, provided that the gene was expressed in at least 10% (gene-gene correlations) or 33% (gene-FSC-A correlations) of cells. This was done using the `cor.test` function from the R `stats` package, which also produces a p-value estimate based on the assumption that correlation coefficients of uncorrelated data follow a student-t distribution. A p-value correction was applied using the `p.adjust` function (Benjamini & Hochberg method).

Transcription and regulatory factor analyses

To identify transcription or regulatory factors that drive expression of groups of genes (such as cluster-enriched genes or modules), we ran Homer, Lisa and/or TRIAGE. HOMER (Homer suite v4.11; human-o v6.3 and human-p v5.5) (Heinz et al., 2010) performs TF motif enrichment analysis in proximal promoters. We used the `findMotifs.pl` function using all expressed genes (expressed in at least 5% of all included cells) as background and promoter location set to -300 to +50 bp (default options). We then show top 5 significant results ($p < .05$ and $q < 0.9$; if available) from the “known results”. Lisa (v. 2.2.5) (Qin et al., 2020) leverages existing H3K27ac ChIP-seq data from transcription regulators to identify regulators that potentially drive gene sets of interest. We ran the “oneshot” Lisa procedure (genome hg38) on gene sets of interest with the “`--rp_map enhanced_10K`” setting and provided a background list of genes (all genes that are expressed in 5% of cells). We then select

significant hits ($p < 0.01$) and show a list that consists of both top-5 hits (by p value only) and top-5 of hits that are observed >1 cell type or CM-specific; hits occurring in both top-fives are indicated with an asterisk. TRIAGE (Shim et al., 2020) leverages H3K27me3 CHIP-seq data to calculate repressive tendency scores (RTS) and discordance scores for genes, with the aim of identifying regulatory genes that control differentiation in a set of genes. To identify potential regulators for each cell cluster, we took differentially expressed genes ($FC > 0$ and adjusted $p < 0.01$) with an $RTS > 0.03$ (deemed priority genes by Shim et al.), and listed the 5 (if available) regulators with the highest RTS score.

SCENIC analysis

To identify regulons, we converted raw count tables into loom files for all of the separate patients and donors from the HCM, Ctrl1 and Ctrl2 datasets, and ran a command line interface (CLI) SCENIC pipeline using “pyscenic” (Aibar et al., 2017). First, we executed the GRN step, using the “pyscenic grn -o adj.csv” command, supplying the `hs_hgnc_curated_tfs.txt` TF list from the pyscenic resource directory. We then executed the “pyscenic ctx” command, where we supplied the `hg19-tss-centered-10kb-7species.mc9nr.feather` and `hg19-500bp-upstream-7species.mc9nr.feather` databases (obtained via <https://resources.aertslab.org/cistarget/>) and the `motifs-v9-nr.hgnc-m0.001-o0.0.tbl` motif file (obtained via <https://resources.aertslab.org/cistarget/motif2tf/>). Finally, the “pyscenic aucell” step was executed. We processed output files further in R. We extracted Normalized Enrichment Scores (NES) from the `reg.csv` output file, from which we determined the median NES score for each respective regulon; the NES score reflects confidence in the link between the TF and gene set. To merge regulons from multiple patients with HCM, we selected those genes that are present in 3 or more patients. Per regulon, we also extracted importance scores for each of the linked genes from the `adj.csv` output file, which we use to rank the genes within the (merged) regulons (here also the median was used to determine importance scores from multiple patients/donors).

Custom gene module analysis

Clusters of genes that show significant correlations with each other were determined using a custom R script, which was applied to the gene expression data of each patient separately. We first selected genes that are expressed in at least 20% of cells pooled for all Patients with HCM. Then, for each patient, we selected genes expressed in 5% of that patient’s cells, and calculated Pearson’s correlations coefficients between all remaining gene pairs, resulting in a large gene-gene correlation

matrix. Subsequently, we calculated p-values for respective correlation coefficients based on the student-t distribution, and applied the Benjamini-Hochberg correction to correct for multiple testing. We then selected genes that had a significant ($p < 0.001$) correlation with at least 10 other genes, resulting in the correlation matrix that was used for the regulon analysis. We applied the `hclust` function (using the `ward.D2` method) to sort rows and columns of the correlation matrix by similarity, and generate a hierarchical tree. Using this tree, we calculated the gap statistic for a range of number of clusters (k), and determined the optimal numbers of clusters (K). (We used the `clusGap` and `maxSE` function from the R cluster package, applying the `Tibs2001SEmax` method.) Genes were assigned to K co-expression modules based on the `cutree` function, resulting 6, 5, 11, 5 and 6 modules for patients 1-5 respectively. Within each module, we ranked genes according to the average correlation to other genes in each module.

To determine final modules presented in the paper, we systematically compared the patient-specific modules for overlap in member genes. We defined gene identity overlap for a pair of modules simply as the number of overlapping genes divided by the size of the smallest regulon in the pair. We used the `hclust` function again to generate a dendrogram, which by eye very clearly showed 5 clusters, as also confirmed by a median gene overlap of 68%, 86%, 62%, 89% and 82% between patients for each of the module groups. We determined our final five modules by joining patient-specific modules based on this clustering, and included genes into each of the final modules if they were identified in at least 3 patient-specific modules of that cluster.

RT-PCR analysis

Total RNA was isolated from 97 myectomy and 9 control samples using TRIzol reagent according to manufacturer's protocol. RNA concentration was determined using Nanodrop 1000 spectrophotometer (ThermoFisher Scientific). Complementary DNA (cDNA) was synthesized from a total of 250 ng of RNA using the iScript cDNA Synthesis Kit (Bio-Rad, #1708891), according to manufacturer's protocol. RT-PCR was performed using gene specific primers (listed below) according to the instructions described by the IQ™ SYBR Green Supermix (Bio-Rad, #170-8885). The RT-PCR protocol was as follows: 95 °C for 15 min, followed by 40 cycles at 95 °C for 15 s, 60 °C for 30 s and 72 °C for 30 s.

Table 1: Quantitative PCR (qPCR) primers

| GENE | FORWARD SEQUENCE (5'-3') | REVERSE SEQUENCE (5'-3') |
|---------|---------------------------|--------------------------|
| ACTA1 | TACCCGCCAGAACTAGAC | ACGATGGACGGGAACACG |
| ACTC1 | CCGTACCACAGGCATTGTC | GACAAAGGAGTAGCCACGCT |
| CKM | GACCCATCATCTCGGATCG | AGGTCGTCTCCACCTTGAG |
| COX6A2 | CATCCGCACCAAGCCCTAC | ACTTTATTGTGTCCGGGGG |
| CRYAB | CCGACGTCTACTTCCCTGAG | CCATGCACCTCAATCACATC |
| CSR3 | ATATGGCCCCAAAGGATCG | CCGGCTTTGGGGACTGTT |
| GAPDH | GGGTATCATCTCTGCCCC | GGTATGAGTCCTTCCACGA |
| HSPB1 | CGCGGAAATACACGCTGC | GTGATCTCGTTGGACTGCGT |
| MB | GCCCATCTTGCTCTTTTTGTC | GGTGACCCTTAAAGAGCCTGAT |
| MYL2 | CCTTCCACCATGGCACCTA | AAGCCATCCCTGTTCTGGT |
| MYL3 | AAGATCACCTACGGGCAGTG | CTGGAGCATAGGCAGGAAAG |
| MYL9 | GCAATGTTTGACCAGTCCCAG | CCTCCAGGTATTCGTCTGTGG |
| NPPA | CGTGAGCTTCTCTTTTA | CCAAATGGTCCAGCAAATTC |
| NPPB | CTCCAGAGACATGGATCCCC | GTTGCGCTGCTCCTGTAAC |
| SLC25A3 | TCTTGTATAGCAATATGCTTGGAGA | GGGCAATGTCAGCAAAGAAT |
| SLC25A4 | GATACTGCCAAGGGGATGCTG | CGACGAACAGTGTCAAAGGG |
| TNNC1 | CTACAAGGCTGCGGTAGAGC | AGCATCCTCATCACCTTGCC |

Ribosomal protein L32 (RPL32) was used as a housekeeping gene, to which all genes were normalized. Expression of NPPA and NPPB in HCM samples and control samples was calculated ($-\Delta Ct$). The results are shown as mean \pm standard error of the mean (SEM). Significance was tested using Students t-test. The number of samples (n) used in each experiment is indicated in the legend or shown in the figures. Plotting was done using PRISM (GraphPad Software Inc.). R and ggplot2 were used to plot correlation analyses. Specifically, based on ΔCt -values of HCM-samples, the Pearson correlation coefficients were determined for gene pairs, and corresponding p-values were calculated by using a t-test (using the `stats::cor.test` function).

Cell size analysis

Cell size was manually measured on sections stained for MLC-2 and labelled with WGA by using ImageJ 1.49v software. Circular events were selected in the WGA channel, to quantify only cells whose cross-section is perpendicular to their long axis. ImageJ was used to measure the area of each identified cell, and fluorescence intensity in the MLC-2 channel within that area. Total MLC-2 fluorescence was nor-

malized to cell area. Cell size and MLC-2 were quantified in 3-5 images each for 6 myectomy samples (326-669 cells per samples, 2931 cells in total).

Acknowledgments

We gratefully acknowledge Roy Huurman, Sylvie Dekker, Martine de Boer, Harm de Wit and Peter van Geel from the Erasmus Medical Center for facilitating sample collection and help with flow cytometry. We thank Stefan van der Elst from the Hubrecht Institute FACS facility for his help with the viability experiments and presenting our flow cytometry data, Jeroen Korving for his help with histology and Anna Alemany for her help with mapping raw data. We further thank Anko de Graaff and the Hubrecht Imaging Center for supporting the imaging. Lastly, we acknowledge Cris dos Remedios for providing us donor heart samples from the Sydney Heart Bank.

Funding

This work was supported by the Leducq Foundation (14CVD04), the European Research Council under the European Union's Seventh Framework Program (ERC Grant Agreement CoG 615708 MICARUS) and the Dutch CardioVascular Alliance (DCVA), an initiative with support of the Dutch Heart Foundation, DCVA2017-18 ARENA-PRIME and DCVA2014-40 CVON-DOSIS.

Author contributions

J.E.C.E., A.E.L., M.W.C., and E.R. designed and performed experiments. M.W., J.E.C.E, C.J.B., and B.M. analyzed the data. P.K., D.K., J.V., M.M., and A.V. provided resources and methodologies J.E.C.E., A.E.L., M.W.C., M.W., and E.R wrote the manuscript. E.R. acquired funding

Disclosures

The authors declare no conflict of interest.

References

- Aibar, S., Gonzalez-Blas, C. B., Moerman, T., Van, A. H. T., Imrichova, H., Hulselmans, G., Rambow, F., Marine, J. C., Geurts, P., Aerts, J., Van Den Oord, J., Atak, Z. K., Wouters, J., Aerts, S., González-Blas, C. B., Moerman, T., Huynh-Thu, V. A., Imrichova, H., Hulselmans, G., ... Aerts, S. (2017). SCENIC: Single-cell regulatory network inference and clustering. *Nature Methods*, 14(11), 1083–1086. <https://doi.org/10.1038/nmeth.4463>
- Berenbrink, M. (2021). The role of myoglobin in the evolution of mammalian diving capacity – The August Krogh principle applied in molecular and evolutionary physiology. *Comparative Biochemistry and Physiology -Part A : Molecular and Integrative Physiology*, 252(November 2020), 110843. <https://doi.org/10.1016/j.cbpa.2020.110843>
- Black, B. L., & Olson, E. N. (1998). Transcriptional control of muscle development by myocyte enhancer factor-2 (MEF2) proteins. *Annu Rev Cell Dev Biol*, 14, 167–196. <https://doi.org/10.1146/annurev.cellbio.14.1.167>
- Chai, J., & Tarnawski, A. S. (2002). Serum Response Factor: discovery, biochemistry, biological roles and implications for tissue injury healing. *Journal of Physiology and Pharmacology*.
- Cui, M., Atmanli, A., Morales, M. G., Tan, W., Chen, K., Xiao, X., Xu, L., Liu, N., Bassel-Duby, R., & Olson, E. N. (2021). Nrf1 promotes heart regeneration and repair by regulating proteostasis and redox balance. *Nature Communications*, 12(1), 1–15. <https://doi.org/10.1038/s41467-021-25653-w>
- Cui, Y., Zheng, Y., Liu, X., Yan, L., Fan, X., Yong, J., Hu, Y., Dong, J., Li, Q., Wu, X., Gao, S., Li, J., Wen, L., Qiao, J., & Tang, F. (2019). Single-Cell Transcriptome Analysis Maps the Developmental Track of the Human Heart. *Cell Rep*, 26(7), 1934–1950 e5. <https://doi.org/10.1016/j.celrep.2019.01.079>
- DeLaughter, D. M., Bick, A. G., Wakimoto, H., McKean, D., Gorham, J. M., Kathiriya, I. S., Hinson, J. T., Homys, J., Gray, J., Pu, W., Bruneau, B. G., Seidman, J. G., & Seidman, C. E. (2016). Single-Cell Resolution of Temporal Gene Expression during Heart Development. *Developmental Cell*, 39(4), 480–490. <https://doi.org/10.1016/j.devcel.2016.10.001>
- Di Domenico, M., Casadonte, R., Ricci, P., Santini, M., Frati, G., Rizzo, A., Carratelli, C. R., Lamberti, M., Parrotta, E., Quaresima, B., Faniello, C. M., Costanzo, F., & Cuda, G. (2012). Cardiac and skeletal muscle expression of mutant beta-myosin heavy chains, degree of functional impairment and phenotypic heterogeneity in hypertrophic cardiomyopathy. *J Cell Physiol*, 227(10), 3471–3476. <https://doi.org/10.1002/jcp.24047>
- Dirx, E., da Costa Martins, P. A., & De Windt, L. J. (2013). Regulation of fetal gene expression in heart failure. *Biochim Biophys Acta*, 1832(12), 2414–2424. <https://doi.org/10.1016/j.bbadis.2013.07.023>
- Dobin, A., Davis, C. A., Schlesinger, F., Drenkow, J., Zaleski, C., Jha, S., Batut, P., Chaisson, M., & Gingeras, T. R. (2013). STAR: Ultrafast universal RNA-seq aligner. *Bioinformatics*, 29(1), 15–21. <https://doi.org/10.1093/bioinformatics/bts635>
- dos Remedios, C. G., Lal, S. P., Li, A., McNamara, J., Keogh, A., Macdonald, P. S., Cooke, R., Ehler, E., Knöll, R., Marston, S. B., Stelzer, J., Granzier, H., Bezzina, C., van Dijk, S., De Man, F., Stienen, G. J. M., Odeberg, J., Pontén, F., Linke, W., & van der Velden, J. (2017). The Sydney Heart Bank: improving translational research while eliminating or reducing the use of animal models of human heart disease. *Biophysical Reviews*, 9(4), 431–441. <https://doi.org/10.1007/s12551-017-0305-3>
- Fan, P., Zhang, L., Cheng, T., Wang, J., Zhou, J., Zhao, L., Hua, C., & Xia, Q. (2021). MiR-590-5p inhibits pathological hypertrophy mediated heart failure by targeting RTN4. *Journal of Molecular Histology*, 52(5), 955–964. <https://doi.org/10.1007/s10735-021-10009-x>
- Farbehi, N., Patrick, R., Dorison, A., Xaymardan, M., Janbandhu, V., Wystub-Lis, K., Ho, J. W.

- K., Nordon, R. E., & Harvey, R. P. (2019). Single-cell expression profiling reveals dynamic flux of cardiac stromal, vascular and immune cells in health and injury. *Elife*, 8, 1–39. <https://doi.org/10.7554/eLife.43882>
- Farrell, E., Armstrong, A. E., Grimes, A. C., Naya, F. J., De Lange, W. J., & Ralphe, J. C. (2018). Transcriptome analysis of cardiac hypertrophic growth in MYBPC3-null mice suggests early responders in hypertrophic remodeling. *Frontiers in Physiology*, 9(OCT), 1–14. <https://doi.org/10.3389/fphys.2018.01442>
- Gladka, M. M., Molenaar, B., de Ruiter, H., Van Der Elst, S., Tsui, H., Versteeg, D., Lacraz, G. P. A. A., Huibers, M. M. H. H., Van Oudenaarden, A., & Van Rooij, E. (2018). Single-Cell Sequencing of the Healthy and Diseased Heart Reveals Cytoskeleton-Associated Protein 4 as a New Modulator of Fibroblasts Activation. *Circulation*, 138(2), 166–180. <https://doi.org/10.1161/CIRCULATIONAHA.117.030742>
- Grun, D., Kester, L., & van Oudenaarden, A. (2014). Validation of noise models for single-cell transcriptomics. *Nat Methods*, 11(6), 637–640. <https://doi.org/10.1038/nmeth.2930>
- Grun, D., Lyubimova, A., Kester, L., Wiebrands, K., Basak, O., Sasaki, N., Clevers, H., van Oudenaarden, A., Grün, D., Lyubimova, A., Kester, L., Wiebrands, K., Basak, O., Sasaki, N., Clevers, H., & van Oudenaarden, A. (2015). Single-cell messenger RNA sequencing reveals rare intestinal cell types. *Nature*, 525(7568), 251–255. <https://doi.org/10.1038/nature14966>
- Grun, D., & van Oudenaarden, A. (2015). Design and Analysis of Single-Cell Sequencing Experiments. *Cell*, 163(4), 799–810. <https://doi.org/10.1016/j.cell.2015.10.039>
- Heinz, S., Benner, C., Spann, N., Bertolino, E., Lin, Y. C., Laslo, P., Cheng, J. X., Murre, C., Singh, H., & Glass, C. K. (2010). Simple Combinations of Lineage-Determining Transcription Factors Prime cis-Regulatory Elements Required for Macrophage and B Cell Identities. *Molecular Cell*, 38(4), 576–589. <https://doi.org/10.1016/j.molcel.2010.05.004>
- Hu, P., Liu, J., Zhao, J., Wilkins, B. J., Lupino, K., Wu, H., & Pei, L. (2018). Single-nucleus transcriptomic survey of cell diversity and functional maturation in postnatal mammalian hearts. *Genes Dev*, 32(19–20), 1344–1357. <https://doi.org/10.1101/gad.316802.118>
- Itoh, K., Ishii, T., Wakabayashi, N., & Yamamoto, M. (1999). Regulatory mechanisms of cellular response to oxidative stress. *Free Radical Research*, 31(4), 319–324. <https://doi.org/10.1080/10715769900300881>
- Kanatous, S. B., Mammen, P. P. A., Rosenberg, P. B., Martin, C. M., White, M. D., DiMaio, J. M., Huang, G., Muallem, S., & Garry, D. J. (2009). Hypoxia reprograms calcium signaling and regulates myoglobin expression. *American Journal of Physiology - Cell Physiology*, 296(3), 393–402. <https://doi.org/10.1152/ajpcell.00428.2008>
- Kannan, M. B., Solovieva, V., & Blank, V. (2012). The small MAF transcription factors MAFF, MAFG and MAFK: Current knowledge and perspectives. *Biochimica et Biophysica Acta - Molecular Cell Research*, 1823(10), 1841–1846. <https://doi.org/10.1016/j.bbamcr.2012.06.012>
- Kannan, S., Miyamoto, M., Lin, B. L., Zhu, R. J., Murphy, S., Kass, D. A., Andersen, P., & Kwon, C. (2019). Large Particle Fluorescence-Activated Cell Sorting Enables High-Quality Single-Cell RNA Sequencing and Functional Analysis of Adult Cardiomyocytes. *Circulation Research*, 125(5), 567–569. <https://doi.org/10.1161/Circresaha.119.315493>
- Kolodziejczyk, A. A., Kim, J. K., Svensson, V., Marioni, J. C., & Teichmann, S. A. (2015). The technology and biology of single-cell RNA sequencing. *Mol Cell*, 58(4), 610–620. <https://doi.org/10.1016/j.molcel.2015.04.005>
- Kolodziejczyk, S. M., Wang, L., Balazsi, K., Derepentigny, Y., Kothary, R., & Megeney, L. A. (1999). MEF2 is upregulated during cardiac hypertrophy and is required for normal post-natal growth of the myocardium. *Current Biology*, 9(20), 1203–1206. [https://doi.org/10.1016/S0960-9822\(00\)80027-5](https://doi.org/10.1016/S0960-9822(00)80027-5)
- Kretzschmar, K., Post, Y., Banner-Helaouet, M., Mattiotti, A., Drost, J., Basak, O., Li, V. S. W.,

- van den Born, M., Gunst, Q. D., Versteeg, D., Kooijman, L., van der Elst, S., van Es, J. H., van Rooij, E., van den Hoff, M. J. B., & Clevers, H. (2018). Profiling proliferative cells and their progeny in damaged murine hearts. *Proc Natl Acad Sci U S A*, 115(52), E12245–E12254. <https://doi.org/10.1073/pnas.1805829115>
- Larson, A., & Chin, M. T. (2021). A method for cryopreservation and single nucleus RNA-sequencing of normal adult human interventricular septum heart tissue reveals cellular diversity and function. *BMC Medical Genomics*, 14(1), 1–8. <https://doi.org/10.1186/s12920-021-01011-z>
- Li, H., & Durbin, R. (2009). Fast and accurate short read alignment with Burrows-Wheeler transform. *Bioinformatics*, 25(14), 1754–1760. <https://doi.org/10.1093/bioinformatics/btp324>
- Liao, Y., Smyth, G. K., & Shi, W. (2014). FeatureCounts: An efficient general purpose program for assigning sequence reads to genomic features. *Bioinformatics*, 30(7), 923–930. <https://doi.org/10.1093/bioinformatics/btt656>
- Lim, D. S., Roberts, R., & Marian, A. J. (2001). Expression profiling of cardiac genes in human hypertrophic cardiomyopathy: insight into the pathogenesis of phenotypes. *Journal of the American College of Cardiology*, 38(4), 1175–1180. [https://doi.org/10.1016/s0735-1097\(01\)01509-1](https://doi.org/10.1016/s0735-1097(01)01509-1)
- Litviňuková, M., Talavera-López, C., Maatz, H., Reichart, D., Worth, C. L., Lindberg, E. L., Kanda, M., Polanski, K., Heinig, M., Lee, M., Nadelmann, E. R., Roberts, K., Tuck, L., Fasouli, E. S., DeLaughter, D. M., McDonough, B., Wakimoto, H., Gorham, J. M., Samari, S., ... Teichmann, S. A. (2020). Cells of the adult human heart. *Nature*, September. <https://doi.org/10.1038/s41586-020-2797-4>
- Long, P. A., Larsen, B. T., Evans, J. M., & Olson, T. M. (2015). Exome sequencing identifies pathogenic and modifier mutations in a child with sporadic dilated cardiomyopathy. *Journal of the American Heart Association*, 4(12), 1–11. <https://doi.org/10.1161/JAHA.115.002443>
- Man, J., Barnett, P., & Christoffels, V. M. (2018). Structure and function of the Nppa-Nppb cluster locus during heart development and disease. *Cell Mol Life Sci*, 75(8), 1435–1444. <https://doi.org/10.1007/s00018-017-2737-0>
- Marian, A. J. (2010). Hypertrophic cardiomyopathy: from genetics to treatment. *Eur J Clin Invest*, 40(4), 360–369.
- Marian, A. J., & Braunwald, E. (2017). Hypertrophic Cardiomyopathy: Genetics, Pathogenesis, Clinical Manifestations, Diagnosis, and Therapy. *Circ Res*, 121(7), 749–770. <https://doi.org/10.1161/CIRCRESAHA.117.311059>
- Maron, B. J., & Maron, M. S. (2013). Hypertrophic cardiomyopathy. *Lancet*, 381(9862), 242–255. [https://doi.org/10.1016/S0140-6736\(12\)60397-3](https://doi.org/10.1016/S0140-6736(12)60397-3)
- Maron, B. J., Ommen, S. R., Semsarian, C., Spirito, P., Olivetto, I., & Maron, M. S. (2014). Hypertrophic cardiomyopathy: Present and future, with translation into contemporary cardiovascular medicine. *Journal of the American College of Cardiology*, 64(1), 83–99. <https://doi.org/10.1016/j.jacc.2014.05.003>
- Martin, M. (2011). Cutadapt removes adapter sequences from high-throughput sequencing reads. *EMBnet.Journal*.
- Mirtschink, P., & Krek, W. (2016). Hypoxia-driven glycolytic and fructolytic metabolic programs: Pivotal to hypertrophic heart disease. *Biochimica et Biophysica Acta - Molecular Cell Research*, 1863(7), 1822–1828. <https://doi.org/10.1016/j.bbamcr.2016.02.011>
- Montag, J., Kowalski, K., Makul, M., Ernstberger, P., Radocaj, A., Beck, J., Becker, E., Tripathi, S., Keyser, B., Muhlfeld, C., Wissel, K., Pich, A., van der Velden, J., dos Remedios, C. G., Perrot, A., Francino, A., Navarro-Lopez, F., Brenner, B., Kraft, T., ... Kraft, T. (2018). Burst-Like Transcription of Mutant and Wildtype MYH7-Alleles as Possible Origin of Cell-to-Cell Contractile Imbalance in Hypertrophic Cardiomyopathy. *Front Physiol*, 9, 359.

- <https://doi.org/10.3389/fphys.2018.00359>
- Morgan, M., Falcon, S., & Gentleman, R. (2021). GSEABase: Gene set enrichment data structures and methods (1.54.0).
- Muraro, M. J., Dharmadhikari, G., Grün, D., Groen, N., Dielen, T., Jansen, E., van Gurp, L., Engelse, M. A., Carlotti, F., de Koning, E. J. P., & van Oudenaarden, A. (2016). A Single-Cell Transcriptome Atlas of the Human Pancreas. *Cell Systems*, 3(4), 385-394.e3. <https://doi.org/10.1016/j.cels.2016.09.002>
- Nomura, S., Satoh, M., Fujita, T., Higo, T., Sumida, T., Ko, T., Yamaguchi, T., Tobita, T., Naito, A. T., Ito, M., Fujita, K., Harada, M., Toko, H., Kobayashi, Y., Ito, K., Takimoto, E., Akazawa, H., Morita, H., Aburatani, H., & Komuro, I. (2018). Cardiomyocyte gene programs encoding morphological and functional signatures in cardiac hypertrophy and failure. *Nat Commun*, 9(1), 4435. <https://doi.org/10.1038/s41467-018-06639-7>
- Numazawa, S., Ishikawa, M., Yoshida, A., Tanaka, S., & Yoshida, T. (2003). Atypical protein kinase C mediates activation of NF-E2-related factor 2 in response to oxidative stress. *American Journal of Physiology - Cell Physiology*, 285(2 54-2), 1–5. <https://doi.org/10.1152/ajpcell.00043.2003>
- Ortega, A., Roselló-Lletí, E., Tarazón, E., Molina-Navarro, M. M., Martínez-Dolz, L., González-Juanatey, J. R., Lago, F., Montoro-Mateos, J. D., Salvador, A., Rivera, M., & Portolés, M. (2014). Endoplasmic reticulum stress induces different molecular structural alterations in human dilated and ischemic cardiomyopathy. *PLoS ONE*, 9(9). <https://doi.org/10.1371/journal.pone.0107635>
- Parbhudayal, R. Y., Garra, A. R., Götte, M. J. W., Michels, M., Pei, J., Harakalova, M., Asselbergs, F. W., van Rossum, A. C., van der Velden, J., & Kuster, D. W. D. (2018). Variable cardiac myosin binding protein-C expression in the myofilaments due to MYBPC3 mutations in hypertrophic cardiomyopathy. *Journal of Molecular and Cellular Cardiology*, 123(August), 59–63. <https://doi.org/10.1016/j.yjmcc.2018.08.023>
- Passier, R., Zeng, H., Frey, N., Naya, F. J., Nicol, R. L., McKinsey, T. A., Overbeek, P., Richardson, J. A., Grant, S. R., & Olson, E. N. (2000). CaM kinase signaling induces cardiac hypertrophy and activates the MEF2 transcription factor in vivo. *Journal of Clinical Investigation*, 105(10), 1395–1406. <https://doi.org/10.1172/JCI8551>
- Pathak, G. P., Shah, R., Kennedy, B. E., Murphy, J. P., Clements, D., Konda, P., Giacomantonio, M., Xu, Z., Schlaepfer, I. R., & Gujar, S. (2018). RTN4 Knockdown Dysregulates the AKT Pathway, Destabilizes the Cytoskeleton, and Enhances Paclitaxel-Induced Cytotoxicity in Cancers. *Molecular Therapy*, 26(8), 2019–2033. <https://doi.org/10.1016/j.ymthe.2018.05.026>
- Qin, Q., Fan, J., Zheng, R., Wan, C., Mei, S., Wu, Q., Sun, H., Zhang, J., Brown, M., Meyer, C. A., & Shirley Liu, X. (2020). Inferring transcriptional regulators through integrative modeling of public chromatin accessibility and ChIP-seq data. *Genome Biology*. <https://doi.org/10.1101/846139>
- Remme, C. A., Verkerk, A. O., Hoogaars, W. M., Aanhaanen, W. T., Scicluna, B. P., Annink, C., van den Hoff, M. J., Wilde, A. A., van Veen, T. A., Veldkamp, M. W., de Bakker, J. M., Christoffels, V. M., & Bezzina, C. R. (2009). The cardiac sodium channel displays differential distribution in the conduction system and transmural heterogeneity in the murine ventricular myocardium. *Basic Res Cardiol*, 104(5), 511–522. <https://doi.org/10.1007/s00395-009-0012-8>
- Ren, Z., Yu, P., Li, D., Li, Z., Liao, Y., Wang, Y., Zhou, B., & Wang, L. (2020). Single-Cell Reconstruction of Progression Trajectory Reveals Intervention Principles in Pathological Cardiac Hypertrophy. *Circulation*, 141(21), 1704–1719. <https://doi.org/10.1161/CIRCULATIONAHA.119.043053>
- Sasagawa, S., Nishimura, Y., Okabe, S., Murakami, S., Ashikawa, Y., Yuge, M., Kawaguchi, K., Kawase, R., Okamoto, R., Ito, M., & Tanaka, T. (2016). Downregulation of GSTK1 is a

- common mechanism underlying hypertrophic cardiomyopathy. *Frontiers in Pharmacology*, 7(JUN), 1–13. <https://doi.org/10.3389/fphar.2016.00162>
- Schauer, A., Adams, V., Poitz, D. M., Barthel, P., Joachim, D., Friedrich, J., Linke, A., & Augstein, A. (2019). Loss of Sox9 in cardiomyocytes delays the onset of cardiac hypertrophy and fibrosis. *International Journal of Cardiology*, 282, 68–75. <https://doi.org/10.1016/j.ijcard.2019.01.078>
- Schroeder, A., Mueller, O., Stocker, S., Salowsky, R., Leiber, M., Gassmann, M., Lightfoot, S., Menzel, W., Granzow, M., & Ragg, T. (2006). The RIN: an RNA integrity number for assigning integrity values to RNA measurements. *Bmc Molecular Biology*, 7. <https://doi.org/Artn 3 10.1186/1471-2199-7-3>
- Selewa, A., Dohn, R., Eckart, H., Lozano, S., Xie, B., Gauchat, E., Elorbany, R., Rhodes, K., Burnett, J., Gilad, Y., Pott, S., & Basu, A. (2020). Systematic Comparison of High-throughput Single-Cell and Single-Nucleus Transcriptomes during Cardiomyocyte Differentiation. *Scientific Reports*, 10(1), 1–13. <https://doi.org/10.1038/s41598-020-58327-6>
- Semsarian, C., Ingles, J., Maron, M. S., & Maron, B. J. (2015). New perspectives on the prevalence of hypertrophic cardiomyopathy. *Journal of the American College of Cardiology*. <https://doi.org/10.1016/j.jacc.2015.01.019>
- Sereti, K. I., Nguyen, N. B., Kamran, P., Zhao, P., Ranjbarvaziri, S., Park, S., Sabri, S., Engel, J. L., Sung, K., Kulkarni, R. P., Ding, Y., Hsiai, T. K., Plath, K., Ernst, J., Sahoo, D., Mikkola, H. K. A., Iruela-Arispe, M. L., & Ardehali, R. (2018). Analysis of cardiomyocyte clonal expansion during mouse heart development and injury. *Nat Commun*, 9(1), 754. <https://doi.org/10.1038/s41467-018-02891-z>
- Sheikh, F., Lyon, R. C., & Chen, J. (2015). Functions of myosin light chain-2 (MYL2) in cardiac muscle and disease. *Gene*, 569(1), 14–20. <https://doi.org/10.1016/j.gene.2015.06.027>
- Shim, W. J., Sinniah, E., Xu, J., Vitrinel, B., Alexanian, M., Andreoletti, G., Shen, S., Sun, Y., Balderson, B., Boix, C., Peng, G., Jing, N., Wang, Y., Kellis, M., Tam, P. P. L., Smith, A., Piper, M., Christiaan, L., Nguyen, Q., ... Palpant, N. J. (2020). Conserved Epigenetic Regulatory Logic Informs Genes Governing Cell Identity. *Cell Systems*, 11(6), 625–639.e13. <https://doi.org/10.1016/j.cels.2020.11.001>
- Skelly, D. A., Squiers, G. T., McLellan, M. A., Bolisetty, M. T., Robson, P., Rosenthal, N. A., & Pinto, A. R. (2018). Single-Cell Transcriptional Profiling Reveals Cellular Diversity and Intercommunication in the Mouse Heart. *Cell Reports*, 22(3), 600–610. <https://doi.org/10.1016/j.celrep.2017.12.072>
- Smith, P. J., Wiltshire, M., & Errington, R. J. (2004). DRAQ5 labeling of nuclear DNA in live and fixed cells. *Curr Protoc Cytom*, Chapter 7, Unit 7 25. <https://doi.org/10.1002/0471142956.cy0725s28>
- Smith, T., Heger, A., & Sudbery, I. (2017). UMI-tools: Modelling sequencing errors in Unique Molecular Identifiers to improve quantification accuracy. *Genome Research*.
- Sorenson D.; Sonnenblick, E.H., Robinson, T.F.; Capasso J.M., A. L. ; T. (1985). Size and shape of enzymatically isolated ventricular myocytes from rats and cardiomyopathic hamsters. *Cardiovasc Res*, 19(12), 793–799.
- Stuart, T., Butler, A., Hoffman, P., Hafemeister, C., Iii, W. M. M., Stoekius, M., Smibert, P., & Satija, R. (2018). Comprehensive integration of single cell data. *BioRxiv*, 1–24. <https://doi.org/10.1101/460147>
- Tan, W. L. W., Lim, B. T. S., Anene-Nzulu, C. G. O., Ackers-Johnson, M., Dashi, A., See, K., Tiang, Z., Lee, D. P., Chua, W. W., Luu, T. D. A., Li, P. Y. Q., Richards, A. M., & Foo, R. S. Y. (2017). A landscape of circular RNA expression in the human heart. *Cardiovascular Research*, 113(3), 298–309. <https://doi.org/10.1093/cvr/cwv250>
- van der Velden, J., Merkus, D., de Beer, V., Hamdani, N., Linke, W. A., Boontje, N. M., Stienen, G. J., & Duncker, D. J. (2011). Transmural heterogeneity of myofilament function and sarcomeric protein phosphorylation in remodeled myocardium of pigs with a recent

- myocardial infarction. *Front Physiol*, 2, 83. <https://doi.org/10.3389/fphys.2011.00083>
- Vigil-Garcia, M., Demkes, C. J., Eding, J. E. C., Versteeg, D., De Ruiter, H., Perini, I., Kooijman, L., Gladka, M. M., Asselbergs, F. W., Vink, A., Harakalova, M., Bossu, A., Van Veen, T. A. B., Boogerd, C. J., & Van Rooij, E. (2021). Gene expression profiling of hypertrophic cardiomyocytes identifies new players in pathological remodelling. *Cardiovascular Research*, 117(6), 1532–1545. <https://doi.org/10.1093/cvr/cvaa233>
- Wang, L., Yu, P., Zhou, B., Song, J., Li, Z., Zhang, M., Guo, G., Wang, Y., Chen, X., Han, L., & Hu, S. (2020). Single-cell reconstruction of the adult human heart during heart failure and recovery reveals the cellular landscape underlying cardiac function. *Nat Cell Biol*, 22(1), 108–119. <https://doi.org/10.1038/s41556-019-0446-7>
- Wang, T. Y., Lee, D., Fox-Talbot, K., Arking, D. E., Chakravarti, A., & Halushka, M. K. (2018). Cardiomyocytes have mosaic patterns of protein expression. *Cardiovascular Pathology*, 34, 50–57. <https://doi.org/https://doi.org/10.1016/j.carpath.2018.03.002>
- Zhang, X., Azhar, G., Chai, J., Sheridan, P., Nagano, K., Brown, T., Yang, J., Khrapko, K., Borras, A. M., Lawitts, J., Misra, R. P., & Wei, J. Y. (2001). Cardiomyopathy in transgenic mice with cardiac-specific overexpression of serum response factor. *American Journal of Physiology - Heart and Circulatory Physiology*, 280(4 49-4), 1782–1792. <https://doi.org/10.1152/ajpheart.2001.280.4.h1782>

Supplemental Material

Supplemental Datasets (available online)

Supplemental Data 1. Full data tables of gene enrichment analysis on clusters in pooled data from HCM, Ctrl1 and Ctrl2.

Supplemental Data 2. Full data tables of gene enrichment analysis on clusters of the HCM CMs.

Supplemental Data 3. Full data table of the correlation analysis of NPPA with all other genes.

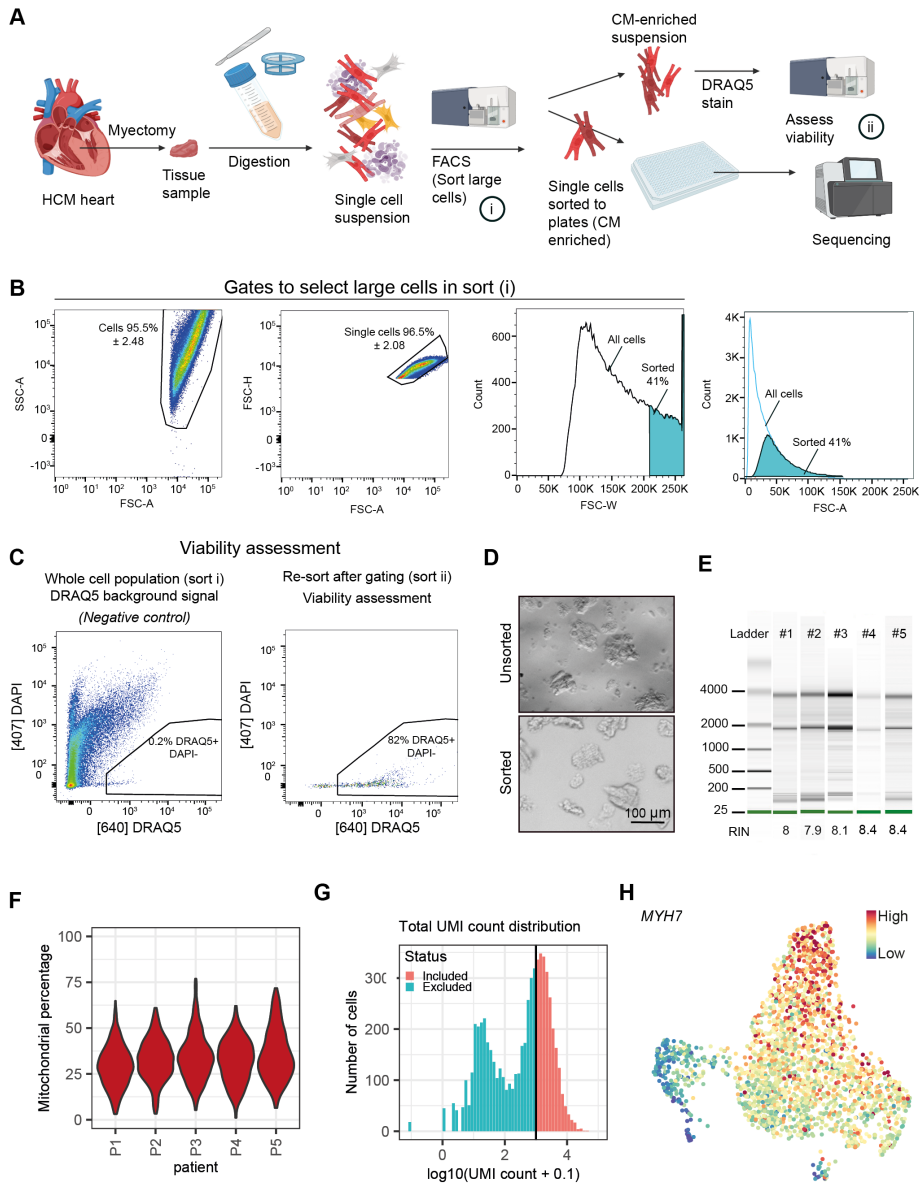
Supplemental Data 4. Full data table of the correlation analysis of XIRP2 with all other genes.

Supplemental Data 5. Full list of regulon member genes and their associated TFs identified by SCENIC for all patients.

Supplemental Data 6. Full list of module member genes identified by our custom co-expression analysis.

Supplemental Data 7. Full data table of the correlation analysis between FSC-A (cell size) and gene expression.

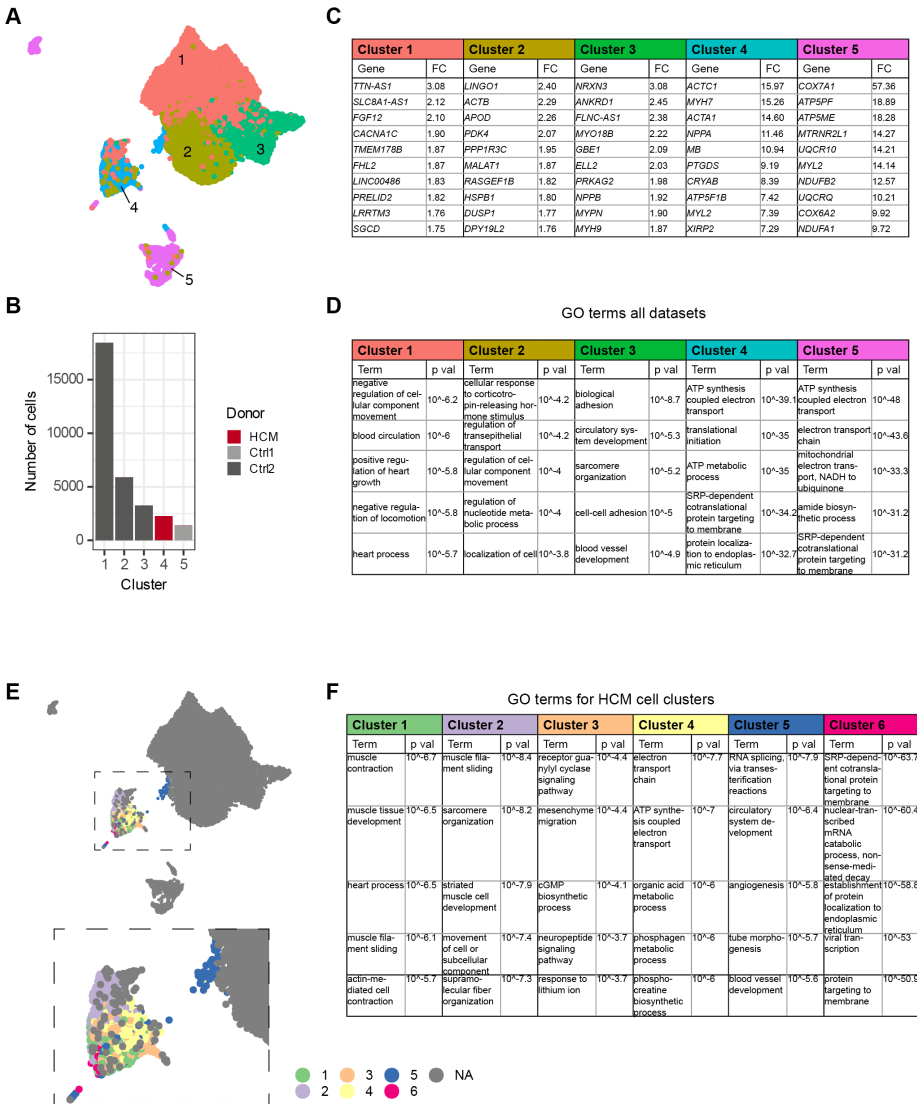
Supplemental Data 8. Full data table with CT values related to the RT-PCR experiments.



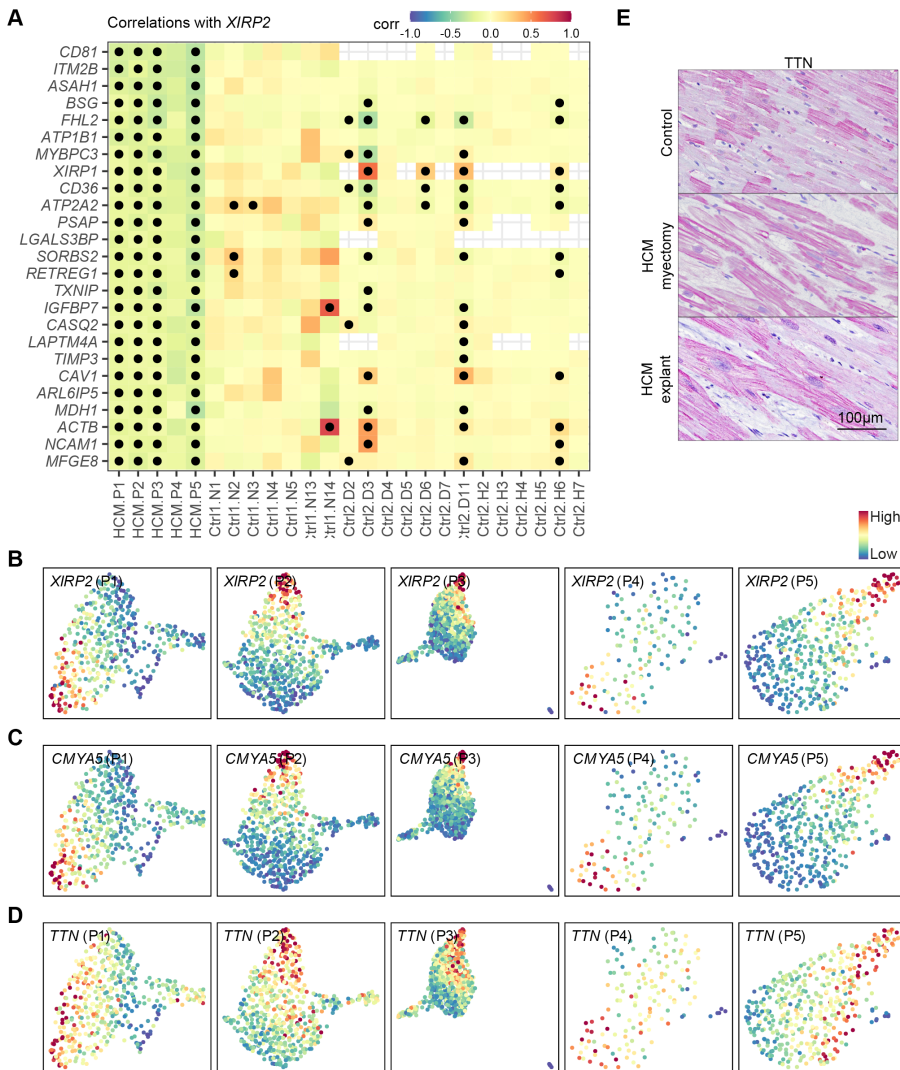
Supplemental Figure 1. FACS gating strategy and quality control for scRNA-seq, related to Figure 1. (A) Cartoon of the experimental strategy used in this paper. HCM myectomy samples were digested and sorted into 384 well plates according to a previously optimized protocol (Gladka et al., 2018). Additionally, quality controls were performed on the cells sorted in (i), by DRAQ5 staining and re-sorting (ii), microscopy and determining RIN values.

(B) Size gates used in the gating protocol. **(C)** DAPI and DRAQ5 staining in combination with FACS to show sorted events are not cells with compromised membranes (which would be DAPI+), but do contain nucleated cells (DRAQ5+). As a control, we first show that the fraction of the whole cell population that is DRAQ5+/DAPI- without DRAQ5 staining, is 0.2%. This shows there is little false positive signal. Then, we added DRAQ5 staining to the sorted cell population, and re-sorted the cells, which showed 82% of cells are DRAQ5 +/DAPI-. (Note that the gates shown here are not used for sorting, but only to calculate the fraction of events

that are DRAQ5+/DAPI-.) **(D)** Representative images of unsorted (top image) and sorted cells (bottom image) showing sorted cells to be intact. **(E)**, RNA quality control of sorted cells from HCM myectomy tissues. **(F)** Violin plot of the percentage mitochondrial genes in sorted cells per HCM patient. **(G)** Histogram showing distribution of number of reads per well. Line represents the 1000 reads/well cut-off for inclusion in the analysis. **(H)** UMAP showing the expression of *MYH7* gene expression in the cells included in this study. SSC indicates side scatter; FACS, fluorescence-activated cell sorting; FSC-A, forward scatter area; FSC-H, forward scatter height; FSC-W, forward scatter width; RIN, RNA integrity number; UMAP, Uniform Manifold Approximation and Projection.

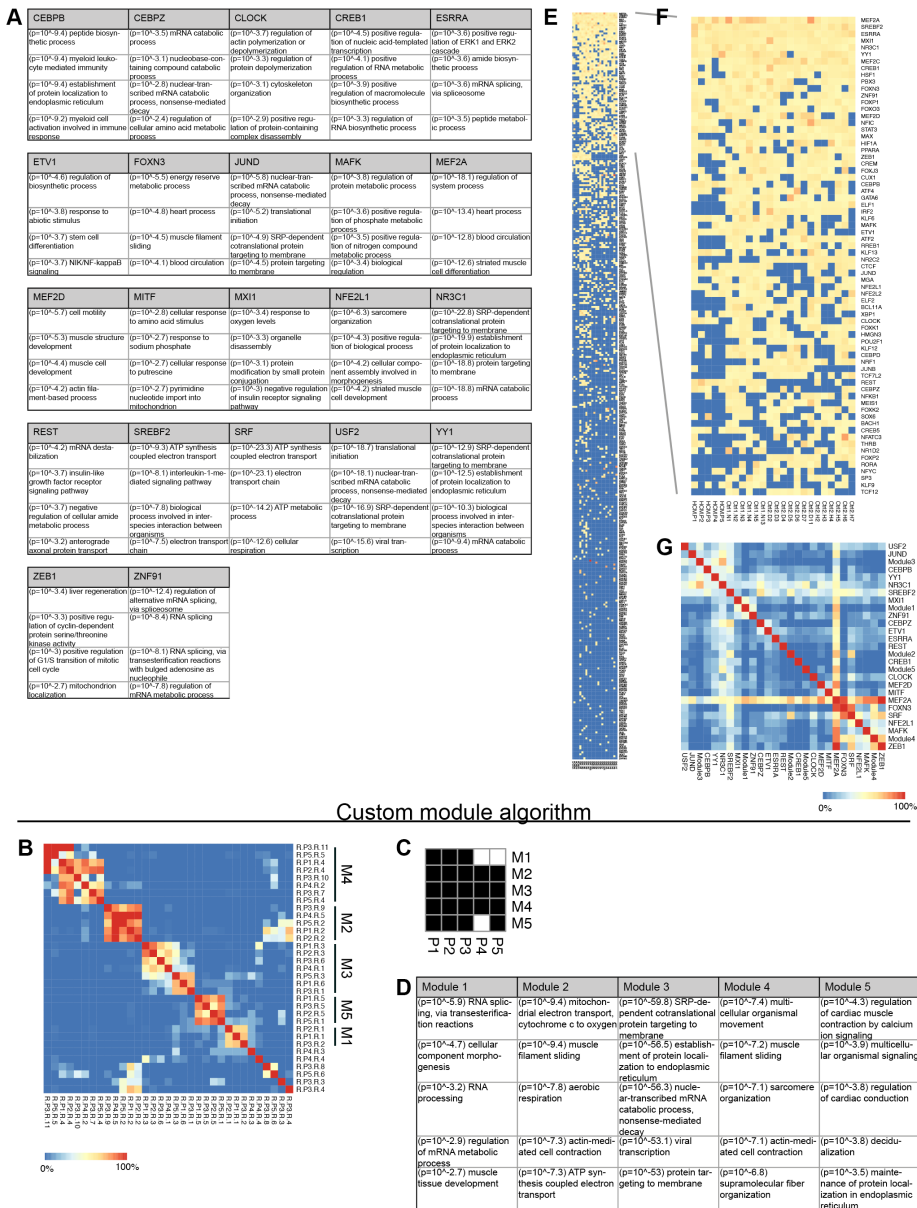


Supplemental Figure 2. Clustering analysis on pooled cells from HCM, Ctrl1 and Ctrl2 and GO terms for HCM clusters, related to Figure 1. (A) UMAP showing cell clusters identified by Seurat in the pooled HCM, Ctrl1 and Ctrl2 data. **(B)** Number of cells per cluster, and the distribution of cell origin over the clusters (HCM, Ctrl1 or Ctrl2 are indicated by red, light gray and dark grey respectively), indicating that the large majority of HCM cells cluster together. **(C)** Table showing the most expressed genes in all clusters, including fold-change enrichment. **(D)** Gene ontology analysis of enriched genes ($p < 0.05$, $FC > 1.1$) identified for clusters shown in (A). **(E)** Clusters determined by Seurat based on HCM cells only (see Fig. 1E), projected on an UMAP of the pooled HCM, Ctrl1 and Ctrl2 datasets. **(F)** Gene ontology analysis of enriched genes ($p < 0.05$, $FC > 1.1$) for clusters determined in the HCM subset of cells.



Supplemental Figure 3. Genes negatively related to *XIRP2*, *TTN* staining, and patient-specific gene expression of *XIRP2*, *CMYA5* and *TTN*, related to Figure 3. (A) Gene expression correlations with *XIRP2* expression for the genes listed, shown separately for each of the patients and donors. A t-test was performed with Benjamini & Hochberg correction, black dots indicate that the correlation is considered significant ($p < 0.05$). **(B-D)** UMAPs showing the expression of *XIRP2*, *CMYA5*, and *TTN* gene expression for each of the HCM patients, respectively. **(E)** Immunohistochemical staining of septal tissue showing *TTN*-expression in an explanted control heart, HCM myectomy tissue and an explanted HCM heart. UMAP, Uniform Manifold Approximation and Projection.

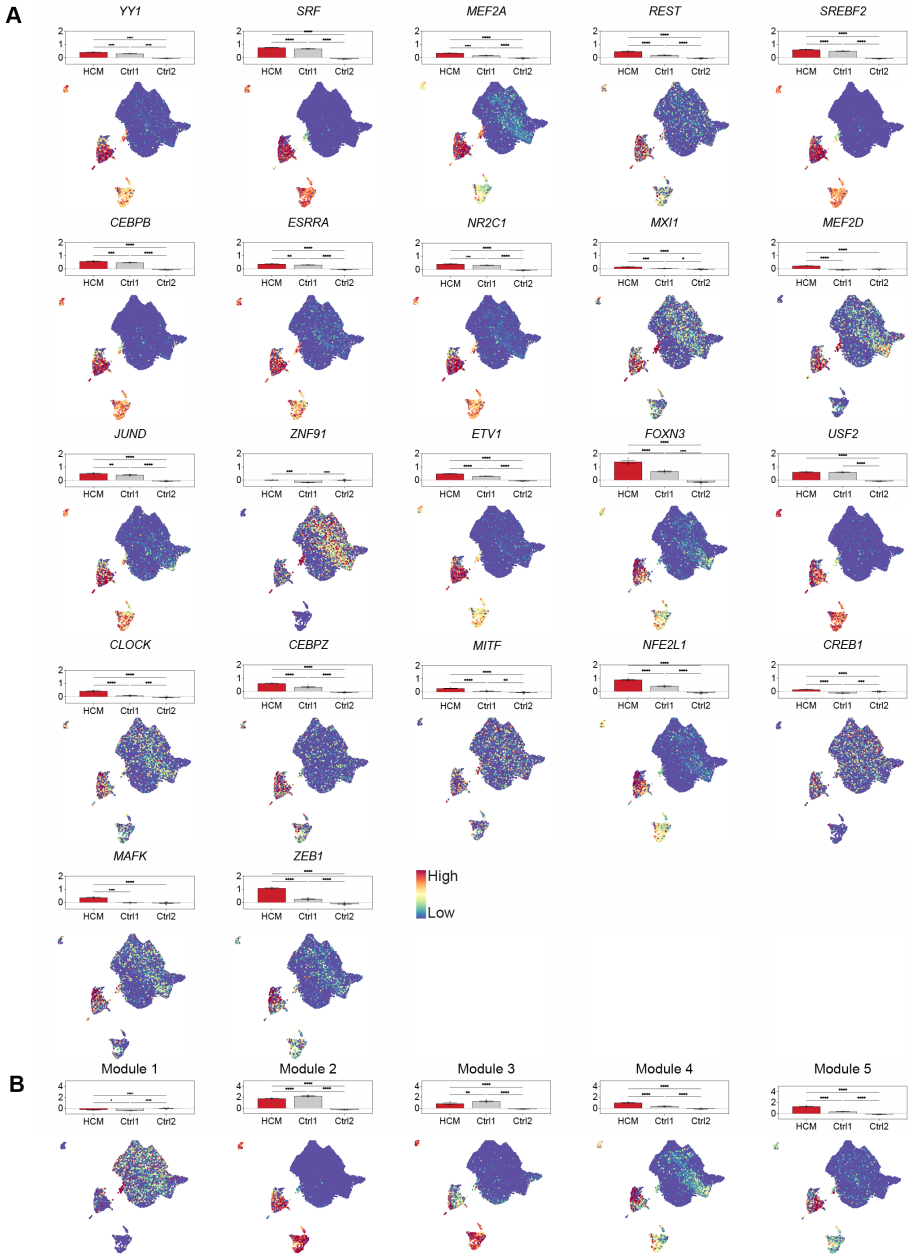
SCENIC



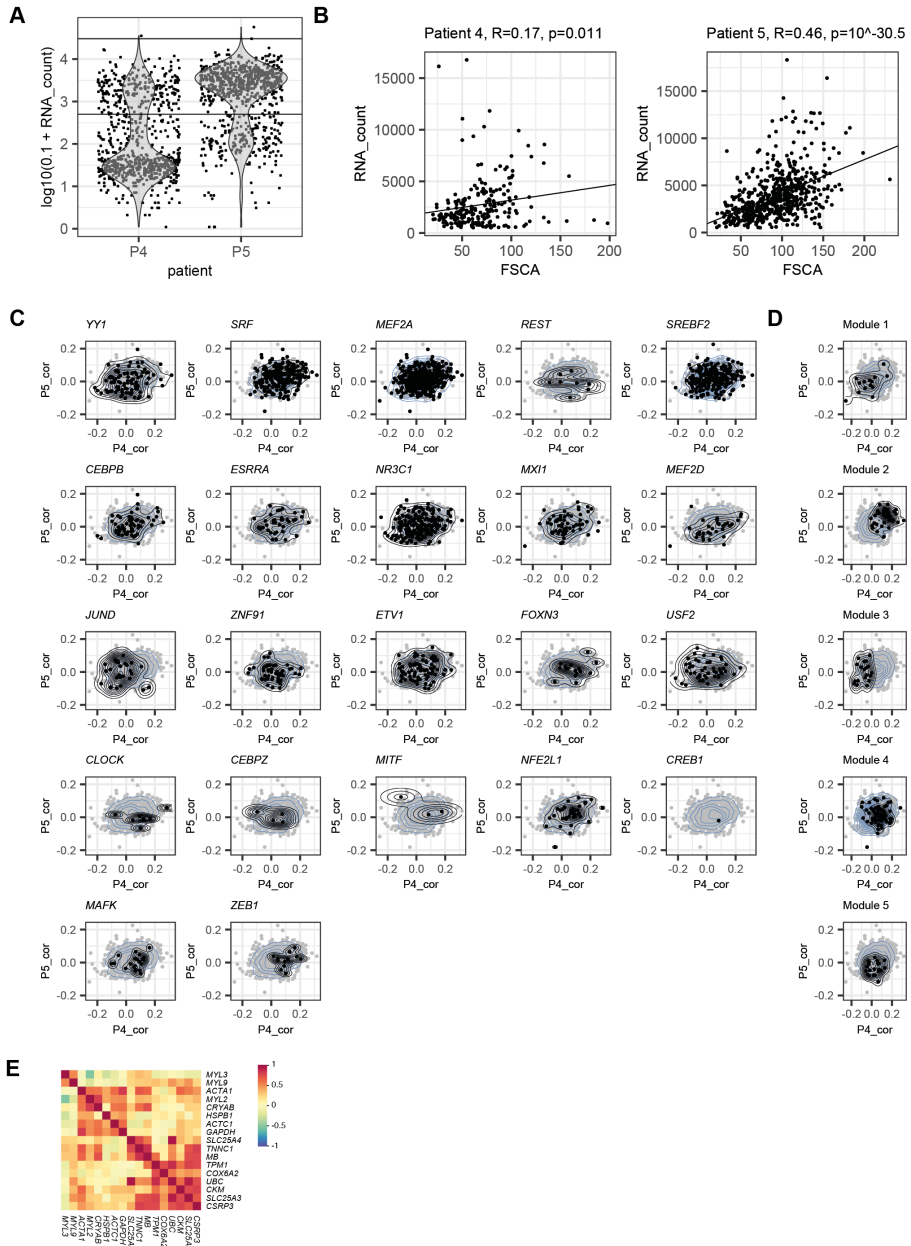
Custom module algorithm

Supplemental Figure 4. GO term analysis and patient-specificity of SCENIC regulons and modules, related to figure 4 and 5. (A) GO term analysis for regulons determined using SCENIC. **(B)** Construction of co-expression modules using a custom algorithm. Initial modules were first identified per patient, and then merged based on member gene similarity, which is indicated in the heatmap. Note that by construction, modules from the same patient cannot have overlapping member genes. **(C)** Specificity of the custom modules for

the different HCM patients. A black square indicates that the respective module (M1-5) was identified in the respective patient (P1-P5). **(D)** GO term analysis for modules determined using our custom algorithm. **(E)** A heatmap showing which SCENIC regulons were identified in which patients and donors over the HCM, Ctrl1 and Ctrl2 datasets. Color coding indicates the absence of the regulon (blue) or reflects the normalized area under the curve score (NES), which indicates the confidence in the link between the respective TFs and its associated genes (yellow to red). **(F)** As E, but only showing first 70 rows. **(G)** Fraction of overlapping member genes between the different SCENIC regulons and custom co-expression modules.



Supplemental Figure 5. Regulons and module expression in pooled HCM, Ctrl1 and Ctrl2 data, related to Figure 4 and Figure 5. (A-B) Bar graphs and UMAPs showing the composite expression (average of Z-score normalized expression of member genes) of SCE-NIC regulons **(A)** or modules **(B)** in all datasets. Bar graphs show mean composite expression per patient. Outliers were removed by using the ROUT test with Q=1% and a one-way ANOVA test was performed. *, $P \leq 0.05$; **, $P \leq 0.01$, ***, $P \leq 0.001$; ****, $P \leq 0.0001$.*, $P \leq 0.05$; **, $P \leq 0.01$, ***, $P \leq 0.001$; ****, $P \leq 0.0001$.



Supplemental Figure 6. Correlations between RNA, regulons, and modules to cell size, and qPCR validation of module 2, related to Figure 6. (A) Violin plot showing the UMI count distribution over wells for patient 4 and 5, lines indicate data used for the correlation calculation in B. **(B)** Correlation analysis between the total mRNA count and cell size according to FSC-A for each well. **(C-D)** Scatter plots of size-expression correlation coefficients per gene (grey dots) determined from patient 4 (X-axis) versus patient 5 (Y-axis). Blue lines indi-

cate the density of grey dots. In black, member genes of respective regulons (C) or modules (D) are highlighted, with black lines indicating the density of the black dots. **(E)** Heatmap of Pearson's correlations between genes identified in module 2 based on RT-PCR data of bulk samples. Samples were normalized to *RPL32*. FSC-A indicates forward scatter area.

| Patients included for Single cell sequencing and histology | | | | | | | |
|--|-----|-------|----------|------------------|---------------|--------------------|---------------|
| FHCM | Sex | Age | Mutation | DNA | Prot | Tissue destination | Manuscript ID |
| HCM202 | F | 65 | unknown | - | - | SCS | HCM.P1 |
| HCM204 | M | 30 | MYBPC3 | c.2373dupG | p.Trp792fs | SCS | HCM.P2 |
| HCM214 | M | 60 | SMN | - | - | Histo | |
| HCM215 | F | 74 | unknown | - | - | SCS/Histo | HCM.P3 |
| HCM218 | M | 50 | unknown | - | - | Histo | |
| HCM229 | M | 57 | SMN | - | - | Histo | |
| HCM230 | M | 66 | MYBPC3 | c.2864_2865delCT | p.Pro955Argfs | Index/SCS/Histo | HCM.P4 |
| HCM234 | M | 72 | TNNT | c.832C>T | p.Arg278Cys | Histo | |
| HCM258 | M | 37 | unknown | - | - | DRAQ5/Index/SCS | HCM.P5 |
| Control cardiomyocytes | | | | | | | |
| Control | Sex | Age | Mutation | DNA | Prot | Tissue destination | Manuscript ID |
| | M | 46 | - | - | - | SCS | Ctrl1.N1 |
| | F | 33 | - | - | - | SCS | Ctrl1.N2 |
| | M | 51 | - | - | - | SCS | Ctrl1.N3 |
| | M | 46 | - | - | - | SCS | Ctrl1.N4 |
| | M | 43 | - | - | - | SCS | Ctrl1.N5 |
| | M | 21 | - | - | - | SCS | Ctrl1.N6 |
| | F | 49 | - | - | - | SCS | Ctrl1.N13 |
| | M | 42 | - | - | - | SCS | Ctrl1.N14 |
| | M | 60-65 | - | - | - | SCS | Ctrl2.D2 |
| | M | 55-60 | - | - | - | SCS | Ctrl2.D3 |
| | F | 70-75 | - | - | - | SCS | Ctrl2.D4 |
| | F | 65-70 | - | - | - | SCS | Ctrl2.D5 |
| | M | 70-75 | - | - | - | SCS | Ctrl2.D6 |
| | M | 60-65 | - | - | - | SCS | Ctrl2.D7 |
| | M | 50-55 | - | - | - | SCS | Ctrl2.H2 |
| | M | 50-55 | - | - | - | SCS | Ctrl2.H3 |
| | M | 55-60 | - | - | - | SCS | Ctrl2.H4 |
| | F | 50-55 | - | - | - | SCS | Ctrl2.H5 |
| | F | 40-45 | - | - | - | SCS | Ctrl2.H6 |
| | F | 45-50 | - | - | - | SCS | Ctrl2.H7 |
| Patients included for quantitative PCR analysis | | | | | | | |
| FHCM | Sex | Age | Mutation | DNA | Prot | Tissue destination | |
| Control1 | M | 24 | - | - | - | qPCR | |
| Control2 | M | 27 | - | - | - | qPCR | |
| Control3 | M | 21 | - | - | - | qPCR | |
| Control4 | M | 21 | - | - | - | qPCR | |
| Control5 | F | 49 | - | - | - | qPCR | |
| Control6 | M | 55 | - | - | - | qPCR | |
| Control7 | M | 40 | - | - | - | qPCR | |

Single-cell transcriptomics provides insights into hypertrophic cardiomyopathy

| | | | | | | |
|----------|------|------|--------------|--------------------------|-----------------------------|------|
| Control8 | M | 33 | - | - | - | qPCR |
| Control9 | F | 50 | - | - | - | qPCR |
| HCM5 | F | 41 | MYBPC3 | c.1458-1G>C | - | qPCR |
| HCM21 | F | 75 | SMN | - | - | qPCR |
| HCM22 | M | 52 | SMN | - | - | qPCR |
| HCM27 | F | 58 | MYH7 | c.4130C>T | p.Thr1377Met | qPCR |
| HCM30 | F | 72 | SMN | - | - | qPCR |
| HCM33 | M | 43 | MYBPC3 | c.927-2A>G | - | qPCR |
| HCM34 | F | 48 | MYBPC3 | c.1790G>A | p.Arg597Gln | qPCR |
| HCM35 | F | 47 | MYBPC3 | c.1608T>A | - | qPCR |
| HCM36 | M | 22 | MYBPC3 | c.927-2A>G | - | qPCR |
| HCM37 | M | 60 | unknown | - | - | qPCR |
| HCM39 | M | 49 | SMN | - | - | qPCR |
| HCM41 | M | 46 | SMN | - | - | qPCR |
| HCM42A | M | 67 | TTN TTN | 33515dupA c.60721G>C | - | qPCR |
| HCM42B | F | 46 | MYH7 | 1816G>A | p.Val606Met | qPCR |
| HCM47 | M | 55 | MYBPC3 | c.3407_3409del | p.Tyr1136del | qPCR |
| HCM48 | M | 49 | unknown | - | - | qPCR |
| HCM50 | M | 32 | unknown | - | - | qPCR |
| HCM51 | M | 59 | TTN TTN | c.65389T>G c.82979T>C | - | qPCR |
| HCM52 | F | 24 | MYBPC3 | c.2827C>T | p.Arg943X | qPCR |
| HCM53 | M | 54 | unknown | - | - | qPCR |
| HCM56 | F | 49 | SMN | - | - | qPCR |
| HCM57 | M | 46 | SMN | - | - | qPCR |
| HCM58 | M | 37 | MYBPC3 | c.927-2A>G | - | qPCR |
| HCM60 | F | 45 | MYBPC3 | c.3029delAG | p.Glu1010fs | qPCR |
| HCM62 | M | 35 | MYBPC3 | c.772G>A | p.Glu258Lys | qPCR |
| HCM63 | M | 33 | MYBPC3 | c.2827C>T | p.Arg943X | qPCR |
| HCM64 | NA ‡ | NA ‡ | unknown | - | - | qPCR |
| HCM65 | F | 72 | unknown | - | - | qPCR |
| HCM66 | M | 45 | MYBPC3 | c.3776delA | p.Gln1259fs | qPCR |
| HCM67 | M | 33 | unknown | - | - | qPCR |
| HCM68 | M | 63 | SMN | - | - | qPCR |
| HCM69 | M | 72 | unknown | - | - | qPCR |
| HCM70 | F | 52 | unknown | - | - | qPCR |
| HCM71 | M | 49 | MYBPC3 | c.2827C>T | p.Arg943X | qPCR |
| HCM72 | M | 47 | unknown | - | - | qPCR |
| HCM73 | M | 60 | MYBPC3 | c.3776delA | - | qPCR |
| HCM74 | F | 46 | SMN | - | - | qPCR |
| HCM76 | F | 56 | SMN | - | - | qPCR |
| HCM77 | F | 79 | unknown | - | - | qPCR |
| HCM78 | M | 52 | SMN | - | - | qPCR |
| HCM79 | M | 58 | unknown | - | - | qPCR |
| HCM80 | M | 34 | MYH7 MYH7 | c.1291G>C c.4327G>A | p.Val431Leu p.Asp1443Asn | qPCR |
| HCM81 | F | 60 | SMN | - | - | qPCR |
| HCM82 | M | 71 | MYBPC3 | c.2783C>T | p.Ser928Leu | qPCR |
| HCM84 | M | 52 | SMN | - | - | qPCR |
| HCM85 | M | 39 | unknown | - | - | qPCR |
| HCM86 | F | 69 | unknown | - | - | qPCR |
| HCM87 | F | 53 | unknown | - | - | qPCR |

| | | | | | | |
|--------|---|----|------------------|------------------------|---------------------------|------|
| HCM88 | F | 57 | MYL2 | c.401A>C | p.Glu134Ala | qPCR |
| HCM89 | M | 59 | SMN | - | - | qPCR |
| HCM90 | M | 53 | SMN | - | - | qPCR |
| HCM91 | M | 26 | SMN | - | - | qPCR |
| HCM92 | M | 66 | MYH7 | c.2685A>C | p.Gln895His | qPCR |
| HCM93 | M | 57 | unknown | - | - | qPCR |
| HCM94 | F | 66 | MYBPC3 | c.1831G>A | - | qPCR |
| HCM95 | M | 62 | unknown | - | - | qPCR |
| HCM96 | M | 74 | SMN | - | - | qPCR |
| HCM97 | M | 62 | unknown | - | - | qPCR |
| HCM98 | M | 63 | SMN | - | - | qPCR |
| HCM99 | F | 42 | unknown | - | - | qPCR |
| HCM100 | M | 41 | unknown | - | - | qPCR |
| HCM101 | M | 20 | MYBPC3 | c.1458-1G>C | - | qPCR |
| HCM102 | F | 69 | SMN | - | - | qPCR |
| HCM103 | M | 26 | MYBPC3 | c.2373dupG | p.Trp792fs | qPCR |
| HCM104 | M | 33 | MYBPC3 | c.2373dupG | p.Trp792fs | qPCR |
| HCM105 | M | 65 | CSRP3 | c.131T>C | p.Leu44Pro | qPCR |
| HCM106 | M | 35 | MYH7 | c.2783A>T | p.Asp928Val | qPCR |
| HCM107 | F | 56 | unknown | - | - | qPCR |
| HCM108 | F | 67 | SMN | - | - | qPCR |
| HCM109 | F | 71 | unknown | - | - | qPCR |
| HCM110 | M | 39 | MYBPC3 MYL2 | c.1000G>T c.64G>A | p.Glu334Ter p.Glu22Lys | qPCR |
| HCM111 | F | 66 | SMN | - | - | qPCR |
| HCM112 | F | 52 | SMN | - | - | qPCR |
| HCM113 | M | 21 | "MYBPC3 DSG2" | c.2827C>T c.2434G>A | p.Arg943X | qPCR |
| HCM114 | M | 69 | MYH7 | c.976G>C | p.Ala326Pro | qPCR |
| HCM115 | F | 21 | SMN | - | - | qPCR |
| HCM116 | F | 53 | MYBPC3 | c.2827C>T | p.Arg943X | qPCR |
| HCM117 | F | 50 | SMN | - | - | qPCR |
| HCM118 | M | 46 | unknown | - | - | qPCR |
| HCM119 | M | 41 | SMN | - | - | qPCR |
| HCM120 | M | 27 | MYBPC3 | c.2373dupG | p.Trp792fs | qPCR |
| HCM121 | F | 55 | MYBPC3 | - | p.Gln1259Arg | qPCR |
| HCM122 | M | 50 | MYBPC3 | c.3331-2A>G | - | qPCR |
| HCM123 | F | 59 | MYBPC3 | c.2373dupG | - | qPCR |
| HCM124 | M | 53 | MYBPC3 ABCC9 | c.2827C>T | p.Arg943X | qPCR |
| HCM125 | M | 66 | SMN | - | - | qPCR |
| HCM126 | F | 64 | unknown | - | - | qPCR |
| HCM127 | M | 33 | unknown | - | - | qPCR |
| HCM128 | F | 62 | unknown | - | - | qPCR |
| HCM129 | F | 45 | SMN | - | - | qPCR |
| HCM130 | M | 72 | MYH7 | c.976G>C | p.Ala326Pro | qPCR |
| HCM131 | F | 52 | MYH7 | - | p.Arg663Cys | qPCR |
| HCM132 | F | 15 | TNNT2 | c.814C>T | p.Gln272* | qPCR |
| HCM133 | M | 58 | MYBPC3 | c.442G>A | p.Gly148Arg | qPCR |
| HCM134 | M | 47 | unknown | - | - | qPCR |
| HCM135 | M | 68 | MYL2 | c.64G>A | p.Glu22Lys | qPCR |
| HCM136 | F | 76 | - | - | - | qPCR |

Patients included for single cell sequencing analysis

| HCM nr. in manuscript | # Cells |
|-----------------------|---------|
| HCM.P1 | 471 |
| HCM.P2 | 607 |
| HCM.P3 | 626 |
| HCM.P4 | 142 |
| HCM.P5 | 446 |

Control cardiomyocytes included for single cell sequencing analysis

| Ctrl nr. in manuscript | # Cells |
|------------------------|---------|
| Ctrl1.N1 | 254 |
| Ctrl1.N2 | 57 |
| Ctrl1.N3 | 27 |
| Ctrl1.N4 | 296 |
| Ctrl1.N5 | 360 |
| Ctrl1.N6 | 68 |
| Ctrl1.N13 | 338 |
| Ctrl1.N14 | 1923 |
| Ctrl2.D2 | 4349 |
| Ctrl2.D3 | 698 |
| Ctrl2.D4 | 1476 |
| Ctrl2.D5 | 949 |
| Ctrl2.D6 | 1896 |
| Ctrl2.D7 | 1303 |
| Ctrl2.H2 | 799 |
| Ctrl2.H3 | 2925 |
| Ctrl2.H4 | 2943 |
| Ctrl2.H5 | 4429 |
| Ctrl2.H6 | 2261 |
| Ctrl2.H7 | 1653 |



Summary

Hypertrophic cardiomyopathy (HCM) is a genetic cardiac disorder affecting 1:500 – 1:200 people worldwide. The phenotype can vary from asymptomatic to unexplained asymmetric left ventricular hypertrophy which inevitably leads to severe cardiac dysfunction and sudden cardiac death. While unexplained, the most pronounced hypertrophy occurs in the intraventricular septum (IVS). Recent studies have identified differentially expressed genes in HCM and healthy hearts, providing insights into HCM-specific cardiomyocyte subpopulations. This yielded many new understandings about cellular heterogeneity in cardiomyocytes but did not explain spatial heterogeneity in phenotype and gene expression.

In an attempt to identify players driving spatial differences in hypertrophy, we made use of Tomo-sequencing (Tomo-Seq). This allowed us to obtain transmural gene expression patterns in the IVS and LV free wall (FW) in an HCM patient harbouring a mutation in myosin binding protein C3 (MYBPC3). By using Principal Component Analysis (PCA) and focusing on the more stressed areas of the IVS, we were able to identify a hypertrophic septal-specific gene expression profile. Motif analysis of enriched genes enabled us to identify the transcription factor Nuclear Receptor Subfamily 2 Group F Member 2 (NR2F2) as a potential regulator. By in vitro knockdown of NR2F2 in stressed human induced pluripotent stem cells-derived cardiomyocytes (hiPSC-CM) we showed that selected NR2F2 target genes increased in hiPSC-CM subjected to hypertrophy-related stress, which subsequently decreased after NR2F2 siRNA knockdown. This implies that NR2F2 is at least partially responsible for the regulation of the hypertrophic septal-specific gene expression program.

Introduction

Hypertrophic cardiomyopathy (HCM) is the most common form of genetic heart disease with an estimated prevalence of 1:500-1:200 patients in the adult population (Bos et al., 2009; Semsarian et al., 2015). The clinical phenotype of HCM patients is highly variable, ranging from asymptomatic to severe cardiac remodelling, which can lead to sudden cardiac arrest, outflow tract obstruction, and eventually heart failure (Antunes & Scudeler, 2020; Bos et al., 2009). On a microscopical level, the principal hallmarks of the disease are cardiomyocyte (CM) disarray, CM hypertrophy, interstitial- and perivascular fibrosis, ischemia and inflammation (Lamke et al., 2003). Remodelling during HCM is characterized by a thickening of the left ventricular (LV) myocardium, specifically the intraventricular septum (IVS). Hypertrophy of the IVS can cause left ventricle outflow track (LVOT) obstruction, impeding efficient blood flow to the aorta. Patients suffering from LVOT may need to undergo a septal myectomy or alcohol ablation to reduce the burden of the hypertrophied IVS (Canepa et al., 2016). Current pharmacological treatments can only alleviate HCM symptoms. Development of better therapeutic opportunities is impaired by a lack of diagnostic markers and therapeutic targets. As such, understanding of the molecular mechanisms driving hypertrophic remodelling would be beneficial.

To address this lack of understanding, several studies aimed at *de novo* identification of genes that drive HCM have been conducted over the last few decades. One strategy has been to study differentially expressed genes in patients with HCM and healthy control samples by performing transcriptomic or proteomic analysis (Bos et al., 2020; Lim et al., 2001; Maron et al., 2021; Pei et al., 2021; C. W. Ren et al., 2016; Schuldt et al., 2021). However, the heart consists of different cell types, and tissue remodelling in HCM shows large spatial and cellular heterogeneity (Becker et al., 2020; Canepa et al., 2016; Cheng et al., 2021; Kirschner et al., 2005; Kraft & Montag, 2019; Sepehrkhoy et al., 2017). Aforementioned bulk analyses on tissue lysates do not capture these aspects of pathogenesis as gene expression from different cell types is mixed and spatial distribution is lost. Recently, our lab and others have applied single-cell RNA sequencing (scRNA-seq) to healthy and diseased human HCM hearts, which allowed for identification of genes that drive disease and cardiomyocyte heterogeneity (Chaffin et al., 2022; Larson et al., 2022; Litviňuková et al., 2020; Nomura et al., 2018; Z. Ren et al., 2020; Wehrens et al., 2022). All these studies

however do not identify the spatial distribution of gene expression patterns, which might be very relevant, as remodelling strongly varies between different anatomical parts of the heart (Ando et al., 2020; Becker et al., 2020; Canepa et al., 2016; Olivotto et al., 2012; Sepehrkhoy et al., 2017). A more recent study has indeed shown that combining single nucleus sequencing with spatial information on frozen tissue section of myectomy tissue can provide us with valuable information about failing status of cardiomyocytes and proximity to other cell types (Liu et al., 2023). This study is however focused on a small area of the septum (myectomy tissue).

In this study, we aimed to identify the mechanisms underlying spatial remodeling responses in HCM. To achieve this, we applied Tomo-sequencing (Tomo-Seq) (Junker et al., 2014; Kruse et al., 2016) to reveal gene expression differences along the transverse axis of the IVS and free wall (FW) of the LV from an HCM patient with a mutation in cardiac myosin binding protein (MYBPC3). Corresponding histological analysis revealed spatial patterns in the degree of disarray and fibrosis, consistent with stress and fibrotic marker gene expression quantified by Tomo-Seq. Application of Principal Component Analysis (PCA) allowed us to link patterns of gene expression to tissue origin (IVS versus FW) and hypertrophy. Promoter sequence analysis revealed transcription factor Nuclear Receptor Subfamily 2 Group F Member 2 (NR2F2) as a potential driver. We observed an increase in expression of 15/19 selected NR2F2 target genes in human induced pluripotent stem cells derived cardiomyocytes (hiPSC-CM) subjected to hypertrophy-related stress, and concurrent decreased expression after NR2F2 siRNA knockdown. These observations are consistent with NR2F2 being at least partially responsible for the septal hypertrophy gene expression program.

Results

Cellular hypertrophy and fibrosis in an HCM explanted heart

To study disease-driving mechanisms underlying HCM, we investigated an explanted heart of a patient harbouring the MYBPC3 c.2373_2374dupG (p.W792fs-X) mutation (Figure 1A-D), the most prevalent HCM-causing mutation in the Netherlands (Christiaans et al., 2010). This mutation leads to the generation of a new splice donor site and in a premature stop codon. In comparison to an age-matched control heart (Control), the HCM heart showed fibrotic deposition in the FW of the LV and fat

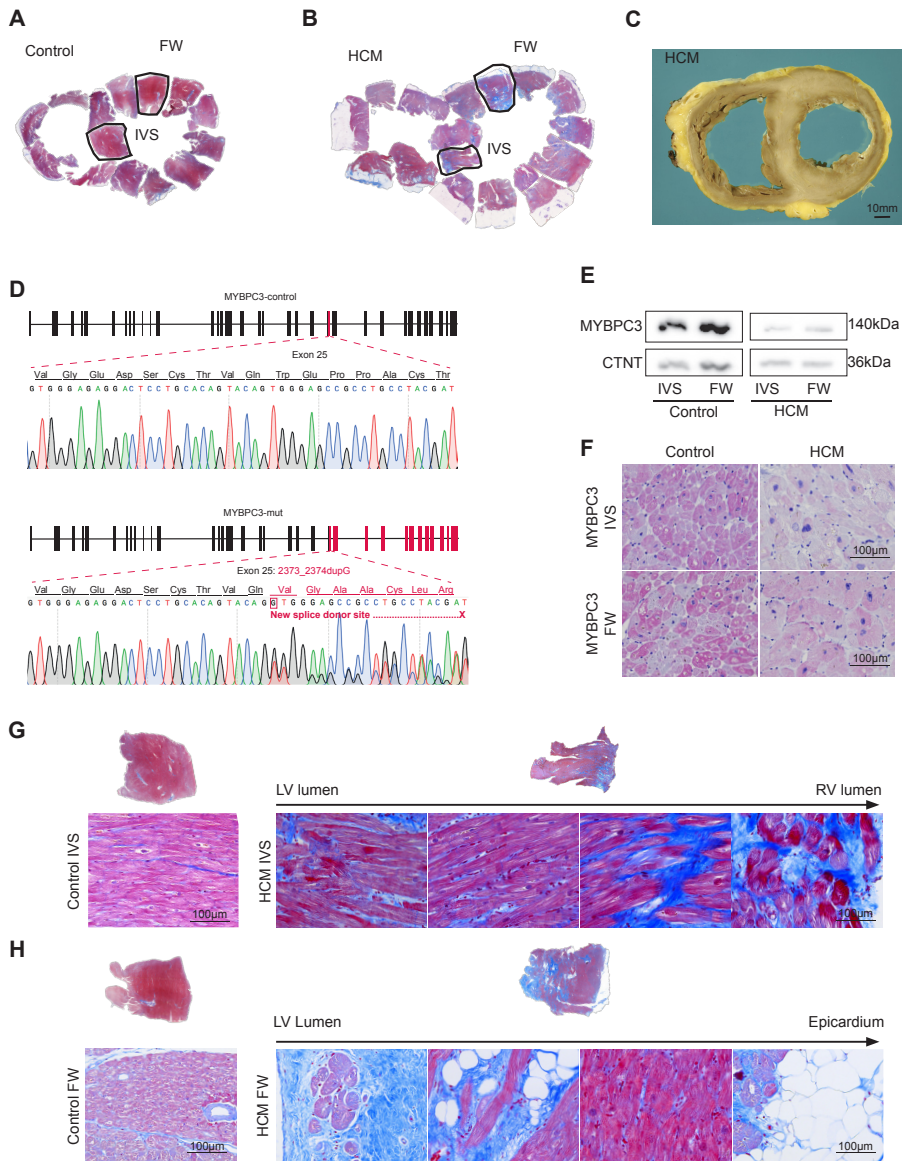


Figure 1. Phenotyping cardiac HCM tissue. (A and B) Masson Trichrome staining on a Control heart **(A)** and an HCM heart **(B)** showing myocardial tissue (red), adipose tissue (white) and fibrotic tissue (blue). Black line indicating the representative sections of the FW and the IVS selected for Tomo-Seq. **(C)** Macro photo of an HCM heart showing hypertrophy in the IVS and in the FW. **(D)** Genomic region showing the exons of MYBPC3 in the Control heart (top) and in the HCM heart (bottom) with an c.2373_2374dupG (p.W792fs-X) mutation. An insertion of a G nucleotide in exon 25 leading to a new splice donor site on exon 25 and a premature stop-codon. **(E)** Western blot showing a decreased expression of MYBPC3 in HCM heart (right) compared to Control heart (left) normalised to Cardiac troponin (TNNT2). **(F)** Immunostaining

showing a decrease in MYBPC3 staining intensity (red) in HCM heart (right) compared to Control heart (left) in both IVS (top) and FW (bottom). Nuclei stained with haematoxylin (dark blue). Scale bars are 100µm. **(G)** Representative Masson Trichrome staining of the Control IVS tissue (left) and HCM IVS tissue (right), the latter shown from lumen of the LV to the lumen of the RV. An overview of the septal block is shown above. **(H)** Representative Masson Trichrome staining of the Control FW tissue (left) and HCM FW tissue (right), the latter shown from lumen of the LV to the (fatty) epicardial region.

deposition around the myocardium (**Figure 1A-B**). Examination of the gross morphology showed hypertrophy in the IVS and in a large part of the FW of the LV (**Figure 1C**). Western blot analysis showed a decrease in MYBPC3 expression in both the IVS and the FW in HCM (right) when compared to Control (left), indicating haploinsufficiency (**Figure 1E**). This decrease was also observed on a histological level, as shown by a decreased MYBPC3 intensity in HCM tissue (right) compared to Control tissue (**Figure 1F, left**). Further histological examination of the myocardium revealed common hallmarks of HCM. In the IVS, the LV side displayed areas of cardiomyocyte disarray and fibrosis was observed throughout the tissue (blue), albeit more pronounced in the right ventricle (RV) side (**Figure 1G**). In the FW, hypertrophic CMs and large fibrotic areas were distributed throughout the tissue. Adipocytes (white) were detected interstitially and at the epicardial site of the wall (**Figure 1H**).

Overall, these results indicate the diseased state of the heart due to a mutation in the MYBPC3 gene with specific HCM hallmarks showing distinct localized patterns.

Local markers for hypertrophy and heart failure in the free wall and the intra-ventricular septum

To understand what drives local remodelling processes in the HCM heart, we applied Tomo-Seq (Junker et al., 2014; Kruse et al., 2016) to investigate spatial gene expression patterns across the IVS and FW. Specifically, we took transmural tissue blocks with a cross-section of approximately 3x3 mm from the IVS and FW and dissected them into consecutive sections of 200 µm (**Figure 2A**). We isolated and bar coded the RNA from each section separately, after which the samples were pooled and submitted for RNA-Seq as previously described (Boogerd et al., 2019; Kruse et al., 2016; Lacraz et al., 2017). Mitochondrial reads were removed, and sections with more than 3000 chromosomal transcripts were used for further analysis (**Supplemen-**

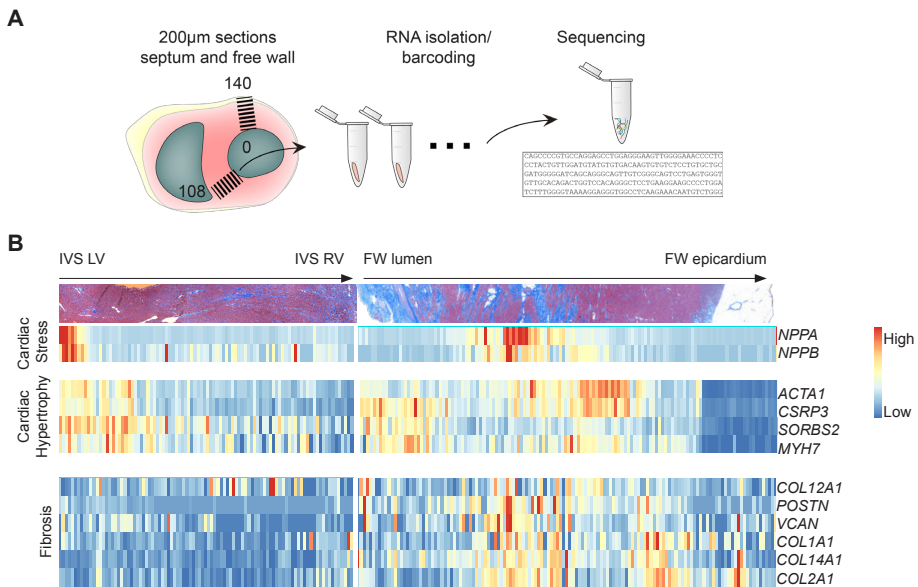


Figure 2. Differential gene expression throughout the myocardial wall in the HCM heart. (A) Graphic depiction of sample and data collection. The IVS and the FW were consecutively sectioned from the lumen of the LV (0) towards the RV and the epicardium, respectively. Samples were collected and processed separately and pooled and sequenced after barcoding. (B) Masson Trichrome staining (top) on an HCM heart showing myocardial tissue (red), fibrotic tissue (blue) and adipose tissue (white). Expression of common cardiac stress marker genes (middle) with a high expression in the LV side of the IVS and a more dispersed expression in the FW. Expression of fibrotic marker genes (bottom) with a low expression in the IVS and a high expression in the FW, in line with the Masson Trichrome staining (top). See also Supplemental Figure 1 and Supplemental Table 1.

tal Figure 1A-C). Thus, a transmural genome-wide expression atlas of the diseased IVS and FW was generated.

To better understand where regional stress might take place in the tissues, we mapped the expression of genes known to be involved in cardiac stress and fibrosis (Figure 2B). Several regions showed increased expression of markers for cardiac stress (*NPPA*, *NPPB*) and hypertrophy (*ACTA1*, *CSRP3*, *MYH7*). The epicardial side of the FW did not show expression of these markers, consistent with this area being identified as adipose tissue. Notably, cardiac stress markers showed an increased expression in the LV side of the IVS, indicating that the stress response might be more local to this region of the IVS (Figure 2B, top). Fibrotic markers (Collagens, *POSTN*, *VCAN*) were also increased in specific regions, mainly in the FW, which overlapped

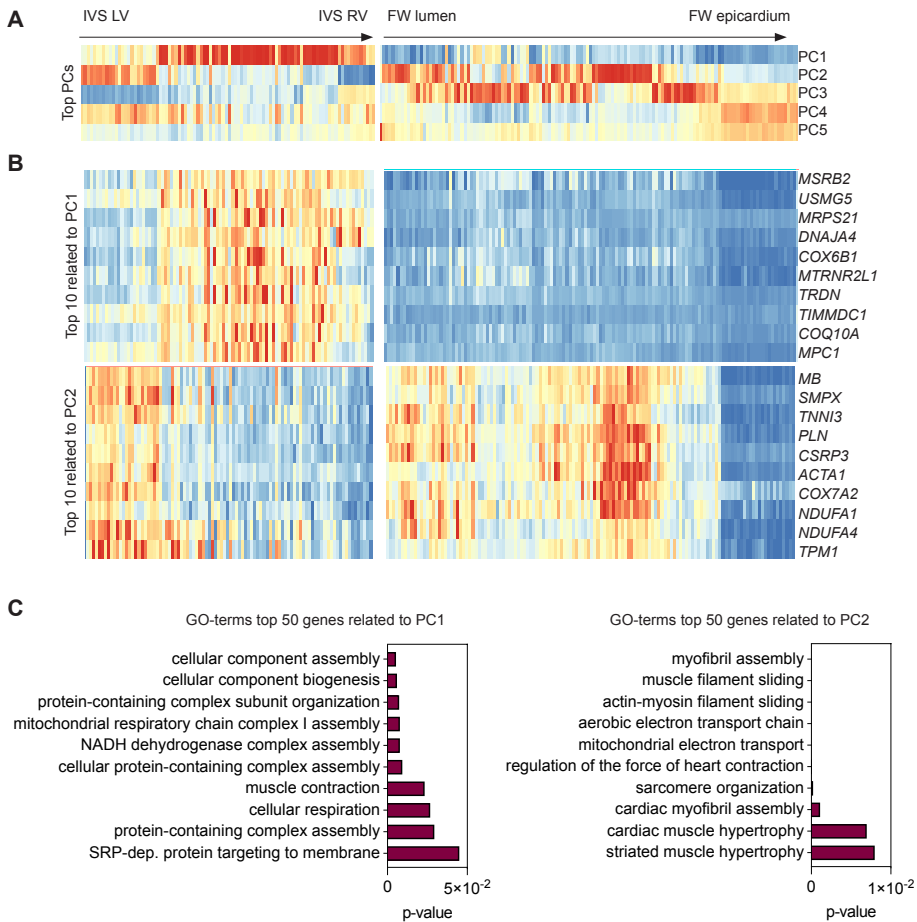


Figure 3. Unsupervised clustering of genes to identify the transcriptome of the more stressed area of the IVS. (A) Principal component analysis of slices in the myocardial wall. The top 5 principal components that respectively explain 13.4%, 6.2%, 3.2%, 2.5% and 2.2% of the data are depicted. (B, top) Top 10 genes with high PC1 loadings showing a more pronounced expression in the IVS. (B, bottom) Top 10 genes with high PC2 loadings showing high expression in the LV side of the IVS, and the lumen side and the middle of the FW. C, Gene ontology analysis of top 50 genes in PC1 (left) and PC2 (right).

with increased stress markers. These findings are consistent with previously published data showing ANP-positive cardiomyocytes to border fibrotic regions in cardiac tissue (Lacruz et al., 2017; Wehrens et al., 2022). The IVS did not show a high expression of fibrotic markers, consistent with the histological observations.

Gene expression patterning reveals a specific signature in LV side of the IVS

Given that we saw clear spatial patterns of gene expression for these specific marker genes, we set out to further investigate the local differences in gene expression for all genes in an unbiased manner. To achieve this, we used PCA, which aims to identify several distinct generalized expression patterns (the principal components, or PCs). This allows for the expression pattern of any gene to be represented as a combination of these PCs. We decided to focus on the first two PCs since, by construction, they explained most variance in the data (roughly 20% of the data where PC1 explained 13.4% of the variance, and PC2 6.2%) (Figure 3A). PC1 appeared to represent septal-specific expression patterns, as it was most pronounced in the IVS. Many genes with high PC1 loading coefficients (meaning the gene's expression pattern was well reflected by the PC pattern) were related to the mitochondria such as *MSRB2*, *MRPS21*, *TIMMDC1* (Figure 3B, upper panel and Supplemental Table 1). GO-term analysis of the top 50 genes with highest PC1 loading coefficients showed enrichment for processes related to the mitochondrial respiratory complex and cellular respiration (Figure 3C, left panel). PC2 showed a high enrichment in the LV side of the IVS and in specific areas of the LV. Genes with high PC2 loading coefficients included mitochondrial genes (*NDUFA1*, *NDUFA4* and *COX7A2*) and, interestingly, markers of cardiac hypertrophy (such as *ACTA1* and *CSRP3*) (Figure 3B, bottom panel and Supplemental Table 1). Indeed, GO-term analysis of the top 50 PC2 genes showed enrichment for processes related to muscle contraction and muscle hypertrophy (Figure 3C, right panel). Overall, these results indicate that the IVS has a specific gene expression signature that distinguishes it from the FW. Additionally, we hypothesize that genes in PC2 are linked to hypertrophic remodelling.

Overlap between PC1 and PC2 identifies septal enriched hypertrophy-related genes

Septal hypertrophic remodelling is a key hallmark of HCM. As such, many patients need to undergo myectomy surgery due to excessive hypertrophy of the IVS. However, the underlying cause for this septal hypertrophy so far remains unknown. With this in mind, we next aimed to identify gene patterns that drive septal hypertrophy. Since we previously linked PC1 genes to septal specificity, and PC2 gene to hypertrophy, we hypothesized that genes with high loading coefficients in both PC1 and PC2 would yield hypertrophic genes specific for the IVS. We therefore selected genes for which both the PC1 and PC2 loading coefficients were in the top quartile.

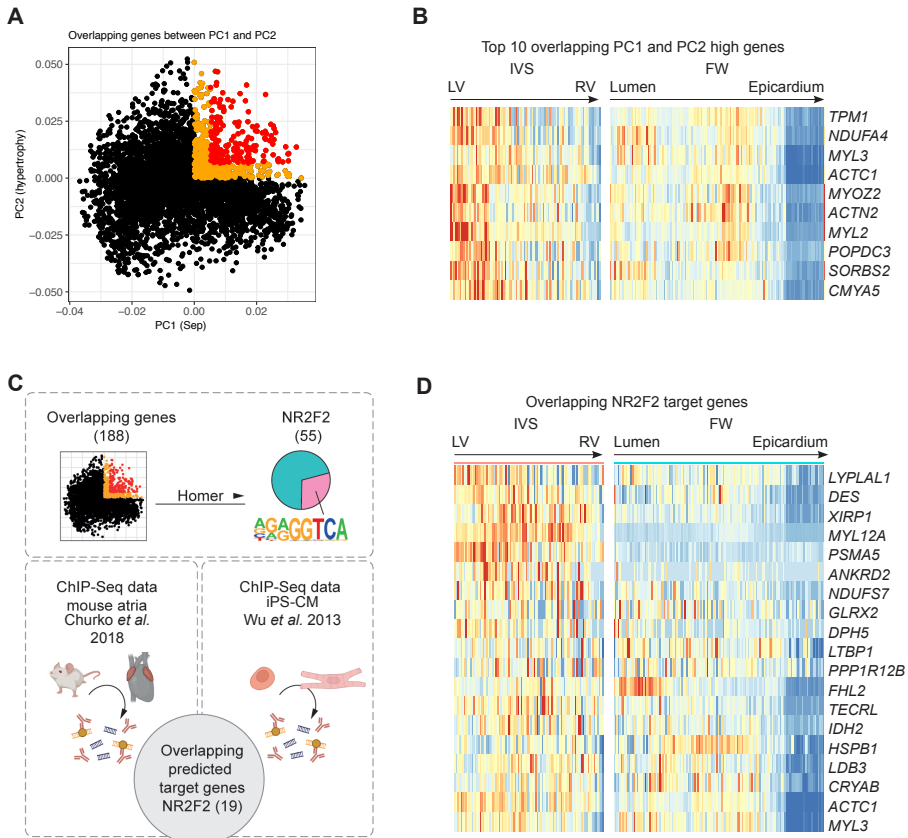


Figure 4. Identification of NR2F2 as a potential driving transcription factor for the septal transcriptome. (A) Dot plot showing the selected cut-off of for genes related to both PC1 and PC2. Genes with positive loadings in both PC1 and PC2 are coloured orange, selected genes are coloured red. (B) Heatmap of the top 10 overlapping genes of PC1 and PC2 showing an enrichment at the LV side of the IVS. (C) Graphical depiction of the identification of NR2F2 as one of the potential transcription factors driving the PC1/PC2 genes. Homer analysis on the 188 overlapping PC1/PC2 genes identified 55 potential target genes for NR2F2 (top). These were overlapped with ChIP-Seq analysis subtracted from the literature (19 genes). (D) Heatmap showing the expression of predicted NR2F2 targets. See also Figure S2 and Table S2 and S3.

This cut-off resulted in a set of 188 genes (Figure 4A). The expression pattern of these genes showed high expression in the LV side of the IVS, consistent with the location of septal hypertrophic remodelling (Figure 4B and Supplemental Figure 2A). The transcriptional program identified by overlying PC1 and PC2 might be specific and relevant for understanding cardiomyocyte stress and hypertrophy in the IVS in

the case of HCM.

Identifying NR2F2 as a potential driver of the septal gene program

To get a better understanding of which transcription factors (TFs) might be driving the IVS-specific hypertrophic gene program, we performed a HOMER analysis on the overlapping PC1 and PC2 genes. A total of 12 motifs were found to be enriched and, after filtering (see Methods), we ended up with 2 TFs; NR2F2 and SOX4 (**Supplemental Table 3**). From these, NR2F2 was predicted to potentially regulate the highest number of targets in our data (55 genes) (**Figure 4C**). NR2F2 plays a key role in atrial identity and cardiac organogenesis, however its expression in the ventricles remains low throughout development (Barth et al., 2005; S. pin Wu et al., 2013). To get a more specific set of potential NR2F2 target genes in the heart, we overlapped our 55 predicted NR2F2 targets with available chromatin immunoprecipitation sequencing (ChIP-Seq) of two individual studies investigating NR2F2 overexpression in the heart (Churko et al., 2018; S. pin Wu et al., 2013) (**Figure 4C**). This yielded 19 potential NR2F2 targets all of which showed a high expression in the IVS (**Figure 4D**).

Knockdown of NR2F2 in hiPSC-CM leads to inhibition of target genes and blunted stress response

To further study the role of NR2F2 in stressed cardiomyocytes, we utilized hiPSC-CM. To mimic a hypertrophic-like phenotype in vitro, we subjected hiPSC-CM to a 72-hour-stress protocol with endothelin-1 (ET-1) (Johansson et al., 2020a). Next, we inhibited NR2F2 expression by using 10 nM of small interfering RNAs (siNR2F2) in hiPSC-CM at day 30 of culture (**Figure 5A, Supplemental Figure 3A**). After 48h, the expression of *NR2F2* mRNA was significantly lower compared to the DMSO treated hiPSC-CM (**Figure 5B**). As expected, western blot also showed a reduction in NR2F2 protein expression after 72 hours of transfection with siNR2F2 compared to the hiPSC-CM transfected with a scramble siRNA (siScr) (**Figure 5C and 5D**). Staining for NR2F2 in ET-1 treated cells showed nuclear expression of NR2F2, indicating the presence of NR2F2 in hiPSC-CMs in all conditions (**Figure 5E**).

Consistent with the hypothesis that NR2F2 is partially responsible for the septal-specific hypertrophic gene program (**Figure 4C-D**), we looked into the expression of potential target genes after the addition of ET-1 in hiPSC-CM. The mRNA expression of several genes, including *ANKRD2*, *GLRX2*, *PPP1R12B*, *XIRP1*, *MYL3*, *MYL12A*

and *CRYAB* were significantly increased (**Figure 5F**). Though not significant, *IDH2*, *NDUFS7*, *FHL2*, *DPH5*, *TECRL*, *LDB3*, *HSPB1*, *ACTC1*, *LYPLAL1*, and *DES* showed similar trends. When the ET-1-treated cells were exposed to siNR2F2, the expression of most of these targets decreased back to control levels, consistent with the hypothesis that these genes are targets of NR2F2 (**Figure 5F**). To determine the role of NR2F2 in an HCM-related cardiac stress more broadly, we examined the expression of common cardiac stress markers (*NPPA*, *MYH7*) in the ET-1 model. After ET-1 exposure, stress markers were significantly increased in the hiPSC-CMs, while the increase was less prominent in cardiomyocytes treated with siNR2F2 (**Figure 5G**, **Supplemental Figure 3B**), suggesting NR2F2 might play a role in regulating cardiomyocyte stress. Additionally, we tested the concentration of proBNP in the supernatant of stressed cells after 72 hours. Although there was an increase of proBNP after ET-1 stress induction, we did not see a significant decrease of the secreted protein after siNR2F2 treatment (**Supplemental Figure 3C**). Furthermore, we did not see significant decrease in cell size in the siNR2F2 treated cells (**Supplemental Figure 3D**). At protein level, the effect of siNR2F2 on target genes was not significant. Nonetheless, Heat Shock Protein B1 (*HSPB1*) expression shows an increase trend after ET-1 and levels are reduced back to control levels after siNR2F2 (**Supplemental Figure 3E-G**).

Overall, these data indicate that we can inhibit the expression of HCM-specific septal genes by knocking down NR2F2 expression. However, over a 72h timespan, there is no direct influence phenotype of these cells.

Discussion

Novel genome sequencing technologies are being applied on human HCM cardiac tissue to better understand the disease-driving mechanism underlying the disease (Laird et al., 2023; Larson et al., 2022; Liu et al., 2023; Pei et al., 2021; Simonson et al., 2023; Wehrens et al., 2022). However, detailed information regarding the specific localization of these genomic changes is often lacking. In this study, we applied Tomo-Seq to identify regional differences in gene expression, that likely relate to areas with different physiological properties. The large amount of quantitative gene expression data collected can therefore contribute to a better understanding of the different local physiological processes that occur in HCM.

In general, HCM patients suffer from asymmetric septal hypertrophy, indicating that

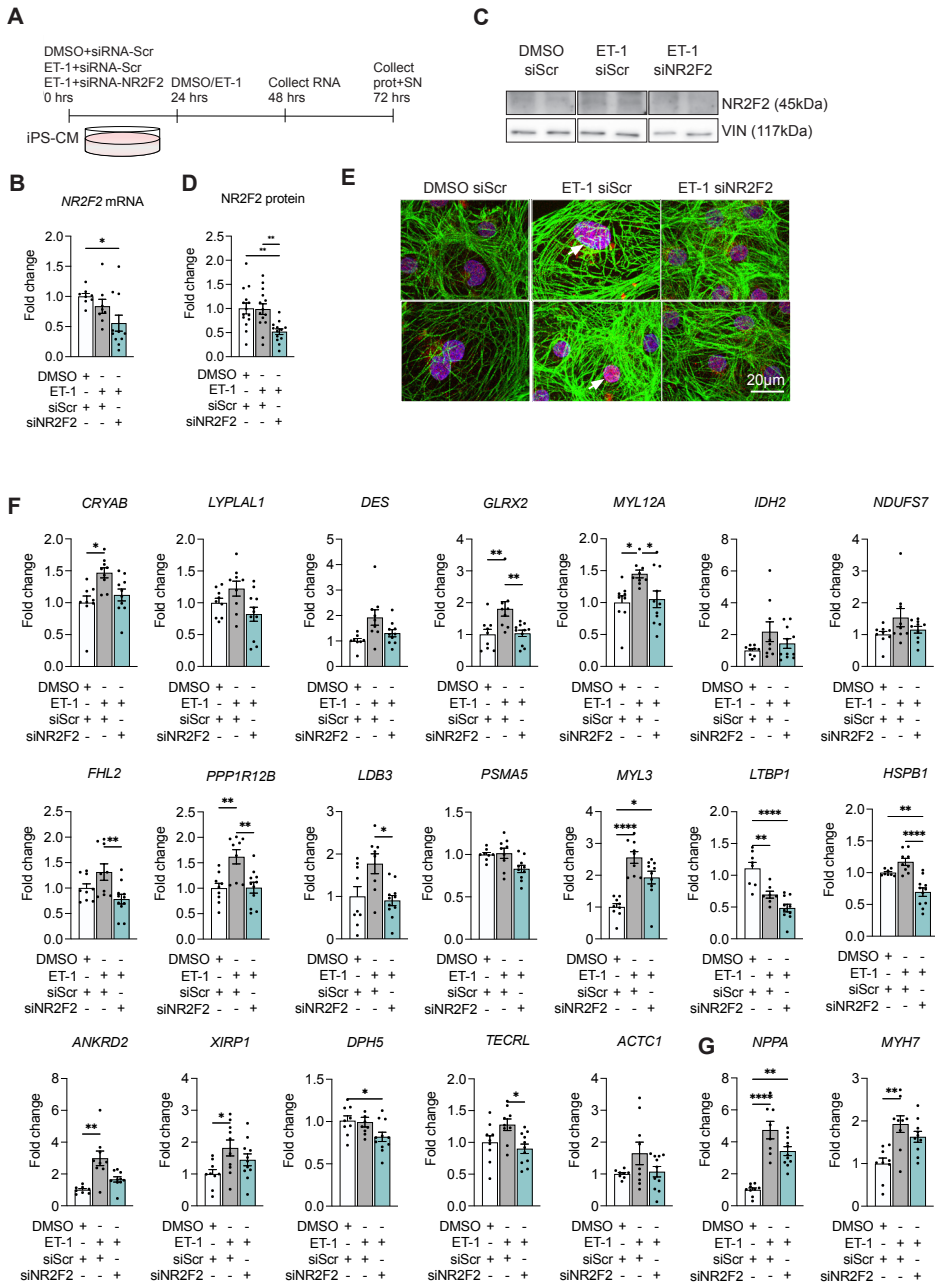


Figure 5. NR2F2 depletion in hiPSC-CMs lowers the stress-induced increase of potential NR2F2 target genes. (A) Graphical timeline of the experimental procedure. **(B)** qPCR analysis showing a decrease in mRNA expression of NR2F2 after siNR2F2 compared to DMSO treated cells. Normalized to RPL32. Fold change is calculated compared to unstressed siScr-treated cells. **(C)** Western blot analysis showing the protein expression of NR2F2. **(D)** Quantifica-

tion of the western blot analysis showing a 50% reduction of NR2F2 protein after treatment with siRNA. Normalized to Vinculin (VIN). Fold change is calculated compared to unstressed siScr-treated cells. **(E)** Immunocytochemistry showing the nuclear expression of NR2F2 (red) co-expressed with nuclear marker DAPI (blue) and the expression of TNNT (green). Treatment with siRNA lead to a reduction in expression of NR2F2. **(F)** qPCR analysis showing the expression of the 19 predicted target genes of NR2F2. Genes are normalized to RPL32. Fold change was calculated with respect to DMSO/siScr treated cells. **(G)** qPCR analysis showing and increase in stress genes after ET-1 treatment. Genes are normalized to *RPL32* housekeeping genes. Fold change was calculated with respect to DMSO/siScr treated cells. Experiment was repeated 3 times (n=3) for mRNA with 4 biological replicates and 3 times for protein (n=4) with an additional time with 2 biological replicates. See also Supplemental Table 3.

3 the IVS is more affected than the FW (Canepa et al., 2016). By contrast, we and others detected a higher fibrotic density in the FWs and trabeculae of explanted HCM hearts (Sepehrkhoy et al., 2017). This indicates that different areas in the myocardial wall may display different histological hallmarks of HCM. Since septal hypertrophy is a common and serious feature in HCM patients, we aimed to better understand which gene expression program specifically drives this septal hypertrophy. Interestingly, PCA analysis revealed a septal-specific gene expression profile enriched in mitochondrial genes (**Figure 2**). Suggesting that the septal side of the IVS is more metabolically active, in line with the fact that LVOT is mainly caused by the outgrowth of the IVS towards the lumen of the LV (Marian & Braunwald, 2017). Additionally, a recent study has shown that disarray in CMs is related to an upregulation of mitochondrial genes and cardiomyocytes with severe disarray showed a downregulation of extracellular matrix genes (Laird et al., 2023). Exploring the extent of disarray of the CMs in this explanted heart offers a compelling area for further investigation.

Overlapping PCA analysis related 188 genes to an IVS-specific expression pattern, and HOMER analysis of the promoter regions of those genes suggested NR2F2 as a potential driver of that specific gene expression. In embryonic stages, NR2F2 plays a key role in cardiac development, mainly expressed in the atria and involved in atria identity. Its expression in the ventricle remains relatively low throughout life (Xie et al., 2017). Under pathological conditions, NR2F2 is increased in the ventricles which causes an alteration to mitochondrial and metabolic genes and processes (Kittleson et al., 2005; Sack et al., 1997; S. P. Wu et al., 2015). The latter results are in line with our results, where we see a high expression of mitochondrial and ribosomal genes and processes in both PC1 and PC2, being more pronounced in PC1 (**Figure 2**).

To further validate the pathological role of NR2F2 in HCM, we performed an in vitro study using hiPSC-CMs. While an elegant model to study human heart tissue (Cohn et al., 2019; Seeger et al., 2019), a major issue concerning the use of hiPSC-CM is their maturation state, which is far from adult (Yang et al., 2014). Since HCM develops in adulthood (Chung et al., 2003), it is challenging to simulate an HCM-related phenotype in a culture dish. Different methods to induce pathological hypertrophy in vitro have been employed, such as endothelin-1 (ET-1), a potent vasoconstrictor (Aggarwal et al., 2014; Davenport et al., 2016; Johansson et al., 2020b). ET-1 showed to induce similar gene expression changes in hiPSC when compared to human hypertrophied left ventricle (Aggarwal et al., 2014). In a more recent study, 24h ET-1 stimulation was sufficient to induce an increase in cell size (Johansson et al., 2020b). Our results show the potential use of ET-1 as compound to induce stress in hiPSC-CM, however, further optimization is required.

Addition of siNR2F2 after ET-1 stress induction re-stabilized the mRNA of the majority of potential targets, suggesting partial role in their regulation. Nonetheless, this effect was not observed as strong on phenotypic or protein levels. Interestingly, there is an increasing trend in HSPB1 after stress, which is then normalized after siNR2F2. HSPB1 plays a role in stabilizing misfolded proteins and therefore preventing their aggregation. Recent studies have shown HCM samples and end-stage heart failure samples to have an increase in HSPB1 when compared to control samples (Jong et al., 2006). These results suggest NR2F2 to potentially play a crucial role in the regulation of Heat Shock Proteins and, consequently, in the overall Protein Quality System (PQS).

All in all, this study has provided an in-depth understanding of the local gene expression profile throughout the hypertrophic heart as well as the identification of a candidate TF which might be playing a crucial role in the pathology of HCM. Currently, HCM patients are treated with medication or (surgical) interventions to relieve the symptoms of the disease, but they do not stop or reverse the adverse remodeling in the heart.

Our findings indicate that stress is regionally different in the HCM heart indicating

that future research should be aimed at specifically targeting disease-driving mechanisms and detecting (early) biomarkers to predict and to detect patients at higher risk of developing the disease.

Limitations of the study

For this study we were able to make use of a heart of an HCM patient for both Tomo-Seq and histological analysis. To the best of our capabilities, we matched the HCM and control heart based on their sex and age, however the collection procedure of each heart was different (explanted failing heart vs. rejected donor heart). Thus, although with Tomo-Seq each sample is its own control, it is challenging to compare the gene expression profile from one human heart to another one, since the handling methods may influence the data. For this reason, we only used the control heart for histological comparison.

Other studies that have used different sequencing techniques on the HCM heart have focused on myectomy tissue (Pei et al., 2021; C. W. Ren et al., 2016; Wehrens et al., 2022), whereas in this study we used an explanted HCM heart, meaning the stage of the disease was more advanced (failing) and this makes it more difficult to compare to available datasets. Nonetheless, by combining RNA-Seq data performed on HCM myectomy tissue and end-stage tissue, we will be able to obtain information regarding the changes in gene expression overtime and, thus, better define novel therapeutic targets to prevent disease progression (Coats et al., 2018; Kraft & Montag, 2019; Marian & Braunwald, 2017; Mirotsoy et al., 2004; Nakamura & Sadoshima, 2018; C. W. Ren et al., 2016; Van Der Velden et al., 2018; Vanderheyden et al., 2004; Varnava et al., 2000)

Acknowledgements

We thank Judith Vivié and Mauro Muraro (Single Cell Discoveries) for technical assistance and helpful discussions.

Methods

Human heart collection

The study met the criteria of the code of proper use of human tissue that is used in the Netherlands. Collection of the human heart tissue was approved by the scientific advisory board of the biobank of the University Medical Center Utrecht, Utrecht, the Netherlands (protocol no. 12/387). Written informed consent was obtained or in certain cases waived by the ethics committee when obtaining informed consent was not possible due to death of the patient.

A human heart of a patient carrying a founder mutation in MYBPC3 (c.2373_2374dupG, p.W792fs-X) was collected during heart transplantation. As a control, we received tissue from a rejected donor heart, which was not transplanted for unspecified reasons. From each heart, a transversal slice was obtained at the apical site, which was subdivided into blocks and flash frozen for storage (-80°C). Frozen tissues from the posterior free wall (FW) and from the septum were selected on the HCM heart, and comparable regions were selected from the control heart.

Histology and immunohistochemistry

From each heart, a superior transversal slice to the apical (frozen) slice was taken, subdivided into smaller blocks and fixed in formalin. These blocks were further processed and embedded in paraffin. Sections ($\pm 4 \mu\text{m}$) were sliced and fixed on microscope slides. Masson Trichrome stains were performed for basic histology and identification of HCM hallmarks, such as; fibrotic areas, fat tissue infiltration, cardiomyocyte hypertrophy, and disarray throughout the myocardial wall. For control, we used a rejected donor heart. Microscope slides were digitalized using a NanoZoomer (Hitachi) scanner and processed with NDP view software. For immunohistochemistry, antigen retrieval was performed by using the appropriate method for a specific antibody (citrate buffer, EDTA or pepsin) and incubated with primary antibody. Slides were then incubated with BrightVision Poly-AP anti-mouse or -rabbit antibody conjugate (Immunologic) and visualized with liquid permanent red (and vector blue [Vector Laboratories] for the double-immunostaining). Slides were counterstained

with hematoxylin to visualize nuclei.

Tomo-Seq on HCM heart

Sample processing and RNA extraction

Sections of whole hearts were frozen and a piece of 3/3-mm/width/height spanning the lumen of the LV to the RV (for the IVS) or the epicardium (for the FW). Tissue was embedded in freezing medium and frozen on dry ice. Cryosections were cut 200µm per sample. RNA was isolated from these samples by TRIzol extraction.

Preparation of sequencing libraries

A cDNA library was prepared for sequencing using the CEL-Seq2 protocol (Boogerd et al., 2019; Junker et al., 2014; Lacraz et al., 2017). A cDNA library was prepared for sequencing using the CEL-Seq2 protocol (Hashimshony et al., 2012; Junker et al., 2014; Lacraz et al., 2017). Briefly, ERCC spike-in and primers with a poly-T sequence, T7 promoter, slice-specific barcode and UMI were added to RNA of each of the

Table 1. Materials for preparation sequencing libraries

| Purpose | Source |
|----------------------------------|---|
| Freezing medium | Tissue Freezing Medium (Leica) |
| RT reaction | SuperScript™ III Reverse Transcriptase (Invitrogen, Thermo Fisher Scientific, 18080093) |
| IVT reaction | 5X MessageAmp™ II aRNA kit (Ambion, Thermo Fisher Scientific, AMB1751-5) |
| RNA and DNA cleanup | Agencourt AMPure XP beads (Beckman Coulter) |
| Spike-in RNA for quality control | ERCC RNA Spike-In Mix (Invitrogen, Thermo Fisher Scientific) |
| PCR reaction | Phusion® High-Fidelity PCR Master Mix with HF Buffer (NEB, M0531L) |
| PCR cleanup | ExoSAP-IT™ PCR Product Cleanup (Affymetrix, Thermo Fisher Scientific) |

slices, from which the RNA was reverse transcribed. The resulting cDNA was then pooled and used for in vitro transcription (IVT). Subsequently, the resulting amplified RNA (aRNA) was subjected to a second round of reverse transcription (using random hexamer primers) to create a cDNA library. The cDNA library is subjected to PCR with Illumina primers to create the final cDNA library that is suitable for sequencing. The libraries were sequenced paired end on an Illumina HiSeq 2500, with read lengths of 50 and 26 nt respectively for read 1 and read 2.

Illumina sequencing libraries were subsequently prepared according to the CEL-seq2 protocol using Superscript® III Double-stranded cDNA synthesis Kit (ThermoFisher), Agencourt AMPure XP beads (Beckman Coulter), and randomhexRT for converting aRNA to cDNA using random priming. The libraries were sequenced paired at 50bp read length on an illumine HiSeq 2500. Samples were sequenced by using Deseq2 (Love et al., 2014).

Mapping

Read 2 was used to determine the slice barcodes and unique molecular identifier (UMI), whilst read 1 was aligned to a reference transcriptome. The reference transcriptome was created by merging all exons in the RefSeq gene models (hg19) from the UCSC genome browser as used previously (Grun et al., 2016). The transcriptome reference is available in fasta format under: <https://github.com/vertesy/TheCorvinas/tree/master/Biology/Sequencing/hg19>. To align the reads, we used the MapAndGo2 wrapper around BWA MEM v07.10 (Li & Durbin, 2009), available under: <https://github.com/anna-alemany/transcriptomics/tree/master/mapandgo>. Reads that mapped equally well to multiple locations were discarded. Unique molecular identifier counts were determined per gene and barcode to determine count tables. UMI counts were subsequently adjusted to account for the expected number of molecules based on counts, 256 possible UMI's and poissonian counting statistics (Muraro et al., 2016).

Bio-informatic analyses

For each sample, the tables with transcript counts were loaded into R (version 4.1.0). Subsequently, the percentage of mitochondrial reads was determined per slice.

Then, the mitochondrial reads and ERCC spike-in reads were excluded from further analysis, as were slices with a total read count of less than 3000. In addition, genes that did not show a read count higher than 5 in at least 3 slices were also excluded from further analysis. The transcript counts were normalized by dividing them by the total amount of reads of the corresponding slice, and multiplying them with the median of R_s , where R_s is the total amount of reads R in a slice s . In addition, Z-scores were determined for the gene expression values by subtraction of that gene's mean expression and division by its standard deviation. A principal component analysis (PCA) was performed on the normalized transcript counts by using the `prcomp` function from the `stats` package (version 4.1.0). For gene expression data presented by heatmaps, Z-score expression values are plotted using the `pheatmap` function from the `pheatmap` package (version 1.0.12); where applicable, that package's default hierarchical clustering algorithm was applied.

GO-term analysis

Top 50 genes related to PC1 and 2 were selected and subjected to GO-term analysis via PANTHER Overrepresentation test (GO Ontology database DOI: 10.5281/zenodo.4437524 Released 2021-01-01). Terms were tested for significance by using a Fishers test, followed by a Bonferroni correction.

Homer analysis

To identify transcription factors potentially driving expression of a specific group of genes, we used HOMER (HOMER version v4.11.1 with packages human-o version 6.3, human-p version 5.5) to perform a sequence motif enrichment analysis on the promoter regions of those genes. The HOMER script `findMotifs.pl` was run with default parameters (considering regions from -300 to 50 bp with respect to the transcription start sites), except that a list of background genes was supplied manually. That list consisted of all 4756 genes detected in our RNA sequencing data that passed the filter criteria described above. In addition, to identify which genes contained specific enriched motifs, we used HOMER's "find" option (using the `.motif` files that contain the enriched motifs from the `knownResults` and `homerResults` folders).

ChIP-Seq analysis

To identify potential direct NR2F2 targets in cardiomyocytes, we obtained NR2F2 ChIP-Seq results from mouse atria and from hiPSC-CMs (Churko et al., 2018; S. pin Wu et al., 2013). Mouse atrial NR2F2 direct target genes were obtained as described in Churko et al., and converted to human orthologous gene symbols using biomaRt v3.13 (Durinck et al., 2005). hiPS-CM NR2F2 ChIP-Seq aligned reads were obtained from NCBI GEO (GSE81585), genome version h19. Peaks were identified using Homer v4.11 findpeaks.pl (Heinz et al., 2010) and annotated using GREAT (McLean et al., 2010) by searching 5.0 kb upstream, 1kb downstream, plus distal up to 1000.0 kb. In addition to GREAT, Homer v4.11 annotatePeaks.pl was used to identify genes with peaks to the nearest transcription start site. Gene lists were overlapped with the 188 overlapping genes between PC1 and PC2, and were overlapped with the 55 predicted target genes among this list which was identified by Homer. This identified to a total of 19 potential NR2F2 target genes (Figure 4D).

Selection of NR2F2

A total of 12 motifs were found to be enriched. Since Myocyte-specific enhancer-binding factors (MEFs) are known to be involved in hypertrophy-related remodelling (Dadson et al., 2015; Desjardins & Naya, 2016; Kolodziejczyk et al., 1999). DMRT6 and DMRT1 were excluded due to the low percentage of targeting sequence with this motif. ZNF263 and THRB were excluded due to the high percentage of background sequences with this motif. The expression levels of TFs with similar parameter values as MEFs was determined by qPCR on hiPSC-CMs. TFs with Ct-values <35 and expressed in the Tomo-Seq data were selected.

Culturing and differentiating human induced pluripotent stem cells

hiPSC were maintained on Geltrex™ (ThermoFisher Scientific, A1413302) cell-culture coated wells in Essential 8™ Medium (GIBCO, A1517001). Medium was refreshed daily. Once 80-100% confluency was reached, hiPSCs were passaged by applying TrypLE Express Enzyme (GIBCO, 12605010) 5 minutes at 37 °C. Next, 4 ml of Essential 8™ Medium was added and cells were transferred to a 15 ml Falcon tube. Cells were centrifuged for 5 minutes at 300 g. Cells were resuspended in 1 ml of Essential 8™ Medium supplemented with 1 μM thiazovivin (Sigma-Aldrich, 420220). Subsequently, cells were seeded at a density of 250,000 cells/cm² in Essential 8™ Medium

supplemented with 2 μM thiazovivin.

Differentiation was induced once hiPSCs reached 80-90% confluency (Day 0). For this, cells were washed once with dPBS (GIBCO, 14190094). Subsequently, cells were cultured with Cardio Differentiation Medium (RPMI-1640-Medium-GlutaMAX™ Supplement-HEPES (Life Technologies, #72400021) supplemented with 0.5 mg/mL human recombinant Albumin (Sigma-Aldrich, #A9731), 0.2 mg/mL L-Ascorbic Acid 2-Phosphate (Sigma-Aldrich, #A8960) containing freshly added 4 μM GSK3B-inhibitor CHIR99021 (Millipore, #361559). After 2 days (Day 2), medium was aspirated and cells were washed once with dPBS and subsequently cultured with Cardio Differentiation Medium supplemented with fresh 5 μM Wnt-inhibitor IWP2 (Millipore, #681671). On day 4 and 6 the cells received fresh Cardio Differentiation Medium without additions. As of day 8, cells were maintained in Cardio Culture Medium (RPMI-1640-Medium-GlutaMAX™-Supplement-HEPES (Life Technologies, #72400021) supplemented with B-27™ Supplement (50x)-serum free (Life Technologies, #17504044). Spontaneous beating cardiomyocytes could be observed between day 8 and day 10. On day 15, cells were passaged at 30% density and expanded by refreshing the media with Cardio Differentiation Medium supplemented with 2 μM of CHIR GSK3B-inhibitor CHIR99021 (Millipore, #361559). Expansion medium was refreshed after 3 days and cells were further passaged. This was performed a maximum of 3 times. To enrich for cardiomyocytes, using selection medium (RPMI without D-glucose (Life Technologies, #11879020), supplemented with Albumin, L-Ascorbic Acid 2-phosphate and Sodium DL-lactate/HEPES buffer (Sigma, #L4263) for 4 days. For downstream applications, hiPSC-CMs were dissociated with TrypLE™ Select Enzyme (10x)-no phenol red (GIBCO, #A1217703) for a maximum of 20 minutes at 37 °C. Cardiomyocytes were seeded at a density of 100,000 cells/cm² in Geltrex-coated wells.

Differentiation efficiency was determined by flow cytometry. Briefly, one million cardiomyocytes were centrifuged for 5 minutes at 300 g. Medium was aspirated and cells were washed once with dPBS. Next, cells were fixed by addition of 1 ml of ice-cold 70% ethanol followed by 4 minutes centrifugation at 300 g. Cells were permeabilized for 10 minutes at 4 °C by resuspension in Blocking Buffer (PBS (pH7.2-7.4) supplemented with 5% fetal bovine serum (FBS), 1% BSA, and 0.5% Triton X-100). Permeabilized cells were then centrifuged for 4 minutes at 300 g and the supernatant was aspirated. After, the cell pellet was resuspended in 100 μL blocking buffer supplemented with anti-Cardiac Troponin T antibody (Abcam, #ab45932; 1:2000) and incubated for 1 hour at 4 °C. After 1 hour, cells were washed with 500 μL of blocking buffer and centrifuged for 4 minutes at 300 g. This washing step was per-

formed twice. Next, cells were resuspended in 100 μ l blocking buffer supplemented with Alexa 488-anti-rabbit antibody (Thermo Fisher Scientific, #A-21206; 1:4000) and incubated for 45 minutes at room temperature (RT). Cells were washed twice as previously described. Finally, cells were resuspended in 1 ml of dPBS and analysed by FACs (BD LSRFortessa™ X-20 Cell Analyzer).

Knockdown experiments

On day 35 of cardiomyocyte differentiation, described above, cells were stressed with 10nM Endothelin-1 (ET-1) (Sigma, E7764-10UG) or 10nM vehicle (Dimethyl sulphoxide, DMSO) (Merk, CAS #: 67-68-5). Cells treated with vehicle were transfected with 10 nM of siRNA scramble (Origene). Cells stressed with ET-1 were transfected with 10 nM of siRNA scramble or a cocktail of 3 siRNA oligo duplexes targeting NR2F2 (Origene, SR303544) using Lipofectamine RNAiMAX (Thermo Fisher Scientific, #13778030) according to the manufacturers' instructions. Cells were refreshed with ET-1 or vehicle every 24 hours. After 48 hours, total RNA was isolated (as described above) and protein samples were collected after 72 hours (as described above).

RNA extraction for Quantitative polymerase chain reaction (qPCR)

RNA was extracted from hiPSC using TRIzol™ Reagent (Thermo Fisher Scientific) according to manufacturers' instructions. RNA concentration was determined using Nanodrop 1000 spectrophotometer (ThermoFisher Scientific). Complementary DNA (cDNA) was synthesized from a total of 500 ng of RNA using the iScript™ cDNA Synthesis Kit (Bio-Rad, #1708891), according to manufacturer's protocol. qPCR was performed using gene specific primers (listed below) according to the instructions described by the IQ™ SYBR Green Supermix (Bio-Rad, #170-8885). The RT-PCR protocol was as follows: 95 °C for 15 minutes, followed by 40 cycles at 95 °C for 15 seconds, 60 °C for 30 seconds and 72 °C for 30 seconds using the CFX96 Realtime PCR system (Bio-Rad). Data was normalized to *RPL32*.

Protein extraction for Western Blot

Protein was extracted from hiPSC-CMs using RIPA lysis buffer (50 mM Tris at pH7.5, 150 mM NaCl, 0.1% SDS, 0.5% sodium deoxycholate, 1% Triton X-100) supplemented with 1 tablet of cComplete™ Protease Inhibitor Cocktail (Roche, #11836170001)

Table 2. quantitative PCR primers

| Gene | FW primer (5'-3') | RV primer (5'-3') |
|-----------------|------------------------|------------------------|
| <i>ACTC1</i> | ATGTGTGACGACGAGGAGAC | ACCCACCATAACTCCCTGGT |
| <i>ANKRD2</i> | AGCAGACACCAATGTGAGGG | GCAGTATCCCCTCCCTGTC |
| <i>CRYAB</i> | CCGACGTCTACTTCCCTGAG | CCATGCACCTCAATCACATC |
| <i>DES</i> | CTCCCCATCCAGACCTACTCT | GGTATGGACCTCAGAACCCCT |
| <i>DPH5</i> | CGAGGAGAAGAACCAGCAGTTA | GCCTGCTGCAATTTTCTGGT |
| <i>FHL2</i> | GCCGTGAGTACCTCCAACC | GTTCTCAGCCACAGTCTCCC |
| <i>GLRX2</i> | GCTCTGACCATGATTTGGCG | GTATTGCTCTCCATCCCAGAGG |
| <i>HSPB1</i> | CGCGGAAATACAGCTGC | GTGATCTCGTTGGACTGCGT |
| <i>IDH2</i> | GCCCTGCTCGTTCGCTCT | TCACCATCCATCTCCACCACG |
| <i>LDB3</i> | CAACCCATTGGCCTGACT | TGCTCAATAGGGGTGCTTGA |
| <i>LTBP1</i> | TGCTCAATAGGGGTGCTTGA | GCTGGGCAAATGCACAAGAA |
| <i>LYPLAL1</i> | TTCTGCAGCGCTGTATCGT | TTGTCCAGAATCACCTGAGCC |
| <i>MYH7</i> | CACTTGAGTAGCCCAGGCACA | CCGCTCCTTCTCTGACTTGC |
| <i>MYL12A</i> | GGTTTTTAGCGCTCTCTGG | ATGGTGGTGGTTAAGTCCCG |
| <i>MYL3</i> | AAGATCACCTACGGGCAGTG | CTGGAGCATAGGCAGGAAAG |
| <i>NDUFS7</i> | GCTACGACATGGACCGCTTT | ATCTGGTCGTAGACCTTGCG |
| <i>NPPA</i> | CCGTGAGCTTCTCTCTTTTA | CCAAATGGTCCAGCAAATTC |
| <i>NPPB</i> | CTCCAGAGACATGGATCCCC | GTTGCGCTGCTCCTGTAAC |
| <i>NR2F2</i> | CGGAGGAACCTGAGCTACAC | CCTCTGCACCGCTTCCC |
| <i>PPP1R12B</i> | TCCCACAGACAATTGCTCCC | TGTAGGGACTTGTGGGGTCA |
| <i>PSMA5</i> | GTTGGTCCTCAGAATCCCCG | GTATTCACGCCCTGTGCGTA |
| <i>RPL32</i> | CAACGTCAAGGAGCTGGAAG | TGGGGTTGGTGACTCTGATG |
| <i>TECL</i> | AACTTGACTCTCAGCGGGC | GGGTACCACTTTGGACATGC |
| <i>XIRP1</i> | GAGGAACGACGAACCCTGAG | GTAGAGGCTGGATGCAAGGG |

per 10 ml of RIPA buffer. Subsequently, samples were boiled for 5 minutes at 99°C in 4x Leammli buffer, including 2% β -mercaptoethanol. Between 5-20 μ g of protein extract was loaded on a 10% SDS-PAGE. Blotted membranes were blocked with 3-5% milk in TBS-Tween for 1 hour at RT. Subsequently, membranes were incubated with primary antibody against the target protein (Antibody) overnight at 4°C. The next day, membranes were washed with 3x with TBS-Tween and incubated with an HRP-conjugated secondary antibody (Jackson Immuno Research Europe Ltd) anti-mouse or anti-rabbit immunoglobulin G for 1 hour at RT. Blots were visualized using Clarity™ Western ECL Substrate (Bio-Rad, #170-5061) and Amersham Imager

600. Western blots were quantified by ImageJ. Data was normalized to Vinculin (antibody).

Immunocytochemistry on hiPSC-CMs

Immunological stainings were performed on cells cultured on glass coverslips, coated with Geltrex. After 72 hours of stress (with/without siRNA), cells were washed and fixed with 2% paraformaldehyde (Klinipath, Duiven) for 10 minutes. Once cells were fixed, they were washed 2x and stored in PBS at 4°C until they were used for staining. Slides were blocked in Blocking Buffer (PBS supplemented with 5% fetal bovine se-

Table 3 List of Antibodies

| Antibody | Source |
|-------------|---------------------------|
| MYBPC3 (E7) | Santa Cruz (sc-137180) |
| TNNT | Abcam (ab8295) |
| VINCULIN | Santa Cruz (sc-25336) |
| NR2F2 | R&D Systems (PP-H7147-00) |
| HSPB1 | Santa Cruz (sc-13132) |
| FHL2 | Sigma (HPA006028) |
| PPP1R12B | Proteintech (13366-1-AP) |

rum (FBS), 1% BSA, and 0.5% Triton X-100) for 30 minutes. Cells were incubated O/N with primary antibodies at 4°C (TNNT mouse 1:600, TNNT 1:600 rabbit, NR2F2 1:300, Antibodies). The next day, slides were washed 3x with PBS-T (PBS supplemented with 0.01% TritonX) and incubated with secondary antibody and DAPI (alexa 488 anti-mouse/rabbit 1:500, alexa 567 anti/mouse rabbit 1:500, DAPI 1:1000) for 1 hour at RT. Slides were washed 3x in PBS-T and mounted on microscope glasses. Microscope slides were visualized using the Leica DM4000 confocal microscope.

Statistical analysis

To compare the difference between the groups in the knockdown experiments on iPS-CMs, Prism 6 (GraphPad Software, Inc.) was used to perform a 2-way-ANOVA followed by a Tukey's multiple comparisons test. P value of <0.05 was interpreted as statistically significant.

Outliers were removed by using a ROUT test with $Q=1\%$, difference between samples was tested for significance by using an ordinary one-way ANOVA followed by a Tukey's multiple comparisons test.

References

- Aggarwal, P., Turner, A., Matter, A., Kattman, S. J., Stoddard, A., Lorier, R., Swanson, B. J., Arnett, D. K., & Broeckel, U. (2014). RNA expression profiling of human iPSC-derived cardiomyocytes in a cardiac hypertrophy model. *PLoS ONE*, *9*(9), 1–10. <https://doi.org/10.1371/journal.pone.0108051>
- Ando, K., Nagao, M., Watanabe, E., Sakai, A., Suzuki, A., Nakao, R., Ishizaki, U., Sakai, S., & Hagiwara, N. (2020). Association between myocardial hypoxia and fibrosis in hypertrophic cardiomyopathy: analysis by T2* BOLD and T1 mapping MRI. *European Radiology*, *30*(8), 4327–4336. <https://doi.org/10.1007/s00330-020-06779-9>
- Antunes, M. de O., & Scudeler, T. L. (2020). Hypertrophic cardiomyopathy. *IJC Heart and Vasculature*, *27*, 100503. <https://doi.org/10.1016/j.ijcha.2020.100503>
- Barth, A. S., Merk, S., Arnoldi, E., Zwermann, L., Kloos, P., Gebauer, M., Steinmeyer, K., Bleich, M., Kääb, S., Pfeufer, A., Überfuhr, P., Dugas, M., Steinbeck, G., & Nabauer, M. (2005). Functional profiling of human atrial and ventricular gene expression. *Pflugers Archiv European Journal of Physiology*, *450*(4), 201–208. <https://doi.org/10.1007/s00424-005-1404-8>
- Becker, R. C., Owens, A. P., & Sadayappan, S. (2020). Tissue-level inflammation and ventricular remodeling in hypertrophic cardiomyopathy. *Journal of Thrombosis and Thrombolysis*, *49*(2), 177–183. <https://doi.org/10.1007/s11239-019-02026-1>
- Boogerd, C. J., Lacraz, G. P., Vértessy, Á., Perini, I., de Ruiter, H., Brodehl, A., van der Kraak, P., Huibers, M., de Jonge, N., Junker, J. P., Vink, A., & van Rooij, E. (2019). Spatial Transcriptomics Unveils ZBTB11 as a Regulator of Cardiomyocyte Degeneration in Arrhythmogenic Cardiomyopathy. *Circulation Research*, *125*(Suppl_1), 1–15. https://doi.org/10.1161/res.125.suppl_1.510
- Bos, J. M., Hebl, V. B., Oberg, A. L., Sun, Z., Herman, D. S., Teekakirikul, P., Seidman, J. G., Seidman, C. E., dos Remedios, C. G., Maleszewski, J. J., Schaff, H. V., Dearani, J. A., Noseworthy, P. A., Friedman, P. A., Ommen, S. R., Brozovich, F. V., & Ackerman, M. J. (2020). Marked Up-Regulation of ACE2 in Hearts of Patients With Obstructive Hypertrophic Cardiomyopathy: Implications for SARS-CoV-2-Mediated COVID-19. *Mayo Clinic Proceedings*, *95*(7), 1354–1368. <https://doi.org/10.1016/j.mayocp.2020.04.028>
- Bos, J. M., Towbin, J. A., & Ackerman, M. J. (2009). Diagnostic, Prognostic, and Therapeutic Implications of Genetic Testing for Hypertrophic Cardiomyopathy. *Journal of the American College of Cardiology*, *54*(3), 201–211. <https://doi.org/10.1016/j.jacc.2009.02.075>
- Canepa, M., Pozios, I., Vianello, P. F., Ameri, P., Brunelli, C., Ferrucci, L., & Abraham, T. P. (2016). Distinguishing ventricular septal bulge versus hypertrophic cardiomyopathy in the elderly. *Heart (British Cardiac Society)*, *102*(14), 1087–1094. <https://doi.org/10.1136/heartjnl-2015-308764>
- Chaffin, M., Papangeli, I., Simonson, B., Akkad, A. D., Hill, M. C., Arduini, A., Fleming, S. J., Melanson, M., Hayat, S., Kost-Alimova, M., Atwa, O., Ye, J., Bedi, K. C., Nahrendorf, M., Kaushik, V. K., Stegmann, C. M., Margulies, K. B., Tucker, N. R., & Ellinor, P. T. (2022). Single-nucleus profiling of human dilated and hypertrophic cardiomyopathy. *Nature*, *608*(7921), 174–180. <https://doi.org/10.1038/s41586-022-04817-8>
- Cheng, Z., Qi, M., Zhang, C., & Mao, Y. (2021). Myocardial Fibrosis in the Pathogenesis, Diagnosis, and Treatment of Hypertrophic Cardiomyopathy. *Cardiovascular Innovations and Applications*, *5*(4), 267–274. <https://doi.org/10.15212/cvia.2021.0008>
- Christiaans, I., Nannenbergh, E. A., Dooijes, D., Jongbloed, R. J. E., Michels, M., Postema, P. G., Majoor-Krakauer, D., van den Wijngaard, A., Mannens, M. M. A. M., van Tintelen, J. P., van Langen, I. M., & Wilde, A. A. M. (2010). Founder mutations in hypertrophic cardiomyopathy patients in the Netherlands. *Neth Heart J*, *18*(5), 248–254. <https://doi.org/10.1007/s12471-010-0008-1>

org/10.1007/BF03091771

- Chung, M. W., Tsoutsman, T., & Semsarian, C. (2003). Hypertrophic cardiomyopathy: from gene defect to clinical disease. *Cell Res*, *13*(1), 9–20. <https://doi.org/10.1038/sj.cr.7290146>
- Churko, J. M., Garg, P., Treutlein, B., Venkatasubramanian, M., Wu, H., Lee, J., Wessells, Q. N., Chen, S. Y., Chen, W. Y., Chetal, K., Mantalas, G., Neff, N., Jabart, E., Sharma, A., Nolan, G. P., Salomonis, N., & Wu, J. C. (2018). Defining human cardiac transcription factor hierarchies using integrated single-cell heterogeneity analysis. *Nature Communications*, *9*(1). <https://doi.org/10.1038/s41467-018-07333-4>
- Coats, C. J., Heywood, W. E., Virasami, A., Ashrafi, N., Syrris, P., Dos Remedios, C., Treibel, T. A., Moon, J. C., Lopes, L. R., McGregor, C. G. A., Ashworth, M., Sebire, N. J., McKenna, W. J., Mills, K., & Elliott, P. M. (2018). Proteomic Analysis of the Myocardium in Hypertrophic Obstructive Cardiomyopathy. *Circulation. Genomic and Precision Medicine*, *11*(12), e001974. <https://doi.org/10.1161/CIRCGEN.117.001974>
- Cohn, R., Thakar, K., Lowe, A., Ladha, F. A., Pettinato, A. M., Romano, R., Meredith, E., Chen, Y. S., Atamanuk, K., Huey, B. D., & Hinson, J. T. (2019). A Contraction Stress Model of Hypertrophic Cardiomyopathy due to Sarcomere Mutations. *Stem Cell Reports*, *12*(1), 71–83. <https://doi.org/10.1016/j.stemcr.2018.11.015>
- Dadson, K., Turdi, S., Hashemi, S., Zhao, J., Polidovitch, N., Beca, S., Backx, P. H., McDermott, J. C., & Sweeney, G. (2015). Adiponectin is required for cardiac MEF2 activation during pressure overload induced hypertrophy. *Journal of Molecular and Cellular Cardiology*, *86*, 102–109. <https://doi.org/10.1016/j.yjmcc.2015.06.020>
- Davenport, A. P., Hyndman, K. A., Dhaun, N., Southan, C., Kohan, D. E., Pollock, J. S., Pollock, D. M., Webb, D. J., & Maguire, J. J. (2016). *Endothelin*. *95499*.
- Desjardins, C., & Naya, F. (2016). The Function of the MEF2 Family of Transcription Factors in Cardiac Development, Cardiogenomics, and Direct Reprogramming. *Journal of Cardiovascular Development and Disease*, *3*(3), 26. <https://doi.org/10.3390/jcdd3030026>
- Durinck, S., Moreau, Y., Kasprzyk, A., Davis, S., De Moor, B., Brazma, A., & Huber, W. (2005). BioMart and Bioconductor: A powerful link between biological databases and microarray data analysis. *Bioinformatics*, *21*(16), 3439–3440. <https://doi.org/10.1093/bioinformatics/bti525>
- Grun, D., Muraro, M. J., Boisset, J. C., Wiebrands, K., Lyubimova, A., Dharmadhikari, G., van den Born, M., van Es, J., Jansen, E., Clevers, H., de Koning, E. J., & van Oudenaarden, A. (2016). De Novo Prediction of Stem Cell Identity using Single-Cell Transcriptome Data. *Cell Stem Cell*, *19*(2), 266–277. <https://doi.org/10.1016/j.stem.2016.05.010>
- Hashimshony, T., Wagner, F., Sher, N., & Yanai, I. (2012). CEL-Seq: Single-Cell RNA-Seq by Multiplexed Linear Amplification. *Cell Reports*, *2*(3), 666–673. <https://doi.org/10.1016/j.celrep.2012.08.003>
- Heinz, S., Benner, C., Spann, N., Bertolino, E., Lin, Y. C., Laslo, P., Cheng, J. X., Murre, C., Singh, H., & Glass, C. K. (2010). Simple Combinations of Lineage-Determining Transcription Factors Prime cis-Regulatory Elements Required for Macrophage and B Cell Identities. *Molecular Cell*, *38*(4), 576–589. <https://doi.org/10.1016/j.molcel.2010.05.004>
- Johansson, M., Ulfenborg, B., Andersson, C. X., Heydarkhan-Hagvall, S., Jeppsson, A., Sartipy, P., & Synnergren, J. (2020a). Cardiac hypertrophy in a dish: A human stem cell based model. *Biology Open*, *9*(9), 1–12. <https://doi.org/10.1242/bio.052381>
- Johansson, M., Ulfenborg, B., Andersson, C. X., Heydarkhan-Hagvall, S., Jeppsson, A., Sartipy, P., & Synnergren, J. (2020b). Cardiac hypertrophy in a dish: A human stem cell based model. *Biology Open*, *9*(9), 1–12. <https://doi.org/10.1242/bio.052381>
- Jong, P. L. De, Michels, M., Kuster, D. W. D., Brundel, B. J. J. M., & Velden, J. Van Der. (2006). *Protein quality control activation and microtubul remodeling in HCM*.
- Junker, J. P., Noël, E. S., Guryev, V., Peterson, K. A., Shah, G., Huisken, J., McMahon, A.

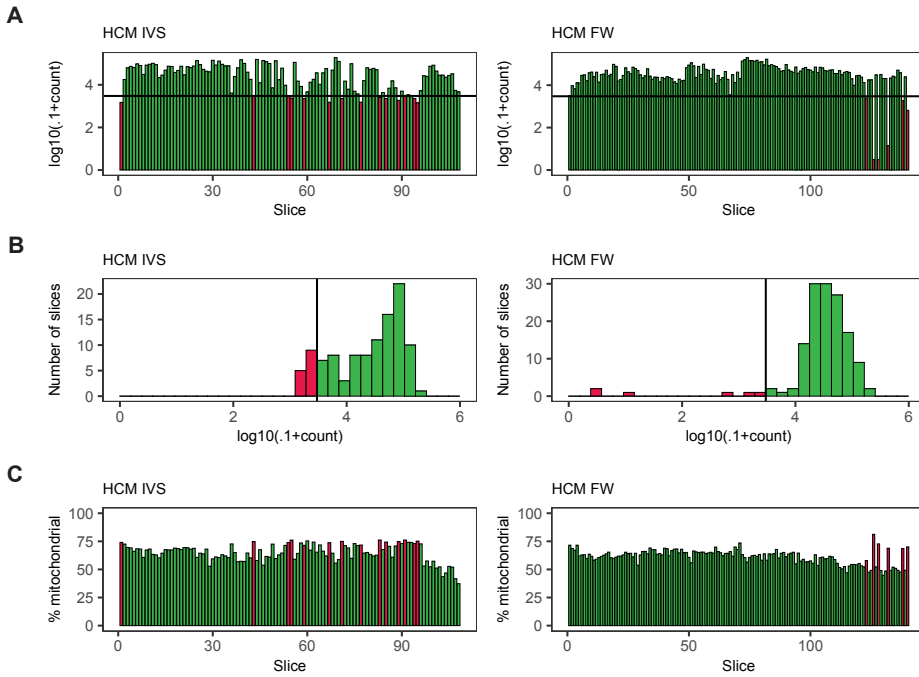
- P., Berezikov, E., Bakkers, J., & Van Oudenaarden, A. (2014). Genome-wide RNA Tomography in the Zebrafish Embryo. *Cell*, *159*(3), 662–675. <https://doi.org/10.1016/j.cell.2014.09.038>
- Kirschner, S. E., Becker, E., Antognozzi, M., Kubis, H. P., Francino, A., Navarro-López, F., Bit-Avragim, N., Perrot, A., Mirrakhimov, M. M., Osterziel, K. J., McKenna, W. J., Brenner, B., & Kraft, T. (2005). Hypertrophic cardiomyopathy-related β -myosin mutations cause highly variable calcium sensitivity with functional imbalances among individual muscle cells. *American Journal of Physiology - Heart and Circulatory Physiology*, *288*(3 57-3), 1242–1251. <https://doi.org/10.1152/ajpheart.00686.2004>
- Kittleson, M. M., Minhas, K. M., Irizarry, R. A., Ye, S. Q., Edness, G., Breton, E., Conte, J. V., Tomaselli, G., Garcia, J. G. N., & Hare, J. M. (2005). Gene expression analysis of ischemic and nonischemic cardiomyopathy: Shared and distinct genes in the development of heart failure. *Physiological Genomics*, *21*, 299–307. <https://doi.org/10.1152/physiolgenomics.00255.2004>
- Kolodziejczyk, S. M., Wang, L., Balazsi, K., Derepentigny, Y., Kothary, R., & Megeney, L. A. (1999). MEF2 is upregulated during cardiac hypertrophy and is required for normal post-natal growth of the myocardium. *Current Biology*, *9*(20), 1203–1206. [https://doi.org/10.1016/S0960-9822\(00\)80027-5](https://doi.org/10.1016/S0960-9822(00)80027-5)
- Kraft, T., & Montag, J. (2019). Altered force generation and cell-to-cell contractile imbalance in hypertrophic cardiomyopathy. *Pflügers Archiv - European Journal of Physiology*, *471*(5), 719–733. <https://doi.org/10.1007/s00424-019-02260-9>
- Kruse, F., Junker, J. P., van Oudenaarden, A., & Bakkers, J. (2016). Tomo-seq: A method to obtain genome-wide expression data with spatial resolution. In *Methods in Cell Biology* (Vol. 135). Elsevier Ltd. <https://doi.org/10.1016/bs.mcb.2016.01.006>
- Lacruz, G. P. A., Junker, J. P., Gladka, M. M., Molenaar, B., Scholman, K. T., Vigil-Garcia, M., Versteeg, D., De Ruiter, H., Vermunt, M. W., Creighton, M. P., Huibers, M. M. H., De Jonge, N., Van Oudenaarden, A., & Van Rooij, E. (2017). Tomo-Seq Identifies SOX9 as a Key Regulator of Cardiac Fibrosis during Ischemic Injury. *Circulation*, *136*(15), 1396–1409. <https://doi.org/10.1161/CIRCULATIONAHA.117.027832>
- Laird, J., Perera, G., Batorsky, R., Wang, H., Arkun, K., & Chin, M. T. (2023). Spatial Transcriptomic Analysis of Focal and Normal Areas of Myocyte Disarray in Human Hypertrophic Cardiomyopathy. *International Journal of Molecular Sciences*, *24*(16). <https://doi.org/10.3390/ijms241612625>
- Lamke, G. T., Allen, R. D., Edwards, W. D., Tazelaar, H. D., & Danielson, G. K. (2003). Surgical pathology of subaortic septal myectomy associated with hypertrophic cardiomyopathy: A study of 204 cases (1996–2000). *Cardiovascular Pathology*, *12*(3), 149–158. [https://doi.org/10.1016/S1054-8807\(03\)00036-X](https://doi.org/10.1016/S1054-8807(03)00036-X)
- Larson, A., Codden, C. J., Huggins, G. S., Rastegar, H., Chen, F. Y., Maron, B. J., Rowin, E. J., Maron, M. S., & Chin, M. T. (2022). Altered intercellular communication and extracellular matrix signaling as a potential disease mechanism in human hypertrophic cardiomyopathy. *Scientific Reports*, *0123456789*, 1–13. <https://doi.org/10.1038/s41598-022-08561-x>
- Li, H., & Durbin, R. (2009). Fast and accurate short read alignment with Burrows-Wheeler transform. *Bioinformatics*, *25*(14), 1754–1760. <https://doi.org/10.1093/bioinformatics/btp324>
- Lim, D. S., Roberts, R., & Marian, A. J. (2001). Expression profiling of cardiac genes in human hypertrophic cardiomyopathy: insight into the pathogenesis of phenotypes. *Journal of the American College of Cardiology*, *38*(4), 1175–1180. [https://doi.org/10.1016/s0735-1097\(01\)01509-1](https://doi.org/10.1016/s0735-1097(01)01509-1)
- Litviňuková, M., Talavera-López, C., Maatz, H., Reichart, D., Worth, C. L., Lindberg, E. L., Kanda, M., Polanski, K., Heinig, M., Lee, M., Nadelmann, E. R., Roberts, K., Tuck, L., Fasouli, E. S., DeLaughter, D. M., McDonough, B., Wakimoto, H., Gorham, J. M., Samari, S., ...

- Teichmann, S. A. (2020). Cells of the adult human heart. *Nature*, September. <https://doi.org/10.1038/s41586-020-2797-4>
- Liu, X., Yin, K., Chen, L., Chen, W., Li, W., Zhang, T., Sun, Y., Yuan, M., Wang, H., Song, Y., Wang, S., Hu, S., & Zhou, Z. (2023). Lineage-specific regulatory changes in hypertrophic cardiomyopathy unraveled by single-nucleus RNA-seq and spatial transcriptomics. *Cell Discovery*, 9(1). <https://doi.org/10.1038/s41421-022-00490-3>
- Love, M. I., Huber, W., & Anders, S. (2014). Moderated estimation of fold change and dispersion for RNA-seq data with DESeq2. *Genome Biology*, 15(12), 1–21. <https://doi.org/10.1186/s13059-014-0550-8>
- Marian, A. J., & Braunwald, E. (2017). Hypertrophic Cardiomyopathy: Genetics, Pathogenesis, Clinical Manifestations, Diagnosis, and Therapy. *Circ Res*, 121(7), 749–770. <https://doi.org/10.1161/CIRCRESAHA.117.311059>
- Maron, B. A., Wang, R. S., Shevtsov, S., Drakos, S. G., Arons, E., Wever-Pinzon, O., Huggins, G. S., Samokhin, A. O., Oldham, W. M., Aguib, Y., Yacoub, M. H., Rowin, E. J., Maron, B. J., Maron, M. S., & Loscalzo, J. (2021). Individualized interactomes for network-based precision medicine in hypertrophic cardiomyopathy with implications for other clinical pathophenotypes. *Nature Communications*, 12(1), 1–11. <https://doi.org/10.1038/s41467-021-21146-y>
- McLean, C. Y., Bristol, D., Hiller, M., Clarke, S. L., Schaar, B. T., Lowe, C. B., Wenger, A. M., & Bejerano, G. (2010). GREAT improves functional interpretation of cis-regulatory regions. *Nature Biotechnology*, 28(5), 495–501. <https://doi.org/10.1038/nbt.1630>
- Mirotsou, M., Watanabe, C. M. H., Schultz, P. G., Pratt, R. E., & Dzau, V. J. (2004). Elucidating the molecular mechanism of cardiac remodeling using a comparative genomic approach. *Physiological Genomics*, 15(Mi), 115–126. <https://doi.org/10.1152/physiolgenomics.00071.2003>
- Muraro, M. J., Dharmadhikari, G., Grün, D., Groen, N., Dielen, T., Jansen, E., van Gurp, L., Engelse, M. A., Carlotti, F., de Koning, E. J. P., & van Oudenaarden, A. (2016). A Single-Cell Transcriptome Atlas of the Human Pancreas. *Cell Systems*, 3(4), 385–394.e3. <https://doi.org/10.1016/j.cels.2016.09.002>
- Nakamura, M., & Sadoshima, J. (2018). Mechanisms of physiological and pathological cardiac hypertrophy. *Nature Reviews Cardiology*, 15(7), 387–407. <https://doi.org/10.1038/s41569-018-0007-y>
- Nomura, S., Satoh, M., Fujita, T., Higo, T., Sumida, T., Ko, T., Yamaguchi, T., Tobita, T., Naito, A. T., Ito, M., Fujita, K., Harada, M., Toko, H., Kobayashi, Y., Ito, K., Takimoto, E., Akazawa, H., Morita, H., Aburatani, H., & Komuro, I. (2018). Cardiomyocyte gene programs encoding morphological and functional signatures in cardiac hypertrophy and failure. *Nat Commun*, 9(1), 4435. <https://doi.org/10.1038/s41467-018-06639-7>
- Olivotto, I., Cecchi, F., Poggesi, C., & Yacoub, M. H. (2012). Patterns of disease progression in hypertrophic cardiomyopathy an individualized approach to clinical staging. *Circulation: Heart Failure*, 5(4), 535–546. <https://doi.org/10.1161/CIRCHEARTFAILURE.112.967026>
- Pei, J., Schuldt, M., Nagyova, E., Gu, Z., el Bouhaddani, S., Yiangou, L., Jansen, M., Calis, J. J. A., Dorsch, L. M., Blok, C. S., van den Dungen, N. A. M., Lansu, N., Boukens, B. J., Efimov, I. R., Michels, M., Verhaar, M. C., de Weger, R., Vink, A., van Steenbeek, F. G., ... Harakalova, M. (2021). Multi-omics integration identifies key upstream regulators of pathomechanisms in hypertrophic cardiomyopathy due to truncating MYBPC3 mutations. *Clinical Epigenetics*, 13(1), 1–20. <https://doi.org/10.1186/s13148-021-01043-3>
- Ren, C. W., Liu, J. J., Li, J. W. H., Li, J. W. H., Dai, J., & Lai, Y. Q. (2016). RNA-seq profiling of mRNA associated with hypertrophic cardiomyopathy. *Molecular Medicine Reports*, 14(6), 5573–5586. <https://doi.org/10.3892/mmr.2016.5931>
- Ren, Z., Yu, P., Li, D., Li, Z., Liao, Y., Wang, Y., Zhou, B., & Wang, L. (2020). Single-Cell Reconstruction of Progression Trajectory Reveals Intervention Principles in Pathological Cardiac

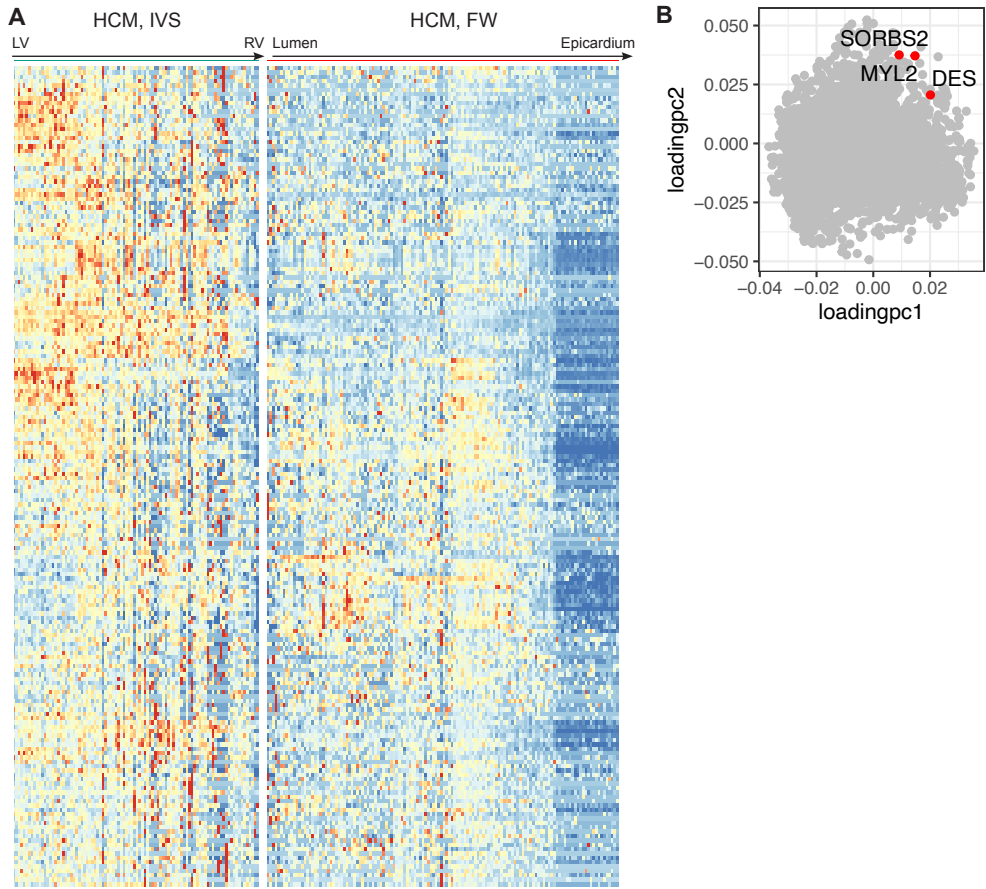
- Hypertrophy. *Circulation*, **141**(21), 1704–1719. <https://doi.org/10.1161/CIRCULATIONAHA.119.043053>
- Sack, M. N., Disch, D. L., Rockman, H. A., & Kelly, D. P. (1997). A role for Sp and nuclear receptor transcription factors in a cardiac hypertrophic growth program. *Proceedings of the National Academy of Sciences of the United States of America*, **94**(12), 6438–6443. <https://doi.org/10.1073/pnas.94.12.6438>
- Schuldt, M., Pei, J., Harakalova, M., Dorsch, L. M., Schlossarek, S., Mokry, M., Knol, J. C., Pham, T. V., Schelfhorst, T., Piersma, S. R., Dos Remedios, C., Dalinghaus, M., Michels, M., Asselbergs, F. W., Moutin, M. J., Carrier, L., Jimenez, C. R., van der Velden, J., & Kuster, D. W. D. (2021). Proteomic and Functional Studies Reveal Detyrosinated Tubulin as Treatment Target in Sarcomere Mutation-Induced Hypertrophic Cardiomyopathy. *Circ Heart Fail*, **14**(1), e007022. <https://doi.org/10.1161/CIRCHEARTFAILURE.120.007022>
- Seeger, T., Shrestha, R., Lam, C. K., Chen, C., McKeithan, W. L., Lau, E., Wnorowski, A., McMullen, G., Greenhaw, M., Lee, J., Oikonomopoulos, A., Lee, S., Yang, H., Mercola, M., Wheeler, M., Ashley, E. A., Yang, F., Karakikes, I., & Wu, J. C. (2019). A Premature Termination Codon Mutation in MYBPC3 Causes Hypertrophic Cardiomyopathy via Chronic Activation of Nonsense-Mediated Decay. *Circulation*, **139**(6), 799–811. <https://doi.org/10.1161/CIRCULATIONAHA.118.034624>
- Semsarian, C., Ingles, J., Maron, M. S., & Maron, B. J. (2015). New Perspectives on the Prevalence of Hypertrophic Cardiomyopathy. *Journal of the American College of Cardiology*, **65**(12), 1249–1254. <https://doi.org/10.1016/j.jacc.2015.01.019>
- Sepehrkhoy, S., Ghossein, J. M. I. H., van Es, R., Harakalova, M., de Jonge, N., Dooijes, D., van der Smagt, J. J., Buijsrogge, M. P., Hauer, R. N. W., Goldschmeding, R., de Weger, R. A., Asselbergs, F. W., & Vink, A. (2017). Distinct fibrosis pattern in desmosomal and phospholamban mutation carriers in hereditary cardiomyopathies. *Heart Rhythm*, **14**(7), 1024–1032. <https://doi.org/10.1016/j.hrthm.2017.03.034>
- Simonson, B., Chaffin, M., Hill, M. C., Atwa, O., Guedira, Y., Bhasin, H., Hall, A. W., Hayat, S., Baumgart, S., Bedi, K. C., Margulies, K. B., Klattenhoff, C. A., & Ellinor, P. T. (2023). Single-nucleus RNA sequencing in ischemic cardiomyopathy reveals common transcriptional profile underlying end-stage heart failure. *Cell Reports*, **42**(2). <https://doi.org/10.1016/j.celrep.2023.112086>
- Van Der Velden, J., Tocchetti, C. G., Varricchi, G., Bianco, A., Sequeira, V., Hilfiker-Kleiner, D., Hamdani, N., Leite-Moreira, A. F., Mayr, M., Falcao-Pires, I., Thum, T., Dawson, D. K., Baligand, J. L., & Heymans, S. (2018). Metabolic changes in hypertrophic cardiomyopathies: Scientific update from the working group of myocardial function of the European Society of Cardiology. *Cardiovascular Research*, **114**(10), 1273–1280. <https://doi.org/10.1093/cvr/cvy147>
- Vanderheyden, M., Goethals, M., Verstreken, S., De Bruyne, B., Muller, K., Van Schuerbeeck, E., & Bartunek, J. (2004). Wall stress modulates brain natriuretic peptide production in pressure overload cardiomyopathy. *Journal of the American College of Cardiology*, **44**(12), 2349–2354. <https://doi.org/10.1016/j.jacc.2004.09.038>
- Varnava, A. M., Elliott, P. M., Sharma, S., McKenna, W. J., & Davies, M. J. (2000). Hypertrophic cardiomyopathy: the interrelation of disarray, fibrosis, and small vessel disease. *Heart (British Cardiac Society)*, **84**(5), 476–482. <https://doi.org/10.1136/HEART.84.5.476>
- Wehrens, M., Leeuw, A. E. De, Wright-clark, M., Eding, J. E. C., Boogerd, C. J., Molenaar, B., Van Der Kraak, P. H., Kuster, D. W. D., van der Velden, J., Michels, M., Vink, A., & van Rooij, E. (2022). Single-cell transcriptomics provides insights into hypertrophic cardiomyopathy. *Cell Reports*, **39**(6), 110809. <https://doi.org/10.1016/j.celrep.2022.110809>
- Wu, S. P., Kao, C. Y., Wang, L., Creighton, C. J., Yang, J., Donti, T. R., Harmancey, R., Vasquez, H. G., Graham, B. H., Bellen, H. J., Taegtmeyer, H., Chang, C. P., Tsai, M. J., & Tsai, S. Y. (2015). Increased COUP-TFII expression in adult hearts induces mitochondrial dysfunction

- tion resulting in heart failure. *Nature Communications*, 6. <https://doi.org/10.1038/ncomms9245>
- Wu, S. pin, Cheng, C. M., Lanz, R. B., Wang, T., Respress, J. L., Ather, S., Chen, W., Tsai, S. J. S. Y. S. J., Wehrens, X. H. T., Tsai, M. J., & Tsai, S. J. S. Y. S. J. (2013). Atrial Identity Is Determined by a COUP-TFII Regulatory Network. *Developmental Cell*, 25(4), 417–426. <https://doi.org/10.1016/j.devcel.2013.04.017>
- Xie, X., Wu, S. P., Tsai, M. J., & Tsai, S. (2017). The Role of COUP-TFII in Striated Muscle Development and Disease. In *Current Topics in Developmental Biology* (1st ed., Vol. 125). Elsevier Inc. <https://doi.org/10.1016/bs.ctdb.2016.12.006>
- Yang, X., Pabon, L., & Murry, C. E. (2014). Engineering Adolescence. *Circulation Research*, 114(3), 511–523. <https://doi.org/10.1161/CIRCRESAHA.114.300558>

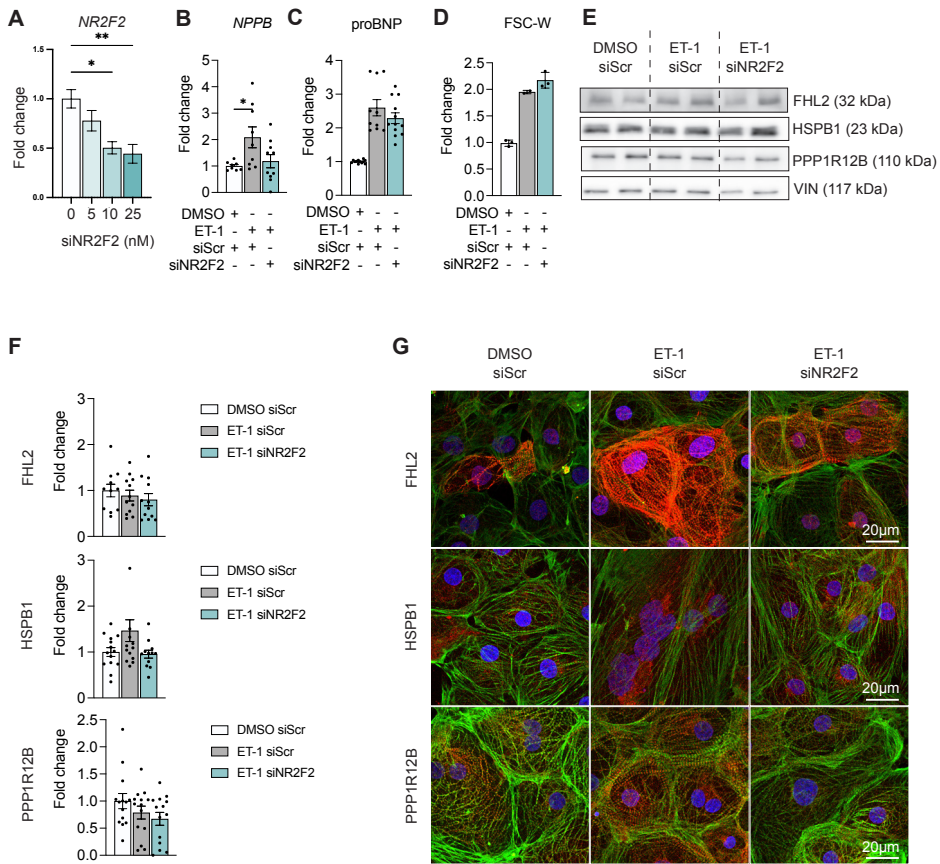
Supplemental material



Supplemental Figure 1. Selection and quality control of sections. (A) Histogram showing the total amount of read counts per consecutive slices. (B) Histogram showing the distribution of reads per slice. Slices with less than 3000 reads were excluded (red). (C) Percentage of mitochondrial reads per slice. Red slices were not selected for further analysis by previous quality controls. Four samples are displayed for each figure; HCM (top) tissue from the septum (left) and the free wall (FW, right). Related to Figure 2.



Supplemental Figure 2. Expression of PC1/PC2 overlapping genes. (A) Heatmap showing the expression of the 188 overlapping genes between PC1 and PC2 in HCM tissue **(B)** Dotplot showing the high loading of *SORBS2*, *MYL2* and *DES* in both PC1 and PC2. Related to Figure 4.



Supplemental Figure 3. The effect of siNR2F2 on target genes. (A) Dose-dependent decrease in NR2F2 mRNA after treatment with siRNA. **(B)** qPCR analysis showing a decreased expression of Natriuretic peptide B (*NPPB*) after siNR2F2 in ET-1 treated cells. Normalized to *RPL32*. Fold change is calculated compared to unstressed siScr-treated cells. **(C)** ELISA analysis showing an increase in proBNP after ET-1 treatment. **(D)** FACS results of FSC-W as an indication of cell size showing an increase in after ET-1 treatment. **(E)** Western blot showing the expression of Four and a half LIM Domains 2 (FHL2), Heat shock protein Family B (small) Member 1 (HSPB1) and Protein Phosphatase 1 regulatory Subunit 12B (PPP1R12B). Normalised to VIN. **(F)** Quantification of western blot in E. **(G)** Immunocytochemistry showing the expression of target genes (red) in cardiomyocytes (counterstained with cTnT (green); DAPI (blue). Forward scatter-Width (FSC-W). Related to Figure 5.

Supplemental Table 1: PC 1-5 genes related to Figure 2

| PC1 | PC2 | PC3 | PC4 | PC5 |
|----------|---------|--------------|----------|----------|
| MSRB2 | MB | IGFBP7 | PSMA5 | GSTM4 |
| USMG5 | SMPX | PEA15 | NPM1 | RBM39 |
| MRPS21 | TNNI3 | COL15A1 | C1orf43 | OR7E37P |
| DNAJA4 | PLN | PCSK6 | ILF2 | EGLN3 |
| COX6B1 | CSRP3 | RPL31 | RPS20 | GOLGA7 |
| MTRNR2L1 | ACTA1 | RPS27L | OXCT1 | RPS6KC1 |
| TRDN | COX7A2 | MRPL30 | PPP2CA | AKAP8 |
| TIMMDC1 | NDUFA1 | MYCT1 | LPAR6 | TBC1D4 |
| COQ10A | NDUFA4 | SRPX | SORT1 | LGALS3BP |
| MPC1 | TPM1 | CCDC80 | RPL41 | IL17RA |
| CAPZA2 | COX5A | RPS23 | CDK2AP1 | CCNL2 |
| TNNT2 | LMOD2 | RPL7A | RBPMS | TRAPP6B |
| UBL5 | NDUFB6 | ZC3H11A | ACBD6 | SELO |
| ATG3 | COX6A2 | LDB2 | TMA7 | R3HDM2 |
| RPS15 | CYCS | PKM | TRIAP1 | MTFR1 |
| TMEM50B | MYL7 | SERPINF1 | VEGFB | DCLK2 |
| HSPE1 | MYOZ2 | PBX1 | CLNS1A | GFM1 |
| FLOT1 | DTNA | C1S | BNIP3 | TCF21 |
| RPL19 | MYH7 | RPS5 | SAP18 | PSMG2 |
| CFL2 | CLIC5 | MBNL2 | CLINT1 | CASP8AP2 |
| RPS28 | PDLIM5 | SLC25A4 | CDC42 | ESRRG |
| S100A1 | CASQ2 | GNB1 | FKBP3 | MDFIC |
| CHCHD10 | COX7A1 | PTPN12 | GSK3B | PSMD12 |
| HRC | MYL3 | SPARCL1 | ATP5J | MED6 |
| NDUFB7 | ACTN2 | ZNF217 | CA4 | COX10 |
| PCBD1 | CKM | FBLN1 | UBR1 | BBX |
| PKIA | POPDC3 | MEA1 | TMEM14B | NDUFS2 |
| MYL12A | NEBL | CFH | ITGB1BP1 | METAP2 |
| FXYD1 | PDLIM1 | TMSB10 | ECH1 | RALB |
| NDUFV3 | NDUFAB1 | SRP14 | MXRA7 | GTDC1 |
| QKI | ATP5B | DCN | PRKAR1A | PPIH |
| NDUFA11 | COX6C | RPL36AL | MARCH2 | MLIP |
| FAM101B | PPDF | CD59 | ZEB2 | FNBP4 |
| ARHGAP1 | SH3RF2 | CANX | ATPAF1 | MED11 |
| LAMTOR5 | EIF1B | FABP5 | SLC39A14 | ABRA |
| CMC2 | NDUFA3 | COL14A1 | SRPK2 | PGR |
| ARL3 | FABP3 | IFI27 | COQ10B | LRRC41 |
| VDAC1 | RCAN2 | LOC100505738 | COX4I1 | NPR2 |
| TAF10 | MASP1 | TOMM6 | PSMB6 | EZR |
| ADPRHL1 | SORBS2 | ARL6IP4 | LYPLAL1 | IMMP1L |
| RPL10 | ATP5G1 | APLNR | CTNNB1 | TRIQK |
| TBX3 | CSDA | COPRS | SF3B4 | DVL1 |

| | | | | |
|---------|----------|--------|--------------|----------|
| TPM3 | C22orf32 | FKBP1A | GPD1L | ILF3-AS1 |
| PROX1 | MYL2 | SCN7A | LOC100131138 | ATP6V1D |
| NDUFAF4 | ACTC1 | COL6A1 | EIF5B | PCM1 |
| PSMA7 | HADHB | SEPT9 | SNHG16 | KLHL15 |
| ACAA2 | MYOM2 | JUND | MAP1LC3A | NREP |
| RPL11 | TIMM8B | GSN | RBX1 | CACYBP |
| SYNGR1 | NDUFS5 | ITFG1 | PPARGC1A | CTR9 |
| PTPRM | CKB | LEFTY2 | CMYA5 | TENM2 |

Supplemental Table 2: PC1 and PC2 188 overlapping genes, related to Figure 4.

| gene | rank | gene | rank | gene | rank | gene | rank | gene | rank |
|---------|------|--------------|------|--------------|------|-----------|------|----------|------|
| TPM1 | 1 | LDB3 | 46 | C7orf73 | 91 | PACSIN3 | 136 | FAM189A2 | 181 |
| NDUFA4 | 2 | DES | 47 | KLHL41 | 92 | ADI1 | 137 | SNTA1 | 182 |
| MYL3 | 3 | MGST3 | 48 | PPP1R3C | 93 | ST3GAL6 | 138 | CISD3 | 183 |
| ACTC1 | 4 | UQCR11 | 49 | NDUFB1 | 94 | CCNB1IP1 | 139 | HYAL1 | 184 |
| MYOZ2 | 5 | GBAS | 50 | NKX2-5 | 95 | UTP11L | 140 | BBS9 | 185 |
| ACTN2 | 6 | ADSSL1 | 51 | MPC2 | 96 | SUPT5H | 141 | PHB | 186 |
| MYL2 | 7 | TECRL | 52 | VDAC2 | 97 | FHIT | 142 | DNAJC4 | 187 |
| POPODC3 | 8 | ANKRD1 | 53 | PPP2R4 | 98 | C9orf123 | 143 | ATP5EP2 | 188 |
| SORBS2 | 9 | VDAC3 | 54 | PSMA5 | 99 | SLC2A4 | 144 | | |
| CMYA5 | 10 | SAMD4A | 55 | SLC25A5 | 100 | MYOT | 145 | | |
| TNNT2 | 11 | COL21A1 | 56 | MRPL15 | 101 | TOM1L2 | 146 | | |
| NPY6R | 12 | NDUFB3 | 57 | NDUFB9 | 102 | ART3 | 147 | | |
| MRPL33 | 13 | RBM24 | 58 | MYPN | 103 | DUSP26 | 148 | | |
| CKMT2 | 14 | NDUFA6 | 59 | SDHB | 104 | GJA4 | 149 | | |
| ATP5J | 15 | ECH1 | 60 | YAF2 | 105 | DDA1 | 150 | | |
| NDUFC1 | 16 | ATP5SL | 61 | EXOG | 106 | ENAM | 151 | | |
| COX8A | 17 | TIMM21 | 62 | TMEM67 | 107 | SPEG | 152 | | |
| C3orf43 | 18 | XIRP2 | 63 | PPP2CA | 108 | KCNH2 | 153 | | |
| ISCU | 19 | RNF115 | 64 | ANKRD2 | 109 | LTBP1 | 154 | | |
| COX4I1 | 20 | COX17 | 65 | NMRK2 | 110 | CTNND2 | 155 | | |
| VDAC1 | 21 | CISD1 | 66 | DLAT | 111 | HMGN3 | 156 | | |
| HRC | 22 | MLLT11 | 67 | C9orf3 | 112 | TBX5 | 157 | | |
| MYL12A | 23 | SAP18 | 68 | SSBP2 | 113 | NUDT7 | 158 | | |
| GNG5 | 24 | CAMTA1 | 69 | DNAJB5 | 114 | GLRX2 | 159 | | |
| NDUFA12 | 25 | ANK1 | 70 | TRIM54 | 115 | PTS | 160 | | |
| ATP5F1 | 26 | SLIRP | 71 | LOC100507537 | 116 | CYB5R1 | 161 | | |
| NDUFB2 | 27 | HSPB3 | 72 | FRMD3 | 117 | MAP4 | 162 | | |
| PKIA | 28 | CRYM | 73 | VPS37A | 118 | BCKDK | 163 | | |
| COX7B | 29 | PKP2 | 74 | AK3 | 119 | PRDX2 | 164 | | |
| TYRP1 | 30 | PPP2R1A | 75 | SVIL | 120 | SRL | 165 | | |
| RYR2 | 31 | FHL2 | 76 | BZW2 | 121 | PPP1R12B | 166 | | |
| ATP5C1 | 32 | IDH2 | 77 | PFKM | 122 | MRPL48 | 167 | | |
| SYNPO2L | 33 | ATP5A1 | 78 | PCGF5 | 123 | USP13 | 168 | | |
| ATP5J2 | 34 | BANF1 | 79 | TXLNB | 124 | CAMK2D | 169 | | |
| SLC25A4 | 35 | MYH7B | 80 | LRRC39 | 125 | APLN | 170 | | |
| HSPB1 | 36 | ATP5L | 81 | THBS4 | 126 | SLCO3A1 | 171 | | |
| C14orf2 | 37 | NDUFV2 | 82 | C14orf159 | 127 | ENO3 | 172 | | |
| XIRP1 | 38 | LOC100131138 | 83 | CADPS | 128 | SDHD | 173 | | |
| SMYD2 | 39 | NDUF57 | 84 | C1orf43 | 129 | CORO6 | 174 | | |
| TNNC1 | 40 | CAMK2B | 85 | NCAM1 | 130 | HIST2H2BE | 175 | | |
| MYOM1 | 41 | ATP5O | 86 | NUDT19 | 131 | CACNA1C | 176 | | |
| LYPLAL1 | 42 | MDH1 | 87 | GYG1 | 132 | C11orf84 | 177 | | |
| CRYAB | 43 | UQCR10 | 88 | TTC1 | 133 | CDK18 | 178 | | |
| UQCRQ | 44 | RPL38 | 89 | SLC39A14 | 134 | ZNF853 | 179 | | |
| ALDOA | 45 | FKBP3 | 90 | DPH5 | 135 | RAB3A | 180 | | |

Supplemental Table 3: Transcription Factors from Homer-analysis, related to Figure 4 and 5.

| Transcription Factor | Motif Name | Consensus | P-value | Log P-value | q-value (Benjamini) |
|----------------------|------------|-----------------|----------|-------------|---------------------|
| Mef2d | GSE61391 | GCTATTTTTAGC | 1.00E-05 | -1.28E+01 | 0.001 |
| Mef2b | GSE67450 | GCTATTTTTGGM | 1.00E-04 | -1.15E+01 | 0.0019 |
| Mef2c | GSE32465 | DCYAAAAATAGM | 1.00E-04 | -1.15E+01 | 0.0019 |
| DMRT6 | GSE60440 | YDGHTACAWTGTADC | 1.00E-03 | -7.46E+00 | 0.0523 |
| Nr2f2 | GSE46497 | AGRGGTCA | 1.00E-03 | -7.33E+00 | 0.0523 |
| Esrrb | GSE11431 | KTGACCTTGA | 1.00E-02 | -6.62E+00 | 0.0811 |
| Mef2a | GSE21529 | CYAAAAATAG | 1.00E-02 | -6.34E+00 | 0.0918 |
| ThRb | GSE52613 | TRAGGTCA | 1.00E-02 | -5.73E+00 | 0.1474 |
| Znf263 | GSE31477 | CVGTSCTCCC | 1.00E-02 | -5.24E+00 | 0.2144 |
| Myf5 | GSE24852 | BAACAGCTGT | 1.00E-02 | -5.24E+00 | 0.2144 |
| DMRT1 | GSE64892 | TWGHWACAWTGTWDC | 1.00E-02 | -5.14E+00 | 0.2144 |
| Sox4 | GSE50066 | YCTTTGTTCC | 1.00E-02 | -4.73E+00 | 0.2672 |



Summary

Myosin binding protein C3 (MYBPC3) is one of the most commonly mutated sarcomeric genes in hypertrophic cardiomyopathy (HCM). Over 350 mutations have been described in MYBPC3, most of which give rise to premature termination codons (PTCs), causing RNA degradation and, consequently, protein reduction in HCM hearts. Nonetheless, the disease-driving mechanisms by which mutations to MYBPC3 result in HCM still remain largely unknown.

In this study, we generated two heterozygous (HET) knock-in (KI) mouse models harbouring mutations in *Mybpc3*; leading to predicted changes in the protein; p.Trp792fs and p.Arg943X. These variants correspond to two Dutch founder mutations, most commonly found in HCM patients in the Netherlands. Cardiac *Mybpc3* transcript levels were significantly decreased in both models, although protein levels did not change. Morphological and functional analysis showed no impairment under physiological conditions. Given that environmental factors can influence HCM onset in humans, we next subjected male mice to Transverse Aortic Binding (TAB) to trigger disease development. Gross morphological and functional studies showed no changes in HET mice when compared to WT mice. Lastly, we investigated mice carrying a homozygous mutation. Here, 2-month-old homozygous KI (HOM) mice showed hallmarks of HCM.

In conclusion, we generated two KI mouse models carrying point mutations known to induce a severe HCM phenotype in humans. Under both physiological and pressure-induced stress conditions, HET mice do not develop an HCM phenotype. These results suggest mice require another additional trigger to develop HCM. This may correspond with patients, since most mutation carriers do not develop a phenotype. Future studies will be required to study the effect of other exogenous stimuli to trigger the development of HCM. On the other hand, HOM mice showed HCM features in early adulthood, indicating that this model may be comparable to patients carrying compound mutations, which are related to childhood-onset HCM, and could be studied for disease progression, or to study potential therapeutic targets. Accordingly, we established valuable models for investigating the molecular mechanisms underlying hypertrophic cardiomyopathy (HCM), induced by a mutation in *Mybpc3*.

Introduction

HCM has a prevalence of 1:200 to 1:500 patients in the adult population, making it one of the most common hereditary cardiomyopathies (B. J. Maron et al., 1995; Semsarian et al., 2015). Although many mutation carriers will never develop a phenotype, those who do exhibit considerable variability, ranging from mild symptoms to end-stage heart failure (B. J. Maron & Maron, 2013). Common HCM traits include (interstitial) fibrosis, cardiomyocyte disarray and cellular hypertrophy. Clinically, HCM is characterized by left-ventricular wall thickness, which is often more prominent in the intraventricular septum (Marian & Braunwald, 2017). Available pharmacological treatments alleviate symptoms, but do not cure the disease (Marian, 2010). In severe cases, patients may need to undergo septal myectomy surgery to relieve the left ventricle outflow obstruction (LVOT) caused by the increased myocardial thickness. Phenotype variability and incomplete penetrance are observed in HCM patients, suggesting that other genetic or environmental factors may play a role in disease development. Several cardiomyopathy studies have employed additional external stresses that have shown to contribute to the onset and course of disease (Barefield et al., 2015; Gramlich et al., 2009; Najafi, Schlossarek, van Deel, et al., 2015). Delineating the molecular mechanisms driving the disease, will give valuable insights into the prediction of onset and the progression, and thereby may shed light on potential biomarkers or the development of novel, personalized therapeutical targets.

MYBPC3 is the most commonly mutated sarcomeric protein in patients with HCM in the Netherlands. This contractile protein plays a key role in the structure and function of the sarcomere, the heart's basic contractile unit (Carrier et al., 2015; Christiaans et al., 2010). It strongly binds to myosin via its C-terminal domain, and to either myosin heads or the actin filament via its N-terminal domain, limiting crossbridge interactions and regulating cardiac contractility (Carrier et al., 2015; Luther et al., 2008). Due to limitations of tracking human tissue over time in HCM pathology, different models have been designed to unravel the causal relationship between HCM and Mybpc3 mutations, however modelling this disease remains a challenge.

Cardiomyocytes, derived from human induced pluripotent stem cells (hiPSC-CMs), and harbouring Mybpc3 pathogenic mutations fail to develop cardiac hypertrophy, which is a key hallmark of HCM (Helms et al., 2020; Seeger et al., 2019). Additionally, most available mouse models in HCM driven by an Mybpc3 mutation are made with

a transgene, or are homozygous knockout (by removing exons), and therefore do not exactly recapitulate the human genetic context (Barefield et al., 2014; Harris et al., 2002). Introducing a human-like point mutation in exon 6 of *Mybpc3* in a mouse model has provided valuable insights into the degradation of mutant protein and the pathology of HCM (Schuldt et al., 2021; Vignier et al., 2009). However, the effect a mutation has on the protein and on the pathogenesis may differ per mutation site.

In the present study, we want to investigate the specific effect common mutations in *Mybpc3* on the pathology of HCM in the adult heart. We generated two *Mybpc3* knock-in (KI) mouse models containing two Dutch founder mutations: c.2373_2374insG and c.2827C>T, both of which give rise to Premature Termination Codons (PTCs). We aimed to obtain insights into disease onset and progression in heterozygous mutant (HET) mice, in both males and females, under physiological and stress conditions. These mice showed no hypertrophy, expression of cardiac stress genes, or cardiac dysfunction. In contrast, 2-month-old homozygous (HOM) mice were heavily affected by their mutation, displaying septal hypertrophy, interstitial fibrosis, and cardiac impairment; mimicking childhood onset HCM. Taken together, this study suggests that heterozygous mouse models harbouring a human pathogenic *Mybpc3* mutation are resilient to HCM pathogenesis, while HOM mice develop a strong phenotype. Both models are interesting to study in more depth, investigating molecular mechanisms driving HCM due to an *Mybpc3* mutation. The HET mice can be used to study the mechanisms driving the onset of the disease, while the HOM mice can be used to study the pathogenesis with compound mutations, the progression to heart failure, or to study therapeutic targets.

Results

Generation of *Mybpc3* knock-in mouse models to study hypertrophic cardiomyopathy

HCM is a genetic disease mainly caused by mutations in sarcomeric genes, of which roughly 20-30% of is located within the *MYBPC3* gene (Figure 1A) (Chung et al., 2003; Zamorano et al., 2014). In an effort to improve our understanding regarding disease-related mechanisms driving HCM, we aimed to generate two KI mouse models representing 2 Dutch founder mutation in *MYBPC3* (c.2373_2374insG or p.Trp792fsX17, and c.2827C>T or p.Arg943X.) (Christiaans et al., 2010). Based on amino acid homology between the human and mouse genome, these mutations corresponded to *MYBPC3* p.Trp796fs and p.Arg947X in mice (Supplemental Figure

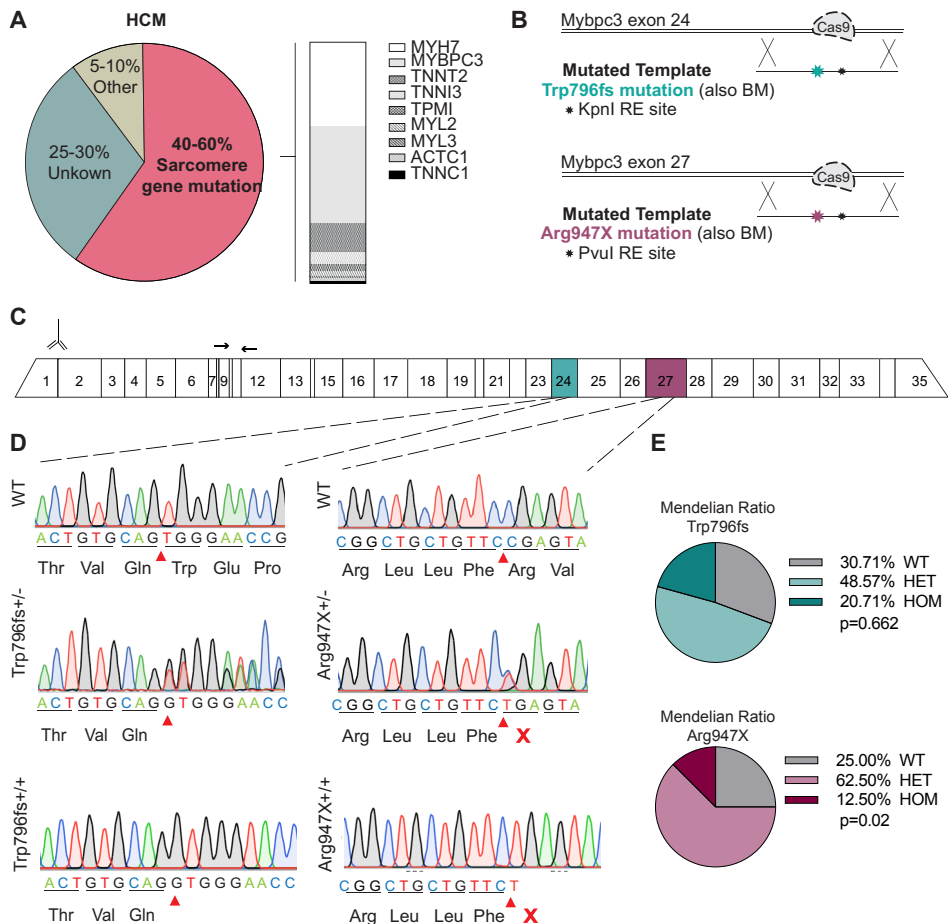


Figure 1. Generation of MYBPC3 knock-in mouse models to study hypertrophic cardiomyopathy. (A) Pie chart and bar graph displaying the percentage of gene mutations known to cause HCM. (B) Schematic representation of the CRISPR/Cas technology used to generate the mouse models. DNA template included the mutation-of-interest, which served as a blocking mutation (BM), and a restriction enzyme (RE) site used to facilitate genotyping. (C) Mouse coding sequence of Mybpc3 showing exons, the binding site of the antibody used for Western blots, and the primers used for qPCR (arrows) (D) Sequencing of region of interest in wild-type, heterozygous (+/-), and homozygous (+/+) mutations for Mybpc3. Red arrow head indicates the mutation site. (E) Mendelian ratios of mice born with either no mutation (WT) a heterozygous mutation (HET, +/-) or a homozygous mutation (HOM, +/+) for both Mybpc3 -Trp796fs (top) and -Arg947X (bottom) mutations. Mendelian ratios were tested for significance with a chi-square test. BM; Blocking mutation, RE; Restriction enzyme.

1A and 1E). These mutations were introduced in the mouse genome by using CRISPR/Cas9 technology (**Figure 1B and 1C**). By using guide RNAs (gRNAs) a template DNA containing the mutation-of-interest was inserted at the directed target site. Next to the mutation-of-interest, we introduced a silent restriction enzyme (RE) site in the template to facilitate genotyping (**Figure 1B**). Targeting was validated by RE analysis of genomic DNA, which indicated the heterozygous and homozygous presence of the inserted template (**Supplemental Figure 1B and Supplemental Figure 1F**). DNA sequencing further validated the correct insertion of the desired mutations (**Figure 1D**). Both mouse models showed intact genomic integrity with > 80% of cells containing 40 chromosomes (**Supplemental Figure 1C and 1G**). Also, no cleavage was observed in the top 3 off-target genes predicted for each gRNA (**Supplemental Figure 1D and 1H**).

For the first mouse model, MYBPC3 Trp796fs mice, the mutation generates a new splice donor site in exon 25, leading to a PTC (**Figure 1D, left**). The second mouse model contained the human MYBPC3 c.2827C>T (p.Arg943X) mutations (referred to as Arg947X mice) (**Figure 1D, right**), which equally introduces a PTC. Mendelian ratios indicated that the number of mice born WT, HET, or HOM is not significantly different from the expected ratio of 25%/50%/25% ($p=0.662$, $n=124$, chi-square) in the Trp796fs mice. However, Arg943X mutation led to a significant reduction in the percentage of HOM mice born, which might indicate increased embryonic lethality ($p=0.02$, $n=89$, chi-square; **Figure 1E**).

A heterozygous mutation in Mybpc3 does not lead to an HCM phenotype up to one year under baseline conditions

Studies have shown that patients are between 40-50 years old when diagnosed with HCM, which would correspond to ± 12 months of age in mice (The Jackson Laboratory, n.d.). Strikingly, women are on average 8 years older than men at the time of diagnosis and, consequently, at the time they go up for myectomy surgery (Nijenkamp et al., 2018; Olivotto et al., 2005). To study the *in vivo* effects of pathogenic Mybpc3 mutations, we first examined hearts of adult HET mice under baseline conditions, which were compared to their wildtype (WT) littermates. We separated males and females to investigate potential sex differences in response to the mutations. Moreover, we incorporated timepoints preceding the 12-month mark into the dataset to ascertain the potential identification of initial alterations in gene expression.

To study the effect of the mutation in HET mice on Mybpc3 transcripts, quantitative PCR (qPCR) analysis was performed over time and normalized in fold-change

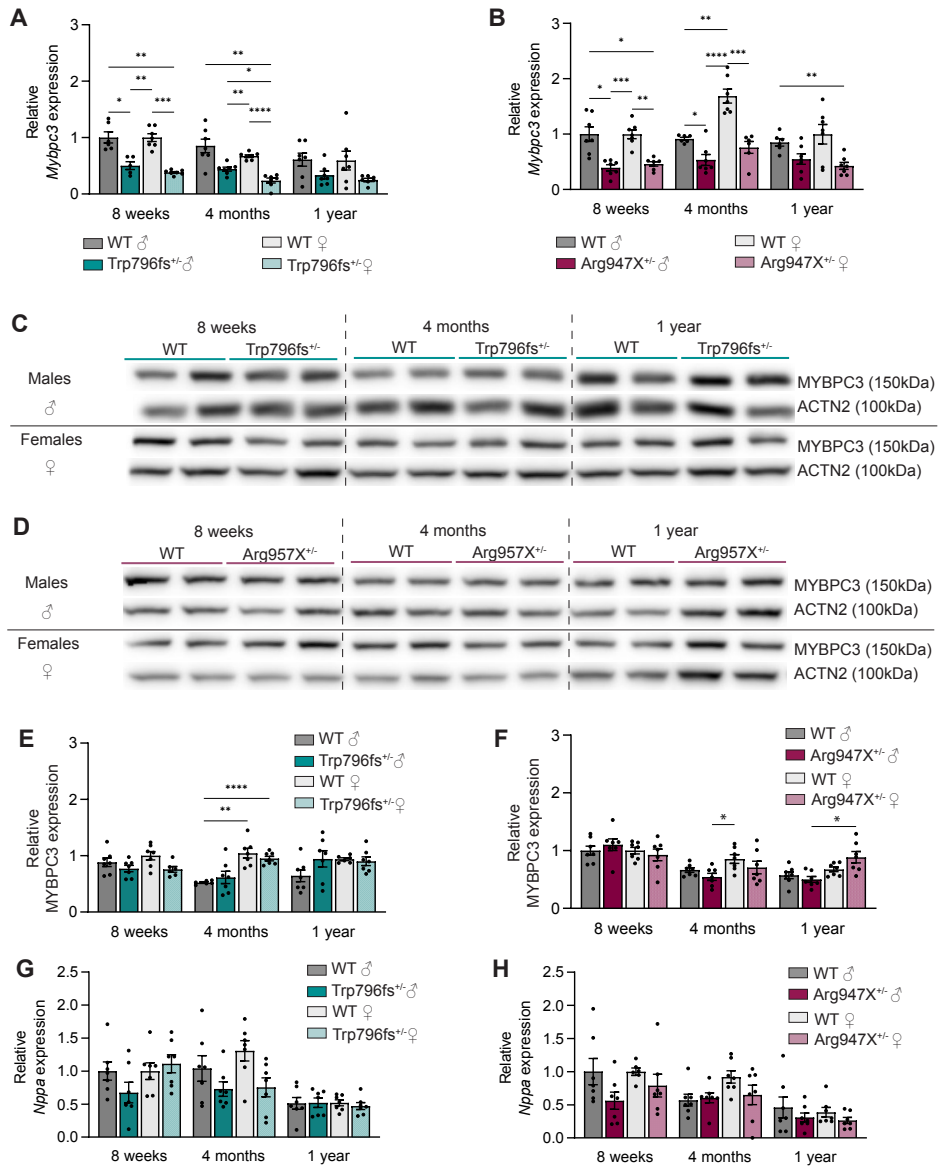


Figure 2. MYBPC3 does not decrease in Trp796fs^{+/-} and Arg947X^{+/-} mice under baseline conditions at 2, 4 and 12 months of age. (A) Relative Mybpc3 expression in 2-, 4- and 12-month-old male WT and Trp796fs^{+/-} mice, both males (darker shades) and females (lighter shades). (B) Relative Mybpc3 expression in 2-, 4- and 12-month-old male WT and Arg947^{+/-} mice, both males (darker shades) and females (lighter shades). (C and D) Western blot of MYBPC3 in 2-, 4- and 12-month-old WT and Trp796fs^{+/-} and Arg947^{+/-} mice. (E and F) Quantification of MYBPC3 protein level. (G and H) Relative Nppa expression in 2-, 4- and 12-month-old WT and HET. RNA and protein expression data plotted as mean \pm SEM (n = 7

per group). RNA is normalized to *Hprt* and protein is normalized to α -ACTININ. Significance was assessed by a 2-way ANOVA (* = p-value < 0.0332; ** = p-value < 0.0021; *** = p-value < 0.0002; **** = p-value < 0.0001).

compared to the adult stage (8 weeks). These data indicated a reduction in *Mybpc3* transcript level in both male and female *Trp796fs*+/- mice at 2 and 4 months of age compared to age-matched WT mice (**Figure 2A**). Although not significant, this reduction was still visible at 12 months of age. By contrast, MYBPC3 protein level was unaltered in the *Trp796fs*+/- mice when compared to age-matched WT mice (**Figure 2C and 2E**), which is in line with the observations made previously in hIPS-CMs and mice carrying the same mutation (Helms et al., 2020; Hilderink et al., 2023). In cardiac tissue from *Arg947X*+/- mice, we were able to show a significant decrease in *Mybpc3* expression at 2 months of age, which remained significant for the females in time, while the males only showed a trend at the later time points (**Figure 2B**). Again, this did not translate into a decrease in MYBPC3 protein compared to WT controls (**Figure 2D and 2F**). Both mutations cause a premature stop codon that potentially could give rise to a truncated protein (95 kDa for *Trp796fs* and 125 kDa for *Arg947X*). In these models, no truncated forms of MYBPC3 were detected in cardiac tissue (**Supplemental Figure 2**).

Cardiac expression of Natriuretic Peptide A (*Nppa*), later translated into ANP, is a marker expressed during cardiac development, and re-expressed during cardiac stress. Therefore, it is commonly used as a marker for cardiac failure or hypertrophy (Man et al., 2018). To test whether our mutant mice showed cardiac stress, we measured *Nppa* levels by qPCR in both HET and WT mice (**Figure 2G and 2H**). These data indicated an expected decline with age with no differences between WT and HET mice for either sex. Furthermore, neither mouse model exhibited gross morphological changes with regards to common hallmarks of HCM, such as cardiac hypertrophy, fibrosis or cell size (**Supplemental Figures 3 and 4**). Although there was an expected difference in heart size between males and females, there was no difference between WT and HET mice (**Supplemental Figure 3 and 4**). Additionally, cardiac function was not significantly altered in the HET mice compared to their respective WT littermates (**Supplemental Tables 1 and 2**). Taken together, these results suggest that the *Trp796fs* and *Arg947X* mutations in *Mybpc3* cause a decline in mRNA transcript level which is compensated for on the protein level. The lack of change in MYBPC3 protein might be contributing to the absence of overt phenotype at the indicated ages.

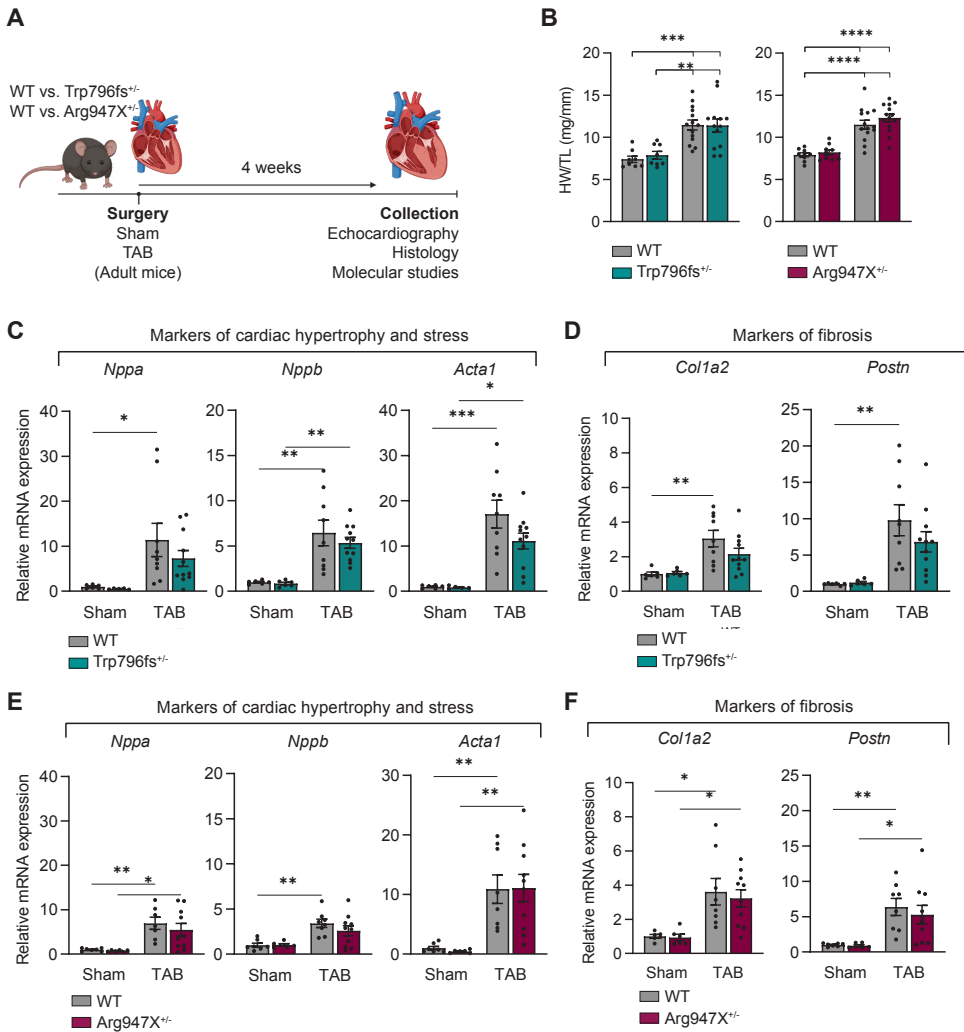


Figure 3. Pressure overload does not induce an HCM phenotype in MYBPC3 *Trp796fs*^{+/-} and *Arg947X*^{+/-} mice. (A) Schematic representation of the Sham and TAB surgery performed on male mice. Mice were 8,5-9,5 weeks old. (B) HW/TL (mg/mm) in WT and *Trp796fs*^{+/-} and *Arg947X*^{+/-} TAB mice compared to Sham mice. (C) qPCRs for common cardiomyocyte stress markers (*Nppa*, *Nppb*, *Acta1*) for WT and *Trp796fs*^{+/-} Sham and TAB mice. (D) qPCRs for common fibrotic markers (*Col1a2* and *Postn*) for WT and *Trp796fs*^{+/-} Sham and TAB mice. (E) qPCRs for common cardiomyocyte stress markers (*Nppa*, *Nppb*, *Acta1*) for WT and *Arg947X*^{+/-} Sham and TAB mice. (F) qPCRs for common fibrotic markers (*Col1a2* and *Postn*) for WT and *Arg947X*^{+/-} Sham and TAB mice. Expression data plotted as mean ± SEM (n = 7 per group). RNA is normalized to *Hprt*. Significance was assessed by a 2-way ANOVA (* = p-value < 0.0332; ** = p-value < 0.0021; *** = p-value < 0.0002; **** = p-value < 0.0001).

Pressure overload does not induce an aggravated phenotype in MYBPC3 Trp796fs^{+/-} and Arg947X^{+/-} mutant mice

Genetic and/or environmental factors have been shown to alter disease development and phenotype (Blankenburg et al., 2014; Christodoulou et al., 2014; Gramlich et al., 2009; Najafi, Schlossarek, van Deel, et al., 2015). Furthermore, pressure overload induced by TAB surgery in mice has been used to trigger disease onset in various cardiomyopathy studies (Barefield et al., 2015; Schmitt et al., 2003; Zhou et al., 2015). To determine the influence of hemodynamic stress on HCM development, TAB surgery was performed on adult male WT and HET mice (8,5-9,5 weeks old). Sham surgery was performed to serve as a control. Mice were sacrificed 4 weeks post-surgery and tissues were collected for functional, morphological and molecular analysis (**Figure 3A**). Both WT and HET mice were significantly affected by the TAB surgery, shown by the increase in heart size, indicated by HW/TL ratios (**Figure 3B**). Furthermore, mice that underwent TAB showed an increase in common markers for cardiac stress (*Nppa*, *Nppb*, *Acta1*) and fibrosis (*Col2a1*, *Postn*) when compared to Sham mice (**Figure 3C to 3F**). This corresponded to an increase in cardiac size (H&E), fibrosis (SR) and cell size (quantified with WGA staining) in response to TAB compared to sham operated mice (**Supplemental Figure 5**). However, at a morphological and functional level, the stress-induced remodelling response appeared comparable for both HET and WT mice (**Figure 3, Supplemental Figure 5, and Supplemental Table 3**).

Since we were unable to detect gross phenotypic differences between WT and HET mice under both baseline and pressure overload conditions, we set out to determine proteomic changes that might be occurring in vivo. For this, we performed proteomics on WT and Trp796fs^{+/-} mice that had undergone a Sham or TAB surgery (n=4 per condition). To confirm the induction of cardiac stress, we first looked at the differentially regulated proteins in response to TAB. A total of 196 proteins were significantly upregulated, and 146 proteins were significantly downregulated (log₂FoldChange > 0.4 or < -0.4), respectively (**Supplemental Figure 6**). As expected, we saw an upregulation in cardiac stress proteins (*Nppa*, *Myh7*, *Nppb*) and fibrosis (*Postn*) after TAB surgery. These markers were also observed to be upregulated at mRNA level by qPCR (**Figure 3C-F**).

To investigate the influence of TAB in a more unbiased way, and to be able to detect early molecular changes, we sought to look into protein differences between WT Sham and Trp796fs^{+/-} Sham mice (**Supplemental Figure 6D-F**). A total of 17 and 20 proteins were up- and downregulated (log₂FoldChange > 0.4 or < -0.4), respectively.

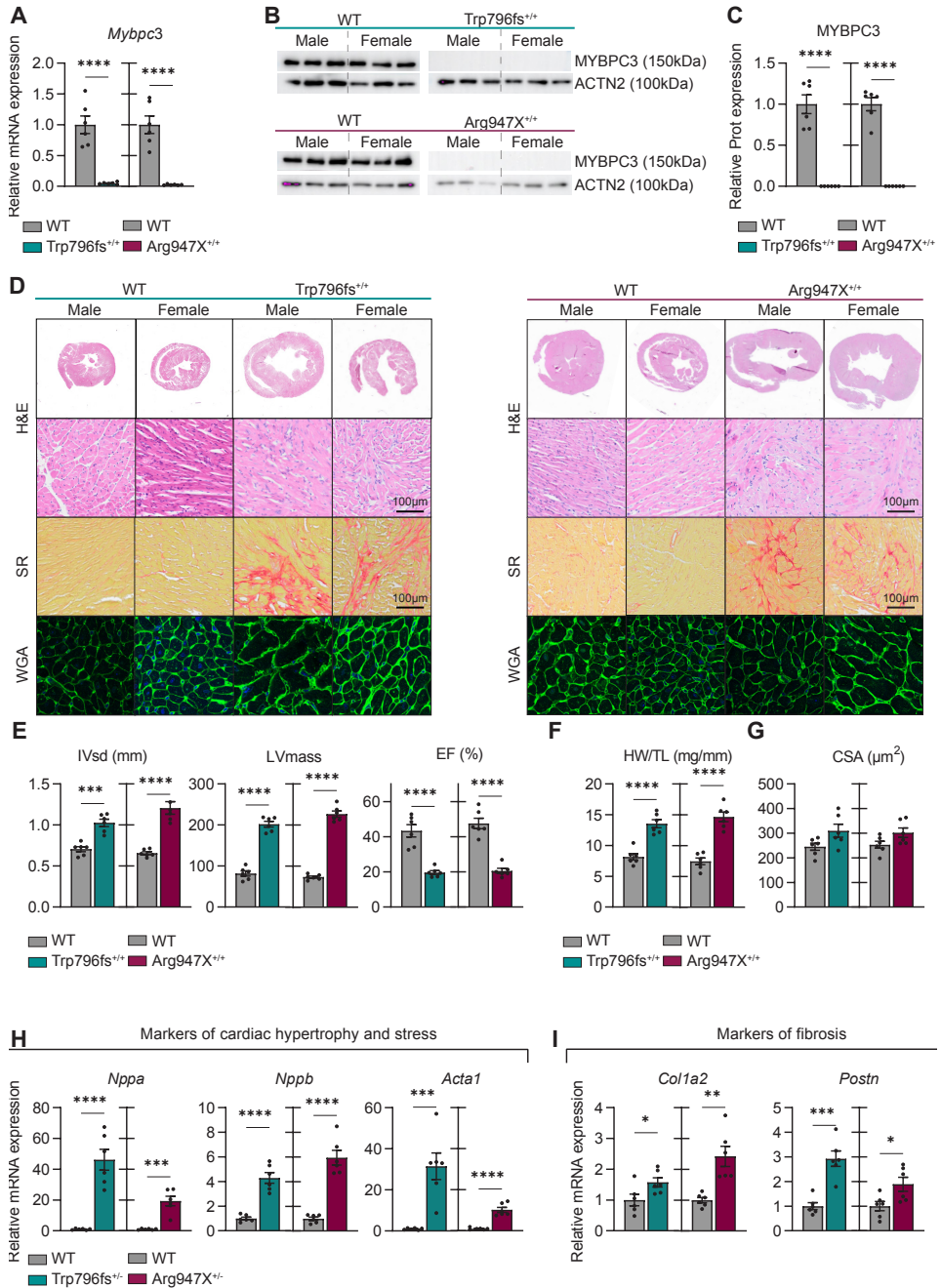


Figure 4. Homozygous male *Trp796fs*^{+/+} and *Arg947X*^{+/+} mice display common features of HCM. (A) Relative *Mybpc3* expression in 2-month-old WT, *Trp796fs*^{+/+} and *Arg947X*^{+/+} mice. **(B)** Western blot of MYBPC3 in 2-month-old WT, *Trp796fs*^{+/+} and *Arg947X*^{+/+} mice.

(C) Quantification of *Mybpc3* protein level. **(D)** Representative H&E staining on heart sections from WT, *Trp796fs+/+* and *Arg947X+/+* mice (top panel, scale 1 mm). Representative H&E, SR and WGA staining on heart sections from WT, *Trp796fs+/+* and *Arg947X+/+* mice (lower panels, scale 50 μm). **(E)** IVSd (mm) in WT, *Trp796fs+/+* and *Arg947X+/+*, corrected LV mass in WT, *Trp796fs+/+* and *Arg947X+/+* mice and EF(%) in WT, *Trp796fs+/+* and *Arg947X+/+* mice. **(F)** HW/TL (mg/mm) in WT, *Trp796fs+/+* and *Arg947X+/+* mice. **(G)** CSA (μm^2) in WT, *Trp796fs+/+* and *Arg947X+/+* mice. **(H)** qPCRs for common cardiomyocyte stress markers (*Nppa*, *Nppb*, *Acta1*) for WT, *Trp796fs+/+* and *Arg947X+/+* mice. **(I)** qPCRs for common fibrotic markers (*Co-11a2* and *Postn*) for WT, *Trp796fs+/+* and *Arg947X+/+* mice. Expression data plotted as mean \pm SEM ($n = 7-9$ per group). RNA is normalized to *Hprt* and protein is normalized to α -Actinin. CSA (μm^2) was measured in ± 50 cells/mouse. Significance was assessed by a 2-way ANOVA (* = p -value < 0.0332; ** = p -value < 0.0021; *** = p -value < 0.0002; **** = p -value < 0.0001).

When comparing WT TAB to *Trp796fs+/-* TAB mice (Supplemental Figure 6G-I) 10 and 55 proteins were up- and downregulated ($\log_2\text{FoldChange} > 0.4$ or < -0.4). Of note, *Mybpc3* levels did not show significant changes in either condition, confirming our previous results. All in all, these results indicate that TAB-induced stress for 4 weeks is not sufficient to trigger mutation related HCM in both mouse models.

Homozygous mutant mice display common features of HCM

In rare, but often very severe cases of HCM, patients are found to have compound mutations. These patients carry two mutations (sometimes on both alleles of *Mybpc3*), which is related to an early/childhood onset and a very severe phenotype (Ingles, 2005; Lekanne Deprez et al., 2006; Marziliano et al., 2012; Wessels et al., 2015). To investigate whether our homozygous mutant mice (*Trp796fs+/+* and *Arg947X+/+*) would recapitulate this phenotype, we collected tissue from both males and females

at 2 months of age (Figure 4). As expected, these mice showed a complete ablation of *Mybpc3* mRNA expression compared to age-matched WT mice (Figure 4A). Consequently, a loss in detectable *Mybpc3* protein was observed (Figure 4B and 4C). Histological analysis showed that HOMs have increased heart size (H&E) regions of disarray (H&E) patches of fibrosis (SR) and areas of increased cardiomyocyte size

(WGA) (Figure 4D). Echocardiographic parameters demonstrate *Trp796fs+/+* and *Arg947+/+* mutant mice to show cardiac remodelling and dysfunction, as characterized by increased intraventricular septum (IVS) thickness and increased LV mass, indicative of cardiac hypertrophy, and reduced ejection fraction (EF) indicative of systolic dysfunction (Figure 4E and Supplemental Table 4). Interestingly, homozygous *Trp796fs+/+* mice showed a decrease in kidney weight (KiW/TL) compared to WT mice (Supplemental Table 4), which could be related to the disease phenotype. HCM patients have been reported to have a higher risk of end-stage renal disease (ESRD) (Lee et al., 2019). Although HW/TL ratio was significantly increased in

both mice carrying mutations, the mean cardiomyocyte cross sectional area (CSA) was not significantly increased, which might be due to an increase in heterogeneity in cardiomyocyte size (**Figure 4B, bottom and 4G**). Homozygous mice showed a significant increase in common markers for cardiac stress (*Nppa*, *Nppb*, *Acta1*) and fibrosis (*Col2a1*, *Postn*) when compared to WT mice (**Figure 4H and 4I**).

Taken together, these results indicate that HOM mice do show a decline in MYBPC3 protein, and a severe cardiac phenotype characterized by impaired cardiac function, cardiac remodelling and fibrosis. Follow up experiments could be focused on studying the underlying mechanism for the progression of the HCM phenotype. Furthermore, this model can be used to investigate therapeutic targets due to its severe phenotype.

Discussion

In this study we aimed to provide further insight into the molecular mechanisms underlying HCM. Here, we generated two *Mybpc3* KI mouse models containing two prevalent mutations found in HCM patients in the Netherlands (MYBPC3 c.2373_2374insG (p.Trp792fs) and c.2827C>T (p.Arg943X)) (Christiaans et al., 2010). We studied HCM onset and progression in HET mice under physiological and stress conditions. Females and males were studied separately in order to discern potential sex-related differences influenced by these mutations. Additionally, we investigated HOM mice to explore the development of traits associated with HCM. We discovered that HET mice do not develop an overt HCM phenotype at an early/adult age, and we could not detect differences between males and females. Since many mutation carriers/relatives of HCM patients do not develop a phenotype, this might be in line with the human situation. Surprisingly, adding a trigger in the form of pressure overload did not aggravate the HCM phenotype in HET mice compared to WT mice. HOM mice however developed an early onset (8 weeks) severe phenotype. This indicates that both models are very suitable for further investigation of the molecular mechanisms driving HCM.

Haploinsufficiency has been suggested as the disease-driving mechanism causing the functional impairments observed in HCM patients. In the advanced stages of HCM, cardiac tissue shows a significant reduction of MYBPC3 protein with an absence of a truncated protein (O'Leary et al., 2019). However, in the current study cardiac protein levels were preserved under baseline conditions, despite the

clear decline in *Mybpc3* transcript expression in HET mice. These results are in line with studies showing unaltered MYBPC3 levels in hiPSC-CMs carrying the MYBPC3 c.2373_2374insG (p.Trp792fs) mutation (Helms et al., 2020) and MYBPC3 c.2827C>T (p.Arg943X) (Seeger et al., 2019). These MYBPC3 heterozygous cells also fail to develop cellular hypertrophy and functional impairments. This also holds true for *Mybpc3* heterozygous knockout mouse models (Barefield et al., 2014; Carrier et al., 2010; Harris et al., 2002). Additionally, a recent paper came out investigating the *Mybpc3* c.2373_2374insG founder mutation in heterozygous and homozygous mice (Hilderink et al., 2023). Consistent with our findings, HET mice did not show a decrease in MYBPC3 protein levels up to 28 weeks, indicating they did not develop haploinsufficiency. Furthermore, these HET mice did not develop a phenotype, consistent with our findings. Altogether, these results indicate that heterozygous mutations in *Mybpc3* are not sufficient to trigger HCM in iPSC-CMs and mouse models.

Interestingly, Helms *et al.* showed that the hiPSC-CMs harboring the MYBPC3 c.2373_2374insG mutation do show a reduction in MYBPC3 protein synthesis which is compensated for by a reduction in MYBPC3 protein degradation and thus results in the maintenance of normal MYBPC3 protein levels (Helms et al., 2020). This finding has yet to be proven in the mouse lines that fail to develop common disease traits. These results suggest that at an early stage, cardiomyocytes are able to successfully compensate for the lack of *Mybpc3* transcript, but at later time points, when the disease is induced, progresses and further impairments across the cell occur, the successful compensation might be disrupted followed by HCM hallmarks such as cardiomyocyte hypertrophy and disarray. Taken together, our results indicate that a heterozygous *Mybpc3* mutation alone is insufficient to trigger disease onset due to compensatory mechanisms. In time or in response to additional triggers these mechanisms might no longer be capable of maintaining suitable protein levels of MYBPC3 which then leads to the development of a HCM phenotype.

The type of mutation may also influence the penetrance of the disease; Some studies have indicated that patients with a *Myh7* mutation have an earlier onset and suffer a more severe phenotype, whereas patients with a *Tnnt* mutation show less hypertrophic remodelling and a higher chance of sudden cardiac death (Bos et al., 2009; Moolman et al., 2000; Varnava et al., 2000). Others argue that it is difficult to link genes to penetrance or disease phenotype, as clinical reports have failed to predict the prognosis of specific mutations (B. J. Maron & Maron, 2013, 2014). Most HCM-causing mutations affect sarcomere genes (**Figure 1**), *Myh7* and *Mybpc3*

being the most commonly mutated genes. Interestingly, patients carrying an Myh7 mutation suffer from a more pronounced HCM phenotype compared to patients carrying Mybpc3 mutations (Velicki et al., 2020). A well-established mouse model generated by Seidman and colleagues contains an Arg404Gln+/- mutation (Geisterfer-Lowrance et al., 1996). These mice, in contrast to HET Mybpc3 mutant mice, show a functional decline and common HCM-related traits such as cardiomyocyte hypertrophy, fibrosis and myocardial disarray (Geisterfer-Lowrance et al., 1996; McConnell et al., 2001). Many *in vitro* and *in vivo* models containing mutations in different sarcomere genes have been developed throughout the years (Bhagwan et al., 2020; Kazmierczak et al., 2014; Mosqueira et al., 2019). Overall, these studies highlight the strong phenotypic variability observed in HCM, with each specific mutation displaying different phenotypes, even when found in the same gene, and moving to a more personalized treatment in the future would be more desirable.

The high variability in phenotype and penetrance observed in HCM patients suggest that internal and external factors play an important role in the disease. Internal factors include sex, age and mental health (Lampert et al., 2010; Nijenkamp et al., 2018), whereas external factors include pregnancy (Goland et al., 2017), competitive exercise (Weissler Snir et al., 2021), cancer therapy (Sabater-Molina et al., 2020), diet (Stauffer et al., 2006) and hypertension (Karam et al., 1989). These have been shown to be involved in the outcome severity of HCM. We hypothesized that pressure overload-induced stress by TAB may trigger disease onset. TAB is a common procedure that induces left ventricle hypertrophy by increasing the workload for the heart (Mohammed et al., 2012; Rockman et al., 1991). We expected that this would be comparable with the increased workload a human heart might have in response LVOT obstruction, and thereby would show a more pronounced HCM phenotype in the mutant mice. Mice that underwent TAB surgery showed an increase in HW/TL and in stress markers compared to unstressed counterparts, indicating that the surgery indeed exposed the hearts of the mice to stress. Surprisingly, this type of stress was not shown to be a trigger for aggravated hypertrophy in CM size, heart weight or echocardiographic markers, indicating LV hypertrophy in HCM caused by an Mybpc3 mutation is not caused by increased pressure to the heart.

Although no significant morphological differences were observed between HET and WT mice, subtle alterations at the protein level were observed by using a more untargeted approach. Specifically, changes observed between HET and WT Sham mice suggest that Mybpc3 mutations cause slight downregulation in mitochondria-relat-

ed proteins such as *Sco2*, *Ndufb1*, *Mtnd1* and *Ndudb3* found in the top 10 down-regulated proteins. These results are in line with recent studies performed on human myectomy samples (Coats et al., 2018; Schuldt et al., 2021). In fact, energy depletion has been proposed as a pathological mechanism underlying HCM. Patients carrying a heterozygous disease-causing mutation, who have not developed severe disease phenotype, show an energy deficit which could then lead to disease development (Crilley et al., 2003).

As our data indicate that 4 weeks of pressure overload is not sufficient to induce HCM in the HET mice, we could consider subjecting mice to a different stressor, such as exercise or a high-fat diet (HFD). Heavy exercise might be a trigger in HCM, as it is the leading cause of sudden cardiac death in competitive athletes, and patients who are performing competitive sports are more at risk of developing life-threatening arrhythmias (Atteya et al., 2017). However, the influence of performing exercise and the development of HCM remains a paradox. In mice, physical exercise has been mimicked by subjecting mice to voluntary wheel-running or a controlled swimming regime (Kazmierczak et al., 2014; Konhilas et al., 2006; Najafi, Schlossarek, Deel, et al., 2015). With controlled swimming, Kazmierczak et al. tested two different HCM-models with a mutation in myosin essential light chain. While one model developed pathologic cardiac remodelling after swimming, the other model did not (Kazmierczak et al., 2014). Additionally, Najafi et al. showed HCM hallmarks in heterozygous *Mybpc3* mutant mice after voluntary wheel running in females, but not in males (Najafi, Schlossarek, Deel, et al., 2015). On the contrary Konhilas et al. indicated that exercise prevented the severity of HCM in mice harbouring a mutation in Myosin heavy chain (Konhilas et al., 2006). These data indicate that the link between exercise and HCM is a challenging link in both humans and mouse models. On the other hand, obesity, which is known to be an increasing problem in developing countries, has been indicated to be correlated to HCM. Indeed, the prevalence of obesity in HCM patients (almost 40% of patients) is remarkably high compared to the general population (Finocchiaro et al., 2017; Fumagalli et al., 2020). Obesity has been associated with an increased risk of LVOT obstruction and adverse events (Balaji et al., 2019; Fumagalli et al., 2020). A study by Olivotto et al. related the magnitude of hypertrophy to BMI (Olivotto et al., 1999). Their results indicated that obesity was independently associated with an increase in LV mass and thus might dictate the progression to heart failure symptoms. Additionally, a high fat diet is known to trigger myocardial hypertrophy and myocardial fibrosis after 6 to 12 months of age (Wang et al., 2015). Another study showed that only HET mice carrying a mutation in *Mybpc3*

developed a cardiac phenotype after being fed a western diet, although this was not accompanied with haploinsufficiency (Nollet et al., 2023). Altogether, both external factors seem to be interesting for further investigation of HCM triggers.

In rare cases, HCM develops at a very young age, and if it does, patients have a higher chance of developing heart failure. This is most often seen in the case of double mutations, or compound mutations, which are a rare phenomenon (0.4% of the HCM patients), related to a more severe outcome (Fourey et al., 2017; B. J. Maron et al., 2012). Compound mutations have been reported most frequently in Mybpc3 (Fourey et al., 2017). These patients are diagnosed at a very young age with biventricular hypertrophy, atrial enlargement and a high risk at neonatal death or a required heart transplant during the first year of life (Fourey et al., 2017; Marziliano et al., 2012). Due to the nature of the mutations in Mybpc3 (most often a pre-mature stop-codon, leading to nonsense mediated decay and no expression of mutant protein), research groups have studied a knockout of Mybpc3 in mice, and detected a hypertrophic phenotype at a very early stage of the development and even alterations in gene expression before birth (Carrier et al., 2004; Farrell et al., 2018); indicating this model might be a relevant model to study childhood-onset HCM due to compound mutations.

In our study, homozygous KI mice were viable until at least 2-months of age, despite ablation of Mybpc3 at both a transcript and protein level. Our data show that these mice develop significant cardiac dysfunction and hypertrophy upon loss of MYBPC3, both clear signs of HCM. This is in line with Hilderink et al., who saw a comparable, to stronger phenotype based on CM CSA in their homozygous KI mice, but at a later age (18-28 weeks) (Hilderink et al., 2023). Indicating the homozygous mice progressively develop an HCM phenotype. Additionally, homozygous Trp796fs+/+ mice showed a significant decrease in kidney weight (KiW/TL) compared to WT, which might suggest renal dysfunction. A nationwide population-based cohort study showed that HCM patients had a higher risk of developing end stage renal disease. The latter was suggested to be caused mainly by diastolic dysfunction. In short, an increase in left ventricle hypertrophy can inevitably cause an increase in left ventricle filling pressure and, consequently, renal venous pressure which can lead to renal dysfunction (Lee et al., 2019). Therefore, it might be another indicator of heart failure in these mice (Gori et al., 2014; Nardi et al., 2007; Verma et al., 2007). Our homozygous mutant mice can be used to study the molecular mechanisms underlying the relationship between cardiac and renal dysfunction. Furthermore, the progression

of heart failure and potential biomarkers could be studied on different timepoints before the 8-week timepoint to delineate at what age these mice develop hypertrophic remodelling, and what proceeds the pathological condition. This might give valuable insights into a better understanding of the pathogenesis of HCM in childhood onset and compound mutations, and enable the investigation of therapeutic targets.

Recently, we have seen a remarkable increase in therapies directly targeting the pathological processes of HCM, including energy depletion (Horowitz & Chirkov, 2010), treatments aiming to manage arrhythmias and sudden cardiac death have also been developed (M. S. Maron et al., 2019), and, although less successfully, targeting fibrosis (Lim et al., 2001). Additionally, Mavacamten has recently been developed (Green et al., 2016; Heitner et al., 2019). The latter is a small molecule that targets myocardial hypercontractility by reversing the enzymatic activity of myosin. It is hypothesized that a reduction in *Mybpc3* due to a mutation leads to hypercontractility due to the nature and function of the protein in holding back myosin heads for contraction (super relaxed state, SRX) (McNamara et al., 2017; Nag et al., 2023). Although Mavacamten (commercialized under the name Cazyos) has shown great results in clinical and pre-clinical settings, it may carry risks due to its effect on systolic function and potential metabolic interactions (Nag et al., 2023). The discovery of this drug, however, underlines the importance of getting a better understanding of the molecular mechanisms driving HCM.

Another angle of targeting genetic diseases is via gene therapy. Cardiac gene therapy with adeno-associated virus (AAV)-based vectors has gained much interest, with the aim to restore function and, potentially, cure HCM. In the context of *MYBPC3*, a single dose of AAV9-*Mybpc3* in neonatal homozygous KI mice was enough to prevent the development of HCM and to increase *Mybpc3* transcript and protein levels (Mearini et al., 2014). Currently, companies such as DiNAQOR and Tenaya Therapeutics are investing in the development of AAVs delivering a functional *MYBPC3* gene. In the recent years, gene editing technologies have been developed to correct disease-driving mutations, many of which require a template-direct repair and, unfortunately, introduce off-target mutations (Li et al., 2020; van Kampen & van Rooij, 2019). DNA base editing systems enable efficient single-nucleotide changes without the need of a double-stranded DNA break (Rees & Liu, 2018). Recently, Shuhong Ma et al. used ABEmax-NG, an adenine base editors (ABEs) technique with an expanded editing scope (Huang et al., 2019), to correct a pathogenic point mutation in *Myh6*

(c.1211C>T) in an HCM mouse model. Compared with single-stranded oligodeoxynucleotides (ssODN)-mediated correction, ABEmax-ING showed to be more efficient with less off-target mutations (Ma et al., 2021). Correction in the germline successfully enabled the elimination of the pathogenic mutation in offspring. The latest gene-editing technology, prime editing, goes a step further by introducing all types of point mutations and small deletions and insertions in a precise manner (Anzalone et al., 2019). At present, prime editing has been used by Olson and co-workers to correct Duchenne muscular dystrophy (DMD) in hiPSC-CMs (Chemello et al., 2021). Although still in its early stages, prime editing shows to be promising technology for therapeutic *in vivo* genome editing.

In summary, hypertrophic cardiomyopathy (HCM) manifests as a multifaceted and heterogeneous disease. Within this study, we engineered two mouse models harbouring the most prevalent Mybpc3 mutations in the Netherlands. Our observations elucidate that a heterozygous mutation is insufficient to elicit a phenotype. Moreover, our data indicated that pressure overload did not lead to diminished Mybpc3 protein levels or an exacerbated HCM phenotype. This observation aligns with the clinical situation, where a substantial proportion of mutation carriers may remain phenotypically asymptomatic. Future studies will focus on the exact trigger to induce the HCM phenotype. Conversely, mice bearing a homozygous mutation demonstrated a pronounced HCM phenotype, rendering this to be a valuable model for investigating early-onset HCM, profiling biomarkers throughout the progression towards heart failure, and exploring potential therapeutic targets. In essence, these models can help us getting a better understanding of the underlying molecular mechanisms driving HCM, which holds promising clinical prospects.

Methods

Animal studies

Animal studies were performed according to the guidelines from Directive 2010/63/EU of the European Parliament on the protection of animals used for scientific purposes. Animal experiments were approved by the institutional guidelines and regulations of the Animal Welfare Committee of the Royal Netherlands Academy of Arts and Sciences and following the guide for the care and use of laboratory animals.

Mouse embryonic stem cell culture

129/Ola-derived IB10 ES cells (Netherlands Cancer Institute, Amsterdam) were cul-

tured on irradiated mouse embryonic fibroblasts (MEFs) in CM^{+/+} medium made with G-MEM (BHK-21) culture media (Life Technologies, 21710-025) supplemented with 1X Glutamax (Life Technologies, 35050-038), 1mM Sodium Pyruvate (Life Technologies, 11360039), 1X Non-Essential Amino Acids (Life Technologies, 11140035, USA), 10% Fetal Bovine Serum (Greiner 758093S4414), 0.1mM β -mercaptoethanol (Merck, 15433) and 10³u/mL LIF (Millipore, ESG 1107). Cells at 80% confluency were dissociated with 10X TVP (dPBS, supplemented with 1mM EDTA, 1% chicken serum (Life Technologies, 16110082) and 10% trypsin 2.5% (Life Technologies, 25090028)) and passaged (1:5) onto fresh irradiated MEFs.

Genome targeting

Mouse models were generated using the clustered regularly interspaced short palindromic repeats (CRISPR-Cas9) technology. For this, guide RNAs (gRNAs) were designed using the CCTop - CRISPR/Cas9 target online predictor tool (Labuhn et al., 2018; Stemmer et al., 2017). gRNAs located adjacent to the mutation-of-interest and with a minimum CRISPR score were selected (Table 1). These were cloned into the pSpCas9(BB)-2A-GFP (PX458) vector backbone, a gift from Feng Zhang (Addgene plasmid #48138; <http://n2t.net/addgene:48138>; RRID: Addgene_48138) (Ran et al., 2013). The reference plasmid was generated by cloning the g-block template (Integrated DNA Technologies), containing the mutant-of-interest, into the pUC19 vector backbone, a gift from Joachim Messing (Addgene plasmid #50005; <http://n2t.net/addgene:50005>; RRID: Addgene_50005) (Norrander et al., 1983). Each g-block template was flanked by roughly a 400bp sequence used for homologous direct repair (HDR) and included a blocking mutation for the protospacer adjacent motif (PAM) sequence which also served as restriction enzyme (RE) site for efficient genotyping (Table 2). Mouse embryonic stem (mES) cells, cultured in a well of 12-well plate, were dissociated and centrifuged at 300g for 5 minutes. Supernatant was aspirated and the cell pellet was resuspended in 500 μ L dPBS (Gibco Life Technologies, 14190094). Next, 5 μ g of gRNA and 5 μ g of reference plasmid were added to the cell suspension. Cells were electroporated with the Biorad Gene Pulser device (Voltage, 0.8kV; Capacitance, 3 μ F) and left at room temperature (RT) for 5 minutes and subsequently seeded on fresh irradiated MEFs. After 24 hours, cells were dissociated and sin-

Table 1. gRNA sequences

| Name | Sequence (5' - 3') |
|---------------|-------------------------|
| gRNA_Trp796fs | AGGACTCCTGCACTGTGCAGTGG |
| gRNA_Arg947X | CCGAGTACGGGCACACAATGTGG |

Table 2. G-block sequence containing the mutation-of-interest.

| Name | Sequence (5' - 3') |
|-------------------|--|
| Trp796fs template | <p>ACGACAGAGCTCATTCACTCAGCTACTCAGCAATGCTCACGGGGACA CTCCAGAGCAGGCAATGGTAGTGACTGGGACTGCTTGAGATGAGTCC TTTGATGGGTGTGTAGAAATGCTACTGTTTGTGGGACAATCACTGTGT CCTGGAGGGCTGGGTGGGGTGGGGTGGATGTAGACATTGGACCTGG GACACACAGGAGGTGAAAGTGAACAGTGGGAGGCATAAGTGTGGAT GGTAGATGATGGATGGTAAGGTAATCCGGGTCTAGATAGCTTGGACT CTGGTGCTGGTGGTGAAGAGAAGGGTGAGCGATGCTGTGGGACTCT GAGTTGGACATAGCTGATGTGGTTCCTCTTCCCCATCAAGATGTCCA GATGCTCCTGCGGCCCTAAGATCAGCAACGTGGGCGAGGACTCCTG CACTGTGCAGGTGGTACCGCCTGCCTATGATGGCGGCAGCCGGT CCTGGGTGAGTTCGGGACAGGGACAGCCAAGGGCAGCTGTCA CCTGAGTGACAGGGCACCGGCCGACTTCTCATCTCCTCTCAGGAT ACATCCTGGAGCGCAAGAAGAAAAAGAGCTACAGGTGGATGAGGCT CAACTTTGATCTGCTGCGGGAGCTGAGCCACGAGGCGAGGCGCATG ATCGAGGGTGTAGCCTATGAGATGCGAGTCTACGCAGTCAATGCCGT GGGAATGTCCAGGCCAGCCCTGCCTCTCAGCCCTTCATGCCTATTG GTGAGCCTGCCAGATCCCAGAATGCAGGGACCAAGGGGTGGATG GTTGCAGCCTCTTAGCCGGCAGGCGGCCTCTGCACAGGGCTTTGAAT TCTATCGG</p> |
| Arg947X template | <p>ACGACAGGTACCTCCTTCTATGAGATCAGCAGACAACCTGAGGTCTCT GGTAATTCATGGCTGCTTCTCTGCATGGTACAGACTCACATCCTCTCT GTCTCTGTCCAGGGCCCCCTGGCGAACCAACCACTTGGCTGTGGAG GATGTGTCAGACACCACTGTCTCACTCAAGTGGCGGCCCCAGAGCG CGTGGGGGCCGGTGGCCTGGACGGATACAGCGTGGAGTACTGCCAG GAGGGATGTGAGTACTCCACCTGGGGCCAGCCCTTGGGTGCTAGCA AGGTAAAGTGTGATTTGACTCATTTATGCCTGCACCCAGGCTCCGAG TGGACACCTGCTCTGCAGGGGCTGACAGAGCGCACATCGATGCTGGT GAAGGACCTACCACTGGGGCACGGCTGCTGTTCTGAGTACGGGCA CACAATGTGGCAGGTCTGGAGGCCCATGCTCACCAAGGAGCCTGT GACAGTGCAGGAGATACTGCGTGAGTGCCCTTCTGCTAAAAGGCCTG CCACTGGCCACCCTTTGCCAATCAAGACAGGCTGGGGACATGGGCTT TAGTAGGCAAGGGCAGGGACAGGGGCTGGGGCAGGAAGGGCCAGG GCCTTCATCTATGCCTTGGGCTCTCTTGGTTCAGTCCCTAATTCTGGAA CAGGTACTIONCAGCATAGGTATTGTCCTCAGAAGTGAACAGTGAGG CTTTTCGGAGCCATTTAGGGTCGTCTGGGATACACTTCCATTCTTCTG TTAGTCTTTGTTGTTGTTGAGACAGGGTCTCTACATAGTCTGGCT GTTCTGGAAGTGAATTCTATCGG</p> |

Red; mutation-of-interest, Orange; PAM Sequence, Blue; RE mutation

Table 3. Primer sequences around the region-of-interest

| Name | Sequence (5' - 3') |
|------------------|---------------------------|
| gRNA_Trp796fs_Fw | CACCGAGGACTCCTGCACTGTGCAG |
| gRNA_Trp796fs_Rv | AAACCTGCACAGTGCAGGAGTCCT |
| gRNA_Arg947X_Fw | CACCGCCACATTGTGTGCCCGTACT |
| gRNA_Arg947X_Rv | AAACAGTACGGGCACACAATGTGG |

gle-cell sorted based on GFP into 96-well plates previously coated with MEFs (BD biosciences, FACSJazz™). After one week, clones were dissociated and transferred onto two MEF-coated 96-well plates. One plate was used to perform DNA genotyping using an ethanol-based precipitation method. A PCR was performed around the region-of-interest (Table 3) followed by a RE digest and analysis on a 2% weight/volume agarose gel. Positive clones were further cultured and stored in liquid nitrogen.

Karyotyping

To determine genomic DNA integrity of successfully modified mES cells, cultured cells were incubated with 0.05μg/mL colcemid (Gibco, 152120012) for 90 minutes at 37°C. Medium was collected and the cells were rinsed once with dPBS (Gibco Life Technologies, 14190094). Next, cells were dissociated with 10X trypsin (TVP) for 5 minutes and subsequently centrifuged at 300g for 5 minutes. The cell pellet was resuspended in 1mL of 75mM KCL prewarmed at 37°C and incubated for 10 minutes at 37°C while shaking. Next, a fixation procedure was performed. In short, 50μL of freshly prepared methanol:acetic acid (3:1 ratio) solution was added dropwise to the cell suspension. Cells were centrifuged at 300g for 5 minutes. Then, the supernatant was removed and 1mL of methanol:acetic acid (3:1 ratio) solution was added dropwise on the cell pellet while shaking and incubated for 20 minutes at 37°C. Cells were centrifuged a second time at 300g for 5 minutes. This procedure was repeated two more times. After the last centrifugation step, the cell pellet was resuspended in 0.5mL methanol:acetic acid (3:1 ratio) solution. Drops of the cell suspension were then dropped from approximately 50cm high on a glass microscope slide and left to dry. Finally, the slides were mounted with ProLong™ Gold Antifade Mountant with DAPI (Thermo Fisher Scientific, P36935). Chromosome spreads were imaged using the Leica TCS SPE Confocal Microscope. Clones showing at least 80% of metaphase spreads with the right karyotype (40 chromosomes) were used for blastocyst injection.

Table 4. Primer sequences of gRNA off-targets

| Name | Sequence (5' - 3') |
|---------------------|-------------------------|
| Trp796fs_Olfr613_Fw | GACCGCTTGGTTGCTATCTG |
| Trp796fs_Olfr613_Rv | CGAAGGTATCACACAATTCTTGA |
| Trp796fs_Aarsd1_Fw | TGGCTCTCTCACCTTCTGTC |
| Trp796fs_Aarsd1_Rv | GGGTGGTGAGACCCTTTGAA |
| Trp796fs_Myh10_Fw | TTGTGGAACGCCTTCACTGT |
| Trp796fs_Myh10_Rv | TCCCTTTCCTGGTCTGGCTA |
| Arg947X_Ankrd24_Fw | TCCTAAGGTCTGTCCTCTGAAC |
| Arg947X_Ankrd24_Rv | AGAAAAAGAGCCTGAGGGGC |
| Arg947X_Arhgef28_Fw | TCTTCCCCCTACCACCCTG |
| Arg947X_Arhgef28_Rv | GCTTGACCGAGAAAAGACCT |
| Arg947X_Mir218-2_Fw | GGAGGTTAGAGAAAACCCACGG |
| Arg947X_Mir218-2_Rv | CCGATGAACCCCGATATCCA |

Off-targets

The top three predicted exonic or intronic off-target sites of the gRNA by CCTop - CRISPR/Cas9 target online predictor tool was assessed by performing PCR (Table 4) and subsequent sequencing.

Blastocyst injection

Modified mES cells were rinsed with dPBS (Gibco Life Technologies, 14190094) and trypsinized with 100µL 10X TVP at RT for 5 minutes. Next, 900µL of CM^{+/+} was added and the cells were resuspended by pipetting until a single cell suspension was obtained. Cells were seeded onto two gelatin-coated wells of a 12-well plates and incubated for one hour at 37°C. Medium was carefully removed and the modified mES cells were collected in 1mL of medium and subsequently centrifuged at 300g for 5 minutes at RT. After discarding the supernatant, the cell pellet was resuspended in 100µL of medium and kept on ice until the blastocyst microinjections. Modified mES were microinjected into B6 mouse blastocysts which were subsequently injected into pseudo pregnant B6 mice. Chimeric offspring were crossbred with C57BL/6 mice.

Genotyping

To determine the genotype of each mouse, genomic DNA was extracted from mouse tissue after following standard digestion and ethanol-based DNA precipitation protocols. PCR was performed around the region-of-interest (Table 3) using GoTaq® G2

Hot Start Green Master Mix protocol (Promega, M7423). Then, PCR products were digested with KpnI (Trp796fs) or PvuI (Arg947X) restriction enzymes (BioLabs[®] New England) for 1 hour at 37°C and subsequently analyzed on a 2% weight/volume agarose gel.

Transverse aortic banding (TAB) surgery

Cardiac remodeling was induced in both WT and HET male mice at 8.5-9.5 weeks of age by constriction of the aorta. Briefly, subcutaneous injections of Buprenorphine (0.1mg/kg) were used as analgesic at least 30 minutes pre surgery. Mice were anesthetized with a mix of Fentanyl (0.05 mg/kg), Midazolam (5 mg/kg), and Dexmedetomidine (0.125 mg/kg) via intraperitoneal injections. If necessary, isoflurane (1-2%) was added to the anesthesia. A tracheal tube was placed which connected the mouse to a ventilator. Hair was removed from the thorax and neck with Veet[®] hair removal cream. After disinfection with Iodine and 70% ethanol, skin was incised left of the midline to allow access to the first intercostal space (between the first and second rib). Pectoral muscles were retracted and the intercostal muscles cut caudal to the first rib. Retractors were placed to separate the thymus from the heart. The aorta was identified within the fatty tissue around the heart and a 6.0 silk suture was placed around the aorta between the first and the second branch. Suture was closed with a 26G needle in between to have a standard size aorta opening. Needle was removed immediately after closing the suture. The thymus was placed back and the rib cage was closed with 5.0 silk sutures. Pectoral muscles were placed back and the skin was closed with a wound clip. Animals were disconnected from the machine and placed on a nose cone with oxygen until recovery, and the mice were antagonized with Atipamezole. A second dose of Buprenorphine (0.1mg/kg) was administered postoperatively after 8-12 hours and a third dose was given the morning after surgery. During the whole surgery and recovery mice were placed on a heating pad at 38-39°C.

Echocardiography

Cardiac function and dimensions were evaluated by two-dimensional transthoracic echocardiography using a Vevo[®] 2100 Ultrasound system (Visual Sonics) connected to a 30MHz transducer. Mice were sedated with 2% isoflurane and placed on a heat mat. In order to verify that the TAB was performed correctly, blood flow was assessed using pulsed wave (PW)-mode, assisted by Color Doppler mode in aortic arch view. For flow measurement near TAB location, descending aorta settings were used. Furthermore, the heart was imaged in a parasternal long-axis as well as short-axis view at the level of the papillary muscles. M-mode tracings from a long-axis enabled the measurement of left ventricle end diastolic diameter (LVIDd), left ventricular end-sys-

tolic diameter (LVIDs), end-diastolic interventricular septal wall thickness (IVSd), end-systolic interventricular septal wall thickness (IVSs), end-diastolic left ventricular posterior wall thickness (LVPWd), end-systolic left ventricular posterior wall thickness (LVPWs) and isovolumic relaxation time (IVRT). For each parameter, the average of at least 6 measurements was used to determine the measurements for each animal. Fractional shortening (FS) and ejection fraction (EF), automatically calculated by the Vevo® LAB 1.7.1 software, was used to assess contractile function.

Tissue collection

After echo measurements, still sedated animals from isoflurane were sacrificed by cervical dislocation. Hearts (and kidneys for homozygous mice) were collected, washed in ice cold PBS, weighed and snap frozen in liquid nitrogen for protein/RNA analysis or fixed in 4% formaldehyde for histological analysis. The heart was cut transversely, using the base section for histology, the center for proteomics and the apex, further cut in half, for protein and RNA. The left leg was enzymatically digested with ProtK (Promega, 0.6µg/µl final concentration) in lysis buffer, after which the tibia length was measured using a digital caliper.

Histology and Microscopy

For histological stainings, hearts were fixed 4% paraformaldehyde (Klinipath, Duiven) for 48 hours at RT, embedded in paraffin and sectioned at 5µm. Hematoxylin and eosin (H&E) staining and picosirius red (SR) were performed for an overall view of the heart and the presence of fibrosis, respectively. Sections were dewaxed and rehydrated and the correspondent staining was performed following standard protocols. Hearts were imaged using a Leica DM 4000 microscope and Leica LAS software. Fibrotic area in the ventricles was quantified using ImageJ.

Cell size

Paraffin-embedded heart sections were dewaxed and rehydrated. Cell borders were stained with fluorescein isothiocyanate (FITC) labeled Wheat Germ Agglutinin (WGA) lectin (100µg/mL, Sigma-Aldrich). Briefly, heart sections were incubated for 1h at RT in WGA solution. After, sections were washed with dPBS and incubated with DAPI solution. All solutions are made with 2% BSA:dPBS. Sections were imaged using 40X oil objective on the Leica TCS SPE and Leica LAS software. Cross-sectional area (CSA) was measured using ImageJ. Quantifications were performed on at least 50 cells per heart and based on the indicated number of hearts.

Protein isolation and Western blot

Cardiac tissue was homogenized in RIPA lysis buffer (50nM Tris, 150nM NaCl, 0.1% SDS, 0.5% sodium deoxycholate, 1% Triton x-100) with a one tablet of of cComplete™ Protease Inhibitor Cocktail (Sigma-Aldrich) per 10mL of RIPA buffer. Protein was subsequently quantified (Bradford Assay, Bio-rad). A total of 25µg of protein was separated on a 10% SDS-PAGE and subsequently transferred to a polyvinylidene difluoride (PVDF) membrane using wet transfer in a mini trans-blot electrophoretic transfer cell (Bio-rad). MYBPC3 (sc-137180, Santa Cruz) was analyzed and α -ACTININ (HPA008315, Sigma) was used as loading control (Table 5) Primary antibodies were incubated overnight at 4°C. Secondary antibodies (anti-mouse or anti-rabbit) coupled to horseradish peroxidase (Jackson ImmunoResearch Europe Ltd) were used,

Table 5. Antibodies used for Western Blot

| Name | Source | Dilution |
|-------------------|------------------------|----------|
| MYBPC3 (E7) | Santa Cruz (sc-137180) | 1:1000 |
| α -ACTININ | Sigma (HPA008315) | 1:500 |

followed by protein detection using Clarity™ Western ECL Substrate kit (Bio-rad). The blots were images using IQ800 RGB Chemiluminescence Imager and quantification analysis were performed using ImageJ.

RNA isolation and real-time PCR (qPCR)

Total RNA was extracted from mouse heart tissue with TRIzol™ Reagent (Thermo Fisher Scientific, 15596026) according to the manufacturer's protocol. cDNA was synthesized from 500ng of RNA using the iScript cDNA Synthesis Kit (Bio-Rad, #1708891). Real-time PCR was performed by using a specific set of primers (Table 6) together with iQ SYBR Green Supermix (Bio-Rad, #170-8885) on a real-time PCR machine (CFX Connect™ Real-Time PCR Detection System, Bio-Rad). Expression

Table 6. Real-time PCR primers

| Name | Forward Sequence (5' - 3') | Reversed Sequence (5'-3') |
|---------------|----------------------------|---------------------------|
| <i>Mybpc3</i> | TTTCCGGAGGGACTCAAAGC | CATGCCTCGAAGGTCTGTGA |
| <i>Hprt</i> | AGCCTAAGATGAGCGCAAGT | ATGGCCACAGGACTAGAACA |
| <i>Nppa</i> | GGTAGGATTGACAGGATTGGAG | GCTTAGGATCTTTTGCATCTG |
| <i>Nppb</i> | GAGTCCTTCGGTCTCAAGGC | CAACTTCAGTGC GTTACAGC |
| <i>Acta1</i> | AGACCACCGCTCTTGTGTG | GGAGTCCTTCTGACCCATACC |
| <i>Col2a1</i> | GCAAAGATGGCTCTAATGGAA | GACTTCCAGGGGGACCAA |
| <i>Postn</i> | AAGAGAATTACTGCAGAGTTGGT | GGTATGAAGTCCTATTCCAAAGTC |

levels were normalized to Hypoxanthine-guanine-fofosforibosyl-transferase (Hprt). Fold changes in gene expression were calculated according to the $2^{-\Delta\Delta CT}$ -method and expressed as mean fold change \pm SEM. Control groups were set at 1.

Proteomics analysis

Proteomics was performed on 4x WT Sham; 4x Trp796fs+/- Sham; 4x WT TAB; 4x Trp796fs+/- TAB. Mouse heart tissue samples (roughly 30 μ g) were placed in Lysing Matrix D tubes containing 800 μ L Tris/SDS lysis buffer (50mM Tris, 0.1% SDS and protease inhibitors, at pH8.8) and homogenized using Lysing Matrix D in a FastPrep homogenizer (MP Biomedicals) twice for 15 seconds. The supernatant was transferred into Eppendorf tubes and sonicated twice for 10 seconds, prior to centrifugation for 30 minutes at 20,000g at 4°C. Protein concentration was measured with Pierce BCA Protein Assay Kit (Thermo Fisher Scientific). Thirty micrograms (30 μ g) of proteins from each sample were denatured by 6 M urea/ 2M thiourea, reduced by 10mM dithiothreitol for 1 hour at 37°C, and alkylated using 50mM iodoacetamide for 1 hour at room temperature in the dark. The samples were precipitated by using 500 μ L of pre-chilled acetone and incubated at -20°C overnight. The samples were centrifugation for 30 minutes at 20,000 g at 4°C, and the supernatant discarded. The protein pellet was dried using a SpeedVac and resuspended in 0.1M triethylammonium bicarbonate (TEAB, pH8.5). Proteins were digested by Trypsin/LysC (enzyme: protein = 1:100) overnight at 37°C with 180rpm shaking. After digestion, peptides were purified on a Bravo AssayMAP liquid handling system using C18 cartridges (Agilent) and resuspended in 0.1M TEAB. A pooled sample was made by mixing the same amount of each sample. Twenty micrograms (20 μ g) of samples along with 2x 20 μ g of pooled samples were labelled with TMT 10plex Reagents (Thermo Fisher Scientific) following the manufacturer's instructions. After quenching with 5% hydroxylamine, 1 pooled sample and 8 samples were mixed together (in total 2 mixed TMT-labelled samples), dried using SpeedVac and resuspended in 60 μ L of 0.1% (v/v) TEA. High pH reversed-phase peptide fractionation was performed using Agilent 300Extend-C18 column (3.5 μ m, 4.6x150mm, Agilent P/N 763973-902) on Ultimate 3000 HPLC (Thermo Fisher Scientific) and 16 fractions were collected for each mixed TMT-labelled sample (120 μ g). The fractionated samples were dried using SpeedVac and resuspended in 30 μ L LC solution (2% acetonitrile, 0.05% trifluoroacetic acid, in LC-MS grade H₂O).

For LC-MS/MS analysis, 10 μ L of each fractionated sample was injected and separated by reversed-phase nano-flow HPLC (Ultimate 3000 RSLCnano, Thermo Fisher Sci-

entific) on a 50cm EASY-SPRAY C18 column (Thermo Fisher Scientific, Cat No. ES803) over 2-hour gradient at a flow rate of 0.2 $\mu\text{l}/\text{min}$: 0-10 minutes, 4%-10%B; 10-75 minutes, 10%-30%B; 75-80 minutes, 30%-40%B; 80-85 minutes, 40-99%B; 85-90 minutes, 99%B; 90-120 minutes, 4%B; where A = 0.1% formic acid, B = 80% acetonitrile, 0.1% formic acid. The separated peptides were directly injected into Orbitrap Fusion Lumos Tribrid Mass Spectrometer (Thermo Fisher Scientific) and analysed using a synchronous precursor selection (SPS) multi-notch MS3 method. Full MS scan range was 375-1500m/z with resolution 120,000 in Orbitrap. Data-dependent MS2 scan was performed on the most abundant precursors using collision-induced dissociation (CID) and detected in linear ion trap. Top 5 fragment ions in MS2 scan were selected for SPS-MS3 scan using higher-energy collisional dissociation (HCD) and detected in Orbitrap with scan range 100-500m/z and resolution 60,000. Cycle time was set at 3 seconds and dynamic exclusion was enabled.

The proteomics data analysis was performed using Proteome Discoverer 2.4 with Mascot 2.6.0. The database search was performed using UniProt/Swiss-Prot mouse database (version 2020_01, 17033 protein entries), 2 missed cleavage allowed, 10ppm precursor mass tolerance and 0.8 Da fragment mass tolerance, TMT 6plex (N-term, K) and carbamidomethylation (C) as fixed modifications, oxidation (M) as variable modifications. With total peptide normalization and on control scaling. The total scaled abundance was exported into Excel and used for further analysis. Proteins of interest were selected using a Log2foldchange < -0,4 or > 0,4.

Statistical analysis

Values are presented as mean \pm standard error of the mean (SEM). Statistical analyses were performed using PRISM software (GraphPad Software Inc. version 8). Outliers were identified and excluded using the Grubbs test with an $\alpha=0.05$. Statistical significance was evaluated using a two-tailed Student's t-test for comparisons between two groups. In case of multiple groups, a 2-way ANOVA including multiple comparisons with Bonferroni correction was performed. Significant differences were achieved when p-values < 0.05 compared to the indicated control. The number of samples (n) and the statistical significance (* = p-value < 0.0332, ** = p-value < 0,021, *** = p-value < 0.0002, **** = p-value < 0.0001) are indicated in the legends of each figure.

References

- Anzalone, A. V., Randolph, P. B., Davis, J. R., Sousa, A. A., Koblan, L. W., Levy, J. M., Chen, P. J., Wilson, C., Newby, G. A., Raguram, A., & Liu, D. R. (2019). Search-and-replace genome editing without double-strand breaks or donor DNA. *Nature*, *576*(7785), 149–157. <https://doi.org/10.1038/s41586-019-1711-4>
- Atteya, G., Day, S., & Lampert, R. (2017). Sports and Exercise in Patients with Hypertrophic Cardiomyopathy: More Questions than Answers. *American College of Cardiology*, 5–7. <https://www.acc.org/latest-in-cardiology/articles/2017/02/20/08/06/sports-and-exercise-in-patients-with-hypertrophic-cardiomyopathy>
- Balaji, S., Dilorenzo, M. P., Fish, F. A., Etheridge, S. P., Aziz, P. F., Russell, M. W., Tisma, S., Pflaumer, A., Sreeram, N., Kubus, P., Law, I. H., & Kantoch, M. J. (2019). Impact of Obesity on Left Ventricular Thickness in Children with Hypertrophic Cardiomyopathy. *Pediatric Cardiology*, *40*(6), 1253–1257. <https://doi.org/10.1007/s00246-019-02145-9>
- Barefield, D., Kumar, M., de Tombe, P. P., & Sadayappan, S. (2014). Contractile dysfunction in a mouse model expressing a heterozygous MYBPC3 mutation associated with hypertrophic cardiomyopathy. *American Journal of Physiology - Heart and Circulatory Physiology*, *306*(6), 807–815. <https://doi.org/10.1152/ajpheart.00913.2013>
- Barefield, D., Kumar, M., Gorham, J., Seidman, J. G., Seidman, C. E., de Tombe, P. P., & Sadayappan, S. (2015). Haploinsufficiency of MYBPC3 exacerbates the development of hypertrophic cardiomyopathy in heterozygous mice. *Journal of Molecular and Cellular Cardiology*, *79*, 234–243. <https://doi.org/10.1016/j.yjmcc.2014.11.018>
- Bhagwan, J. R., Mosqueira, D., Chairez-Cantu, K., Mannhardt, I., Bodbin, S. E., Bakar, M., Smith, J. G. W. W., & Denning, C. (2020). Isogenic models of hypertrophic cardiomyopathy unveil differential phenotypes and mechanism-driven therapeutics. *Journal of Molecular and Cellular Cardiology*, *145*(March), 43–53. <https://doi.org/10.1016/j.yjmcc.2020.06.003>
- Blankenburg, R., Hackert, K., Wurster, S., Deenen, R., Seidman, J. G., Seidman, C. E., Lohse, M. J., & Schmitt, J. P. (2014). beta-Myosin heavy chain variant Val606Met causes very mild hypertrophic cardiomyopathy in mice, but exacerbates HCM phenotypes in mice carrying other HCM mutations. *Circ Res*, *115*(2), 227–237. <https://doi.org/10.1161/CIRCRESAHA.115.303178>
- Bos, J. M., Towbin, J. A., & Ackerman, M. J. (2009). Diagnostic, Prognostic, and Therapeutic Implications of Genetic Testing for Hypertrophic Cardiomyopathy. *Journal of the American College of Cardiology*, *54*(3), 201–211. <https://doi.org/10.1016/j.jacc.2009.02.075>
- Carrier, L., Knöll, R., Vignier, N., Keller, D. I., Bausero, P., Prudhon, B., Isnard, R., Ambroisine, M.-L., Fiszman, M., Ross, J., Schwartz, K., & Chien, K. R. (2004). Asymmetric septal hypertrophy in heterozygous cMyBP-C null mice. *Cardiovascular Research*, *63*(2), 293–304. <https://doi.org/10.1016/j.cardiores.2004.04.009>
- Carrier, L., Mearini, G., Stathopoulou, K., & Cuello, F. (2015). Cardiac myosin-binding protein C (MYBPC3) in cardiac pathophysiology. *Gene*, *573*(2), 188–197. <https://doi.org/10.1016/j.gene.2015.09.008>
- Carrier, L., Schlossarek, S., Willis, M. S., & Eschenhagen, T. (2010). The ubiquitin-proteasome system and nonsense-mediated mRNA decay in hypertrophic cardiomyopathy. *Cardiovascular Res*, *85*(2), 330–338. <https://doi.org/10.1093/cvr/cvp247>
- Chemello, F., Chai, A. C., Li, H., Rodriguez-Caycedo, C., Sanchez-Ortiz, E., Atmanli, A., Mireault, A. A., Liu, N., Bassel-Duby, R., & Olson, E. N. (2021). Precise correction of Duchenne muscular dystrophy exon deletion mutations by base and prime editing. *Sci Adv*, *7*(18). <https://doi.org/10.1126/sciadv.abg4910>
- Christiaans, I., Nannenbergh, E. A., Dooijes, D., Jongbloed, R. J. E., Michels, M., Postema, P. G., Majoor-Krakauer, D., van den Wijngaard, A., Mannens, M. M. A. M., van Tintelen,

- J. P., van Langen, I. M., & Wilde, A. A. M. (2010). Founder mutations in hypertrophic cardiomyopathy patients in the Netherlands. *Neth Heart J*, *18*(5), 248–254. <https://doi.org/10.1007/BF03091771>
- Christodoulou, D. C., Wakimoto, H., Onoue, K., Eminaga, S., Gorham, J. M., DePalma, S. R., Herman, D. S., Teekakirikul, P., Conner, D. A., McKean, D. M., Domenighetti, A. A., Aboukhalil, A., Chang, S., Srivastava, G., McDonough, B., De Jager, P. L., Chen, J., Bulyk, M. L., Muehlschlegel, J. D., ... Seidman, J. G. (2014). 5'RNA-Seq identifies Fhl1 as a genetic modifier in cardiomyopathy. *Journal of Clinical Investigation*, *124*(3), 1364–1370. <https://doi.org/10.1172/JCI70108>
- Chung, M. W., Tsoutsman, T., & Semsarian, C. (2003). Hypertrophic cardiomyopathy: from gene defect to clinical disease. *Cell Res*, *13*(1), 9–20. <https://doi.org/10.1038/sj.cr.7290146>
- Coats, C. J., Heywood, W. E., Virasami, A., Ashrafi, N., Syrris, P., Dos Remedios, C., Treibel, T. A., Moon, J. C., Lopes, L. R., McGregor, C. G. A., Ashworth, M., Sebire, N. J., McKenna, W. J., Mills, K., & Elliott, P. M. (2018). Proteomic Analysis of the Myocardium in Hypertrophic Obstructive Cardiomyopathy. *Circulation. Genomic and Precision Medicine*, *11*(12), e001974. <https://doi.org/10.1161/CIRCGEN.117.001974>
- Crilly, J. G., Boehm, E. A., Blair, E., Rajagopalan, B., Blamire, A. M., Styles, P., McKenna, W. J., Ostman-Smith, I., Clarke, K., Watkins, H., Östman-Smith, I., Clarke, K., & Watkins, H. (2003). Hypertrophic cardiomyopathy due to sarcomeric gene mutations is characterized by impaired energy metabolism irrespective of the degree of hypertrophy. *J Am Coll Cardiol*, *41*(10), 1776–1782. [https://doi.org/10.1016/s0735-1097\(02\)03009-7](https://doi.org/10.1016/s0735-1097(02)03009-7)
- Farrell, E., Armstrong, A. E., Grimes, A. C., Naya, F. J., De Lange, W. J., & Ralphe, J. C. (2018). Transcriptome analysis of cardiac hypertrophic growth in MYBPC3-null mice suggests early responders in hypertrophic remodeling. *Frontiers in Physiology*, *9*(OCT), 1–14. <https://doi.org/10.3389/fphys.2018.01442>
- Finocchiaro, G., Magavern, E., Sinagra, G., Ashley, E., Papadakis, M., Tome-Esteban, M., Sharma, S., & Olivetto, I. (2017). Impact of demographic features, lifestyle, and comorbidities on the clinical expression of hypertrophic cardiomyopathy. *Journal of the American Heart Association*, *6*(12), 1–11. <https://doi.org/10.1161/JAHA.117.007161>
- Fourey, D., Care, M., Siminovitch, K. A., Weissler-Snir, A., Hindieh, W., Chan, R. H., Gollob, M. H., Rakowski, H., & Adler, A. (2017). Prevalence and Clinical Implication of Double Mutations in Hypertrophic Cardiomyopathy. *Circulation: Cardiovascular Genetics*, *10*(2), 1–10. <https://doi.org/10.1161/CIRCGENETICS.116.001685>
- Fumagalli, C., Maurizi, N., Day, S. M., Ashley, E. A., Michels, M., Colan, S. D., Jacoby, D., Marchionni, N., Vincent-tompkins, J., Ho, C. Y., Olivetto, I., & Investigators, S. (2020). Association of Obesity With Adverse Long-term Outcomes in Hypertrophic Cardiomyopathy. *5*(1), 65–72. <https://doi.org/10.1001/jamacardio.2019.4268>
- Geisterfer-Lowrance, A. A., Christe, M., Conner, D. A., Ingwall, J. S., Schoen, F. J., Seidman, C. E., & Seidman, J. G. (1996). A mouse model of familial hypertrophic cardiomyopathy. *Science*, *272*(5262), 731–734. <https://doi.org/10.1126/science.272.5262.731>
- Goland, S., van Hagen, I. M., Elbaz-Greener, G., Elkayam, U., Shotan, A., Merz, W. M., Enar, S. C., Gaisin, I. R., Pieper, P. G., Johnson, M. R., Hall, R., Blatt, A., & Roos-Hesselink, J. W. (2017). Pregnancy in women with hypertrophic cardiomyopathy: data from the European Society of Cardiology initiated Registry of Pregnancy and Cardiac disease (ROPAC). *Eur Heart J*, *38*(35), 2683–2690. <https://doi.org/10.1093/eurheartj/ehx189>
- Gori, M., Senni, M., Gupta, D. K., Charytan, D. M., Kraigher-Krainer, E., Pieske, B., Claggett, B., Shah, A. M., Santos, A. B., Zile, M. R., Voors, A. A., McMurray, J. J., Packer, M., Bransford, T., Lefkowitz, M., Solomon, S. D., & Investigators, P. (2014). Association between renal function and cardiovascular structure and function in heart failure with preserved ejection fraction. *Eur Heart J*, *35*(48), 3442–3451. <https://doi.org/10.1093/eurheartj/ehu254>

- Gramlich, M., Michely, B., Krohne, C., Heuser, A., Erdmann, B., Klaassen, S., Hudson, B., Magarin, M., Kirchner, F., Todiras, M., Granzier, H., Labeit, S., Thierfelder, L., & Gerull, B. (2009). Stress-induced dilated cardiomyopathy in a knock-in mouse model mimicking human titin-based disease. *J Mol Cell Cardiol*, *47*(3), 352–358. <https://doi.org/10.1016/j.yjmcc.2009.04.014>
- Green, E. M., Wakimoto, H., Anderson, R. L., Evanchik, M. J., Gorham, J. M., Harrison, B. C., Henze, M., Kawas, R., Oslob, J. D., Rodriguez, H. M., Song, Y., Wan, W., Leinwand, L. A., Spudich, J. A., McDowell, R. S., Seidman, J. G., & Seidman, C. E. (2016). Heart disease: A small-molecule inhibitor of sarcomere contractility suppresses hypertrophic cardiomyopathy in mice. *Science*, *351*(6273), 617–621. <https://doi.org/10.1126/science.aad3456>
- Harris, S. P., Bartley, C. R., Hacker, T. A., McDonald, K. S., Douglas, P. S., Greaser, M. L., Powers, P. A., & Moss, R. L. (2002). Hypertrophic cardiomyopathy in cardiac myosin binding protein-C knockout mice. *Circulation Research*, *90*(5), 594–601. <https://doi.org/10.1161/01.RES.0000012222.70819.64>
- Heitner, S. B., Jacoby, D., Lester, S. J., Owens, A., Wang, A., Zhang, D., Lambing, J., Lee, J., Semigran, M., & Sehnert, A. J. (2019). Mavacamten Treatment for Obstructive Hypertrophic Cardiomyopathy: A Clinical Trial. *Ann Intern Med*, *170*(11), 741–748. <https://doi.org/10.7326/M18-3016>
- Helms, A. S., Tang, V. T., O’Leary, T. S., Friedline, S., Wauchope, M., Arora, A., Wasserman, A. H., Smith, E. D., Lee, L. M., Wen, X. W., Shavit, J. A., Liu, A. P., Previs, M. J., & Day, S. M. (2020). Effects of MYBPC3 loss-of-function mutations preceding hypertrophic cardiomyopathy. *JCI Insight*, *5*(2). <https://doi.org/10.1172/jci.insight.133782>
- Hilderink, S., Schuldt, M., Goebel, M., Jansen, V. J., Manders, E., Moorman, S., Dorsch, L. M., van Steenbeek, F. G., van der Velden, J., & Kuster, D. W. D. (2023). Characterization of heterozygous and homozygous mouse models with the most common hypertrophic cardiomyopathy mutation MYBPC3 in the Netherlands. *Journal of Molecular and Cellular Cardiology*, *185*, 65–76. <https://doi.org/10.1016/j.yjmcc.2023.10.008>
- Horowitz, J. D., & Chirkov, Y. Y. (2010). Perhexiline and hypertrophic cardiomyopathy: a new horizon for metabolic modulation. *Circulation*, *122*(16), 1547–1549. <https://doi.org/10.1161/CIRCULATIONAHA.110.981464>
- Huang, S., Liao, Z., Li, X., Liu, Z., Li, G., Li, J., Lu, Z., Zhang, Y., Li, X., Ma, X., Sun, Q., & Huang, X. (2019). Developing ABEmax-NG with Precise Targeting and Expanded Editing Scope to Model Pathogenic Splice Site Mutations In Vivo. *IScience*, *15*, 640–648. <https://doi.org/10.1016/j.isci.2019.05.008>
- Ingles, J. (2005). Compound and double mutations in patients with hypertrophic cardiomyopathy: implications for genetic testing and counselling. *Journal of Medical Genetics*, *42*(10), e59–e59. <https://doi.org/10.1136/jmg.2005.033886>
- Karam, R., Lever, H. M., & Healy, B. P. (1989). Hypertensive hypertrophic cardiomyopathy or hypertrophic cardiomyopathy with hypertension? A study of 78 patients. *J Am Coll Cardiol*, *13*(3), 580–584. [https://doi.org/10.1016/0735-1097\(89\)90596-2](https://doi.org/10.1016/0735-1097(89)90596-2)
- Kazmierczak, K., Yuan, C. C., Liang, J., Huang, W., Rojasand, A. I., & Szczesna-Cordary, D. (2014). Remodeling of the heart in hypertrophy in animal model with myosin essential light chain mutations. *Frontiers in Physiology*, *5*(September), 1–12. <https://doi.org/10.3389/fphys.2014.00353>
- Konhilas, J. P., Watson, P. A., Maass, A., Boucek, D. M., Horn, T., Stauffer, B. L., Luckey, S. W., Rosenberg, P., & Leinwand, L. A. (2006). Exercise can prevent and reverse the severity of hypertrophic cardiomyopathy. *Circulation Research*, *98*(4), 540–548. <https://doi.org/10.1161/01.RES.0000205766.97556.00>
- Labuhn, M., Adams, F. F., Ng, M., Knoess, S., Schambach, A., Charpentier, E. M., Schwarzer, A., Mateo, J. L., Klusmann, J. H., & Heckl, D. (2018). Refined sgRNA efficacy prediction improves large- and small-scale CRISPR-Cas9 applications. *Nucleic Acids Res*, *46*(3),

- 1375–1385. <https://doi.org/10.1093/nar/gkx1268>
- Lampert, R., Salberg, L., & Burg, M. (2010). Emotional stress triggers symptoms in hypertrophic cardiomyopathy: a survey of the Hypertrophic Cardiomyopathy Association. *Pacing Clin Electrophysiol*, 33(9), 1047–1053. <https://doi.org/10.1111/j.1540-8159.2010.02770.x>
- Lee, H., Han, K., Park, J. B., Hwang, I. C., Yoon, Y. E., Park, H. E., Choi, S. Y., Kim, Y. J., Cho, G. Y., Kim, H. K., & Ommen, S. R. (2019). Risk of end-stage renal disease in patients with hypertrophic cardiomyopathy: A nationwide population-based cohort study. *Sci Rep*, 9(1), 14565. <https://doi.org/10.1038/s41598-019-50993-5>
- Lekanne Deprez, R. H., Muurling-Vlietman, J. J., Hruđa, J., Baars, M. J. H., Wijnaendts, L. C. D., Stolte-Dijkstra, I., Alders, M., & van Hagen, J. M. (2006). Two cases of severe neonatal hypertrophic cardiomyopathy caused by compound heterozygous mutations in the MYBPC3 gene. *Journal of Medical Genetics*, 43(10), 829–832. <https://doi.org/10.1136/jmg.2005.040329>
- Li, H., Yang, Y., Hong, W., Huang, M., Wu, M., & Zhao, X. (2020). Applications of genome editing technology in the targeted therapy of human diseases: mechanisms, advances and prospects. *Signal Transduct Target Ther*, 5(1), 1. <https://doi.org/10.1038/s41392-019-0089-y>
- Lim, D. S., Lutucuta, S., Bachireddy, P., Youker, K., Evans, A., Entman, M., Roberts, R., & Marian, A. J. (2001). Angiotensin II blockade reverses myocardial fibrosis in a transgenic mouse model of human hypertrophic cardiomyopathy. *Circulation*, 103(6), 789–791. <https://doi.org/10.1161/01.cir.103.6.789>
- Luther, P. K., Bennett, P. M., Knupp, C., Craig, R., Padron, R., Harris, S. P., Patel, J., & Moss, R. L. (2008). Understanding the organisation and role of myosin binding protein C in normal striated muscle by comparison with MyBP-C knockout cardiac muscle. *J Mol Biol*, 384(1), 60–72. <https://doi.org/10.1016/j.jmb.2008.09.013>
- Ma, S., Jiang, W., Liu, X., Lu, W. J., Qi, T., Wei, J., Wu, F., Chang, Y., Zhang, S., Song, Y., Bai, R., Wang, J., Lee, A. S., Zhang, H., Wang, Y., & Lan, F. (2021). Efficient Correction of a Hypertrophic Cardiomyopathy Mutation by ABEmax-NG. *Circ Res*, 129(10), 895–908. <https://doi.org/10.1161/CIRCRESAHA.120.318674>
- Man, J., Barnett, P., & Christoffels, V. M. (2018). Structure and function of the Nppa-Nppb cluster locus during heart development and disease. *Cell Mol Life Sci*, 75(8), 1435–1444. <https://doi.org/10.1007/s00018-017-2737-0>
- Marian, A. J. (2010). Hypertrophic cardiomyopathy: from genetics to treatment. *Eur J Clin Invest*, 40(4), 360–369. <https://www.ncbi.nlm.nih.gov/pubmed/20503496>
- Marian, A. J., & Braunwald, E. (2017). Hypertrophic Cardiomyopathy: Genetics, Pathogenesis, Clinical Manifestations, Diagnosis, and Therapy. *Circ Res*, 121(7), 749–770. <https://doi.org/10.1161/CIRCRESAHA.117.311059>
- Maron, B. J., Gardin, J. M., Flack, J. M., Gidding, S. S., Kurosaki, T. T., & Bild, D. E. (1995). Prevalence of Hypertrophic Cardiomyopathy in a General Population of Young Adults (pp. 785–789). *Circulation*. <https://doi.org/https://doi.org/10.1161/01.CIR.92.4.785>
- Maron, B. J., & Maron, M. S. (2013). Hypertrophic cardiomyopathy. *Lancet*, 381(9862), 242–255. [https://doi.org/10.1016/S0140-6736\(12\)60397-3](https://doi.org/10.1016/S0140-6736(12)60397-3)
- Maron, B. J., & Maron, M. S. (2014). The 25-year genetic era in hypertrophic cardiomyopathy: Revisited. *Circulation: Cardiovascular Genetics*, 7(4), 401–404. <https://doi.org/10.1161/CIRCGENETICS.114.000741>
- Maron, B. J., Maron, M. S., & Semsarian, C. (2012). Double or compound sarcomere mutations in hypertrophic cardiomyopathy: A potential link to sudden death in the absence of conventional risk factors. *Heart Rhythm*, 9(1), 57–63. <https://doi.org/10.1016/j.hrthm.2011.08.009>
- Maron, M. S., Rowin, E. J., Wessler, B. S., Mooney, P. J., Fatima, A., Patel, P., Koethe, B. C., Romashko, M., Link, M. S., & Maron, B. J. (2019). Enhanced American College of Car-

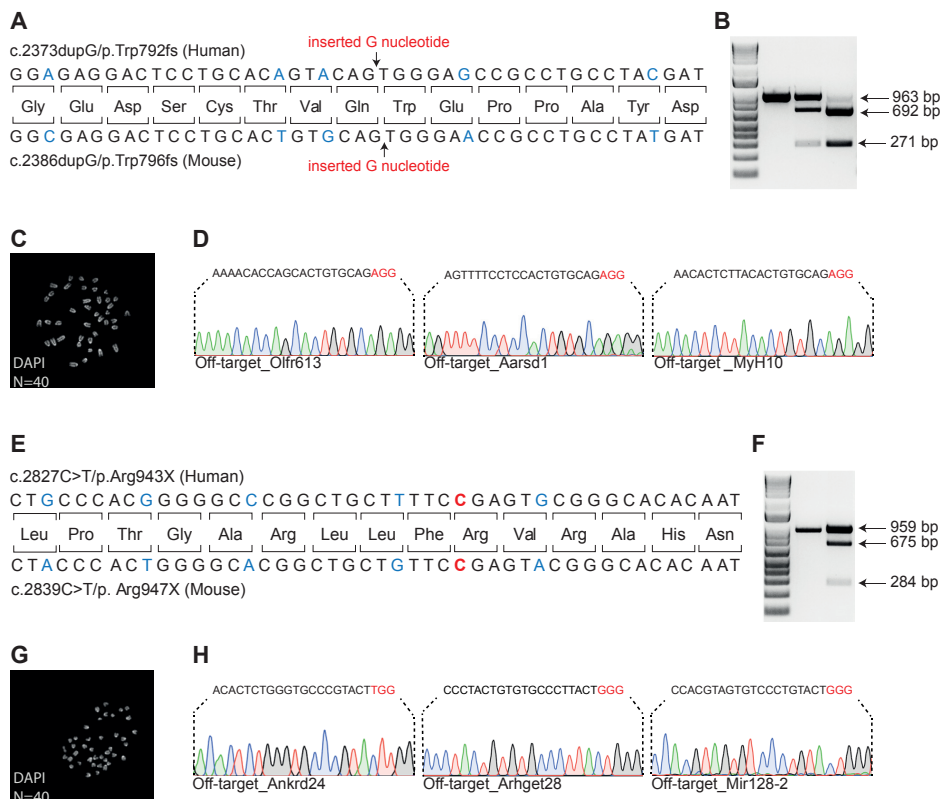
- diology/American Heart Association Strategy for Prevention of Sudden Cardiac Death in High-Risk Patients With Hypertrophic Cardiomyopathy. *JAMA Cardiol*, 4(7), 644–657. <https://doi.org/10.1001/jamacardio.2019.1391>
- Marziliano, N., Merlini, P. A., Vignati, G., Orsini, F., Motta, V., Bandiera, L., Intrieri, M., & Veronese, S. (2012). A case of compound mutations in the MYBPC3 gene associated with biventricular hypertrophy and neonatal death. *Neonatology*, 102(4), 254–258. <https://doi.org/10.1159/000339847>
- McConnell, B. K., Fatkin, D., Semsarian, C., Jones, K. A., Georgakopoulos, D., Maguire, C. T., Healey, M. J., Mudd, J. O., Moskowitz, I. P. G., Conner, D. A., Giewat, M., Wakimoto, H., Berul, C. I., Schoen, F. J., Kass, D. A., Seidman, C. E., & Seidman, J. G. (2001). Comparison of two murine models of familial hypertrophic cardiomyopathy. *Circulation Research*, 88(4), 383–389. <https://doi.org/10.1161/01.RES.88.4.383>
- McNamara, J. W., Li, A., Lal, S., Bos, J. M., Harris, S. P., Van Der Velden, J., Ackerman, M. J., Cooke, R., & Dos Remedios, C. G. (2017). MYBPC3 mutations are associated with a reduced super-relaxed state in patients with hypertrophic cardiomyopathy. *PLoS ONE*, 12(6), 1–22. <https://doi.org/10.1371/journal.pone.0180064>
- Mearini, G., Stimpel, D., Geertz, B., Weinberger, F., Kramer, E., Schlossarek, S., Mouro-Filiatre, J., Stoehr, A., Dutsch, A., Wijnker, P. J. M., Braren, I., Katus, H. A., Muller, O. J., Voit, T., Eschenhagen, T., Carrier, L., Krämer, E., Schlossarek, S., Mouro-Filiatre, J., ... Carrier, L. (2014). Mybpc3 gene therapy for neonatal cardiomyopathy enables long-term disease prevention in mice. *Nat Commun*, 5(May), 5515. <https://doi.org/10.1038/ncomms6515>
- Mohammed, S. F., Storlie, J. R., Oehler, E. A., Bowen, L. A., Korinek, J., Lam, C. S., Simari, R. D., Burnett Jr., J. C., & Redfield, M. M. (2012). Variable phenotype in murine transverse aortic constriction. *Cardiovasc Pathol*, 21(3), 188–198. <https://doi.org/10.1016/j.carpath.2011.05.002>
- Moolman, J. A., Reith, S., Kerstin, U. I., Bailey, S., Gautel, M., Jeschke, B., Fischer, C., Ochs, J., McKenna, W. J., Klues, H., & Vosberg, H. P. (2000). A newly created splice donor site in exon 25 of the MyBP-C gene is responsible for inherited hypertrophic cardiomyopathy with incomplete disease penetrance. *Circulation*, 101(12), 1396–1402. <https://doi.org/10.1161/01.CIR.101.12.1396>
- Mosqueira, D., Bhagwan, J. R., Denning, C., Smith, J. G. W., Bhagwan, J. R., & Denning, C. (2019). Modeling Hypertrophic Cardiomyopathy: Mechanistic Insights and Pharmacological Intervention. *Trends Mol Med*, 25(9), 775–790. <https://doi.org/10.1016/j.molmed.2019.06.005>
- Nag, S., Gollapudi, S. K., del Rio, C. L., Spudich, J. A., & McDowell, R. (2023). *Mavacamten, a precision medicine for hypertrophic cardiomyopathy: From a motor protein to patients*. <https://www.science.org>
- Najafi, A., Schlossarek, S., Deel, E. D. Van, Heuvel, N. Van Den, & Güçlü, A. (2015). Sexual dimorphic response to exercise in hypertrophic. 1303–1317. <https://doi.org/10.1007/s00424-014-1570-7>
- Najafi, A., Schlossarek, S., van Deel, E. D., van den Heuvel, N., Guclu, A., Goebel, M., Kuster, D. W., Carrier, L., & van der Velden, J. (2015). Sexual dimorphic response to exercise in hypertrophic cardiomyopathy-associated MYBPC3-targeted knock-in mice. *Pflugers Arch*, 467(6), 1303–1317. <https://doi.org/10.1007/s00424-014-1570-7>
- Nardi, E., Cottone, S., Mule, G., Palermo, A., Cusimano, P., & Cerasola, G. (2007). Influence of chronic renal insufficiency on left ventricular diastolic function in hypertensives without left ventricular hypertrophy. *J Nephrol*, 20(3), 320–328. <https://www.ncbi.nlm.nih.gov/pubmed/17557265>
- Nijkamp, L., Bollen, I. A. E., van Velzen, H. G., Regan, J. A., van Slegtenhorst, M., Niessen, H. W. M., Schinkel, A. F. L., Kruger, M., Poggesi, C., Ho, C. Y., Kuster, D. W. D., Michels, M., & van der Velden, J. (2018). Sex Differences at the Time of Myectomy in Hypertrophic

- Cardiomyopathy. *Circ Heart Fail*, 11(6), e004133. <https://doi.org/10.1161/CIRCHEARTFAILURE.117.004133>
- Nollet, E. E., Algül, S., Goebel, M., Schlossarek, S., van der Wel, N. N., Jans, J. J. M., van de Wiel, M. A., Knol, J. C., Pham, T. V., Piersma, S. R., de Goeij-de Haas, R., Hermans, J., van Klinken, J. B., van Weeghel, M., Houtkooper, R. H., Carrier, L., Jimenez, C. R., Kuster, D. W. D., & van der Velden, J. (2023). Western diet triggers cardiac dysfunction in heterozygous Mybpc3-targeted knock-in mice: A two-hit model of hypertrophic cardiomyopathy. *Journal of Molecular and Cellular Cardiology Plus*, 100050. <https://doi.org/10.1016/j.jmccpl.2023.100050>
- Norrander, J., Kempe, T., & Messing, J. (1983). Construction of improved M13 vectors using oligodeoxynucleotide-directed mutagenesis. *Gene*, 26(1), 101–106. [https://doi.org/10.1016/0378-1119\(83\)90040-9](https://doi.org/10.1016/0378-1119(83)90040-9)
- O’Leary, T. S., Snyder, J., Sadayappan, S., Day, S. M., & Previs, M. J. (2019). MYBPC3 truncation mutations enhance actomyosin contractile mechanics in human hypertrophic cardiomyopathy. *Journal of Molecular and Cellular Cardiology*, 127(December 2018), 165–173. <https://doi.org/10.1016/j.yjmcc.2018.12.003>
- Olivotto, I., Maron, B. J., Monteregeggi, A., Mazzuoli, F., Dolara, A., & Cecchi, F. (1999). Prognostic value of systemic blood pressure response during exercise in a community-based patient population with hypertrophic cardiomyopathy. *Journal of the American College of Cardiology*, 33(7), 2044–2051. [https://doi.org/10.1016/S0735-1097\(99\)00094-7](https://doi.org/10.1016/S0735-1097(99)00094-7)
- Olivotto, I., Maron, M. S., Adabag, A. S., Casey, S. A., Vargiu, D., Link, M. S., Udelson, J. E., Cecchi, F., & Maron, B. J. (2005). Gender-related differences in the clinical presentation and outcome of hypertrophic cardiomyopathy. *J Am Coll Cardiol*, 46(3), 480–487. <https://doi.org/10.1016/j.jacc.2005.04.043>
- Ran, F. A., Hsu, P. D., Wright, J., Agarwala, V., Scott, D. A., & Zhang, F. (2013). Genome engineering using the CRISPR-Cas9 system. *Nat Protoc*, 8(11), 2281–2308. <https://doi.org/10.1038/nprot.2013.143>
- Rees, H. A., & Liu, D. R. (2018). Base editing: precision chemistry on the genome and transcriptome of living cells. *Nat Rev Genet*, 19(12), 770–788. <https://doi.org/10.1038/s41576-018-0059-1>
- Rockman, H. A., Ross, R. S., Harris, A. N., Knowlton, K. U., Steinhilper, M. E., Field, L. J., Ross Jr., J., & Chien, K. R. (1991). Segregation of atrial-specific and inducible expression of an atrial natriuretic factor transgene in an in vivo murine model of cardiac hypertrophy. *Proc Natl Acad Sci U S A*, 88(18), 8277–8281. <https://doi.org/10.1073/pnas.88.18.8277>
- Sabater-Molina, M., Navarro-Penalver, M., Munoz-Esparza, C., Esteban-Gil, A., Santos-Mateo, J. J., & Gimeno, J. R. (2020). Genetic Factors Involved in Cardiomyopathies and in Cancer. *J Clin Med*, 9(6). <https://doi.org/10.3390/jcm9061702>
- Schmitt, J. P., Semsarian, C., Arad, M., Gannon, J., Ahmad, F., Duffy, C., Lee, R. T., Seidman, C. E., & Seidman, J. G. (2003). Consequences of pressure overload on sarcomere protein mutation-induced hypertrophic cardiomyopathy. *Circulation*, 108(9), 1133–1138. <https://doi.org/10.1161/01.CIR.0000086469.85750.48>
- Schuldt, M., Pei, J., Harakalova, M., Dorsch, L. M., Schlossarek, S., Mokry, M., Knol, J. C., Pham, T. V., Schelfhorst, T., Piersma, S. R., Dos Remedios, C., Dalinghaus, M., Michels, M., Asselbergs, F. W., Moutin, M. J., Carrier, L., Jimenez, C. R., Van Der Velden, J., & Kuster, D. W. D. (2021). Proteomic and functional studies reveal deetyrosinated tubulin as treatment target in sarcomere mutation-induced hypertrophic cardiomyopathy. *Circulation: Heart Failure*, January, 39–55. <https://doi.org/10.1161/CIRCHEARTFAILURE.120.007022>
- Seeger, T., Shrestha, R., Lam, C. K., Chen, C., McKeithan, W. L., Lau, E., Wnorowski, A., McMullen, G., Greenhaw, M., Lee, J., Oikonomopoulos, A., Lee, S., Yang, H., Mercola, M., Wheeler, M., Ashley, E. A., Yang, F., Karakikes, I., & Wu, J. C. (2019). A Premature Termination Codon Mutation in MYBPC3 Causes Hypertrophic Cardiomyopathy via

- Chronic Activation of Nonsense-Mediated Decay. *Circulation*, 139(6), 799–811. <https://doi.org/10.1161/CIRCULATIONAHA.118.034624>
- Semsarian, C., Ingles, J., Maron, M. S., & Maron, B. J. (2015). New Perspectives on the Prevalence of Hypertrophic Cardiomyopathy. *Journal of the American College of Cardiology*, 65(12), 1249–1254. <https://doi.org/10.1016/j.jacc.2015.01.019>
- Stauffer, B. L., Konhilas, J. P., Luczak, E. D., & Leinwand, L. A. (2006). Soy diet worsens heart disease in mice. *J Clin Invest*, 116(1), 209–216. <https://doi.org/10.1172/JCI24676>
- Stemmer, M., Thumberger, T., Del Sol Keyer, M., Wittbrodt, J., & Mateo, J. L. (2017). Correction: CCTop: An Intuitive, Flexible and Reliable CRISPR/Cas9 Target Prediction Tool. *PLoS One*, 12(4), e0176619. <https://doi.org/10.1371/journal.pone.0176619>
- The Jackson Laboratory. (n.d.). *Life span as a biomarker*. Retrieved 15 October 2023, from <https://www.jax.org/research-and-faculty/research-labs/the-harrison-lab/gerontology/life-span-as-a-biomarker>
- van Kampen, S. J., & van Rooij, E. (2019). CRISPR Craze to Transform Cardiac Biology. *Trends Mol Med*, 25(9), 791–802. <https://doi.org/10.1016/j.molmed.2019.06.008>
- Varnava, A. M., Elliott, P. M., Sharma, S., McKenna, W. J., & Davies, M. J. (2000). Hypertrophic cardiomyopathy: the interrelation of disarray, fibrosis, and small vessel disease. *Heart (British Cardiac Society)*, 84(5), 476–482. <https://doi.org/10.1136/HEART.84.5.476>
- Velicki, L., Jakovljevic, D. G., Preveden, A., Golubovic, M., Bjelobrk, M., Ilic, A., Stojisic, S., Barlocco, F., Tafelmeier, M., Okwose, N., Tesic, M., Brennan, P., Popovic, D., Ristic, A., MacGowan, G. A., Filipovic, N., Maier, L. S., & Olivotto, I. (2020). Genetic determinants of clinical phenotype in hypertrophic cardiomyopathy. *BMC Cardiovasc Disord*, 20(1), 516. <https://doi.org/10.1186/s12872-020-01807-4>
- Verma, A., Anavekar, N. S., Meris, A., Thune, J. J., Arnold, J. M., Ghali, J. K., Velazquez, E. J., McMurray, J. J., Pfeffer, M. A., & Solomon, S. D. (2007). The relationship between renal function and cardiac structure, function, and prognosis after myocardial infarction: the VALIANT Echo Study. *J Am Coll Cardiol*, 50(13), 1238–1245. <https://doi.org/10.1016/j.jacc.2007.06.018>
- Vignier, N., Schlossarek, S., Fraysse, B., Mearini, G., Krämer, E., Pointu, H., Mougnot, N., Guiard, J., Reimer, R., Hohenberg, H., Schwartz, K., Vernet, M., Eschenhagen, T., & Carrier, L. (2009). Nonsense-mediated mrna decay and ubiquitin-proteasome system regulate cardiac myosin-binding protein c mutant levels in cardiomyopathic mice. *Circulation Research*, 105(3), 239–248. <https://doi.org/10.1161/CIRCRESAHA.109.201251>
- Wang, Z., Li, L., Zhao, H., Peng, S., & Zuo, Z. (2015). Chronic high fat diet induces cardiac hypertrophy and fibrosis in mice. *Metabolism: Clinical and Experimental*, 64(8), 917–925. <https://doi.org/10.1016/j.metabol.2015.04.010>
- Weissler Snir, A., Connelly, K. A., Goodman, J. M., Dorian, D., & Dorian, P. (2021). Exercise in hypertrophic cardiomyopathy: restrict or rethink. *Am J Physiol Heart Circ Physiol*, 320(5), H2101–H2111. <https://doi.org/10.1152/ajpheart.00850.2020>
- Wessels, M. W., Herkert, J. C., Frohn-Mulder, I. M., Dalinghaus, M., van den Wijngaard, A., de Krijger, R. R., Michels, M., De Coo, I. F., Hoedemaekers, Y. M., & Dooijes, D. (2015). Compound heterozygous or homozygous truncating MYBPC3 mutations cause lethal cardiomyopathy with features of noncompaction and septal defects. *Eur J Hum Genet*, 23(7), 922–928. <https://doi.org/10.1038/ejhg.2014.211>
- Zamorano, J. L., Anastakis, A., Borger, M. A., Borggrefe, M., Cecchi, F., Charron, P., Hagege, A. A., Lafont, A., Limongelli, G., Mahrholdt, H., McKenna, W. J., Mogensen, J., Nihoyannopoulos, P., Nistri, S., Piepe, P. G., Pieske, B., Rapezzi, C., Rutten, F. H., Tillmanns, C., ... Watkins, H. (2014). 2014 ESC Guidelines on diagnosis and management of hypertrophic cardiomyopathy: the Task Force for the Diagnosis and Management of Hypertrophic Cardiomyopathy of the European Society of Cardiology (ESC). *Eur Heart J*, 35(39), 2733–2779. <https://doi.org/10.1093/eurheartj/ehu284>

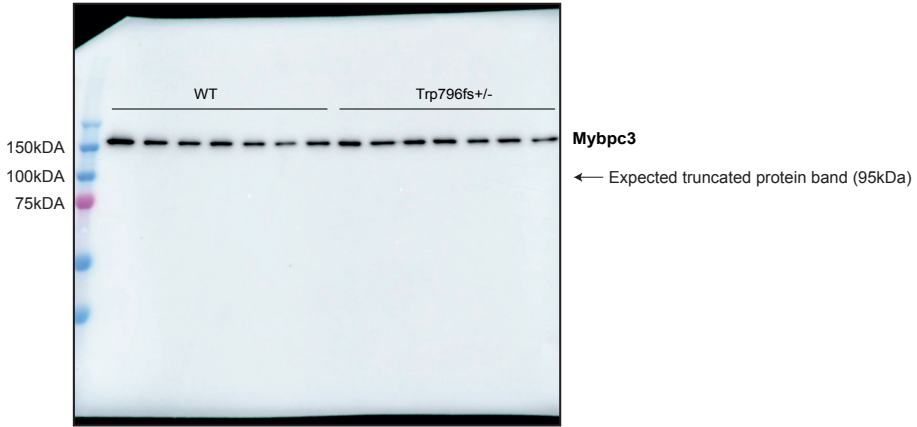
Zhou, Q., Kesteven, S., Wu, J., Aidery, P., Gawaz, M., Gramlich, M., Feneley, M. P., & Harvey, R. P. (2015). Pressure Overload by Transverse Aortic Constriction Induces Maladaptive Hypertrophy in a Titin-Truncated Mouse Model. *Biomed Res Int*, 2015, 163564. <https://doi.org/10.1155/2015/163564>

Supplemental material

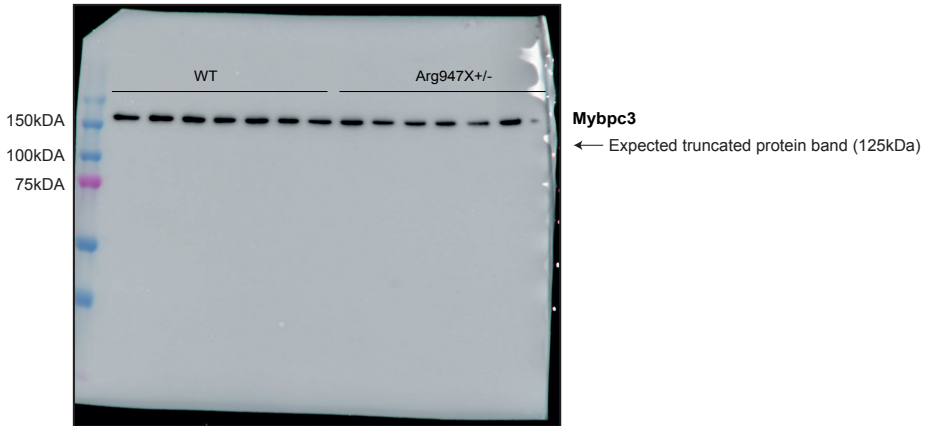


Supplemental Figure 1. Generation of MYBPC3 knock-in mouse models to study hypertrophic cardiomyopathy. (A) Genomic sequences of MYBPC3 human and mouse showing conservation of the region containing the c.2373dupG/p.Trp792fs mutation (B) Representative agarose gel displaying the genotyping strategy used. (C) Representative karyotype image showing a cell containing 40 chromosomes. (D) Genomic DNA sequences of the top 3 predicted off-target sites of the gRNA used for gene editing. (E) Genomic sequences of MYBPC3 human and mouse showing conservation of the region containing the c.2827C>T/p.Arg943X mutation (F) Representative agarose gel displaying the genotyping strategy used. (G) Representative karyotype image showing a cell containing 40 chromosomes. (H) Genomic DNA sequences of the top 3 predicted off-target sites of the gRNA used for gene editing.

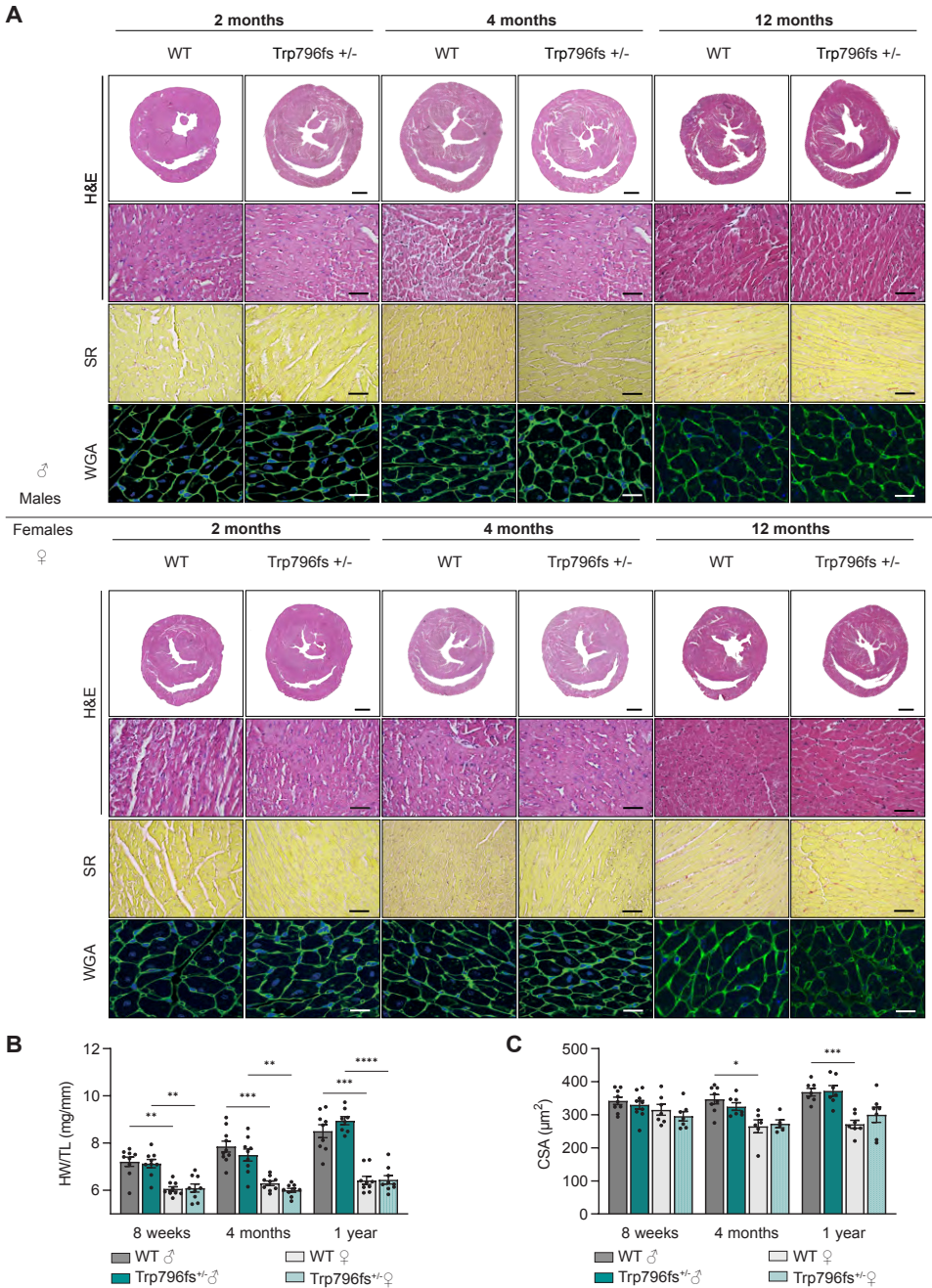
A



B

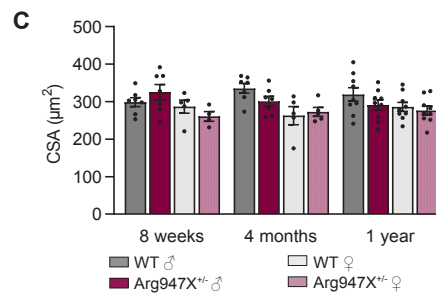
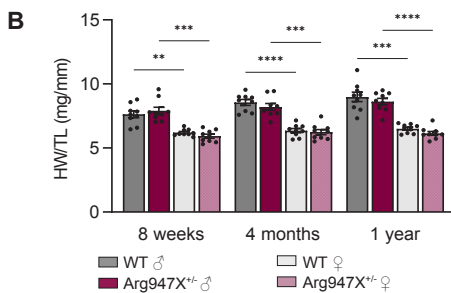
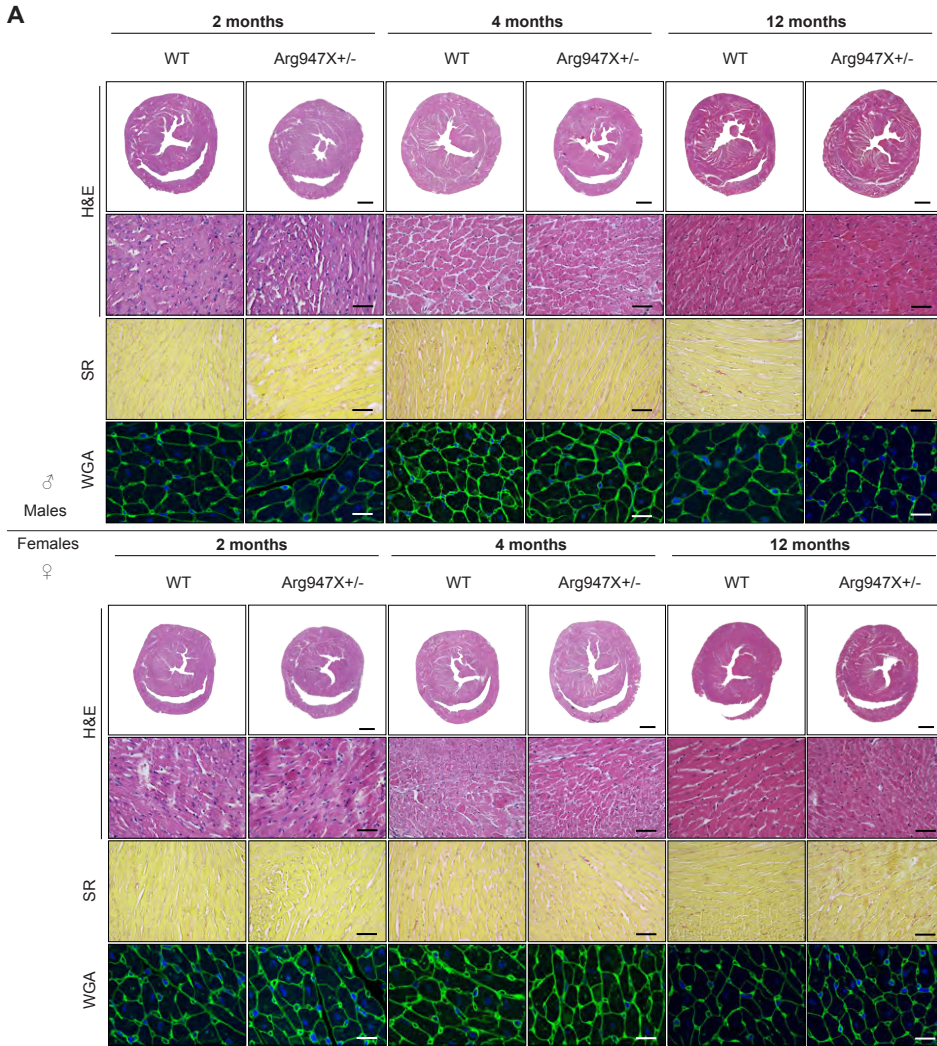


Supplemental Figure 2. Western blots for MYBPC3 in WT and HET. (A) Representative western blot for MYBPC3 (150kDa) and expected truncated protein (95kDa) in WT and Trp796fs+/- . **(B)** Representative western blot for MYBPC3 (150kDa) and expected truncated protein (125kDa) in WT and Arg947X+/- .



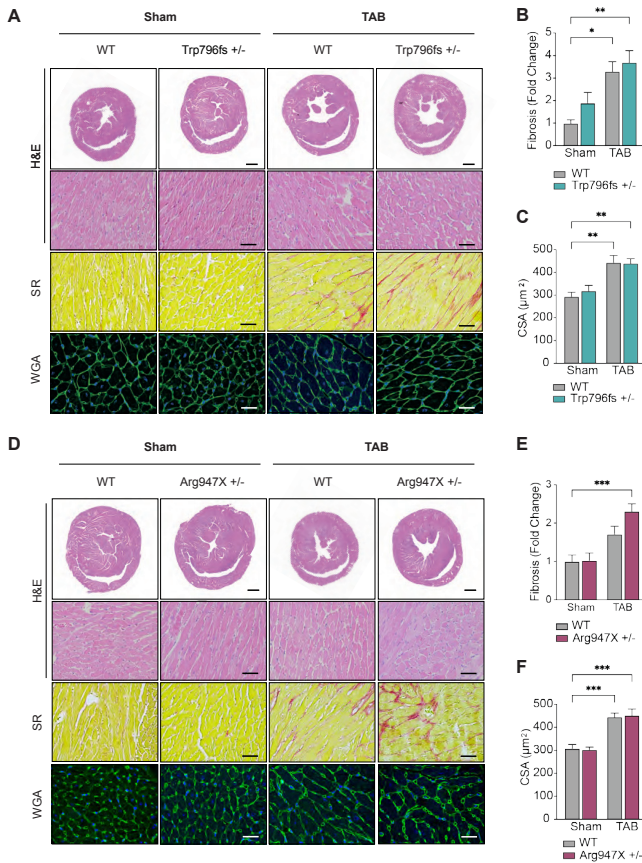
Supplemental Figure 3. Morphological features of male and female WT and Trp796fs^{+/-} mice. (A) Representative H&E staining on heart sections from 2-, 4- and 12-month-old male WT and Trp796fs^{+/-} mice (top panel, scale 1 mm). Representative H&E, SR and WGA staining on heart sections from female WT and Trp796fs^{+/-} mice (lower panels, scale 50 µm). B, HW/TL

(mg/mm) in male WT and Trp796fs+/- mice. **(B)** HW/TL (mg/mm) in male and female WT and Trp796fs+/- mice. **(C)** CSA (μm^2) in male WT and Trp796fs+/- mice. Expression data plotted as mean \pm SEM (n = 7-9 per group). CSA (μm^2) was measured in 50 cells/mouse. Significance was assessed by a 2-way ANOVA (* = p-value < 0,0332; ** = p-value < 0,0021; *** = p-value < 0,0002; **** = p-value < 0.0001).

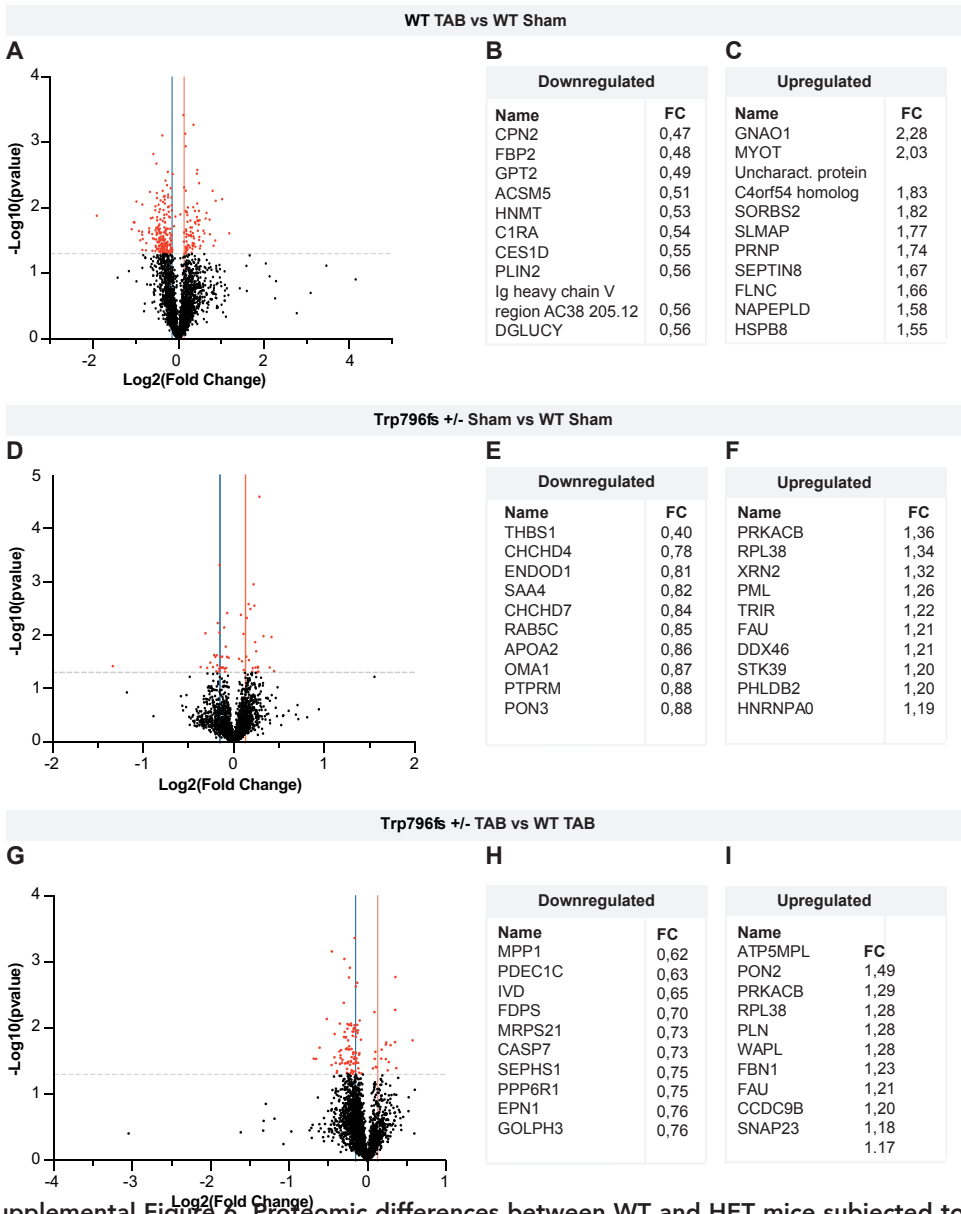


Supplemental Figure 4. Morphological features of male and female WT and Arg947X^{+/-} mice. (A) Representative H&E staining on heart sections from 2-, 4- and 12-month-old male WT and Arg947X^{+/-} mice (top panel, scale 1 mm). Representative H&E, SR and WGA staining on heart sections from female WT and Trp796fs^{+/-} mice (lower panels, scale 50 µm). B, HW/TL

(mg/mm) in male WT and Arg947X^{+/-} mice. **(B)** HW/TL (mg/mm) in male and female WT and Arg947X^{+/-} mice. **(C)** CSA (μm^2) in male WT and Arg947X^{+/-} mice. Expression data plotted as mean \pm SEM (n = 7-9 per group). CSA (μm^2) was measured in 50 cells/mouse. Significance was assessed by a 2-way ANOVA (* = p-value < 0,0332; ** = p-value < 0,0021; *** = p-value < 0,0002; **** = p-value < 0.0001).



Supplemental Figure 5. Morphological features of WT and HET mice subjected to Sham or TAB-induced stress. (A) Representative H&E staining on heart sections from Sham and TAB WT and Trp796fs +/- mice (top panel, scale 1 mm). Representative H&E, SR and WGA staining on heart sections from Sham and TAB WT and Trp796fs +/- mice (lower panels, scale 50 μm). (B) Fibrosis quantification in Sham and TAB WT and Trp796fs +/- mice. (C) CSA (μm²) in Sham and TAB WT and Trp796fs +/- mice. (D) Representative H&E staining on heart sections from Sham and TAB WT and Arg947X +/- mice (top panel, scale 1 mm). Representative H&E, SR and WGA staining on heart sections from Sham and TAB WT and Arg947X +/- mice (lower panels, scale 50 μm). (E) Fibrosis quantification in Sham and TAB WT and Arg947X +/- mice. (F) CSA (μm²) in Sham and TAB WT and Arg947X +/- mice. Expression data plotted as mean ± SEM (n = 7-9 per group). CSA (μm²) was measured in 50 cells/mouse. Significance was assessed by a 2-way ANOVA (* = p-value < 0,0332; ** = p-value < 0,0021; *** = p-value < 0,0002; **** = p-value < 0.0001).



Supplemental Figure 8. Proteomic differences between WT and HET mice subjected to Sham or TAB-induced stress. (A) Volcano plot displaying proteomic changes between WT TAB and Trp796fs+/- TAB mice. Red dots depict proteins with a log₂FoldChange < -0,4 and > 0,4. **(B)** Top 10 downregulated proteins. **(C)** Top 10 upregulated proteins. **(D)** Volcano plot displaying proteomic changes between Trp796fs+/- Sham and WT Sham mice. Red dots depict proteins with a log₂FoldChange < -0,4 and > 0,4. **(E)** Top 10 downregulated proteins. **(F)** Top 10 upregulated proteins. **(G)** Volcano plot displaying proteomic changes between Trp796fs+/- TAB and WT TAB mice. Red dots depict proteins with a log₂FoldChange < -0,4 and > 0,4. **(H)** Top 10 downregulated proteins. **(I)** Top 10 upregulated proteins.

Supplemental Table 1. Morphological and echocardiographical parameters of WT and Trp796fs+/-

| Morphological parameters | | | | | | | |
|--------------------------|---------|---------------|---------------|----------------|---------------|---------------|---------------|
| Parameter | Sex | 2 months | | 4 months | | 12 months | |
| | | WT | Trp796fs +/- | WT | Trp796fs +/- | WT | Trp796fs +/- |
| BW (g) | Males | 26,18 ± 0,68 | 26,5 ± 0,65 | 31,89 ± 0,96§ | 29,20 ± 0,61 | 33,93 ± 0,92 | 35,80 ± 0,77 |
| | Females | 20,9 ± 0,40 | 20,59 ± 0,59 | 23,38 ± 0,38* | 23,48 ± 0,55* | 24,98 ± 0,40 | 25,72 ± 0,73 |
| HW (mg) | Males | 119,87 ± 3,34 | 118,99 ± 3,28 | 139,54 ± 4,09* | 133,11 ± 4,47 | 154,78 ± 5,51 | 163,40 ± 3,38 |
| | Females | 98,74 ± 2,17 | 100,34 ± 2,70 | 107,92 ± 1,78 | 102,30 ± 1,28 | 116,56 ± 3,28 | 115,67 ± 3,20 |
| HW/TL (mg/mm) | Males | 7,38 ± 0,11 | 7,13 ± 0,17 | 7,85 ± 0,25 | 7,5 ± 0,25 | 8,5 ± 0,28* | 9,03 ± 0,17 |
| | Females | 6,06 ± 0,10 | 6,10 ± 0,17 | 6,29 ± 0,10 | 6,00 ± 0,08 | 6,42 ± 0,17 | 6,44 ± 0,17 |
| LwW/TL (mg/mm) | Males | 87,13 ± 3,99 | 90,92 ± 3,07 | 86,30 ± 3,30 | 74,48 ± 2,98 | 91,41 ± 2,51 | 96,50 ± 2,32 |
| | Females | 75,94 ± 6,19 | 65,43 ± 3,43 | 65,95 ± 2,00 | 63,92 ± 1,54 | 66,56 ± 1,05 | 62,13 ± 1,42 |
| LuW/TL (mg/mm) | Males | 9,01 ± 0,09 | 8,41 ± 0,36 | 9,36 ± 0,28 | 8,36 ± 0,56 | 9,20 ± 0,23 | 8,87 ± 0,21 |
| | Females | 8,41 ± 0,22 | 8,47 ± 0,17 | 8,81 ± 0,12 | 8,23 ± 0,43 | 8,30 ± 0,14 | 8,32 ± 0,11 |
| KiW/TL (mg/mm) | Males | 10,85 ± 0,43 | 10,15 ± 0,32 | 11,48 ± 0,45 | 10,29 ± 0,42 | 14,14 ± 0,53 | 14,05 ± 0,24 |
| | Females | 8,45 ± 0,37 | 8,12 ± 0,22 | 8,59 ± 0,20 | 8,02 ± 0,14 | 9,19 ± 0,16 | 9,04 ± 0,33 |

| Echocardiographical parameters | | | | | | | |
|--------------------------------|---------|----------------|----------------|----------------|----------------|----------------|----------------|
| Parameter | Sex | 2 months | | 4 months | | 12 months | |
| | | WT | Trp796fs +/- | WT | Trp796fs +/- | WT | Trp796fs +/- |
| EF (%) | Males | 38,61 ± 4,28 | 45,20 ± 4,33 | 40,69 ± 2,21 | 39,82 ± 3,08 | 50,39 ± 1,92 | 45,92 ± 3,34 |
| | Females | 37,93 ± 2,03 | 38,04 ± 2,67 | 41,64 ± 2,64 | 46,91 ± 4,38 | 54,32 ± 3,98 | 54,53 ± 3,54 |
| IVSd (mm) | Males | 0,82 ± 0,05 | 0,97 ± 0,07 | 0,92 ± 0,04 | 0,84 ± 0,03 | 1,02 ± 0,03 | 0,99 ± 0,03 |
| | Females | 0,74 ± 0,03 | 0,84 ± 0,02 | 0,89 ± 0,08 | 0,96 ± 0,05 | 0,87 ± 0,04 | 0,90 ± 0,02 |
| IVSs (mm) | Males | 1,10 ± 0,05 | 1,31 ± 0,11 | 1,19 ± 0,04 | 1,11 ± 0,03 | 1,43 ± 0,04 | 1,35 ± 0,03 |
| | Females | 1,00 ± 0,06 | 1,14 ± 0,04 | 1,20 ± 0,08 | 1,31 ± 0,13 | 1,27 ± 0,06 | 1,35 ± 0,04 |
| LVPWd (mm) | Males | 0,67 ± 0,04 | 0,84 ± 0,08 | 0,69 ± 0,07 | 0,75 ± 0,07 | 0,89 ± 0,06 | 0,85 ± 0,06 |
| | Females | 0,78 ± 0,06 | 0,79 ± 0,07 | 0,63 ± 0,04 | 0,70 ± 0,05 | 0,84 ± 0,05 | 0,64 ± 0,03 |
| LVPWs (mm) | Males | 0,86 ± 0,05 | 1,02 ± 0,10 | 0,90 ± 0,07 | 1,00 ± 0,08 | 1,10 ± 0,07 | 1,11 ± 0,09 |
| | Females | 0,95 ± 0,07 | 0,91 ± 0,08 | 0,77 ± 0,05 | 0,98 ± 0,05 | 1,06 ± 0,06 | 0,88 ± 0,03 |
| LVIDd (mm) | Males | 4,15 ± 0,11 | 4,01 ± 0,06 | 4,23 ± 0,04 | 4,13 ± 0,05 | 4,15 ± 0,11 | 4,22 ± 0,06 |
| | Females | 4,07 ± 0,06 | 4,09 ± 0,03 | 4,03 ± 0,08 | 3,64 ± 0,11* | 3,74 ± 0,12 | 3,84 ± 0,10 |
| LVIDs (mm) | Males | 3,38 ± 0,16 | 3,11 ± 0,14 | 3,44 ± 0,09 | 3,33 ± 0,05 | 2,99 ± 0,15 | 3,26 ± 0,10 |
| | Females | 3,25 ± 0,11 | 3,34 ± 0,07 | 3,32 ± 0,11 | 2,80 ± 0,17 | 2,70 ± 0,16 | 2,77 ± 0,14 |
| Heart rate (bpm) | Males | 394,44 ± 8,83 | 418,36 ± 11,05 | 432,16 ± 20,07 | 437,38 ± 14,69 | 474,65 ± 11,32 | 480,53 ± 10,20 |
| | Females | 378,62 ± 12,01 | 412,51 ± 8,18 | 397,20 ± 10,29 | 401,46 ± 10,09 | 520,08 ± 12,58 | 516,35 ± 22,87 |
| IVRT (ms) | Males | 22,21 ± 0,85 | 19,62 ± 0,33 | 17,18 ± 1,62 | 16,66 ± 1,56 | 17,44 ± 1,04 | 17,68 ± 0,50 |
| | Females | 21,19 ± 0,45 | 20,93 ± 0,52 | 17,47 ± 0,72 | 17,55 ± 0,98 | 16,83 ± 0,36 | 16,61 ± 0,72 |

BW; Body weight, HW; Heart weight, TL; Tibia length, EF; Ejection fraction, IVSd; Intraventricular septum diastole, IVSs; Intraventricular septum systole, LVPWd; Left ventricle posterior wall diastole, LVPWs; Left ventricle posterior wall systole, LVIDd; Left ventricle interior diameter diastole, LVIDs; Left ventricle interior diameter systole, IVRT; Isovolumic relaxation time, bpm; Beats per minute, * = p-val<0,03 vs corresponding WT; ** = p-val<0,002 vs corresponding WT; *** = p-val<0,0002 vs corresponding WT; **** = p-val<0,0001 vs corresponding WT.

Supplemental Table 2. Morphological and echocardiographical parameters of WT and Arg947X+/- mice

| Morphological parameters | | | | | | | |
|--------------------------|---------|---------------|---------------|---------------|---------------|---------------|---------------|
| Parameter | Sex | 2 months | | 4 months | | 12 months | |
| | | WT | Arg947X +/- | WT | Arg947X +/- | WT | Arg947X +/- |
| BW (g) | Males | 25,42 ± 0,64 | 26,74 ± 0,42 | 30,6 ± 0,95 | 30,54 ± 0,99 | 34,8 ± 0,89 | 34,62 ± 1,50 |
| | Females | 20,77 ± 0,78 | 20,48 ± 0,46 | 23,97 ± 0,64 | 23,90 ± 0,79 | 26,60 ± 0,89 | 27,19 ± 0,64 |
| HW (mg) | Males | 127,57 ± 4,65 | 132,82 ± 4,89 | 147,44 ± 4,39 | 143,07 ± 5,91 | 164,46 ± 7,46 | 154,98 ± 5,33 |
| | Females | 101,70 ± 1,66 | 96,16 ± 2,73 | 108,79 ± 2,93 | 107,89 ± 4,03 | 118,47 ± 2,57 | 111,78 ± 3,18 |
| HW/TL (mg/mm) | Males | 7,63 ± 0,26 | 7,90 ± 0,29 | 8,56 ± 0,23 | 8,21 ± 0,26 | 8,99 ± 0,37* | 8,63 ± 0,25 |
| | Females | 6,20 ± 0,09 | 5,92 ± 0,16 | 6,35 ± 0,16 | 6,24 ± 0,20 | 6,51 ± 0,12 | 6,15 ± 0,15 |
| LwW/TL (mg/mm) | Males | 82,15 ± 2,73 | 83,06 ± 3,26 | 90,73 ± 3,58 | 85,71 ± 2,69 | 88,53 ± 5,58 | 90,72 ± 4,12 |
| | Females | 63,02 ± 3,28 | 61,88 ± 2,42 | 66,11 ± 2,59 | 66,34 ± 4,16 | 68,17 ± 2,00 | 67,14 ± 1,77 |
| LuW/TL (mg/mm) | Males | 8,88 ± 0,26 | 9,06 ± 0,19 | 9,10 ± 0,20 | 8,95 ± 0,28 | 8,82 ± 0,45 | 9,44 ± 0,27 |
| | Females | 8,52 ± 0,19 | 8,41 ± 0,23 | 8,41 ± 0,21 | 8,28 ± 0,28 | 8,44 ± 0,38 | 8,07 ± 0,15 |
| KiW/TL (mg/mm) | Males | 10,6 ± 0,23 | 10,52 ± 0,47 | 11,25 ± 0,42 | 10,99 ± 0,46 | 13,79 ± 1,13 | 13,30 ± 0,64 |
| | Females | 8,30 ± 0,11 | 7,77 ± 0,20 | 8,47 ± 0,23 | 7,69 ± 0,17 | 9,16 ± 0,30 | 8,55 ± 0,29 |

| Echocardiographical parameters | | | | | | | |
|--------------------------------|---------|----------------|----------------|----------------|----------------|----------------|----------------|
| Parameter | Sex | 2 months | | 4 months | | 12 months | |
| | | WT | Arg947X +/- | WT | Arg947X +/- | WT | Arg947X +/- |
| EF (%) | Males | 36,81 ± 3,66 | 39,85 ± 4,37 | 46,75 ± 2,66 | 42,32 ± 2,67 | 46,08 ± 2,84 | 47,38 ± 2,67 |
| | Females | 40,76 ± 4,47 | 47,61 ± 2,81 | 43,74 ± 3,24 | 44,26 ± 3,02 | 50,22 ± 3,03 | 48,31 ± 2,63 |
| IVSd (mm) | Males | 0,82 ± 0,05 | 0,93 ± 0,04 | 1,10 ± 0,06 | 0,99 ± 0,07 | 0,94 ± 0,04 | 0,99 ± 0,05 |
| | Females | 0,77 ± 0,05 | 0,82 ± 0,06 | 0,89 ± 0,11 | 0,78 ± 0,05 | 0,90 ± 0,05 | 0,89 ± 0,02 |
| IVSs (mm) | Males | 1,11 ± 0,06 | 1,25 ± 0,05 | 1,38 ± 0,07 | 1,25 ± 0,09 | 1,29 ± 0,04 | 1,25 ± 0,08 |
| | Females | 1,13 ± 0,07 | 1,14 ± 0,07 | 1,22 ± 0,11 | 1,05 ± 0,07 | 1,28 ± 0,04 | 1,20 ± 0,03 |
| LVPWd (mm) | Males | 0,66 ± 0,04 | 0,70 ± 0,06 | 0,76 ± 0,02 | 0,84 ± 0,06 | 0,76 ± 0,07 | 0,87 ± 0,06 |
| | Females | 0,64 ± 0,06 | 0,56 ± 0,04 | 0,61 ± 0,05 | 0,62 ± 0,04 | 0,79 ± 0,06 | 0,80 ± 0,05 |
| LVPWs (mm) | Males | 0,70 ± 0,06 | 0,85 ± 0,08 | 1,04 ± 0,05 | 1,02 ± 0,07 | 0,87 ± 0,05 | 1,16 ± 0,08 |
| | Females | 0,73 ± 0,05 | 0,76 ± 0,04 | 0,75 ± 0,04 | 0,81 ± 0,10 | 0,98 ± 0,07 | 1,06 ± 0,07 |
| LVIDd (mm) | Males | 4,20 ± 0,08 | 4,13 ± 0,08 | 4,20 ± 0,08 | 4,24 ± 0,12 | 4,45 ± 0,14 | 4,09 ± 0,10 |
| | Females | 3,88 ± 0,05 | 3,78 ± 0,07 | 4,03 ± 0,10 | 3,97 ± 0,07 | 3,87 ± 0,05 | 3,74 ± 0,06 |
| LVIDs (mm) | Males | 3,46 ± 0,13 | 3,32 ± 0,13 | 3,23 ± 0,12 | 3,37 ± 0,15 | 3,30 ± 0,10 | 3,12 ± 0,11 |
| | Females | 3,12 ± 0,014 | 2,89 ± 0,10 | 3,16 ± 0,13 | 3,11 ± 0,12 | 2,89 ± 0,10 | 2,84 ± 0,08 |
| Heart rate (bpm) | Males | 404,04 ± 11,50 | 395,04 ± 18,10 | 493,81 ± 9,16 | 482,49 ± 15,30 | 462,06 ± 11,73 | 490,01 ± 14,92 |
| | Females | 450,39 ± 12,72 | 543,53 ± 14,64 | 450,39 ± 12,72 | 452,53 ± 14,64 | 496,13 ± 7,43 | 477,29 ± 17,44 |
| IVRT (ms) | Males | 16,12 ± 0,53 | 17,89 ± 1,43 | 12,11 ± 0,45 | 11,79 ± 0,74 | 17,29 ± 0,63 | 16,82 ± 0,84 |
| | Females | 17,05 ± 1,17 | 16,36 ± 0,87 | 13,85 ± 0,65 | 13,91 ± 0,59 | 16,93 ± 0,64 | 18,77 ± 0,60 |

BW; Body weight, HW; Heart weight, TL; Tibia length, LwW; Liver weight, LuW; Lung weight, KiW; Kidney weight, EF; Ejection fraction, IVSd; Intraventricular septum diastole, IVSs; Intraventricular septum systole, LVPWd; Left ventricle posterior wall diastole, LVPWs; Left ventricle posterior wall systole, LVIDd; Left ventricle interior diameter diastole, LVIDs; Left ventricle interior diameter systole, IVRT; Isovolumic relaxation time, bpm; Beats per minute.

Supplemental Table 3. Morphological and echocardiographical parameters of WT and Trp796fs+/- Sham and TAB mice and Arg947X+/- Sham and TAB mice

| Morphological parameters | | | | | | | | |
|--------------------------|---------------|---------------|-------------------|-------------------|---------------|---------------|------------------|------------------|
| Parameter | Sham | | TAB | | Sham | | TAB | |
| | WT | Trp796fs +/- | WT | Trp796fs +/- | WT | Arg947X +/- | WT | Arg947X +/- |
| BW (g) | 26,30 ± 0,79 | 28,13 ± 0,48 | 28,74 ± 0,44* | 28,49 ± 0,51 | 29,22 ± 0,99 | 29,88 ± 1,01 | 28,66 ± 0,61 | 29,78 ± 0,58 |
| HW (mg) | 128,86 ± 7,81 | 134,90 ± 8,24 | 198,17 ± 10,00*** | 198,07 ± 11,41*** | 139,19 ± 4,85 | 143,43 ± 5,90 | 200,32 ± 9,40*** | 215,20 ± 9,02*** |
| HW/TL (mg/mm) | 7,41 ± 0,37 | 7,87 ± 0,45 | 11,47 ± 0,56*** | 11,32 ± 0,69*** | 7,92 ± 0,24 | 8,21 ± 0,33 | 11,50 ± 0,53*** | 12,21 ± 0,49*** |
| LvW/TL (mg/mm) | 81,93 ± 6,20 | 83,52 ± 4,59 | 84,67 ± 2,91 | 76,98 ± 2,64 | 84,69 ± 4,10 | 92,25 ± 4,78 | 82,71 ± 2,17 | 90,30 ± 3,45 |
| LuW/TL (mg/mm) | 8,31 ± 0,30 | 8,82 ± 0,21 | 11,06 ± 1,22 | 10,83 ± 1,09 | 9,61 ± 0,38 | 9,71 ± 0,34 | 12,54 ± 1,57 | 11,17 ± 0,72 |
| KiW/TL (mg/mm) | 10,23 ± 0,48 | 10,70 ± 0,37 | 10,61 ± 0,41 | 9,87 ± 0,31 | 11,33 ± 0,53 | 11,40 ± 0,52 | 10,04 ± 0,27 | 10,72 ± 0,26 |

| Echocardiographical parameters | | | | | | | | |
|--------------------------------|----------------|----------------|----------------|----------------|----------------|----------------|----------------|----------------|
| Parameter | Sham | | TAB | | Sham | | TAB | |
| | WT | Trp796fs +/- | WT | Trp796fs +/- | WT | Arg947X +/- | WT | Arg947X +/- |
| EF (%) | 41,245 ± 2,96 | 45,61 ± 3,13 | 39,40 ± 3,06 | 45,04 ± 3,76 | 42,52 ± 2,07 | 42,76 ± 4,34 | 40,03 ± 3,13 | 40,62 ± 2,66 |
| IVSd (mm) | 0,93 ± 0,07 | 0,91 ± 0,05 | 1,11 ± 0,06 | 1,12 ± 0,06 | 0,92 ± 0,06 | 0,88 ± 0,04 | 1,16 ± 0,06 | 1,17 ± 0,07 |
| IVSs (mm) | 1,25 ± 0,07 | 1,22 ± 0,02 | 1,42 ± 0,05* | 1,49 ± 0,05 | 1,24 ± 0,06 | 1,24 ± 0,08 | 1,50 ± 0,07 | 1,51 ± 0,07 |
| LVPWd (mm) | 0,74 ± 0,08 | 0,78 ± 0,09 | 0,82 ± 0,09 | 0,98 ± 0,07 | 0,65 ± 0,04 | 0,75 ± 0,03 | 0,89 ± 0,06 | 0,98 ± 0,09* |
| LVPWs (mm) | 0,94 ± 0,11 | 1,03 ± 0,12 | 1,06 ± 0,09 | 1,21 ± 0,08 | 0,80 ± 0,05 | 0,93 ± 0,06 | 1,11 ± 0,08 | 1,16 ± 0,11 |
| LVIDd (mm) | 4,22 ± 0,08 | 4,02 ± 0,08 | 4,40 ± 0,08 | 4,06 ± 0,11 | 4,40 ± 0,04 | 4,22 ± 0,09 | 4,25 ± 0,07 | 4,15 ± 0,07 |
| LVIDs (mm) | 3,38 ± 0,10 | 3,11 ± 0,11 | 3,56 ± 0,10 | 3,17 ± 0,14 | 3,48 ± 0,06 | 3,33 ± 0,16 | 3,42 ± 0,09 | 3,35 ± 0,10 |
| Heart rate (bpm) | 408,41 ± 25,89 | 420,89 ± 28,28 | 437,83 ± 24,02 | 433,72 ± 15,05 | 390,71 ± 16,42 | 418,18 ± 22,15 | 412,48 ± 16,77 | 411,69 ± 14,76 |

BW; Body weight, HW; Heart weight, TL; Tibia length, LvW; Liver weight, LuW; Lung weight, KiW; Kidney weight, EF; Ejection fraction, IVSd; Intraventricular septum diastole, IVSs; Intraventricular septum systole, LVPWd; Left ventricle posterior wall diastole, LVPWs; Left ventricle posterior wall systole, LVIDd; Left ventricle interior diameter diastole, LVIDs; Left ventricle interior diameter systole, bpm; Beats per minute, * = p-val<0,03 vs Sham WT; *** = p-val<0,0002 vs Sham WT;

Supplemental Table 4. Morphological and echocardiographical parameters of Trp796fs+/+ and Arg947X+/+ mice compared to their WT littermates

| Morphological parameters | | | | |
|---------------------------------|-----------------|---------------------|-----------------|--------------------|
| Parameter | 2 months | | 2 months | |
| | WT | Trp796fs +/+ | WT | Arg947X +/+ |
| BW (g) males | 22,33 ± 1,38 | 22,63 ± 1,11 | 20,47 ± 0,25 | 23,07 ± 0,60** |
| BW (g) females | 18,27 ± 0,29 | 17,33 ± 0,31* | 16,63 ± 1,01 | 18,30 ± 0,45 |
| HW (mg) males | 136,8 ± 20,9 | 233,2 ± 10,2** | 120,4 ± 14,7 | 251,7 ± 17,2** |
| HW (mg) females | 115,6 ± 9,2 | 186,7 ± 6,2*** | 107,8 ± 20,7 | 199,1 ± 11,1** |
| HW/TL (mg/mm) | 82 ± 12 | 13,6 ± 1,5**** | 74 ± 12 | 147 ± 17**** |
| LvW/TL (mg/mm) | 64,8 ± 10,7 | 70,3 ± 7,3 | 65,3 ± 8,0 | 73,6 ± 9,3 |
| LuW/TL (mg/mm) | 9,6 ± 0,6 | 8,9 ± 0,4* | 9,7 ± 0,9 | 9,0 ± 0,9 |
| KiW/TL (mg/mm) | 18,2 ± 2,6 | 14,8 ± 1,8* | 16,8 ± 4,0 | 15,4 ± 2,6 |
| Parameter | | | | |
| EF (%) | 43,36 ± 7,94 | 19,68 ± 2,44**** | 47,57 ± 6,69 | 20,58 ± 3,17**** |
| IVSd (mm) | 0,71 ± 0,07 | 1,03 ± 0,10*** | 0,66 ± 0,04 | 1,21 ± 0,17**** |
| IVSs (mm) | 0,93 ± 0,11 | 1,15 ± 0,10** | 0,95 ± 0,04 | 4,68 ± 0,33**** |
| LVPWd (mm) | 0,76 ± 0,08 | 1,17 ± 0,07**** | 0,76 ± 0,08 | 1,31 ± 0,09**** |
| LVPWs (mm) | 0,98 ± 0,11 | 1,33 ± 0,12*** | 0,94 ± 0,12 | 1,46 ± 0,06**** |
| LVIDd (mm) | 3,93 ± 0,31 | 4,90 ± 0,08**** | 3,80 ± 0,31 | 4,68 ± 0,336** |
| LVIDs (mm) | 3,10 ± 0,30 | 4,46 ± 0,10**** | 2,91 ± 0,31 | 4,25 ± 0,33**** |

BW; Body weight, HW; Heart weight, TL; Tibia length, EF; Ejection fraction, IVSd; Intraventricular septum diastole, IVSs; Intraventricular septum systole, LVPWd; Left ventricle posterior wall diastole, LVPWs; Left ventricle posterior wall systole, LVIDd; Left ventricle interior diameter diastole, LVIDs; Left ventricle interior diameter systole, Tested for significance with an Unpaired t-test; WT vs. HOM mutant: * = p-val<0,05, ** = p-val<0,01, *** = p-val<0,001, **** = p-val<0,0001



Hypertrophic cardiomyopathy (HCM) is the most common genetic heart disease, characterized by a thickening of the myocardial wall in the absence of any other loading condition on the heart (Marian & Braunwald, 2017; Semsarian et al., 2015). Mutation carriers may develop life-threatening arrhythmias, or pathological remodeling which can eventually progress to heart failure (Marian & Braunwald, 2017). The broad clinical presentation and high variability in disease penetrance make it complicated to predict onset and development.

In this thesis, our objective was to dive deeper into the molecular mechanisms underpinning this pathological condition. Enhancing our understanding of the altered pathways in HCM holds significance for the prospect of discovering therapeutic interventions, as well as identifying (hematological) serum markers for the early detection and prevention of the disease.

We hypothesized to find heterogeneity among cardiomyocytes (CMs), distinguishing cells with varying degrees of pathology or hypertrophy. Single cell RNA sequencing (scRNA-seq) was used in **Chapter 2** to elucidate the molecular landscape of individual cells, enabling comprehensive examination of the cellular diversity within the HCM tissue. We next studied gene expression patterns in the HCM-intraventricular septum (IVS) and in the left ventricular free wall (LVFW) to get a better understanding of the susceptibility of the IVS in becoming hypertrophic in patients with HCM (**Chapter 3**). Lastly, we developed a mouse model of HCM by knocking in two different well-known disease-causing mutations in *Mybpc3* (**Chapter 4**). Our findings and conclusions are discussed below.

Unravelling molecular mechanisms driving HCM using scRNA-seq

Hypertrophy can be located anywhere in the left ventricle, but the IVS is affected in almost all cases (Canepa et al., 2016). Therefore, patients with severe HCM (IVS >15mm) will often go for septal reduction therapy, by alcohol ablation or by myectomy surgery. To the best of our knowledge, we were the first to perform scRNA-seq on freshly isolated CMs from HCM-myectomy tissue (**Chapter 2**). By doing so, we aimed to find more hypertrophied or stressed CMs, and link their transcriptional program

to relevant molecular pathways in HCM.

ScRNA-seq has been used to detect differences in gene expression between cell types, heterogeneity in cells from the same cell type, or for the discovery of new cell types (Grun et al., 2015; Kolodziejczyk et al., 2015). Our lab and others have been able to perform scRNA-seq on the adult mammalian heart (Cui et al., 2019; Farbehi et al., 2019; Gladka et al., 2018; Kretzschmar et al., 2018; Nomura et al., 2018; Wang et al., 2020). In this Chapter, we chose to specifically focus on CMs as their heterogeneity has been suggested as a trigger for HCM hallmarks (Kraft & Montag, 2019; Montag et al., 2018; Parbhudayal et al., 2018). We compared HCM CMs to healthy CMs extracted from available databases (Litviňuková et al., 2020; Wang et al., 2020) and confirmed the pathological state of our CMs by verification of upregulated stress genes (*NPPA*, *NPPB*, *ACTA1*, and *MYH7*).

Next, we aimed to identify common subpopulations of CMs in HCM samples. Variation between patients might be a risk in identification of CM subpopulations, as you might be biased by patient-specific traits (sex/age/mutation status). In this study, we collected 5 different samples for scRNA-seq (3 males and 2 females), of which two patients were identified mutation carriers (**Supplemental Table 1, Chapter 2**). The CMs from all patients were pooled, and by looking at gene-gene correlations in this heterogeneous population, we were able to detect distinct patterns which could be linked to biological processes such as cardiac stress, and interaction of proteins at the costamere and intercalated disks. These gene correlations were present in each patient individually (**Supplemental Figure 3, Chapter 2**), indicating that we found genetic pathways which are general for the HCM phenotype. The impact of specific traits on gene expression at the single-cell level remains uncertain. Existing literature employing single nucleus RNA sequencing (snRNA-seq) in patients with dilated cardiomyopathy indicated that there was little difference in cell composition and gene expression between males and females, but age might have a significant influence on the results (Koenig et al., 2022). Conversely, Chaffin *et al.* observed sex-dependent effects on certain genes, while they did not observe differences between patients carrying an *Mybpc3*, or *Myh7* mutation and other patients with HCM (Chaffin et al., 2022). These studies and our study are limited by the number of patient samples for establishing meaningful correlations. Expanding or combining these datasets with additional samples would enable a more comprehensive examination to

study the effect of confounding factors on the phenotype and on cellular behavior.

Detected gene patterns and cellular heterogeneity were further investigated with two different techniques: SCENIC (Aibar et al., 2017) which can be used to identify groups of co-expressed genes driven by specific transcription factors (TFs), and by defining Modules, which we identified by co-regulated gene clusters. We could link the genes expressed in Module 2 (Figure 5B and 5C, Chapter 2) to cell size by making use of the scatter properties from the Fluorescence-activated Cell Sorting (FACS) data. Additionally, we validated the expression of the top gene from Module 2; Myosin light chain 2 (MYL2/MLC-2) in a large dataset of HCM samples and on histological analysis of myectomy samples. This provided us insight into which marker genes might be expressed in more hypertrophic cells; one of the main characteristics of HCM, and enables future studies on which pathways might be activated in these cells.

Using this size data has given us an interesting angle for the investigation of gene expression in more hypertrophic cells. However, there are disadvantages to our methods; we used enzymatic and mechanical digestion of fresh tissue. This might be a limitation, as enzymatic digestion on its own can lead to the induction of a stress program (Van Den Brink et al., 2017). Furthermore, cells might break during the FACS process, which could increase the risk of only sorting cell fragments. We were able to show with a dual DRAQ5 experiment that the sorted cells were alive and contained a nucleus. We only focused on sorting CMs; therefore, we may miss important information as fibroblasts, vascular cells and immune cells play a great role in pathological remodeling of the heart (Abplanalp et al., 2020; Farbehi et al., 2019; Gladka et al., 2018; Martini et al., 2019; Zhao et al., 2022). However, if we would have gated for smaller cells, we would have increased the chance at sorting cell fragments. One way to circumvent this, is by performing snRNA-seq. Other groups have compiled extensive datasets encompassing diverse cell types. These datasets provide substantial insights into changes in cell composition and intercellular communication occurring in the heart, and in HCM tissue specifically (Chaffin et al., 2022; Larson et al., 2022; Litviňuková et al., 2020; X. Liu et al., 2023). A limitation inherent to snRNA-seq resides in its potential to oversee aspects of cellular heterogeneity, as it only picks up on transcripts that are located in the nucleus. In this study, we were able to combine whole cell sequencing with snRNA-seq (Litviňuková et al., 2020). In

this way, we were able to combine HCM datasets with datasets coming from healthy donor hearts, which is a great advantage in understanding the data. However, one might also argue that the differences in the collection of the tissue and the data might be an issue. It would be interesting to see whether we can also detect similarities and unique data-aspects from whole cell, and nuclear sequencing in HCM tissue.

Identification of NR2F2 as a potential driver of the genetic program in the diseased HCM septum by using Tomo-seq

Aside from studying CM heterogeneity in HCM (Chapter 2), we were interested in regional gene expression and heterogeneity throughout the myocardial wall. In Chapter 3, we aimed to better understand local differences in HCM tissue, such as the predominant hypertrophy in the IVS. By using Tomo-seq, we were able to detect distinct patterns of stress, hypertrophy and fibrosis in the left ventricular free wall (LVFW) and the IVS, indicating we could study specific regions such as local hypertrophy and fibrotic patterns, known to be present in HCM (Canepa et al., 2016; J. Liu et al., 2022; Sepehrkhoy et al., 2017) in more detail. Principle component (PC) analysis indicated that most genes were explained by PC1 in the IVS, containing mitochondrial genes, and PC2 in the IVS and the LVFW containing many known stress genes (e.g., *CSRP3*, and *ACTA1*) and was related to hypertrophy. By overlapping PC1 and PC2, we aimed to get a specific gene program which could be related to both the IVS and hypertrophy-related genes. Hence, we performed a HOMER analysis on the overlapping PC1/PC2 genes to identify TFs driving this genetic program, which returned with Nuclear Receptor Subfamily 2 Group F Member 2 (NR2F2) as a potential candidate. NR2F2 is already known for its role in atrial development, and it was shown to be upregulated in the ventricles under pathological conditions altering mitochondrial processes (Kittleson et al., 2005; Sack et al., 1997; Wu et al., 2015; Xie et al., 2017). These results indicated that it might be an interesting target to block remodeling processes in HCM.

In order to model hypertrophy *in vitro*, we used Endothelin-1 (ET-1) on human induced pluripotent stem cell-derived CMs (hiPS-CM) (Johansson et al., 2020). We could observe an increase in many of the predicted target genes of NR2F2, which was inhibited upon NR2F2 knockdown. These data indicate that NR2F2 could be the potential driver of the genes related to the hypertrophic area of the IVS. However,

we could not detect an (expected) increase of NR2F2 expression after stressing the hiPS-CMs with ET-1. The same was true for in the expression of *NPPB*/proBNP (as a marker for stress) and protein levels of target genes. Additionally, we could not detect an inhibition of increase in cell size by NR2F2 knockdown. These data indicate that ET-1 might not be stressing the cells enough to see an effect at phenotypic level of NR2F2. Furthermore, 2D culture of hiPS-CMs might not be an ideal model to mimic hypertrophy, due to their low maturity (Ahmed et al., 2020), indicating that optimization of this experimental setup is required to be able to study the role of NR2F2 in HCM.

Studying regional and cellular heterogeneity with in-depth sequencing techniques

Together, in **Chapter 2**, we used scRNA-seq on myectomy (diseased) tissue, and in **Chapter 3**, we used Tomo-seq on the transplanted (failing) heart. These novel techniques provide valuable perspectives into the gene expression heterogeneity in HCM. Nonetheless, due to the different disease states of these tissues, comparison between datasets is challenging. Additionally, each Tomo-seq slice contained a mixture of different cell types, whereas scRNA-seq comprised of CMs only. Despite this, we can find an overlap in the hypertrophy related genes in Module 2 of **Chapter 2**, and the hypertrophy related genes in PC2 of **Chapter 3**. These datasets can be studied further to identify overlapping patterns. Additionally, we identified MYL2 as a marker for more hypertrophic cells in **Chapter 2**, and we saw it expressed in the top 10 genes of PC1/2 overlapping genes in **Chapter 3**. Others have also picked up on this gene as being more expressed in a local area of a failing heart or overlapping in areas with high *NPPB* expression when performing spatial sequencing (Asp et al., 2017; X. Liu et al., 2023). With spatial sequencing, circular areas from a tissue section are sequenced by putting them on an oligoDT loaded glass. Some studies have extended this further by combining the data with snRNA-seq (Asp et al., 2019; Laird et al., 2023; Li & Wang, 2021; Liao et al., 2021; X. Liu et al., 2023; Vandereyken et al., 2023). By using these sequencing techniques in a higher resolution, different areas of hypertrophy, myocyte disarray and fibrosis were detected. Furthermore, combining this data with scRNA-seq or snRNA-seq can broaden our understanding of inter-cellular communication and the local biological processes leading to pathological remodeling.

Modeling HCM in mice carrying a known pathogenic mutation in patients

In 40-60% of the cases, patients with HCM are found to carry a sarcomere mutation (Zamorano et al., 2014). In the Netherlands, the majority of these mutations are two founder mutations in the gene encoding cardiac myosin binding protein C3 (*Mybpc3*); c.2373_2374insG (p.Trp792fs) and c.2827C>T (p.Arg943X). In **Chapter 4**, we generated mouse models harboring these Dutch founder mutations with the aim to investigate their effect on the heart and HCM triggers. For both mouse models, our data shows that a heterozygous mutation (HET) leads to a reduction in *Mybpc3* transcripts, but not to reduction in protein levels. No significant changes were detected in heart function, histology or stress genes when compared to their wildtype (WT) littermates. These results are in line with previous studies, where they used heterozygous knockout animals of *Mybpc3* (Harris et al., 2002), although some showed contractile dysfunction (Barefield et al., 2014) or a reduction in protein and asymmetrical hypertrophy after 1 year (Carrier et al., 2004). Our results indicate that the mice need to be studied at either an older age, or an additional trigger is required to induce HCM onset.

In attempt to trigger the HCM phenotype, we performed transverse aortic binding (TAB). This is a common procedure to increase the pressure on the ventricles and hereby induce hypertrophy (Mohammed et al., 2012; Rockman et al., 1991). Despite the onset of hypertrophy, TAB did not worsen the hypertrophic phenotype in HET mice, based on physiological parameters, echo data, or gene expression. This is in conflict with results from Barefield et al, where the same procedure led to a worsened phenotype and increased force development and calcium sensitivity in mutant animals (Barefield et al., 2015). Discrepancies with our results could be explained by differences in the mouse model or in the procedure. The absence of a worsened phenotype in our mutated animals indicate that we might need another stressor to induce HCM. Although we were not able to trigger a (worsened) phenotype in HET mice with pressure overload, this model is very interesting to study other triggers for the onset of HCM. There is a large population of carriers that do not develop any phenotype, and this model might recapitulate the human situation. It would be interesting to find out whether non-affected humans are also able to maintain their levels of MYBPC3-protein, and whether this also prevents the onset of HCM in this situation.

By contrast, homozygous mutant mice exhibited a discernable HCM phenotype.

Transcript levels of *Mybpc3* were not detectable, as well as the protein levels. Both mouse models showed an increase in hypertrophy based on the heart weight to tibia length ratio, decreased heart function and an increase in stress markers. This is in line with studies of homozygous knockout mice of *Mybpc3*, which developed hypertrophy after day 1, paired with a high expression of stress genes (*Acta1*, *Nppb*, and *Myh7*) and mitochondrial alterations (Carrier et al., 2004; Farrell et al., 2018; Harris et al., 2002). These data correspond with the phenotype seen in humans carrying a double or a compound mutation. These patients develop HCM at a very young age and the phenotype is often much more severe (Wessels et al., 2015). These data indicate that our model might exhibit similarities to HCM caused by compound mutations. This model can be used in further research, by studying a timeline to find the exact time and trigger of the onset of HCM and when the lack of *Mybpc3* protein is going to be detrimental. Furthermore, this model can be used to study the regional and cellular heterogeneity as found in the human samples, or to study therapeutic targets.

What comes first, haploinsufficiency or cellular stress?

The question remains whether haploinsufficiency triggers the disease, or whether there is another trigger preceding disease onset. In **Chapter 3**, we studied the heart of a patient with a heterozygous mutation, the most common *Mybpc3* mutation in the Netherlands (p.Trp792fs) (Christiaans et al., 2010). This mutation was mimicked in a mouse model in **Chapter 4** (p.Trp796fs). In **Chapter 3**, we could detect a clear decrease in MYBPC3 protein levels in the HCM heart, which is in line with what others have found in the advanced stages of HCM (O'Leary et al., 2019). However, no reduction in protein levels was detected in the HET mice. This is more in line with results found in hiPSC-CMs or mice carrying an *Mybpc3* mutation (Helms et al., 2020; Hilderink et al., 2023). In this study there was no reduction in MYBPC3 protein found, and it was suggested that the reduction in *Mybpc3* transcripts due to the mutation was compensated for by a reduction in protein degradation. Whether this would also be the case in mice is yet to be investigated. Moreover, inducing a stress in the heart with hemodynamic pressure did not alter the hypertrophy in HET mice compared to WT mice, indicating that another stress might exceed the loss in MYBPC3 protein. Interestingly, others have triggered the HCM phenotype in mice carrying a heterozygous *Mybpc3* mutation with a western diet, while having an unaltered protein level compared to WT (Nollet et al., 2023). It will be intriguing to further investigate the role of loss of protein and additional triggers in the manifestation of HCM hallmarks.

Future perspectives in early detection of HCM

Getting a better understanding of HCM can improve predictions on disease progression. Other studies have suggested that biomarkers used to predict heart failure such as proBNP, cardiac Troponin (cTnT) and LDL cholesterol can be used as prognostic markers in HCM (Jansen et al., 2022). Furthermore, a metabolomics study has identified several differentially expressed metabolites in carriers of an HCM mutation without a phenotype and mutations carriers with a severe phenotype (Jansen et al., 2023). In our studies, we identified myoglobin (MB) as potential biomarker by performing scRNA-seq in **Chapter 2**. Furthermore, in **Chapter 3**, MB was most strongly related to PC2, the PC that was related to hypertrophy. Myoglobin is used as a marker for muscle injury (Berenbrink, 2021), but hasn't been tested as a biomarker for HCM. A more thorough study of potentially secreted factors, combined with serum analysis of a timeline model of the mice study could provide valuable insight into potential biomarkers to predict HCM.

Future perspectives in the treatment of HCM

Although septal reduction therapy is considered a very safe and effective procedure to relieve outflow tract obstruction, pharmacological interventions are currently mostly focused on relieving symptoms (Maron & Maron, 2014). Recently, a myosin inhibitor, Mavacamten, proved to reduce the symptom burden by blocking the myosin heads and thereby reducing the contraction force (Ho et al., 2020; Tuohy et al., 2020). Additionally, recent studies have indicated that a protein lost by an HCM mutation could be replenished by using adeno-associated virus-9 (AAV-9) and with base editing (Gedicke-Hornung et al., 2013; Mearini et al., 2014; Reichart et al., 2023). Moreover, the first clinical trial using AAV techniques has recently been announced by Tenaya Therapeutics, holding promising findings in the therapeutic options for HCM patients in the future. We hope that our data can contribute to such findings or can be used to study novel targets.

Concluding remarks

Within this thesis, we introduce pertinent models aimed to enhance our understanding of the pathogenesis of HCM. By combining these models and subsequent research, we can further examine the initiation and progression of the disease, as well

as assess potential therapeutic interventions.

References

- Abplanalp, W. T., John, D., Cremer, S., Assmus, B., Dorsheimer, L., Hoffmann, J., Becker-Perkola, G., Rieger, M. A., Zeiher, A. M., Vasa-Nicotera, M., & Dimmeler, S. (2020). Single cell RNA sequencing reveals profound changes in circulating immune cells in patients with heart failure. *Cardiovascular Research*. <https://doi.org/10.1093/cvr/cvaa101>
- Ahmed, R. E., Anzai, T., Chanthra, N., & Uosaki, H. (2020). A Brief Review of Current Maturation Methods for Human Induced Pluripotent Stem Cells-Derived Cardiomyocytes. *Frontiers in Cell and Developmental Biology*, 8(March), 1–9. <https://doi.org/10.3389/fcell.2020.00178>
- Aibar, S., Gonzalez-Blas, C. B., Moerman, T., Van, A. H. T., Imrichova, H., Hulselmans, G., Rambow, F., Marine, J. C., Geurts, P., Aerts, J., van den Oord, J., Atak, Z. K., Wouters, J., Aerts, S., González-Blas, C. B., Moerman, T., Huynh-Thu, V. A., Imrichova, H., Hulselmans, G., ... Aerts, S. (2017). SCENIC: single-cell regulatory network inference and clustering. *Nature Methods*, 14(11), 1083–+. <https://doi.org/10.1038/Nmeth.4463>
- Asp, M., Giacomello, S., Larsson, L., Wu, C., Fürth, D., Qian, X., Wårdell, E., Custodio, J., Reimegård, J., Salmén, F., Österholm, C., Ståhl, P. L., Sundström, E., Åkesson, E., Bergmann, O., Bienko, M., Månsson-Broberg, A., Nilsson, M., Sylvén, C., & Lundeberg, J. (2019). A Spatiotemporal Organ-Wide Gene Expression and Cell Atlas of the Developing Human Heart. *Cell*, 179(7), 1647–1660.e19. <https://doi.org/10.1016/j.cell.2019.11.025>
- Asp, M., Salmén, F., Ståhl, P. L., Vickovic, S., Felldin, U., Löfling, M., Navarro, J. F., Maaskola, J., Eriksson, M. J., Persson, B., Corbascio, M., Persson, H., Linde, C., & Lundeberg, J. (2017). Spatial detection of fetal marker genes expressed at low level in adult human heart tissue. *Scientific Reports*, 7(1). <https://doi.org/10.1038/s41598-017-13462-5>
- Barefield, D., Kumar, M., de Tombe, P. P., & Sadayappan, S. (2014). Contractile dysfunction in a mouse model expressing a heterozygous MYBPC3 mutation associated with hypertrophic cardiomyopathy. *American Journal of Physiology - Heart and Circulatory Physiology*, 306(6), 807–815. <https://doi.org/10.1152/ajpheart.00913.2013>
- Barefield, D., Kumar, M., Gorham, J., Seidman, J. G., Seidman, C. E., de Tombe, P. P., & Sadayappan, S. (2015). Haploinsufficiency of MYBPC3 exacerbates the development of hypertrophic cardiomyopathy in heterozygous mice. *Journal of Molecular and Cellular Cardiology*, 79, 234–243. <https://doi.org/10.1016/j.yjmcc.2014.11.018>
- Berenbrink, M. (2021). The role of myoglobin in the evolution of mammalian diving capacity – The August Krogh principle applied in molecular and evolutionary physiology. *Comparative Biochemistry and Physiology -Part A : Molecular and Integrative Physiology*, 252(November 2020), 110843. <https://doi.org/10.1016/j.cbpa.2020.110843>
- Canepa, M., Pozios, I., Vianello, P. F., Ameri, P., Brunelli, C., Ferrucci, L., & Abraham, T. P. (2016). Distinguishing ventricular septal bulge versus hypertrophic cardiomyopathy in the elderly. *Heart (British Cardiac Society)*, 102(14), 1087–1094. <https://doi.org/10.1136/heart-jnl-2015-308764>
- Carrier, L., Knöll, R., Vignier, N., Keller, D. I., Bausero, P., Prudhon, B., Isnard, R., Ambroisine, M.-L., Fisman, M., Ross, J., Schwartz, K., & Chien, K. R. (2004). Asymmetric septal hypertrophy in heterozygous cMyBP-C null mice. *Cardiovascular Research*, 63(2), 293–304. <https://doi.org/10.1016/j.cardiores.2004.04.009>
- Chaffin, M., Papangeli, I., Simonson, B., Akkad, A. D., Hill, M. C., Arduini, A., Fleming, S. J., Melanson, M., Hayat, S., Kost-Alimova, M., Atwa, O., Ye, J., Bedi, K. C., Nahrendorf, M., Kaushik, V. K., Stegmann, C. M., Margulies, K. B., Tucker, N. R., & Ellinor, P. T. (2022). Single-nucleus profiling of human dilated and hypertrophic cardiomyopathy. *Nature*, 608(7921), 174–180. <https://doi.org/10.1038/s41586-022-04817-8>

- Christiaans, I., Nannenbergh, E. A., Dooijes, D., Jongbloed, R. J. E., Michels, M., Postema, P. G., Majoor-Krakauer, D., van den Wijngaard, A., Mannens, M. M. A. M., van Tintelen, J. P., van Langen, I. M., & Wilde, A. A. M. (2010). Founder mutations in hypertrophic cardiomyopathy patients in the Netherlands. *Neth Heart J*, *18*(5), 248–254. <https://doi.org/10.1007/BF03091771>
- Cui, Y., Zheng, Y., Liu, X., Yan, L., Fan, X., Yong, J., Hu, Y., Dong, J., Li, Q., Wu, X., Gao, S., Li, J., Wen, L., Qiao, J., & Tang, F. (2019). Single-Cell Transcriptome Analysis Maps the Developmental Track of the Human Heart. *Cell Rep*, *26*(7), 1934–1950 e5. <https://doi.org/10.1016/j.celrep.2019.01.079>
- Farbehi, N., Patrick, R., Dorison, A., Xaymardan, M., Janbandhu, V., Wystub-Lis, K., Ho, J. W. K., Nordon, R. E., & Harvey, R. P. (2019). Single-cell expression profiling reveals dynamic flux of cardiac stromal, vascular and immune cells in health and injury. *Elife*, *8*, 1–39. <https://doi.org/10.7554/eLife.43882>
- Farrell, E., Armstrong, A. E., Grimes, A. C., Naya, F. J., De Lange, W. J., & Ralphe, J. C. (2018). Transcriptome analysis of cardiac hypertrophic growth in MYBPC3-null mice suggests early responders in hypertrophic remodeling. *Frontiers in Physiology*, *9*(OCT), 1–14. <https://doi.org/10.3389/fphys.2018.01442>
- Gedicke-Hornung, C., Behrens-Gawlik, V., Reischmann, S., Geertz, B., Stimpel, D., Weinberger, F., Schlossarek, S., Précigout, G., Braren, I., Eschenhagen, T., Mearini, G., Lorain, S., Voit, T., Dreyfus, P. A., Garcia, L., & Carrier, L. (2013). Rescue of cardiomyopathy through U7snRNA-mediated exon skipping in Mybpc3-targeted knock-in mice. *EMBO Molecular Medicine*, *5*(7), 1060–1077. <https://doi.org/10.1002/emmm.201202168>
- Gladka, M. M., Molenaar, B., de Ruiter, H., Van Der Elst, S., Tsui, H., Versteeg, D., Lacraz, G. P. A. A., Huibers, M. M. H. H., Van Oudenaarden, A., & Van Rooij, E. (2018). Single-Cell Sequencing of the Healthy and Diseased Heart Reveals Cytoskeleton-Associated Protein 4 as a New Modulator of Fibroblasts Activation. *Circulation*, *138*(2), 166–180. <https://doi.org/10.1161/CIRCULATIONAHA.117.030742>
- Grun, D., Lyubimova, A., Kester, L., Wiebrands, K., Basak, O., Sasaki, N., Clevers, H., van Oudenaarden, A., Grün, D., Lyubimova, A., Kester, L., Wiebrands, K., Basak, O., Sasaki, N., Clevers, H., & van Oudenaarden, A. (2015). Single-cell messenger RNA sequencing reveals rare intestinal cell types. *Nature*, *525*(7568), 251–255. <https://doi.org/10.1038/nature14966>
- Harris, S. P., Bartley, C. R., Hacker, T. A., McDonald, K. S., Douglas, P. S., Greaser, M. L., Powers, P. A., & Moss, R. L. (2002). Hypertrophic cardiomyopathy in cardiac myosin binding protein-C knockout mice. *Circulation Research*, *90*(5), 594–601. <https://doi.org/10.1161/01.RES.0000012222.70819.64>
- Helms, A. S., Tang, V. T., O’Leary, T. S., Friedline, S., Wauchope, M., Arora, A., Wasserman, A. H., Smith, E. D., Lee, L. M., Wen, X. W., Shavit, J. A., Liu, A. P., Previs, M. J., & Day, S. M. (2020). Effects of MYBPC3 loss-of-function mutations preceding hypertrophic cardiomyopathy. *JCI Insight*, *5*(2). <https://doi.org/10.1172/jci.insight.133782>
- Hilderink, S., Schuldt, M., Goebel, M., Jansen, V. J., Manders, E., Moorman, S., Dorsch, L. M., van Steenbeek, F. G., van der Velden, J., & Kuster, D. W. D. (2023). Characterization of heterozygous and homozygous mouse models with the most common hypertrophic cardiomyopathy mutation MYBPC3 in the Netherlands. *Journal of Molecular and Cellular Cardiology*, *185*, 65–76. <https://doi.org/10.1016/j.yjmcc.2023.10.008>
- Ho, C. Y., Olivotto, I., Jacoby, D., Lester, S. J., Roe, M., Wang, A., Waldman, C. B., Zhang, D., Sehnert, A. J., & Heitner, S. B. (2020). Study Design and Rationale of EXPLORER-HCM: Evaluation of Mavacamten in Adults with Symptomatic Obstructive Hypertrophic Cardiomyopathy. *Circulation: Heart Failure*, *June*, 59–67. <https://doi.org/10.1161/CIRCHEARTFAILURE.120.006853>
- Jansen, M., Algül, S., Bosman, L. P., Michels, M., van der Velden, J., de Boer, R. A., van Tintel-

- en, J. P., Asselbergs, F. W., & Baas, A. F. (2022). Blood-based biomarkers for the prediction of hypertrophic cardiomyopathy prognosis: a systematic review and meta-analysis. *ESC Heart Failure*, 9(5), 3418–3434. <https://doi.org/10.1002/ehf2.14073>
- Jansen, M., Schuldt, M., van Driel, B. O., Schmidt, A. F., Christiaans, I., van der Crabben, S. N., Hoedemaekers, Y. M., Dooijes, D., Jongbloed, J. D. H., Boven, L. G., Deprez, R. H. L., Wilde, A. A. M., Jans, J. J. M., van der Velden, J., de Boer, R. A., van Tintelen, J. P., Asselbergs, F. W., & Baas, A. F. (2023). Untargeted Metabolomics Identifies Potential Hypertrophic Cardiomyopathy Biomarkers in Carriers of MYBPC3 Founder Variants. *International Journal of Molecular Sciences*, 24(4). <https://doi.org/10.3390/ijms24044031>
- Johansson, M., Ulfenborg, B., Andersson, C. X., Heydarkhan-Hagvall, S., Jeppsson, A., Sartip, P., & Synnergren, J. (2020). Cardiac hypertrophy in a dish: A human stem cell based model. *Biology Open*, 9(9), 1–12. <https://doi.org/10.1242/bio.052381>
- Kittleson, M. M., Minhas, K. M., Irizarry, R. A., Ye, S. Q., Edness, G., Breton, E., Conte, J. V., Tomaselli, G., Garcia, J. G. N., & Hare, J. M. (2005). Gene expression analysis of ischemic and nonischemic cardiomyopathy: Shared and distinct genes in the development of heart failure. *Physiological Genomics*, 21, 299–307. <https://doi.org/10.1152/physiolgenomics.00255.2004>
- Koenig, A. L., Shchukina, I., Amrute, J., Andhey, P. S., Zaitsev, K., Lai, L., Bajpai, G., Brede-meyer, A., Smith, G., Jones, C., Terrebonne, E., Rentschler, S. L., Artyomov, M. N., & Lavine, K. J. (2022). Single-cell transcriptomics reveals cell-type-specific diversification in human heart failure. *Nature Cardiovascular Research*, 1(3), 263–280. <https://doi.org/10.1038/s44161-022-00028-6>
- Kolodziejczyk, A. A., Kim, J. K., Svensson, V., Marioni, J. C., & Teichmann, S. A. (2015). The technology and biology of single-cell RNA sequencing. *Mol Cell*, 58(4), 610–620. <https://doi.org/10.1016/j.molcel.2015.04.005>
- Kraft, T., & Montag, J. (2019). Altered force generation and cell-to-cell contractile imbalance in hypertrophic cardiomyopathy. *Pflügers Archiv - European Journal of Physiology*, 471(5), 719–733. <https://doi.org/10.1007/s00424-019-02260-9>
- Kretzschmar, K., Post, Y., Bannier-Helaouet, M., Mattiotti, A., Drost, J., Basak, O., Li, V. S. W., van den Born, M., Gunst, Q. D., Versteeg, D., Kooijman, L., van der Elst, S., van Es, J. H., van Rooij, E., van den Hoff, M. J. B., & Clevers, H. (2018). Profiling proliferative cells and their progeny in damaged murine hearts. *Proc Natl Acad Sci U S A*, 115(52), E12245–E12254. <https://doi.org/10.1073/pnas.1805829115>
- Laird, J., Perera, G., Batorsky, R., Wang, H., Arkun, K., & Chin, M. T. (2023). Spatial Transcriptomic Analysis of Focal and Normal Areas of Myocyte Disarray in Human Hypertrophic Cardiomyopathy. *International Journal of Molecular Sciences*, 24(16). <https://doi.org/10.3390/ijms241612625>
- Larson, A., Codden, C. J., Huggins, G. S., Rastegar, H., Chen, F. Y., Maron, B. J., Rowin, E. J., Maron, M. S., & Chin, M. T. (2022). Altered intercellular communication and extracellular matrix signaling as a potential disease mechanism in human hypertrophic cardiomyopathy. *Scientific Reports*, 12(1). <https://doi.org/10.1038/s41598-022-08561-x>
- Li, X., & Wang, C. Y. (2021). From bulk, single-cell to spatial RNA sequencing. *International Journal of Oral Science*, 13(1), 1–6. <https://doi.org/10.1038/s41368-021-00146-0>
- Liao, J., Lu, X., Shao, X., Zhu, L., & Fan, X. (2021). Uncovering an Organ's Molecular Architecture at Single-Cell Resolution by Spatially Resolved Transcriptomics. *Trends in Biotechnology*, 39(1), 43–58. <https://doi.org/10.1016/j.tibtech.2020.05.006>
- Litviňuková, M., Talavera-López, C., Maatz, H., Reichart, D., Worth, C. L., Lindberg, E. L., Kanda, M., Polanski, K., Heinig, M., Lee, M., Nadelmann, E. R., Roberts, K., Tuck, L., Fasouli, E. S., DeLaughter, D. M., McDonough, B., Wakimoto, H., Gorham, J. M., Samari, S., ... Teichmann, S. A. (2020). Cells of the adult human heart. *Nature*, September. <https://doi.org/10.1038/s41586-020-2797-4>

- Liu, J., Zhao, S., Yu, S., Wu, G., Wang, D., & Liu, M. B. L. (2022). *Patterns of Replacement Fibrosis in Hypertrophic*.
- Liu, X., Yin, K., Chen, L., Chen, W., Li, W., Zhang, T., Sun, Y., Yuan, M., Wang, H., Song, Y., Wang, S., Hu, S., & Zhou, Z. (2023). Lineage-specific regulatory changes in hypertrophic cardiomyopathy unraveled by single-nucleus RNA-seq and spatial transcriptomics. *Cell Discovery*, 9(1). <https://doi.org/10.1038/s41421-022-00490-3>
- Marian, A. J., & Braunwald, E. (2017). Hypertrophic Cardiomyopathy: Genetics, Pathogenesis, Clinical Manifestations, Diagnosis, and Therapy. *Circ Res*, 121(7), 749–770. <https://doi.org/10.1161/CIRCRESAHA.117.311059>
- Maron, B. J., & Maron, M. S. (2014). The 25-year genetic era in hypertrophic cardiomyopathy: Revisited. *Circulation: Cardiovascular Genetics*, 7(4), 401–404. <https://doi.org/10.1161/CIRCGENETICS.114.000741>
- Martini, E., Kunderfranco, P., Peano, C., Carullo, P., Cremonesi, M., Schorn, T., Carriero, R., Termanini, A., Colombo, F. S., Jachetti, E., Panico, C., Faggian, G., Fumero, A., Torracca, L., Molgora, M., Cibella, J., Pagiatakis, C., Brummelman, J., Alvisi, G., ... Kallikourdis, M. (2019). Single-Cell Sequencing of Mouse Heart Immune Infiltrate in Pressure Overload-Driven Heart Failure Reveals Extent of Immune Activation. *Circulation*, 140(25), 2089–2107. <https://doi.org/10.1161/CIRCULATIONAHA.119.041694>
- Mearini, G., Stimpel, D., Geertz, B., Weinberger, F., Kramer, E., Schlossarek, S., Mourot-Filiatre, J., Stoehr, A., Dutsch, A., Wijinker, P. J. M., Braren, I., Katus, H. A., Muller, O. J., Voit, T., Eschenhagen, T., Carrier, L., Krämer, E., Schlossarek, S., Mourot-Filiatre, J., ... Carrier, L. (2014). Mybpc3 gene therapy for neonatal cardiomyopathy enables long-term disease prevention in mice. *Nat Commun*, 5(May), 5515. <https://doi.org/10.1038/ncomms6515>
- Mohammed, S. F., Storlie, J. R., Oehler, E. A., Bowen, L. A., Korinek, J., Lam, C. S., Simari, R. D., Burnett Jr., J. C., & Redfield, M. M. (2012). Variable phenotype in murine transverse aortic constriction. *Cardiovasc Pathol*, 21(3), 188–198. <https://doi.org/10.1016/j.carpath.2011.05.002>
- Montag, J., Kowalski, K., Makul, M., Ernstberger, P., Radocaj, A., Beck, J., Becker, E., Tripathi, S., Keyser, B., Muhlfeld, C., Wissel, K., Pich, A., van der Velden, J., dos Remedios, C. G., Perrot, A., Francino, A., Navarro-Lopez, F., Brenner, B., Kraft, T., ... Kraft, T. (2018). Burst-Like Transcription of Mutant and Wildtype MYH7-Alleles as Possible Origin of Cell-to-Cell Contractile Imbalance in Hypertrophic Cardiomyopathy. *Front Physiol*, 9, 359. <https://doi.org/10.3389/fphys.2018.00359>
- Nollet, E. E., Algül, S., Goebel, M., Schlossarek, S., van der Wel, N. N., Jans, J. J. M., van de Wiel, M. A., Knol, J. C., Pham, T. V., Piersma, S. R., de Goeij-de Haas, R., Hermans, J., van Klinken, J. B., van Weeghel, M., Houtkooper, R. H., Carrier, L., Jimenez, C. R., Kuster, D. W. D., & van der Velden, J. (2023). Western diet triggers cardiac dysfunction in heterozygous Mybpc3-targeted knock-in mice: A two-hit model of hypertrophic cardiomyopathy. *Journal of Molecular and Cellular Cardiology Plus*, 100050. <https://doi.org/10.1016/j.jmccpl.2023.100050>
- Nomura, S., Satoh, M., Fujita, T., Higo, T., Sumida, T., Ko, T., Yamaguchi, T., Tobita, T., Naito, A. T., Ito, M., Fujita, K., Harada, M., Toko, H., Kobayashi, Y., Ito, K., Takimoto, E., Akazawa, H., Morita, H., Aburatani, H., & Komuro, I. (2018). Cardiomyocyte gene programs encoding morphological and functional signatures in cardiac hypertrophy and failure. *Nat Commun*, 9(1), 4435. <https://doi.org/10.1038/s41467-018-06639-7>
- O'Leary, T. S., Snyder, J., Sadayappan, S., Day, S. M., & Previs, M. J. (2019). MYBPC3 truncation mutations enhance actomyosin contractile mechanics in human hypertrophic cardiomyopathy. *Journal of Molecular and Cellular Cardiology*, 127(December 2018), 165–173. <https://doi.org/10.1016/j.yjmcc.2018.12.003>
- Parbhudayal, R. Y., Garra, A. R., Götte, M. J. W., Michels, M., Pei, J., Harakalova, M., Asselbergs, F. W., van Rossum, A. C., van der Velden, J., & Kuster, D. W. D. (2018). Variable

- cardiac myosin binding protein-C expression in the myofilaments due to MYBPC3 mutations in hypertrophic cardiomyopathy. *Journal of Molecular and Cellular Cardiology*, 123(August), 59–63. <https://doi.org/10.1016/j.yjmcc.2018.08.023>
- Reichart, D., Newby, G. A., Wakimoto, H., Lun, M., Gorham, J. M., Curran, J. J., Raguram, A., DeLaughter, D. M., Conner, D. A., Marsiglia, J. D. C., Kohli, S., Chmatal, L., Page, D. C., Zabaleta, N., Vandenberghe, L., Liu, D. R., Seidman, J. G., & Seidman, C. (2023). Efficient in vivo genome editing prevents hypertrophic cardiomyopathy in mice. *Nature Medicine*, 29(2), 412–421. <https://doi.org/10.1038/s41591-022-02190-7>
- Rockman, H. A., Ross, R. S., Harris, A. N., Knowlton, K. U., Steinhilber, M. E., Field, L. J., Ross Jr., J., & Chien, K. R. (1991). Segregation of atrial-specific and inducible expression of an atrial natriuretic factor transgene in an in vivo murine model of cardiac hypertrophy. *Proc Natl Acad Sci U S A*, 88(18), 8277–8281. <https://doi.org/10.1073/pnas.88.18.8277>
- Sack, M. N., Disch, D. L., Rockman, H. A., & Kelly, D. P. (1997). A role for Sp and nuclear receptor transcription factors in a cardiac hypertrophic growth program. *Proceedings of the National Academy of Sciences of the United States of America*, 94(12), 6438–6443. <https://doi.org/10.1073/pnas.94.12.6438>
- Semsarian, C., Ingles, J., Maron, M. S., & Maron, B. J. (2015). New Perspectives on the Prevalence of Hypertrophic Cardiomyopathy. *Journal of the American College of Cardiology*, 65(12), 1249–1254. <https://doi.org/10.1016/j.jacc.2015.01.019>
- Sepehrkhoy, S., Gho, J. M. I. H., van Es, R., Harakalova, M., de Jonge, N., Dooijes, D., van der Smagt, J. J., Buijsrogge, M. P., Hauer, R. N. W., Goldschmeding, R., de Weger, R. A., Asselbergs, F. W., & Vink, A. (2017). Distinct fibrosis pattern in desmosomal and phospholamban mutation carriers in hereditary cardiomyopathies. *Heart Rhythm*, 14(7), 1024–1032. <https://doi.org/10.1016/j.hrthm.2017.03.034>
- Tuohy, C. V., Kaul, S., Song, H. K., Nazer, B., & Heitner, S. B. (2020). Hypertrophic cardiomyopathy: the future of treatment. *Eur J Heart Fail*, 22(2), 228–240. <https://doi.org/10.1002/ejhf.1715>
- Van Den Brink, S. C., Sage, F., Vértesy, Á., Spanjaard, B., Peterson-Maduro, J., Baron, C. S., Robin, C., Van Oudenaarden, A., Vertesy, A., Spanjaard, B., Peterson-Maduro, J., Baron, C. S., Robin, C., & Van Oudenaarden, A. (2017). Single-cell sequencing reveals dissociation-induced gene expression in tissue subpopulations. *Nature Methods*, 14(10), 935–936. <https://doi.org/10.1038/nmeth.4437>
- Vandereyken, K., Sifrim, A., Thienpont, B., & Voet, T. (2023). Methods and applications for single-cell and spatial multi-omics. *Nature Reviews Genetics*. <https://doi.org/10.1038/s41576-023-00580-2>
- Wang, Y., Yao, F., Wang, L., Li, Z., Ren, Z., Li, D., Zhang, M., Han, L., Wang, S. qiang, Zhou, B., & Wang, L. (2020). Single-cell analysis of murine fibroblasts identifies neonatal to adult switching that regulates cardiomyocyte maturation. *Nature Communications*, 11(1). <https://doi.org/10.1038/s41467-020-16204-w>
- Wessels, M. W., Herkert, J. C., Frohn-Mulder, I. M., Dalinghaus, M., van den Wijngaard, A., de Krijger, R. R., Michels, M., De Coo, I. F., Hoedemaekers, Y. M., & Dooijes, D. (2015). Compound heterozygous or homozygous truncating MYBPC3 mutations cause lethal cardiomyopathy with features of noncompaction and septal defects. *Eur J Hum Genet*, 23(7), 922–928. <https://doi.org/10.1038/ejhg.2014.211>
- Wu, S. P., Kao, C. Y., Wang, L., Creighton, C. J., Yang, J., Donti, T. R., Harmancey, R., Vasquez, H. G., Graham, B. H., Bellen, H. J., Taegtmeier, H., Chang, C. P., Tsai, M. J., & Tsai, S. Y. (2015). Increased COUP-TFII expression in adult hearts induces mitochondrial dysfunction resulting in heart failure. *Nature Communications*, 6. <https://doi.org/10.1038/ncomms9245>
- Xie, X., Wu, S. P., Tsai, M. J., & Tsai, S. (2017). The Role of COUP-TFII in Striated Muscle Development and Disease. In *Current Topics in Developmental Biology* (1st ed., Vol. 125).

Elsevier Inc. <https://doi.org/10.1016/bs.ctdb.2016.12.006>

- Zamorano, J. L., Anastasakis, A., Borger, M. A., Borggrefe, M., Cecchi, F., Charron, P., Hagege, A. A., Lafont, A., Limongelli, G., Mahrholdt, H., McKenna, W. J., Mogensen, J., Nihoyannopoulos, P., Nistri, S., Piepe, P. G., Pieske, B., Rapezzi, C., Rutten, F. H., Tillmanns, C., ... Watkins, H. (2014). 2014 ESC Guidelines on diagnosis and management of hypertrophic cardiomyopathy: the Task Force for the Diagnosis and Management of Hypertrophic Cardiomyopathy of the European Society of Cardiology (ESC). *Eur Heart J*, 35(39), 2733–2779. <https://doi.org/10.1093/eurheartj/ehu284>
- Zhao, W., Wu, T., Zhan, J., & Dong, Z. (2022). Identification of the Immune Status of Hypertrophic Cardiomyopathy by Integrated Analysis of Bulk- and Single-Cell RNA Sequencing Data. *Computational and Mathematical Methods in Medicine*, 2022. <https://doi.org/10.1155/2022/7153491>



Nederlandse samenvatting

Hypertrofe cardiomyopathie (HCM) is een aandoening waarbij een verdikking in de hartspier optreedt die niet te herleiden is aan andere condities, zoals hypertensie, die de druk op het hart verhogen. Het is een veelvoorkomende ziekte; 1:500 – 1:200 mensen van de algemene bevolking leiden eraan. Daarmee is het ook de meest voorkomende genetische hartziekte. Bij het overgrote gedeelte van de patiënten met HCM wordt een mutatie gevonden in een van de genen die een rol hebben in het samentrekken van de hartspier. Als we specifiek naar Nederland kijken, hebben de meeste dragers een mutatie in myosine bindend eiwit c3 (MYBPC3 c.2373_2374insG (p.Trp792fs) en c.2827C>T (p.Arg943X), deze twee mutaties zijn ook in Nederland ontstaan en zijn aan een groot gedeelte van de populatie doorgegeven.

De symptomen variëren sterk; vele dragers van een mutatie zullen nooit de ziekte (het fenotype) ontwikkelen, maar bij sommige patiënten kan het hebben van een enkele mutatie ernstige gevolgen hebben. Bij een deel is het eerste symptoom direct een hartstilstand, hierdoor is HCM is doodsoorzaak nr. 1 bij jonge atleten. Bij andere patiënten kan er remodelering in het hart optreden. Deze remodelering wordt gekenmerkt door een toename in de celgrootte van de hartspiercellen (hypertrofie) en een toename in de hoeveelheid lidtekenweefsel in de spierlaag. De verdikking van de gehele hartspier kan zich overal voordoen, maar in bijna alle gevallen is het intra ventriculaire septum (**IVS, Figuur 1, midden**) aangedaan. Doordat hier verdikking optreedt wordt de doorgang naar de aorta vernauwd, waardoor de hartkleppen naar het septum gezogen worden (Venturi effect) en waardoor de weg van het linkerventrikel (LV) naar de aorta (het outflow tract, LVOT) geblokkeerd wordt. Bij een zogenoemde obstructie van het LVOT, of wanneer het septum dikker wordt dan 15mm, kunnen patiënten een ingreep ondergaan, waarbij er door middel van het inspuiten van alcohol, of door het wegsnijden van een deel van het septum in een myectomie operatie (**Figuur 1, rechts**) de weg weer vrij wordt gemaakt. Hoewel dit in veel gevallen een zeer effectieve methode is om de ziekte te verhelpen, blijft het hart van ongeveer 10% van de patiënten door remodeleren, waardoor er veel littekenweefsel in de hartspier komt en de hartspier uiteindelijk dunner wordt (dilateren). Hierdoor ontstaat er een nieuwe fase van de ziekte: hartfalen. Wanneer een patient deze fase bereikt kan hij/zij alleen behandeld worden door het ontvangen van een donorhart.

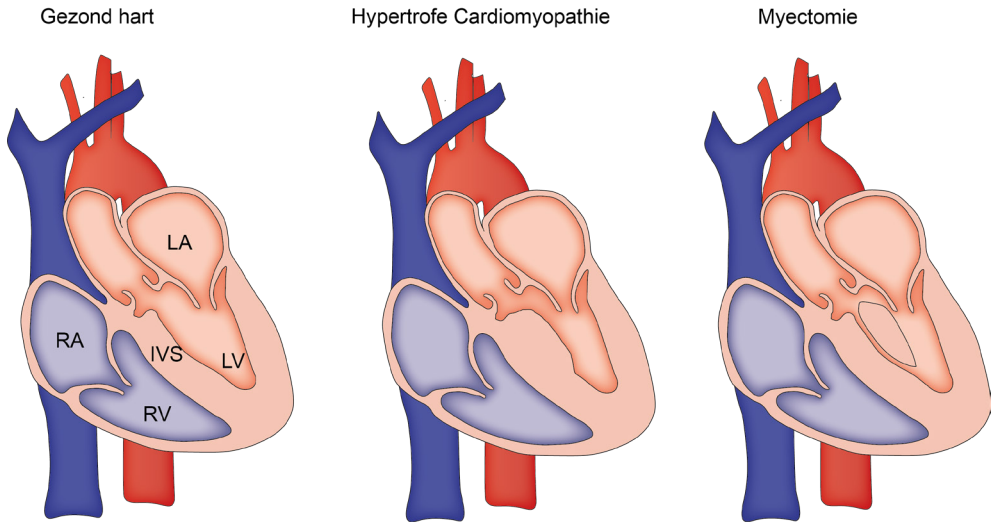


De reden waarom het septum begint met remodeleren, of waarom de ene patiënt een ernstig fenotype ontwikkelt en de andere juist geen last heeft van de mutatie blijft een complexe vraag. Als we beter zouden kunnen voorspellen wie HCM ontwikkelt en waarom, dan kunnen wij specifiek op zoek gaan naar een methode om de patiënten te behandelen, of om het remodeleren voor te zijn. Het doel van mijn promotieonderzoek was om gericht op het verkrijgen van een beter beeld van de ontwikkeling van HCM op een moleculair niveau.

In **hoofdstuk 2** hebben wij gekeken naar de verschillen tussen hartspiercellen uit het HCM-hart. Andere onderzoekers hebben aangetoond dat er variatie is tussen (het functioneren van) hartspiercellen uit hetzelfde weefsel, en dat dit een trigger zou kunnen zijn voor hypertrofie. Wij waren benieuwd of we onderscheid konden maken tussen de hartspiercellen, en konden definiëren welke cel zieker was dan de andere, en welke achterliggende mechanismen dit zouden kunnen aansturen. Om dit te onderzoeken hebben wij gebruik mogen maken van hartweefsel wat werd weggesneden in myectomie operaties in Rotterdam. Van dit weefsel hebben wij een oplossing gemaakt van enkele cellen met behulp van enzymen en mechanische digestie. Met behulp van Fluorescentie-geactiveerde sortering (FACS) konden wij de levende hartspiercellen per cel sorteren en per cel het RNA af te lezen (sequenzen, scRNA-seq), waarbij wij hebben gekeken naar de genexpressie van zieke hartspiercellen. Door deze data te vergelijken met dat van hartspiercellen uit gepubliceerde datasets konden wij verifiëren dat de hartspiercellen die wij uit het myectomie weefsel hebben geïsoleerd een hoge expressie hebben van stress genen, zoals *NPPA*, *NPPB*, *ACTA1* en *MYH7*.

Verder onderzoek heeft ons geleerd dat wij, ondanks dat alle cellen hartspiercellen waren, onderlinge heterogeniteit konden detecteren. Ook zagen wij sterke gradiënten in genexpressies door de cel populatie. Deze correlaties waren aanwezig in alle 5 samples, wat bevestigde dat dit een biologisch fenomeen is en niet een verschil tussen patiënten onderling. Dit heeft ons ertoe geleid om te zoeken naar gen-gen correlaties. Door gebruik te maken van verschillende bioinformatische analyses konden we patronen in genen ontdekken die gekoppeld konden worden aan de activatie van transcriptiefactoren (TFs) en we konden Modules met een specifiek genexpressiepatroon identificeren. Door gebruik te maken van de FACS-data konden wij de Modules relateren aan de celgrootte. Dit leverde ons waardevolle inzichten op over de genen die in grotere (en eventueel de meest hypertrofe) cellen tot expressie komen, en de TFs die dit programma aan kunnen sturen. Alles bij elkaar hebben wij





Figuur 1. Representatie van het gezonde hart, en het hart met hypertrofe cardiomyopathie. (A) Gezond hart. **(B)** HCM-hart met verdikt septum wat kan leiden tot een obstructie van het outflow tract (LVOT-obstructie) **(C)** Myectomie operatie, waarbij het deel van het septum wat in de weg zit operatief wordt weggesneden. LA; Linker atrium, RA; Rechter atrium, LV; Linkerventrikel, RV; Rechterventrikel, IVS; Intra ventriculair septum.

met dit hoofdstuk een waardevolle dataset geproduceerd waarin we in detail kunnen bestuderen wat het verschil is tussen hartspiercellen, en wat de mechanismen zijn die de hartspiercellen dikker of meer gestrest kunnen maken.

In hoofdstuk 3 zijn wij in meer detail getreden over de reden waarom het IVS de primaire plek is waar verdikking optreedt in HCM. Wij wilden graag het genexpressie patroon onderzoeken in het septum en in de vrije wand van het LV. Dit hebben wij gedaan door middel van Tomo sequencing (Tomo-seq), wat inhoudt dat we een deel van IVS (van LV naar RV) en een deel van de vrije wand hebben opgesneden in hele dunne plakjes en RNA-sequencing op elk individueel plakje hebben gedaan. Hierdoor konden we patronen vinden in de expressie van genen door de hartspierwand heen. Eerst hebben wij gekeken naar de locatie van marker genen door de wand heen. Hierbij detecteerde wij dat stress en hypertrofie genen in zowel het IVS als in de vrije wand tot expressie kwamen, hoewel de stress genen meer aan de LV kant van het septum tot expressie kwamen. Genen kenmerkend voor littekenweefsel hadden daarentegen een hogere expressie in de vrije wand. Daarna hebben

wij op een onbevooroordeelde manier naar de data gekeken door middel van een Principle Component Analyse (PCA). De meeste genen in de dataset vielen in PC1 en PC2. PC1 was het meest gerelateerd aan het IVS en was kon in verband gebracht worden met mitochondriale processen. PC2 werd gekenmerkt door genen die gerelateerd waren aan hypertrofie. Ook kwam PC2 voornamelijk aan de linkerventrikel-kant van het septum tot expressie, wat ons deed vermoeden dat dit gedeelte ook onder meer stress zou hebben gestaan.

Omdat erachter wilde komen waarom juist het septum dikker wordt in HCM, onderzochten wij de overlappende genen tussen PC1 en PC2 vinden om zo de specifieke genen te vinden die én in het hypertofe/meer gestreste deel van het septum tot expressie kwamen én die septum specifiek waren. Door deze set met genen te onderwerpen aan een HOMER analyse, waarbij wij kijken naar de motieven rondom de genen die door TFs kunnen worden aangestuurd, identificeerde wij NR2F2 als potentiële modulator van dit gen programma. Om dit te valideren hebben wij gebruik gemaakt van geïnduceerde pluripotente stamcellen die gedifferentieerd waren in hartspiercellen in een 2D cultuur (iPSC-CM). Door deze aan endotheline-1 (ET-1) bloot te stellen konden wij hypertrofie nabootsen. Wanneer wij een silencing RNA (siRNA) voor NR2F2 toevoegde, konden wij de expressie van NR2F2 verminderen en daarbij het voorspelde gen programma dat omhoogging na stress met ET-1 voor een groot deel inhiberen. Deze stress en deze siRNA waren echter niet genoeg om het fenotype van hypertrofie te inhiberen of om veranderingen te zien op eiwit niveau. Tot slot konden wij concluderen dat we een specifiek genprogramma in het IVS en in het LV konden detecteren, en dat we deze aan stress konden relateren. Verder onderzoek zal uitwijzen hoe deze genprogramma's precies worden aangestuurd.

In het laatste hoofdstuk, **hoofdstuk 4** hebben wij onderzocht wat de exacte trigger voor HCM kan zijn in de aanwezigheid van een mutatie. Wij hebben twee muismodellen gecreëerd die dragers zijn van de twee meest voorkomende mutaties in MYB-PC3 in Nederland. Zonder een extra stress toe te voegen zagen wij geen verschil in het hart tussen de muizen met een heterozygote mutatie (met één van de twee allelen gemuteerd) en hun wild-type (WT) broers/zussen die geen mutatie hadden. Daarna wilde we onderzoeken of in de aanwezigheid van zo'n enkele mutatie geïnduceerde hypertrofie versterkt wordt door stress op het hart. Deze stress hebben wij gegeven door verhoogde druk op het hart aan te brengen door middel van een band om de aorta (Transaortic binding; TAB). Ook hier vonden wij geen verschil in



hartfunctie of genexpressie in vergelijking met WT. De muizen die een homozygote mutatie droegen waren daarentegen zwaar aangedaan. Na twee maanden zagen wij al een sterke verdikking in het hart, vermindering van hartfunctie en hoge expressie van stress genen. Bij elkaar hebben wij dus nog niet de exacte trigger kunnen vinden die leidt tot HCM in de heterozygote dieren, maar laten de homozygote dieren duidelijke kenmerken van HCM zien. Beide modellen kunnen gebruikt worden in verder onderzoek naar de trigger of naar de progressie van HCM.

In conclusie hebben we in deze thesis met uitgebreide sequencing technieken veel geleerd over de verschillende moleculaire paden die bijdragen aan het veranderen van een gezond naar een HCM-hart. Daarbij hebben wij modellen ontwikkeld waarbij we de start en de progressie van HCM kunnen bestuderen. Verder onderzoek naar de factoren die wij hebben geïdentificeerd kunnen potentieel helpen bij de ontwikkeling en de ontdekking van biomarkers om de ziekte beter te kunnen voorspellen, of naar therapieën om de ziekte te voorkomen.





Acknowledgements

Allereerst wil ik graag **Eva** bedanken voor dit promotietraject. Ik heb een fijne tijd op het Hubrecht gehad en ik heb veel geleerd van de dynamische leeromgeving. Bedankt dat jouw kantoor altijd open stond, voor de begeleiding en de sturing die je mij hebt gegeven, en de momenten die we hebben gelachen en gediscussieerd over de projecten. Jouw enthousiasme voor het onderzoek is aanstekelijk en het overzicht wat je van alle projecten weet bij te houden is bewonderingswaardig. Ik heb veel van je mogen leren, zo moet ik nog altijd aan je denken als ik een project of bespreking begin met een leeg A4-tje en vervolgens alvast alle geplande figuur-panels van het eindproduct aan het uittekenen ben.

Martijn, hoewel je pas in een late fase mijn co-promotor bent geworden ben ik ontzettend blij met de laatste rondes kritische feedback die ik van je heb mogen ontvangen, en dat ik jou als klankbord kon gebruiken. Daarnaast is jouw bijdrage aan deze thesis is enorm geweest met alle analyses die je voor ons hebt gedaan, het 'Decoding' is voornamelijk voor jouw werk! Ik kon altijd bij jou terecht met random ideeën en brainstormsessies waarin we vaak in gedachtekronkels verdwaald raakten. Ik waardeer ook heel erg al je pogingen om mij wat vaardiger en zelfstandiger te maken met R, bedankt voor al je geduld!

Ik wil graag mijn leescommissie, **Dominique de Kleijn, Joost Sluijter, Hester den Ruijter, Jeroen Bakkers** en **Rudolf de Boer** bedanken dat zij de tijd hebben genomen om deze thesis na te lezen en te beoordelen.

My paranymphs; **Roxanne&Clement** Our PhD's started with a spontaneous decision to fly to Brazil when we were practically strangers. From here, we travelled to Paris together, explored Portugal, organized events in the PV, and enjoyed many parties and balcony sessions. Nearly every Friday around 5PM I hopped up the stairs to grab you guys for a beer. Beyond this, you have been my go-to people for scientific questions, or to be my guineapigs for practicing my presentations. You have always come up with valuable feedback, even though cardiac research not within your comfort zones. I might have sprung the "paranymphs" title on you in the first year, causing a bit of a stir, but looking back, I couldn't be happier that we have started, and will finish this journey together!



I would also kindly like to thank all my past supervisors: **Carol, Regis, Linde, Ed, Rudolf** and **Monika**. You have triggered my interest in science and shaped me into a PhD student. Thank you for including me in your thought processes and letting me do really cool projects. Thanks a lot for teaching me how to perform experiments, process and analyze, present and write it down. Besides learning a great deal at all my internships, I also really enjoyed my time here at all your different institutes.

I would also like to thank all the (old) members of the **van Rooij lab**, to begin with **Maya** the bee! My partner in PhD! You served as my literary guide with your exceptional writing (and fast reading) skills. You have an impeccable talent for time and project management (and pushing people before 8:00 in the morning with texts ;)). You have always been able to uplift me when I was feeling a bit lost and your super bubbly personality was good fun to have around! I'm looking forward to see what the future holds for you and to see mini-Maya grow! **Joep!** De grondlegger van hoofdstuk 2, bedankt voor de opzet en de klinische kijk die je kon geven bij onze hoofdstukken en voor je droge humor. **Eirini&Suji!** Thanks a lot for all the times in cell culture, boosting the volume of the music in cell culture and hanging out at or outside of work. **Elvira&Thomas**, the new kids on the block (toen ik weg ging). Ik heb jullie niet lang als PhD studenten meegemaakt, maar ik vond het heel gezellig om jullie als student in het lab te hebben en ik weet zeker dat jullie dit traject succesvol zullen gaan verlopen! (En **Thomas**, bedankt voor de aanvullende data die ik nog even nodig had om hoofdstuk 4 af te maken). **Brian**, mijn lab-buurman! Bedankt voor jouw hulp met het ontwerpen van iPS studies, en bedankt voor al jouw herinneringen, zelfs toen ik het Hubrecht verlaten had in Leiden, zonder jou zou ik bijna vergeten zijn een boekje te schrijven ;). **Louk**, je lijkt altijd te rennen! Bedankt dat je je overschot aan energie met ons wilt delen ;). **Marta**, I enjoyed working with you so much! We had so many fun moments in and outside of the lab and you are the best at laughing off serious situations! It was good fun meeting you in Sri Lanka and I really hope we will go surfing together again someday! **Arwa**, Habibi! You were the fellow ex-student of Moni and I've always looked up to you! I've learned a lot from you, the way you present, and from reading your reports ;-). **Bas**, Bureau-buurman! Bedankt voor al onze discussies en borrels! Ook bedankt aan mijn mede-minions tijdens de stagetijd in de van Rooij-groep; **Merijn, Janita** en **Evelyne** bedankt voor de leuke tijd! **Evelyne**, met jou heb ik daarna nog veel contact gehouden en ik vond het heel fijn om samen naar werk te kunnen fietsen en je op te zoeken in Doorn, waar we zelfs nog even samen aan onze thesissen hebben gewerkt (en geschaatst)! Ook



heel erg bedankt aan de andere Demkes; **Charlotte!** Bedankt voor al jouw goede adviezen, coaching sessies en altijd vrolijke humeur. Al was onze overlap in het van Rooij lab niet heel groot, je hebt me heel erg geholpen bij de afronding, wat fijn dat we de deadline van een datum aanvragen voor het einde van 2023 precies hebben gehaald!

Bedankt aan alle fantastische analisten uit het van Rooij lab: **Hesther**, bedankt voor de lange tomo-seq experimenten die wij samen hebben kunnen doen. Ik heb deze dagen heel leuk en leerzaam gevonden. Daarnaast was je ook altijd in voor een praatje en voor advies. **Lieneke** mijn fijne ex-kantoorgenootje, bedankt voor je hulp bij het muizenhoofdstuk. **Jantine** baas van de iPS cellen, bedankt voor al jouw hulp met het opzetten van de validatie experimenten voor tomo-seq en voor jouw hulp bij het maken van microtissues (al hebben we ze later nooit gebruikt). **Ilaria** my Italian mum! I always enjoyed our little talks about Cloe in the lab. And thank you too much for all your mental support! En altijd relaxte **Danielle!** Ik vond het heel fijn om met je samen te werken in de laatste maanden bij de muizen! Bedankt voor al je hulp in deze studie!

And our (ex-)post-docs; **Monika**, I learned so much from you. It's always fun to work with you and you always come with good advice about experiments and critical questions. **Andrea**, my sub-paranymph! Thanks a lot for organizing Maya's defense with me, it was great fun doing this together. It was always good to have you and your creative brain around. **Jenny** (the selfie stick) and **Kees** thanks both for your advice, support and questions. Lastly, thanks to **Marjolein** for bio-informatic discussions, **Gregory** (the photographer) and **Iliana** for work and not work-related conversations!

I'd like to thank the Hubrecht's for the great time and the scientific and non-scientific discussions. We were sharing offices (**Pim, Jingchao, Anko, Bana, Thomas**), cell culturing (**Bas, Timo, Kim, Spiros** - still in Leiden, yay! -, **Lorena, Maaïke**) the second floor and the cuddle corner (**Sjoerd, Niko, Joana&Dani** (Bob's burgers family with **Gabi**), **Ajit** (the party-starter) **Bram, Stein, Micha&Max, Lotte&Tim** (The mischievous duo in the Ardennes), **Sanne** (You were the happiest skier on Winterberg), our upstairs neighbors (**Bruna** (your wedding will always be one of my favorite Brazil-memories!), **Themis, Sonja, Niels, Juliette**) and the people that were key in organizing our still occurring Ardennes weekends; **Jamie&Erik** (the king-wizzards), **Rob** (thanks for all the cheezes!).



Ik wil ook graag de andere zeer belangrijke Hubrechtters bedanken: de dames van de receptie voor het warme welkom elke dag, HR voor het regelen van alle contracten en documenten, Technical&domestic service (in het bijzonder **Bart, Elroy** en **Jules**) voor alle gezelligheid in het magazijn, het regelen van mijn pasje, het meewerken met organisatie van evenementen, en voor alle tijd die ze voor mij hebben genomen toen ik meer informatie over het gebouw wilde voor het green team, de mensen bij IT, in het bijzonder **Peter-Erik** voor het oplossen van al mijn Mac-vragen, de mensen bij de FACS **Stephan** en **Reinier**, jullie hebben mij ontzettend veel geholpen bij mijn experimenten en bedankt voor het inwerken op alle apparaten en de mannen bij de histologie **Jeroen** en **Harry**! Niet alleen hebben jullie heel veel histologie gesneden voor hoofdstuk 4, ik heb ook veel van jullie geleerd en ik vond het altijd gezellig om bij jullie in het histologie lab te werken! En natuurlijk **Litha**! Bedankt voor al je fantastische en snelle antwoorden en hulp in de afrondende fase van mijn PhD.

Aside from my paranymphs, I also really want to thank the rest of best PV ever; PV2019! The DJ (**Wouter T**) father of the discoball and Sean Paul lover (**Wouter B**), The only rational one (**Jorik**) and our puppies (**Joris** and **Reinier**). We never printed dates right on our posters (which might have been my fault), we were slightly disorganized, but we also had a lot of fun! I really enjoy that we still see each other and come together every once in a while, and I hope that we will keep on doing this in the future!

I'd also like to thank some ex-colleagues from the AMC (**Angela, Judith, Teresa, Bea, Nadia, Daphne, Anouk, Abel, Xu, and Wessel**) for the great times at BMEP. **Natalja** and **Jiska** for my warm visits to the VU and Biesmortel. **Arjen, Roger, Mieke** and **Han** for the time at the RMI, **Arie, Zoe, Kai**, for the wonderful time at the University of Otago. And my fellow master students **Natasa** and **Giulia**.

I want to extend my gratitude to my new department, the Islet lab! Special thanks to **Eelco, Françoise** and **Marten** to have me and for the nice collaborations. **Roxanna, Amadeo, Yun, Miriam, Fransje, Maarten1/2** (van Aagje en Tall), **Maaïke1/2/3, Ferdy, Lizanne, Anagha, Esther, Natas(ch/j)a, Cyriel1/2, de E(s/z)ra's, DJ, Corine, Evelien, Rutger, Jason** en de dames van nephrology (**Rianne, Anneloes, Novella, Rosalie**, en de rest!). Bedankt voor de fantastische werksfeer, de samenwerkingen, de 12 pubs, de pubquizen (Temptation Islets/Insulin it to win it!) labweekenden en vele borrels! Thanks for asking me every once in a while, (but not too often) about the current



state of my PhD and for giving me the time and support to finish it! **Hanegraafje**, voor jou heb ik waarschijnlijk nog drie bladzijdes nodig om je te bedanken. Ik ben zo blij dat je mij binnen hebt gehaald en dat we nu samen projecten kunnen opzetten en uitvoeren. Je was al een vriendin en nu ook een collega, en jouw kritische blik, plan-vaardigheden, nieuwsgierigheid en daadkracht maken je een heerlijk persoon om mee samen te werken. Ik heb een hoop van je mogen leren, ik heb tegen je mogen klagen, maar ik heb ook vooral onwijs veel met je gelachen de afgelopen twee jaar en dat blijven we vooral nog heel lang doen!

Thanks to the people with which we had a lot of fun on the Salamancapad (of which the name of the app group cannot be mentioned here). **Alex, Peggy, Mariah, Miguel** and my dearest neighbors, **Dennis, Hassan** and **Kinan** (I've spent so many hours at your place, you are the best host!). Bedankt aan de vrienden in het oude bowlingteam, **Hizkia, Laura, Esther, Daniel**. Bedankt **Jeroen, Arnaud** en familie, voor jullie support. Ik wil ook graag mijn lieve vriendinnen **Caroline, Sophie, Laura, Ellen** en **Janneke** bedanken voor alle wijntjes, feestjes, en in de tuin hangen. Ook mijn Leidse vriendinnen **Tisra, Hesther** en **Benthe** en **Pam** wil ik bedanken, dat we nog vaak in de kroeg of op het terras mogen hangen! Ik wil **Etmee** en **Linda** bedanken, voor de nieuwe hobby's (longboarden, surfen, kamperen) die we in corona hebben opgepakt en nog altijd met elkaar kunnen delen (hoewel we dit allemaal misschien beter in onze tienerjaren hadden kunnen leren).

Bedankt aan alle **ouwe lullen van Uranymus** waarmee ik nog jaarlijks mee mag met het weekendje weg, en derde kerstdag vieren! Een bijzonder bedankje aan **Marlies**, voor alle momenten die ik met je heb mogen delen, en **Rienko**, ik heb zoveel bewondering voor jouw veerkracht. Bedankt aan mijn lieve vrienden, met wie ik nog altijd feestjes, festivals, oud en nieuw en andere belangrijke dingen mag delen. **Tom!** Mijn Uranymus-papa! Bedankt dat je altijd voor iedereen aan het zorgen bent, niemand hoeft ook met een leeg glas bier te staan als jij rondloopt. **Giertje!** De meest fanatieke wie is de Mol apper, **TimB**, de beste volkszanger (als je durft). **Iris** en **Malou**, bedankt voor de gezellige logeerpartijtjes! En **Bas**, nog bedankt voor je CV! Bedankt **Kim** (trots!), bedankt **Arno** (de strijkplank-DJ) en **Rianne**, ik kom snel eens met jou Amber en Emely op de bank hangen! Bedankt aan de mensen uit de vriendengroep die mij voor zijn gegaan in het promoveren en van wie ik veel advies heb mogen ontvangen; **Nol** voor je relativerende blik, **Dieke** de beste reporter die overal wel een woordgrapje van weet te maken. **Maarten**, de eeuwige optimist! Ik vond het zo'n eer om naast jou te mogen staan met jou promotie en ik ben blij dat



je er nu ook bij kan zijn voor mij! Bedankt aan mijn tweede huis in Utrecht, **Rianne**, je mag mij altijd wakker maken om met jou, Hannah en wijn slechte films te kijken! En natuurlijk **Rob**, maat! We hebben al een mooie lijst met artiesten samen gezien (of juist niet gezien en festivals afgestruind). Ik kon je telefonische checkups woensdagavond 18:00 ook altijd heel erg waarderen! Bedankt dat je wilde helpen met het design van deze thesis (behalve dat je er een "home is where the heart is"-associatie aan hebt gehangen die ik niet meer kan loslaten). Voor altijd linksvoor!

Als laatste, bedankt aan mijn lieve zus **Maike**, met wie ik mijn hele leven al zoveel heb kunnen delen. Ook bedankt aan mijn zwager **Mike**, en de liefste nichtjes; **Emelie**, **Lauri**, en **Nummer Drie** die nog onderweg is voor het altijd warme onthaal in Culemborg. **Papa** en **mama**, zonder jullie was ik hier nooit gekomen. Jullie hebben altijd mijn nieuwsgierigheid beloond, geen vraag was jullie ooit te veel, jullie zijn mijn wandelende Wikipedia (en als jullie het even niet weten worden mijn vragen altijd tot in detail uitgezocht). Daarnaast kan ik altijd bij jullie terecht voor wijze raad of voor het controleren van mijn teksten. Ik hou van jullie!



Curriculum Vitae

Anne Elisabeth de Leeuw was born the 3rd of February 1991 in Leiden, the Netherlands. After graduating high school, she moved to Utrecht to study Life Sciences with a specialization in Zoology. She started developing great interest in pursuing her career in science from the moment of her first internship in New Zealand. Here, she was at the University of Otago with prof. dr. Regis R. Lamberts and dr. Carol T. Bussey. She investigated the role of catecholamines on the heart rate and blood pressure in a diabetic, and obese context. After this internship she did another internship at the



Rudolf Magnus Institute (UMC Utrecht) in the group of prof. dr. Roger Adan under supervision of Linde Boekhoudt to investigate the role of the dopaminergic system in the brain from the nucleus accumbens to the ventral tegmental area. She finished her Bachelor's degree in 2013 and continued with her Master's degree at the VU in Amsterdam. During this time, she investigated remodelling of small arteries in an *ex vivo* setup in the lab of prof. dr. Ed van Bavel. For her master thesis, she went to Groningen, to perform a literature study on the cardioprotective role of SGLT2 inhibition, which was supervised by prof. dr. Rudolf de Boer, and published in *European Heart Journal - Cardiovascular Pharmacotherapy*. For the last internship, Anne was at prof. dr. Eva van Rooij's lab at the Hubrecht Institute in Utrecht. Supervised by dr. Monika Gladka she investigated the role of ZEB2 in hypoxia-induced stress. Anne was awarded her masterdiploma of cardiovascular research *cum laude*. She enjoyed her time at the Hubrecht and returned to the lab of Eva van Rooij in 2018 to start a PhD on investigating the molecular mechanisms driving genetic heart diseases. The results of this research are presented in this thesis.



List of publications

Wehrens, M., **Leeuw, A. E. de**, Wright-clark, M., Eding, J. E. C., Boogerd, C. J., Molenaar, B., van der Kraak, P. H., Kuster, D. W. D., van der Velden, J., Michels, M., Vink, A., & van Rooij, E. (2022). Single-cell transcriptomics provides insights into hypertrophic cardiomyopathy. *CellReports*, 39(6), 110809. <https://doi.org/10.1016/j.celrep.2022.110809>

Gladka, M., Kohela, A., **Leeuw, A.E. de**, Molenaar, B., Versteeg, D., Kooijman, L., Geldorp, M. van, Ham, W.B. van, Haigh, J.J., Veen, T.A.B. van, Rooij, E. van (2023). Hypoxia-responsive ZEB2 regulates a network of calcium handling genes in the injured heart (manuscript submitted).

Palao, T., van Weert, A., **de Leeuw, A.**, de Vos, J., Bakker, E. N. T. P., & van Bavel, E. (2018). Sustained conduction of vasomotor responses in rat mesenteric arteries in a two-compartment in vitro set-up. *Acta Physiologica*, 224(3). <https://doi.org/10.1111/apha.13099>

Boekhoudt, L., Roelofs, T. J. M., de Jong, J. W., **de Leeuw, A. E.**, Luijendijk, M. C. M., Wolterink-Donselaar, I. G., van der Plasse, G., & Adan, R. A. H. (2017). Does activation of midbrain dopamine neurons promote or reduce feeding? *International Journal of Obesity*, 41(7), 1131–1140. <https://doi.org/10.1038/ijo.2017.74>

de Leeuw, A. E., & de Boer, R. A. (2016). Sodium-glucose cotransporter 2 inhibition: Cardioprotection by treating diabetes—a translational viewpoint explaining its potential salutary effects. In *European Heart Journal - Cardiovascular Pharmacotherapy* (Vol. 2, Issue 4, pp. 244–255). Oxford University Press. <https://doi.org/10.1093/ehjcvp/pvw009>

Bussey, C. T., **de Leeuw, A. E.**, & Lamberts, R. R. (2014). Increased haemodynamic adrenergic load with isoflurane anaesthesia in type 2 diabetic and obese rats in vivo. *Cardiovascular Diabetology*, 13(1). <https://doi.org/10.1186/s12933-014-0161-4>

Bussey, C. T. T., **de Leeuw, A. E.**, Cook, R. F. F., Ashley, Z., Schofield, J., & Lamberts, R. R. R. (2014). Dual implantation of a radio-telemeter and vascular access port allows repeated hemodynamic and pharmacological measures in conscious lean and obese rats. *Laboratory Animals*, 48(3), 250–260. <https://doi.org/10.1177/0023677214530687>



